lv-Infra

TU Delft

Vertical Flow-Induced Vibrations of Valves in Navigation Locks

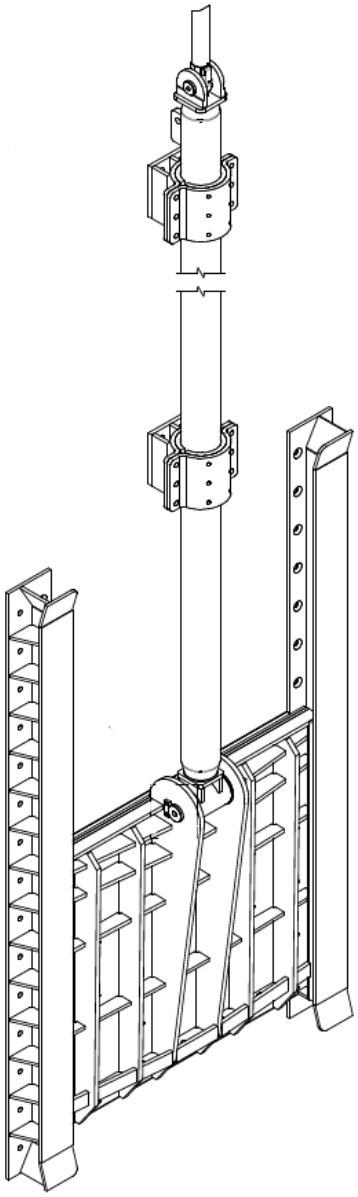

T.J.A. Korevaar

[Page intentionally left blank]

Vertical Flow-Induced Vibrations of Valves in Navigation Locks

Master of Science Thesis

BY

T.J.A. Korevaar

October 4, 2016

For the degree of Master of Science in Hydraulic Engineering
at Delft University of Technology

Graduation Committee	
Prof. dr. ir. W.S.J. Uijttewaal (chairman)	Delft University of Technology
Ir. W.F. Molenaar	Delft University of Technology
Dr. ir. B. Hofland	Delft University of Technology
Ing. M. van Almen	IV-Infra B.V.

Faculty of Civil Engineering and Geosciences (CEG)
Delft University of Technology

[Page intentionally left blank]

Preface

This report is the final result of my master thesis and is part of the master track Hydraulic Engineering at Delft University of Technology. This research could not have been realised without the help of my supervisors.

First of all, I would like to thank the engineering company IV-Infra for providing me with a pleasant work environment. In special, I want to thank Matthijs van Almen for his daily support during the entire process of the thesis.

I also want to thank my supervisors from the University of Technology Delft, which are Wim Uijttewaal, Wilfred Molenaar and Bas Hofland, for their advice and help with the research.

Special thanks go to my parents for their support during my entire study and for providing me with the opportunities to achieve my goals.

Tom Korevaar

Delft, October 2016

[Page intentionally left blank]

Abstract

Navigation locks are used to transport vessels between waterways with different water levels. In the nearby future many navigation locks will be renovated or replaced. During the design of a new lock still some unknown factors are encountered. One of these factors is the vibration of the valve.

The valve is part of the filling and emptying system that is responsible for the levelling of the water in the lock chamber. The most used valve type is a vertical-lift valve. During the filling and emptying of the lock, water flows with high velocity underneath the valve. The flow of water can cause vibrations. These vibrations are called flow-induced vibrations and could lead to failure of the valve system. Possible failures are for example that the operating machinery will not be able to open the valve or that the valve will hit other elements due to the vibrations. As a consequence the lock gate complex cannot meet its requirements anymore.

Several types of flow-induced vibrations can be distinguished. This distinction is based on the cause of the vibration. The three most important types regarding the flow underneath a valve are:

- Excitation due to turbulence of the water flow;
- Excitation due to instability of the water flow;
- Self-excitation of the valve.

The above-mentioned types can be experienced in two directions. The two directions are in-flow (horizontal in the direction of the flow) and cross-flow (perpendicular to the direction of the flow). A valve is more likely to vibrate in a vertical direction (cross-flow) than a horizontal direction (in-flow), because the majority of the valves is positioned in a niche of a gate or culvert.

Currently not much information regarding the flow-induced vibrations due to turbulence or instability of the water flow is available and the information that is available is often out dated. The shape of the lower edge seal of the valve has an effect on both types of flow-induced vibrations. This seal has to ensure the water tightness of the valve. No research has been done on the effects of the seal shapes, which are used nowadays, on the dynamic behaviour. Therefore, the information of the effect of seal shapes as used in practice is missing. In the current situation a guideline involving the natural frequency of the valve system is used. This guideline states that the natural frequency of the valve (f_n) has to be larger than three times the excitation frequency (f_{exc}). Therefore, the main research question of this research is:

> *What is the effect of the shape of the lower edge seal on the vertical flow-induced vibrations of a valve in a filling and emptying culvert?*

The vibration phenomena have been investigated by means of a physical model. A simplified scale model of the valve is constructed and tested in a current flume under varying conditions. The varying parameters during these tests are the flow velocity underneath the valve, the stiffness of the vertical suspension (one extreme stiff and four lower kinds of stiffness), the gate opening underneath the valve and the shape of the lower edge seal. Four different seal shapes have been tested, the shapes are shown in figure 1. The tests have been executed under steady state conditions. In addition to the steady state tests, free-decay tests (to determine the natural frequency and damping) and tests to determine the contraction have been executed.

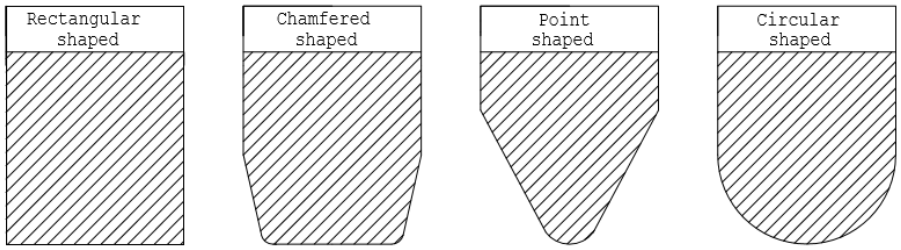

Figure 1: Lower edge seal shapes used during the physical model tests

A total of 227 steady state tests have been done, 177 of these tests were executed with a low vertical stiffness. A total of 71 tests (40%) showed a clear dominant response. The majority of the responses were found in the tests with the chamfered-shaped lower edge (60% of total tests with chamfered-shaped lower edge) and the least with the point-shaped (15% of total tests with point-shaped lower edge). The range of the parameters was similar during all tests. The gate opening was varied between 5 and 45 mm and the flow velocity was varied between 0.3 and 1.9 m/s.

In addition to the influence on the existence of a dominant response, the shape of the lower edge seems to have an effect on the amplitude of the vibration (vertical force amplitude) as well. The rectangular-shaped seal showed significantly larger amplitudes, while the point-shaped seal showed the smallest amplitudes.

The shape of the lower edge seal did not affect the excitation frequency. For all shapes a Strouhal number (a dimensionless quantity for the excitation frequency) of 0.13 was found. It was experienced that the Strouhal number was influenced by the Reynolds number. The Strouhal number showed a constant trend for a Reynolds number above a lower limit ($> 3\,10^4$). The Reynolds numbers reached during the physical model tests were relatively low compared to the Reynolds numbers reached in real-life designs. This could lead to a different response in a real-life situation. Therefore, it is recommended to conduct similar tests, as done during this research, but with larger Reynolds numbers.

The relative gate opening (gate opening/thickness of the valve) had an effect on the existence of vibrations. The largest vibrations occurred when the relative gate opening was between 0.5 and 1.0. Above a ratio of 1.5 no vibrations were experienced at all.

The structural damping of the model has an effect on the resonance frequencies of the valve. The damping shifts the resonance frequency. Theoretically the critical area for resonance is at $f/f_n = 1.0$ (excitation frequency/natural frequency). The presence of the damping shifts the resonance peak to $f/f_n < 1.0$. The damping in the model was viscous damping, where the main contributor to the damping in a real-life situation is friction. The real amount of damping in a valve system is still unknown. It is recommended to get a clearer view of this damping, since it can have a significant effect on the resonance frequency.

The current guidelines regarding a vibration free design, suggest that the natural frequency of the system should be three times the excitation frequency. If this rule is followed the dynamic amplification factor will not exceed 1.1. Any form of resonance can be prevented. If the present damping reaches significant values the resonance frequency of the system becomes smaller. Consequently, the resonance frequency will be closer to the excitation frequency.

The study has proven the presence of the flow-induced vibrations. However, the executed physical model test should be optimized to get a more accurate view on the different phenomena. Also should the effect of certain parameters (Reynolds number, water levels) be further investigated.

Table of Contents

Chapter 1 Introduction

The first chapter of this report will give an introduction of the research and will describe the structure of the report and methodology. This will be done by the sections listed below.

- Navigation Lock (§ 1.1). A short introduction is given of the navigation lock and the function of the valve in this lock system.
- Problem (§ 1.2). This paragraph exists of a brief description of the problem and a problem statement.
- Objectives (§ 1.3). The objectives stated in this paragraph result from the problem analysis presented in the previous paragraph.
- Research Questions (§ 1.4). The research questions as presented in this section follow from the objectives in § 1.3.
- Research Methodology (§ 1.5). This part will shortly elaborate the choice for a physical model test. Also the steps taken during this process will be explained
- Assumptions and Limitations (§ 1.6). After the methodology has been explained the important assumptions and limitations made during the course of the research are given.
- Report Structure (§ 1.7). The final part of this chapter will be dedicated to the structure of the remaining part of the report.

1.1 Navigation Lock

A navigation lock is a type of sluice that is used to transport vessels between two waterways with a different water level. A navigation lock is most of the time located at the beginning or the end of a channel with a regulated water level. Figure 1-1 shows a schematization of the most important elements of a navigation lock.

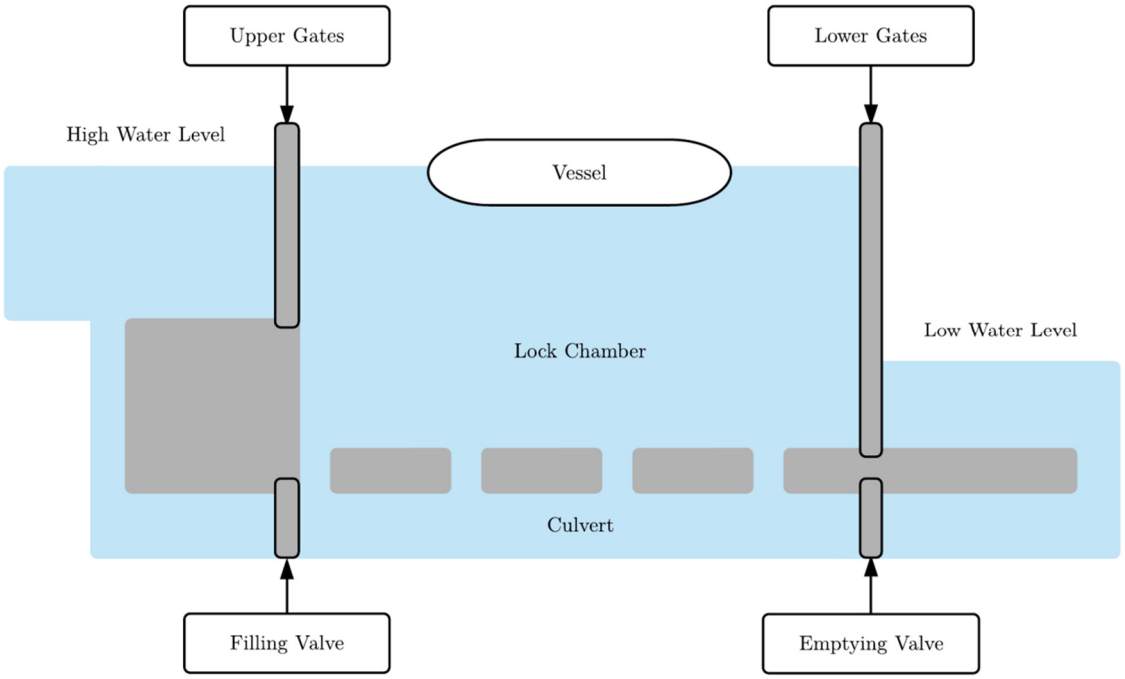

Figure 1-1: Schematization of a navigation lock

One of the main functions of a navigation lock is the levelling of the water in the lock chamber. This enables the vessels to pass the water level differences of the two waterways. The levelling is done by a filling and emptying system of which the valve is an important element. The valves control the in- and outflow of water. Figure 1-2 shows a flowchart of the overarching definition of sluices. The flowchart is concentrated to the individual elements of the valve. A more detailed background of all the components from Figure 1-2 is given in Appendix A. The next paragraph will give a brief description of the valve and some elements.

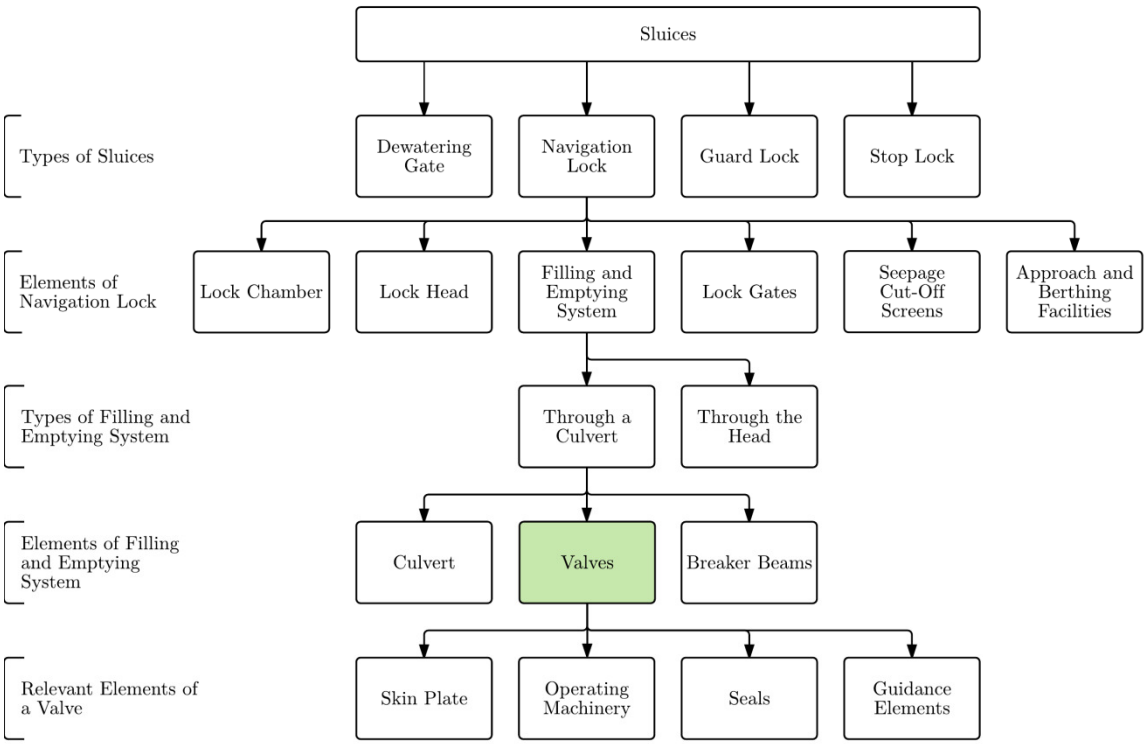

Figure 1-2: Flowchart from the definition of a sluice concentrated to the individual elements of the valve

1.1.1 Valve

The main function of a valve is to control the water flow in a pipeline [35]. In this report the pipeline is considered a filling and emptying culvert of a navigation lock as shown in Figure 1-3 (L). Valves are designed in different shapes and types, but this research will focus on the vertical lift valve as shown in Figure 1-3. A basic valve design exists of several basic elements. A more detailed description of the valve and these elements can be found in Appendix A. In this paragraph a short description is given. The basic elements are:

- Skin plate (Figure 1-3 (R), no. 1). The skin plate is the main part of the valve and has to withstand the hydrostatic pressure when the valve is closed.
- Operating machinery (Figure 1-3 (R), no. 2). In the present designs the valve is opened and closed by a hydraulic cylinder that is located above the valve. The figure below does not show the cylinder but shows the vertical rod that is connected to the cylinder. The hydraulic cylinder is the main contributor of vertical stiffness of the valve system.
- Seals (Figure 1-3 (R), no. 3). The seals are positioned at all edges (top, bottom and side) of the valve and have to prevent (major) leakage.
- Guidance elements (Figure 1-3 (R), no. 4). The guidance elements are located on the side of the valve and have to guide the valve (skin plate) during opening and closing. The elements can be applied as a rolling system or as a sliding system. The figure below shows a sliding system. A sliding system is the most applied type of guidance element in the Netherlands. At the contact points of the guidance elements and the skin plate friction takes place. This friction is an important damping force in the valve system.

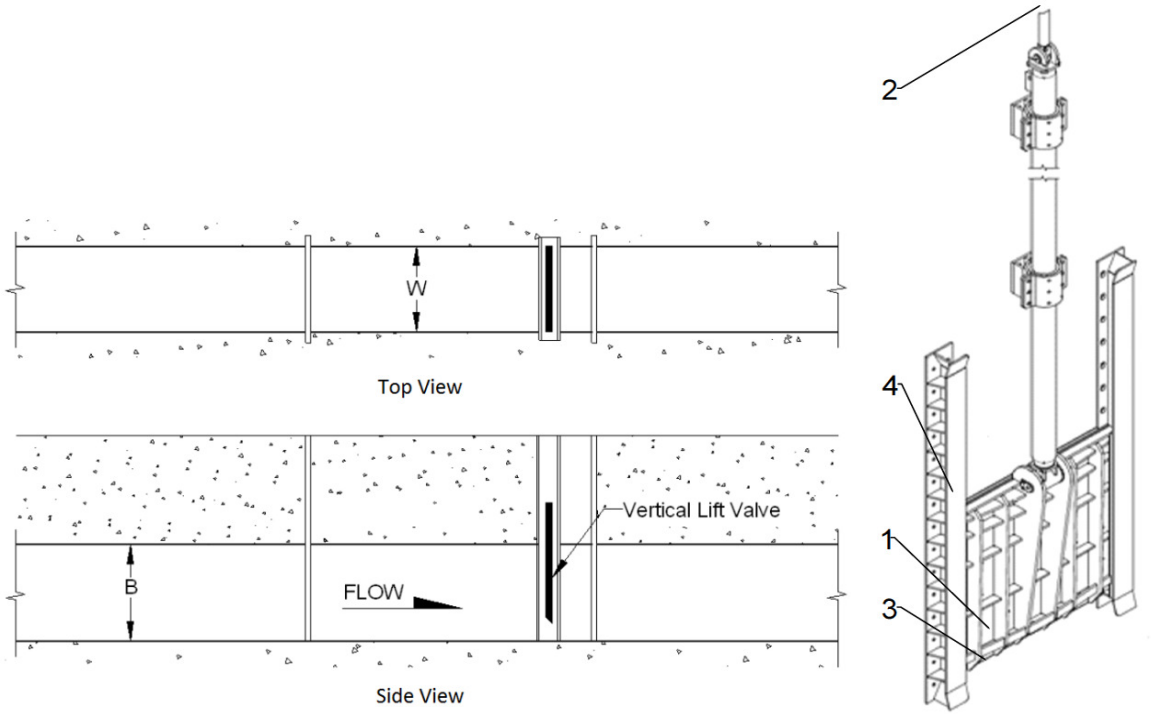

Figure 1-3: (L) Top and side view of a vertical lift vale in a culvert [49] & (R) Valve including guidance elements and a part of the suspension system

1.2 Problem

This paragraph gives a brief description of the problem. The description is based on the results of a literature study. In § 1.2.1 a problem description is given. After the problem description, a short problem statement will be presented in § 1.2.2.

1.2.1 Problem Description

In the near future a major amount of locks has to be constructed or replaced over the whole area of the Netherlands [62]. The process of constructing and designing a new lock still has some unknown factors. One of these factors is the dynamic behaviour of the valve in a filling and emptying culvert.

A filling and emptying culvert is mostly used in navigation locks with a high head difference. Figure 1-4 (L) shows an example of a culvert inside the lock chamber. Another option is to position the culverts outside the lock chamber. One of the main reasons to apply a culvert system is to reduce the disturbance of the water in the lock chamber due to turbulence of the in- or out flowing water. By reducing the disturbances, the vessels will be more stable during the levelling. The in- and outflow of water in a culvert is regulated by one or multiple valves.

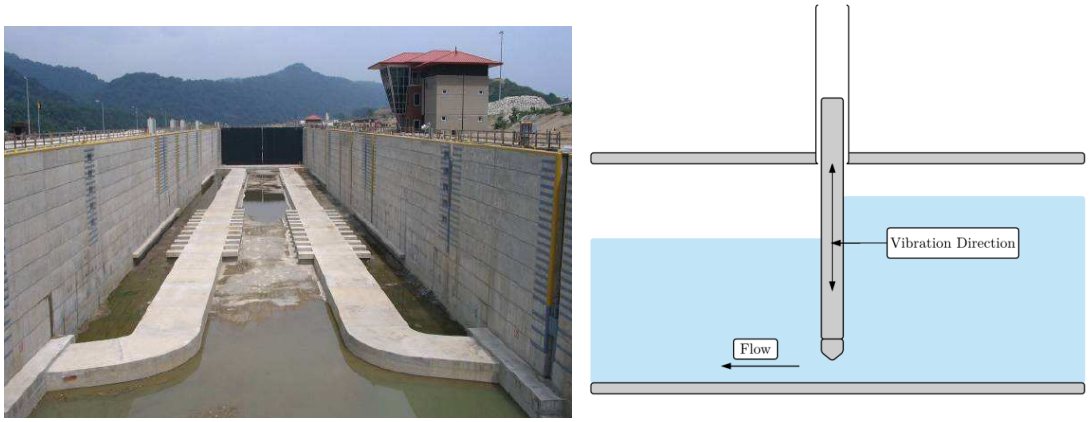

Figure 1-4: (L) In-chamber longitudinal culvert system, Marmet Lock (US) [40] & (R) Vertical cross-flow vibrations of a valve

During the levelling of the water in the lock chamber, water will flow underneath the valves. Figure 1-3 (L) shows the top and the side view of an underflow vertical-lift valve. Large flow velocities under the valve can be reached due to the head differences. This flow of water could lead to multiple phenomena. One of these phenomena is the vertical vibration of the valve. These vibrations could lead to (partial) failure of the valves and the navigation lock will no longer able to level the water. Failure of the valves can cause additional amounts of levelling time. This additional levelling time will eventually lead to additional costs.

In the present situation the knowledge regarding vertical cross-flow vibrations on valves in a filling and emptying culvert of a navigation lock is limited. Experiences from the past prove the presence of the vibrations. In most cases it was impossible to recreate the related hydraulic conditions to study these experiences [35]. Nevertheless, some research has been done on vertical cross-flow vibrations. Most of these researches were based on straightforward and simplified design shapes of the lower edge of the valve. These shapes are not often used in practice. Therefore, the results are not conform a real-life situation. A desk study was done by Erdbrink and Jongeling [19] in which they stated that the vertical type of vibration is known for its large amplitudes and relative low frequencies and therefore the vibrations could be very destructive.

Kolkman and Jongeling [33] give multiple causes for the emergence of vibrations of a valve. One of the most unknown types is the vibration due to the instability of the flowing water. This type is caused in most cases by an instable separation point of the flow or an instable reattachment point of the flow. Another important type is the vibration due to turbulence that depends on the shape of the lower edge.

During the design phase of new locks, new questions regarding the present theories and assumptions of the flow-induced vibrations emerged. Based on this background this research will focus on the blank spots of our knowledge regarding the flow-induced cross-flow vibrations of a valve. In the case of a vertical-lift valve in a culvert, these cross-flow vibrations are in the vertical direction. Figure 1-4 (R) shows the direction of the vibration.

1.2.2 Problem Statement

In the present situation a lot of literature is available regarding the cross-flow vertical vibrations of a valve. Most of the literature is based on physical model tests. Some of the researches give contradictory results. These results lead to different advices regarding a vibration free design. In an ideal situation clear, precise and correct guidelines would be available for the vibration free design of a valve. This thesis should bring the current situation and the ideal situation closer to each other.

1.3 Objectives

Based on the problem description and the problem statement from previous paragraph some objectives were set. The objectives are listed below.

- The field of study regarding vibrations on a valve is fairly undeveloped. A few studies have been done from which several standard design rules were retrieved. An objective is to make an inventory of this information and discuss the missing and contradictory information and incorrect guidance.
- The research will be done using physical laboratory tests. Therefore, it should be pursued that the design of the physical model will be as close to the reality as possible. By achieving this objective, the results from the physical model tests will be more accurate and useful in practice.
- Vibrations on a valve depend on multiple external variables, for example flow velocity, head difference and the ratio between the thickness of the valve and the opening underneath the valve. Therefore, one objective will be to get an overview of the different related external variables and the magnitude of their positive or negative contributions to the vibrations.
- From the structural elements the major contributor to the vertical vibrations will be the shape of the lower edge with the attached watertight closing seal. In this research the effect of different shaped seals on the vibrations should be made clear. The seals tested are seals as used in practice.

1.4 Research Questions

The objectives presented in the previous paragraph are summarised in research questions. The questions can be divided into a main question and several sub-questions. The questions are presented in this paragraph. The main question of the research is defined as:

What is the effect of the shape of the lower edge seal on the vertical flow-induced vibrations of a valve in a filling and emptying culvert?

The sub-questions are formulated as:

- *What are the critical conditions for the initiation of the flow-induced vertical vibrations of a valve in a culvert?*
- *What is the relation between the excitation frequency of the flow, the response frequency of the system and the natural frequency of the system?*
- *What is the difference in excitation frequency for the different lower edge seal shapes? And is this coupled to a constant critical Strouhal number for a specific shape?*
- *What is the impact of the shape of the lower edge seal on the hydraulic down pull force? And is there a clear way to quantify the value of the hydraulic down pull force?*

1.5 Research Methodology

The complete system of the valve including the suspension system and the culvert involves many fundamental principles from multiple fields of study. The fields that are involved in the problem are amongst others structural engineering, mechanical engineering and fluid engineering. Therefore, the production of a numerical or analytical model of the whole system is extremely complex. Some attempts to create a numerical model have been made, but were never able to capture all features relevant for a complete representation of the excitation mechanisms [18]. A complete numerical model would be too complex for the scope of this study. For this reason, a choice has been made to retrieve the results based on the outcome of a physical model test. During the process the first step was to retrieve the most import information already available regarding the problem. Based on this information the physical model and the methodology have been designed.

After the model has been designed and the tests have been executed, the data has been analysed. The results and conclusions are retrieved from this analysis. More clarity on the exact steps of the research is given in § 1.7. This paragraph explains the full structure of the report.

1.6 Assumptions and Limitations

This paragraph will discuss the assumptions and limitations regarding the research. The assumptions and limitations are based on a literature study from which the most important results can be found in Chapter 2 and Appendix C.

1.6.1 Assumptions

During the course of the research some assumptions were made. The initial assumptions are stated below.

- The valve plate is infinitely stiff. The focus of the research is set on the vertical degree of freedom of the rigid valve. By making the valve infinitely stiff it will not be able to undergo a flexural movement. Also the rotational movement of the valve should be prevented. This assumption is important during the design of the model set-up.

- No added structural damping in the model. The model will always include a small amount of structural damping. It is chosen to not to add any additional damping in the model. The damping in the model should be kept as minimal as possible. The low value of damping will be beneficial for the initiation of the vibrations. Therefore, more insight can be given in the different phenomena.
- The tests are done under steady state flow conditions. The experiment will be executed using a steady state flow. This is in contrast with the real situation in which the boundary conditions change continuously. With changing boundary conditions an unsteady state will be present. The results of the research will identify conditions which are unfavourable for the initiation of the vibrations. These conditions are not related to the state of the flow.
- The problem is considered to be a two dimensional problem. In this research the problem is considered as a two dimensional problem. This means that the effect due to friction with the side of the culvert and other related three-dimensional phenomena are neglected. The parameters of the model are assumed constant over the width of the valve/flume.

1.6.2 Limitations

In additions to the assumptions made in the previous paragraph the research will also have certain limitations. The limitations are:

- The dimensions of the laboratory flume. The major part of limitations regarding the physical laboratory tests will be related to the use of a flume. Most vertical-lift valves are situated in a culvert, which is seen as a closed conduit in terms of fluid mechanics. It will not be possible to recreate a closed conduit state with the available current flumes. The relevant parameters (the flow velocity, gate opening and lower edge shape) do not depend tremendously on this difference.
- Scale model. Because of the size of the available flume it will not be possible to simulate the situation in a 1:1 scale. For this reason, a scale model is used. When the correct and relevant scaling factors are used the use of a scale model should give a similar result.
- Validation of the test results. In addition to the limitations regarding the laboratory flume there will also be limitations regarding the validation of the test results. Because of the complexity of the problem no useful numerical model exists and the development of a numerical model would be too complex. Validation could be done by making simple calculations based on current design rules.

1.7 Report Structure

The report structure is shown in Figure 1-5. The content of the report has been divided into several sections. The sections are listed below.

- Introduction (Chapter 1). This first chapter gave a first overview of the problem and the goals of the research. A detailed description of the entire lock system and the important components can be found in Appendix A.
- Theoretical Background (Chapter 2). This part gives and introduction of the flow-induced vibrations of a valve. The theoretical background is retrieved from a literature study. The information will be divided into two parts:
    - Dynamics of the System (§ 2.1 and Appendix B). This paragraph gives a theoretical background of the dynamic system.
    - Flow-Induced Vibrations of the Valve (§ 2.2 and Appendix C). This section describes the definitions and causes of the vibrations of the valve. It will also contain an elaboration of the already existing guidelines for a vibration free design.

- Test Conditions and Settings (Chapter 3). This section will explain the physical model test. This is done in two parts:
  - Methodology (§ 3.1, Appendix D and Appendix E). This section describes all relevant parameters during the physical model test and elaborates the steps taken during the testing process.
  - Model Set-Up (§ 3.2, Appendix F and Appendix G). This part discusses the details of the designed model set-up and all the choices and calculations made to come to this set-up.
- Results and Discussion (Chapter 4, Appendix H, Appendix I and Appendix J). This section discusses the results from the physical test. During this process the retrieved results are compared to already existing information. Appendix H shows how the data has been processed from the rough data files. Appendix I gives an overview of all the tests with the test conditions and Appendix J shows some explained power spectra resulted from the processing of the data.
- Conclusion and Recommendations (Chapter 5). The final part of the report exists of the conclusions of this research and recommendations regarding any possible future research.

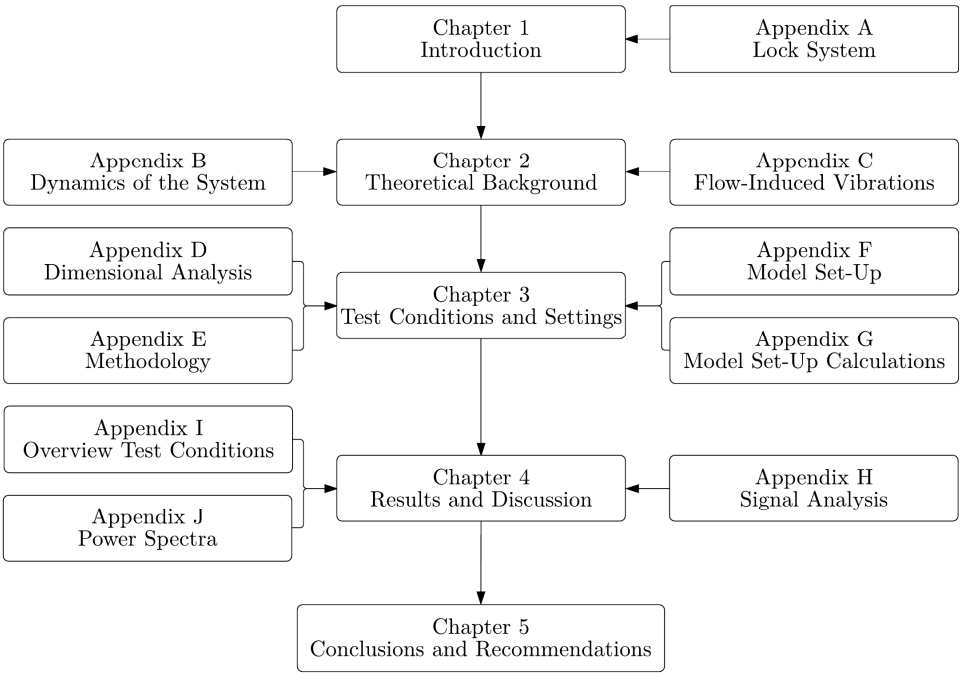

Figure 1-5: The structure of the report

Chapter 2 Theoretical Background

This chapter will give a theoretical background regarding the flow-induced vibrations of a valve in a culvert of a navigation lock, based on a literature study. The chapter has been divided into two subsections. The structure of the chapter is given in Figure 2-1. The sections are:

- Dynamics of the system (§ 2.1). In this paragraph the equation of motion and added water effects will be discussed. Additional information regarding the dynamics can be found in Appendix B.
- Flow-induced vibrations of a valve (§ 2.2). This section focusses on the different types and definitions of the vibrations. It will also elaborate the current knowledge regarding the vibrations and the commonly used design guidelines. A more detailed description of the different vibrations can be found in Appendix C.

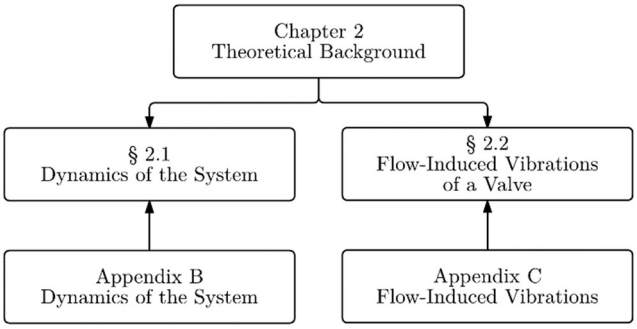

Figure 2-1: The structure of chapter 2

2.1 Dynamics of the System

An understanding of the dynamic behaviour of the system is important to understand the problem. This paragraph will go deeper into the theory of the dynamics. This will be done by treating the following subjects:

- A simple mass-spring-dashpot system with only one degree of freedom (§ 2.1.1). This paragraph gives the description of a basic dynamic system with the corresponding equation of motion. Special attention is paid to the damping in such a system.
- Additional hydrodynamic terms due to the presence of water (§ 2.1.2). Because the valve is positioned under water the basic equation of motion is adjusted with additional terms. The Additional hydrodynamic terms due to the presence of water are called the water effects.
- The response of the system (§ 2.1.3). The final part describes the response of the system. A distinction is made between the response frequency and the natural frequency.

2.1.1 Equation of Motion

When the valve system has one degree of freedom (vertical) and the problem is discussed in a two dimensional way, it can be modelled as a simple mass-spring-dashpot system as shown in Figure 2-2. The equation of motion coupled to this basic model is given in equation 2.1 [9]:

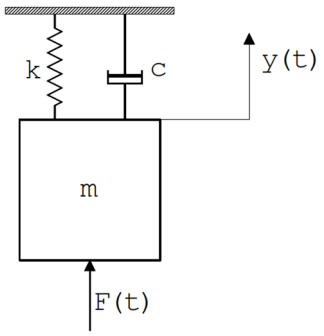

Figure 2-2: Basic one degree of freedom mass-spring-dashpot system

$$m \cdot \frac{\partial^2 y}{\partial t^2} + c \cdot \frac{\partial y}{\partial t} + k \cdot y = F(t) \qquad 2.1$$

In which:

m	=	mass [kg]
c	=	damping [Ns/m]
k	=	spring stiffness [N/m]
F(t)	=	external force [N]
t	=	time [s]
y	=	vertical position [m]

This exact equation is only relevant when the system moves in free air. When the mass-spring-dashpot system is used under water some hydrodynamic terms have to be added to the equation of motion. This is explained in the next paragraph (§ 2.1.2).

Damping

An aspect in this system that requires some more attention is the damping (c). In Equation 2.2 the definition of the critical damping (c_{cr}) of the system is given. This critical damping is often expressed by a dimensionless number, which is shown in equation 2.3 [9] and is called the damping factor (ζ).

$$c_{cr} = 2 \cdot \sqrt{k \cdot m} \qquad 2.2$$

$$\zeta = \frac{c}{c_{cr}} = \frac{c}{2 \cdot \sqrt{k \cdot m}} \qquad 2.3$$

A distinction can be made between five types of damping. These forms are all related to the damping factor [9]. The forms are displayed in Figure F-12. The types are:

- $\zeta = 0 \rightarrow$ no damping. When the damping factor is 0, there is no damping (c = 0) in the system. This means the amplitude of the vibration will not change in time.
- $0 < \zeta < 1 \rightarrow$ underdamped. If the damping factor has a value between 0 and 1 the vibration is damped and the amplitude will decrease in time.
- $\zeta > 1 \rightarrow$ overdamped. A system with a damping factor larger than 1 has a high amount of damping. Theoretically this means that the vibration will not pass the equilibrium point again. In certain cases, this could happen. It could be that the system does not return to the initial equilibrium state.
- $\zeta = 1 \rightarrow$ critically damped. When the damping factor is exactly 1 a transition point between an underdamped system and an overdamped system is reached, this is called critically damped. When

a system is critically damped it returns to the equilibrium state as fast as possible without vibrating.

- $\zeta < 0 \rightarrow$ negative damped. When the damping factor is lower than 0 the damping is negative. In a system with negative damping the amplitude can increase to infinity. The system is unstable.

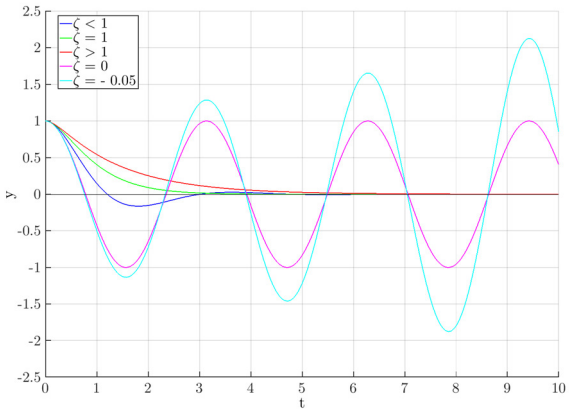

Figure 2-3: Examples of vibrations with the theoretical forms of damping related to the damping factor (ζ)

2.1.2 Added Water Effects

When a valve moves under water additional terms are added to the basic equation of motion. These terms are defined as the added water effects. When these terms are added the analysis of the structural motion can remain similar to that of a system in free air. Figure 2-4 shows a valve in flowing water.

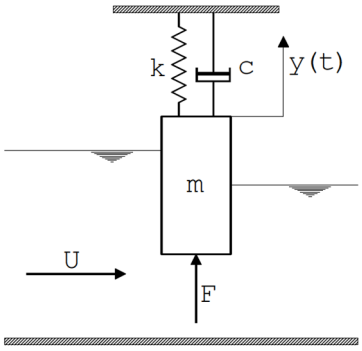

Figure 2-4: Basic one degree of freedom mass-spring-dashpot system in flowing water

Equation 2.4 [33] shows the equation of motion of the previous paragraph adjusted for movement under water. The additional terms are called the added water terms.

$$(m + m_w)\cdot\frac{\partial^2 y}{\partial t^2} + (c + c_w)\cdot\frac{\partial y}{\partial t} + (k+k_w)\cdot y = F\left(t, y, \frac{dy}{dt}, \text{etc.}\right) \qquad 2.4$$

In which:

m_w	=	added water mass [kg]
c_w	=	added water damping [Ns/m]
k_w	=	added water stiffness [N/m]

From equation 2.4 three kinds of added water effects can be defined. A more detailed description of these effects is given in Appendix B. The effects are:

- Added water mass (m_w);
- Added water stiffness (k_w);
- Added water damping (c_w).

2.1.3 Dynamic Response

During the tests a steady state situation has been created. The researches done in the past have presented their results in varying types of frequencies. It is important to make a clear distinction between these frequencies and the relations to each other. The frequencies often used are:

- The excitation frequency (f_{exc});
- The natural frequency (f_n);
- The response frequency (f_{resp}).

In this specific case the excitation frequency is the most unknown frequency. The fluctuations and the instability of the water flow will give a frequency in the hydraulic down pull force, which is going to excite the system. The excitation frequency will be dealt with in Chapter 3. In this paragraph the focus will be on the natural frequency and the response frequency.

The Natural Frequency

An important characteristic of the system is the natural frequency. The natural frequency is defined as the frequency of a free vibrating system without external force, lacking any form of damping. The equation of motion presented in equation 2.1 will be reduced to equation 2.5.

$$m \cdot \frac{d^2y}{dt^2} + k \cdot y = 0 \qquad 2.5$$

The result of this equation will be a harmonic vibration. This leads to the definition of the natural frequency as shown in equation 2.6.

$$f_n = \frac{\omega_n}{2\pi} = \frac{1}{2\pi} \cdot \sqrt{\frac{k}{m}} \qquad 2.6$$

In which: f_n = natural frequency [Hz]
ω_n = natural angular frequency [rad/s]

With a same approach the natural frequency for an underwater system can be determined. The natural frequency for a system under water is shown in equation 2.7.

$$f_n = \frac{1}{2 \cdot \pi} \cdot \sqrt{\frac{k+k_w}{m+m_w}} \qquad 2.7$$

When the natural frequency is (almost) equal to the excitation frequency, resonance phenomena may arise. When resonance occurs the amplitude of the vibrations can become infinitely large, leading to an unstable system. A significant amount of damping in the system could influence the natural frequency. A new obtained frequency, that is called the damped natural frequency ($f_{n,damped}$), is shown in equation 2.8 [20].

$$f_{n,damped} = \frac{1}{2 \cdot \pi} \cdot \sqrt{\frac{k}{m} - \left(\frac{c}{2 \cdot m}\right)^2} = \frac{1}{2 \cdot \pi} \cdot \sqrt{\frac{k}{m} \cdot (1 - \zeta)^2} \qquad 2.8$$

Appendix B gives a more detailed description of resonance, a more detailed derivation of the natural frequency and an explanation of other important dynamical characteristics.

The Response Frequency

The response frequency is the frequency of the valve when it is excited by a force. Some important remarks can be made regarding the response frequency. In a steady-state situation the response frequency of the system is equal to that of the forcing, when the force is pure harmonic [10]. Mathematically the response has a solution as shown in equation 2.9.

$$y(t) = Y_0 \cdot \sin(\omega \cdot t + \phi) \tag{2.9}$$

In which:

	Y_0	=	vertical amplitude of the vibration [m]
	ω	=	angular force frequency [rad/s]
	ϕ	=	phase difference [rad]

This solution shows that in a steady-state situation the response frequency solely depends on the frequency of the force and not on the properties of the spring-mass system (k and m). However, the vibrations will be excited by multiple phenomena and unpredictable turbulence. Therefore, the force will not be pure harmonic. The response frequency will therefore be a combination between the excitation frequency and the natural frequency.

Lock-in Effect

A phenomenon that should be kept in mind is the lock-in effect. This effect synchronizes the excitation frequency of the water with the natural frequency of the system. The effect has never been observed with vertical vibrating valves with only underflow. However, some effects of the phenomena could be encountered and could therefore influence the results. Figure 2-5 shows a visualization of the lock-in effect. On the x-axis the excitation frequency (f_{exc}) is displayed and on the y-axis the ratio between the natural frequency and the excitation frequency (f_{exc}/f_n). The figure shows that when the ratio approaches 1.0 the excitation frequency shifts to the natural frequency.

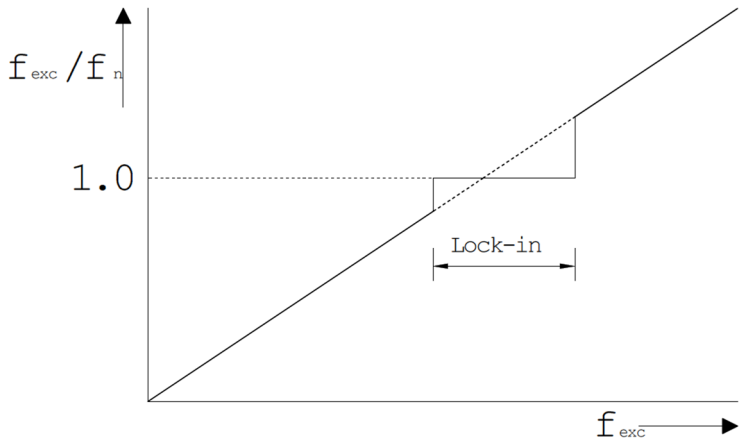

Figure 2-5: The lock-in effect on the excitation frequency with the natural frequency

2.2 Flow-Induced Vibrations of a Valve

This paragraph gives a theoretical background of the different vibrations. This will be done by elaborating the next subjects:

- Causes (§ 2.2.1). The vibrations can have multiple causes. This section shortly discusses the different relevant causes.
- Flow-induced vibrations (§ 2.2.2). This paragraph will describe in more detail the different types and definitions of flow-induced vibrations. The key vibrations of this study are identified and explained in more detail.

2.2.1 Causes

The initiation of vibrations of a valve can have different causes. The main causes of the vibrations are:

- Flow-induced;
- Wave-induced;
- Cavitation;
- Leakage.

This research will focus on the flow-induced vibrations and therefore the vibrations due to waves are neglected. The vibrations due to leakage and cavitation can be interpreted as flow-induced effects, but will be neglected in this research. For an explanation of these effects a reference is made to Appendix C. The next paragraph will focus only on the flow-induced vibrations.

2.2.2 Flow-Induced Vibrations

Flow-induced vibrations are defined as the vibration and noise phenomena due to the flow of water or gas [32]. Because water will flow underneath the valve during opening, the valve is vulnerable to the effects of flow-induced vibrations. These vibrations can have two main directions. The directions are:

- In-flow. The vibrations are in the same direction as the flow of water. In the case of a vertical lift valve in a culvert, the in-flow vibrations are in a horizontal direction;
- Cross-flow. The vibrations are perpendicular to the direction of the flow. As earlier discussed in Chapter 1 the problem will be considered from a two-dimensional point of view. The relevant cross-flow vibrations that remain are the vertical vibrations. Figure 2-6 shows the direction of the cross-flow vibrations of the valve. In the remainder of this study the focus is set on the vertical cross-flow vibrations.

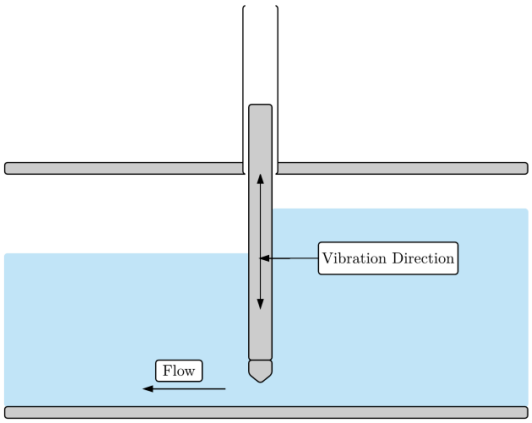

Figure 2-6: The direction of the cross-flow vibrations in a two-dimensional problem

Definitions

Some important definitions have to be made clear to get a better understanding of the flow-induced vibrations. The most important definitions in flow-induced vibrations phenomena are [41]:

- Body oscillators. A body oscillator exists in two different forms. One form is a rigid structure or rigid element that is able to perform angular or linear movements. The other form is a structure or structural part that has elastic properties and can perform flexural movement.
- Fluid oscillators. In contrast to a body oscillator, a fluid oscillator exists of mass that can oscillate due to gravity or fluid compressibility. When an excitation frequency of the fluid oscillator coincides with the natural frequency of a body oscillator it could amplify the vibration of the body oscillator.

The sources for excitation of the fluid or body oscillator can be a great many. These sources of excitation are divided into three main categories [41]. These three categories are listed below.

- Extraneously Induced Excitation (EIE). This type of excitation arises from fluctuations in flow velocity or fluctuations in pressure that are independent of the structure. Examples of EIE sources are waves, external created turbulence and earthquakes.
- Instability-Induced Excitation (IIE). In the case of IIE the source of the excitation is the flow instability. By definition the flow instability is inherent to the flow created by the shape of the structure. Examples of IIE sources are vortex shedding behind the structure and impinging of a free shear layer.
- Movement-Induced Excitation (MIE). This type of excitation depends on the fluctuating forces that arise from the movement of the vibrating oscillator. These kind of excitations are self-excited.

Types

There are 5 main types of flow-induced vibrations regarding hydraulic structures [33]. Figure 2-7 gives an overview of the different types of vibrations. The figure makes a distinction between a rod or beam (top row) and a gate or valve (bottom row). The 5 main types of excitation are:

- Excitation due to turbulence (Figure 2-7, no. 1);
- Excitation due to flow instability (Figure 2-7, no. 2)
- Self-excitation (Figure 2-7, no. 3);
- Increase of excitation by liquid resonance (Figure 2-7, no. 4);
- Excitation due to liquid oscillations in a basin (Figure 2-7, no. 5).

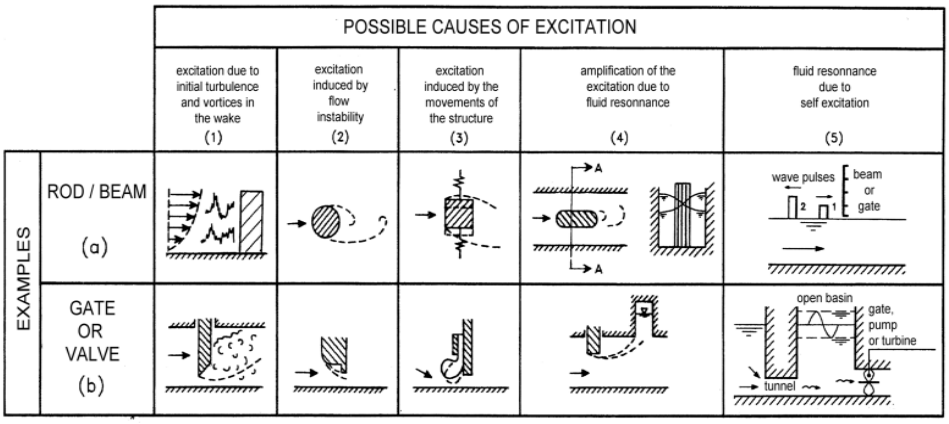

Figure 2-7: Different types of vibrations of hydraulic structures [33]

A more detailed description of all the types of vibrations is given in Appendix C. In this paragraph only the excitation due to flow instability and due to turbulence induced by the shape of the valve are elaborated in more detail. These excitations both can be classified under the instability-induced excitations (IIE).

Excitation due to flow instability

One kind of vibration is the excitation due to instability of the water flow. The causes for this kind of vibration are:

- an instable separation point (Figure 2-8);
- a reattachment point;
  - an instable reattachment point (Figure 2-9 (L));
  - a shear layer deflection of entrapped fluid (Figure 2-9 (R));

Instable separation point

Figure 2-8 shows an example of an instable separation point. An instable separation point occurs when the position of the separation point fluctuates in time. The figure shows that the pressure on both sides of the valve is different due to the head difference and a change in position of the separation point can lead to fluctuations in the vertical hydrodynamic drag and lift force. This force will eventually initiate the vertical vibrations. When the structure has a predefined sharp separation point, this phenomenon will most likely not occur. The guidelines regarding the shape and material of the lower edge to create a predefined separation point are in contrast with the requirements regarding the watertight lower seals that should prevent leakage. Any initial vibrations can amplify the phenomenon by an increase in fluctuations of the separation point.

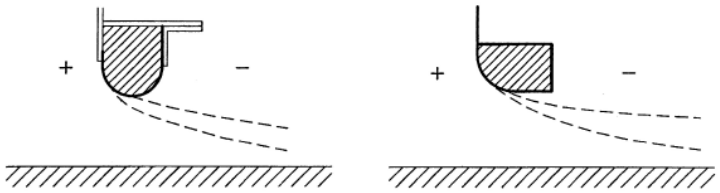

Figure 2-8: Instable separation point [19]

Reattachment Point

In contrast to the earlier discussed instable separation point, a reattachment point does not immediately lead to vibration phenomena. The presence of a reattachment point can still lead to a stable situation. A stable situation is shown in Figure 2-9 (no. 1). The position of the reattachment point does not move and is stable. Figure 2-9 (no. 2, no. 4) shows two situations with a reattachment point that could lead to vibrations. The first situation shows the presence of an instable reattachment point (no. 2). The instable reattachment point is comparable with the instable separation point. The second situation (no. 4) shows deflection in the entrapped fluid. This event leads to pressure fluctuations underneath the valve which will influence the drag and lift force. Literature suggests that shapes with an angle of at least 60° downstream of the valve can prevent a reattachment point [35].

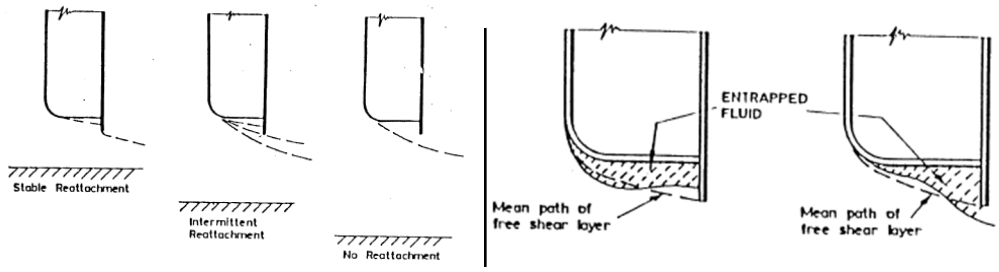

Figure 2-9: (L) Reattachment point options [35] & (R) Possible shear layer deflection of entrapped fluid [35]

Excitation due to turbulence

The excitation due to turbulence discussed in this research is the turbulence caused by the shape of the valve. Therefore, the excitation can be classified as an IIE. It should be noted that initial turbulence is not taken into account with this vibration. Figure 2-10 shows turbulence in the wake of the valve. The irregularities in the emergence of the turbulence can initiate a vibration in the vertical direction (cross-flow) as well in the horizontal direction (in-flow).

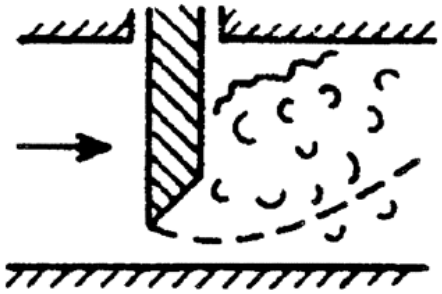

Figure 2-10: Excitation due to turbulence in the wake [19]

An important number regarding vibration phenomena related to the turbulence is the Strouhal number. The number is often used in the design phase of the project to determine the excitation frequency. The number is defined as a dimensionless parameter that gives a relation between the excitation frequency and the flow velocity of the water [33] (equation 2.10).

$$S = \frac{f_{exc} \cdot L}{U} \qquad 2.10$$

In which:

S	=	Strouhal number [-]
f_{exc}	=	excitation frequency [Hz]
L	=	a representative length of the flow geometry [m]
U	=	flow velocity [m/s]

The Strouhal number will return in the dimensional analysis of Chapter 3. The current design rules regarding the vibrations for horizontal as well as vertical vibrations of a valve are based on the Strouhal number and is given in equation 2.11 [33].

$$\frac{f_n \cdot L}{U} > (2 \text{ to } 3) \cdot S \qquad 2.11$$

This condition shows that the natural frequency of the system should be at least two or three times as large as the excitation frequency. The determination of the excitation frequency is done using results from researches from the past. These researches are based on basic shaped valves (rectangular valve) and often have an unclear definition of the characteristic length (L). For example, Vrijer [59] and Uwland [56] used the gate opening in contrast to Erdbrink [20] that used the gate thickness.

2.3 Conclusion

When the valve is assumed to be a rigid body (no flexural movement is possible) with a single degree of freedom (vertical direction) a basic form of the equation of motion can be applied. When the system is located in flowing water the basic equation must be rewritten with additional hydrodynamic terms. Because of these terms the structural analysis can stay similar to the one of a system in free air.

A crucial theoretical condition is when the natural frequency of the system is (almost) similar to the excitation frequency of the flowing water. Such a situation could lead to resonance, a phenomenon in which the amplitude of the vibration can become infinitely large. In almost all cases this leads to failure of the valve system. When both frequencies are close to each other there is a risk that both frequencies synchronize and a lock-in effect occurs. The lock-in effect has not yet been encountered with solely under flown valves.

The research focusses on the response frequency and the excitation frequency. When the force is pure harmonic the properties of the system (k and m) are no longer relevant. Because the force is related to turbulence it will not be pure harmonic and the dynamic properties of the system will have an influence on the response.

The main focus of this research is the flow-induced vibrations. The flow-induced cross-flow vibrations of a valve are considered in the vertical direction. Therefore, the problem is assumed to be two-dimensional. Because the focus will be on the flow-induced vibrations the effects related to cavitation, leakage and wave phenomena will be neglected in the further course of the research. All these effects could cause vibrations, however, they are independent of the flow-induced vibrations.

The valve is a body oscillator which is able to perform linear movement. Different sources can initiate the linear vibrations. The most uncertain source is the flow instability which leads to instability induced vibrations. It is uncertain what the forces and frequencies are that arise during these vibrations. Because it is impossible to uncouple this type from the vibrations due to turbulence of the water flow, both types of vibrations will be taken into account. During the physical model tests an attempt is made to make a distinction between the effects of the different types of flow-induced vibrations.

For both vibrations some guidelines regarding the instability induced vibrations are available, these guide lines are mainly focussed on the shape and the dimensions of the valve. For the vibrations due to turbulence a statement is made that the natural frequency (f_n) should be three times larger than the excitation frequency (f_{exc}). With this statement the dynamic amplification factor is kept under 1.1 and resonance of the system can be prevented. The uncertainty lies in the determination of the excitation frequency, which is not easily known.

From the previous executed researches, results and conclusions vary and contradict. This leads to uncertainties in the design process. An example is the lack of clarity in the definition of the characteristic length (L) in the Strouhal number and the reduced velocity.

Chapter 3 Test Conditions and Settings

This chapter describes the test conditions and settings of the physical model test. This information is divided into two main subsections. Figure 3-1 shows the structure of the chapter. The subsections are:

- The methodology (§ 3.1). This section exists of a short description of the dimensional analysis and the process steps. More details regarding the methodology can be found in Appendix D and Appendix E.
- The model set-up (§ 3.2). The section of the model set-up exists of a short elaboration of the used model set-up with the related choices. More information and calculations regarding the model set-up can be found in Appendix F and Appendix G.

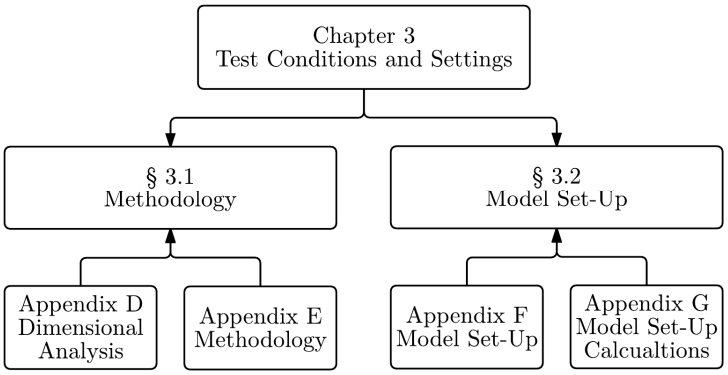

Figure 3-1: The structure of chapter 3

3.1 Methodology

The methodology used during the physical tests will be explained on the basis of:

- Dimensional analysis (§ 3.1.1). This paragraph explains the dimensional analysis. The dimensional analysis presents all the dimensionless numbers that are involved in the problem. Appendix D gives a more detailed elaboration of the dimensional analysis and the execution of the Buckingham-Π theorem.
- Test conditions (§ 3.1.2). This paragraph elaborates the steps taken during the testing process and the parameters that have been varied.

3.1.1 Dimensional Analysis

This paragraph will describe the variables that have an effect on the vibration phenomena. A distinction is made between input variables and output variables. The input variables will be determined before the test and will be varied during the tests. The output variables are measured during the tests and lead to possible results. All the variables involved are shown in Figure 3-2. The problem is considered to be two dimensional. This means that the variables are assumed to be constant over the width of the model.

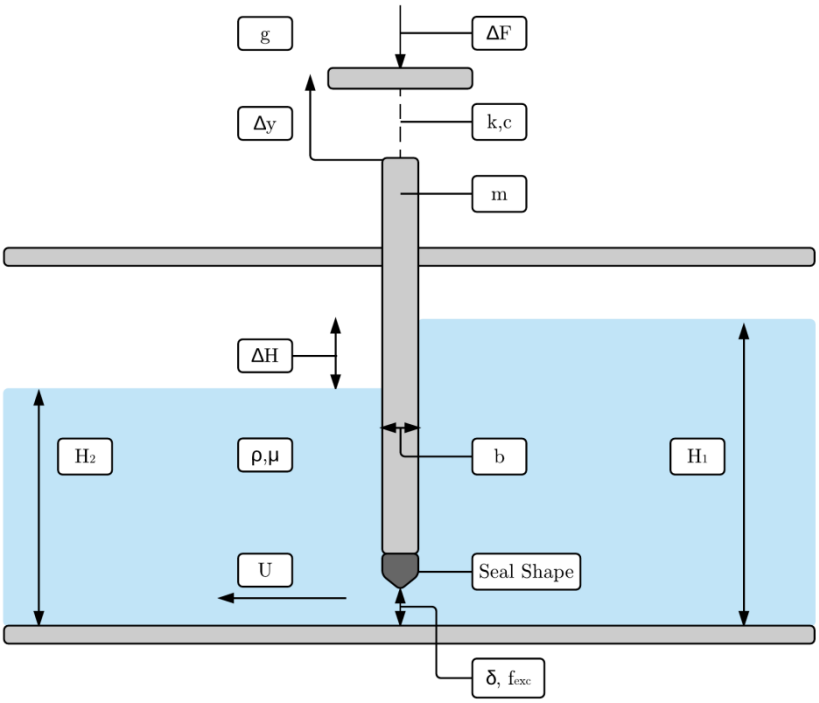

Figure 3-2: Overview of variables in the system

The first step in the design of a proper physical model is the execution of a dimensional analysis. This analysis will lead to a dimensionless space in which all the dimensionless numbers that are connected to the topic have a place. At first all variables involved in the problem are defined and afterwards the Buckingham Π-theorem is used to execute a dimensional analysis. The outcome parameters could be used as input, output or scale parameters. All the relevant variables are given in Table 3-1 and can also be found in Figure 3-2. The downstream water level (H_2) has been let out of the table because it can be based on the upstream water level (H_1) and the head difference (ΔH). A total number of 15 variables could play a role in the problem. The seal shape is regarded an external variable and will be left out of the dimensional analysis. The shape is already assumed to be dimensionless. Appendix D gives a more detailed elaboration of the executed Buckingham Π-analysis.

Variables	**Symbol**	**Variables**	**Symbol**
Stiffness	k	Water Density	ρ
Mass	m	Excitation Frequency	f_{exc}
Damping	c	Flow Velocity	U
Vertical Displacement	Δy	Dynamic Viscosity	μ
Upstream Water Level	H_1	Gravitational Acceleration	g
Head Difference	ΔH	Vertical Force Amplitude	ΔF
Gate Thickness	b	Seal Shape	-
Gate Opening	δ		

Table 3-1: Overview of the variables that play a significant role within the problem

Table 3-2 shows the dimensionless parameters retrieved from the Buckingham Π-theorem and their role in the model (input/output or scale parameter). The seal shape has been added again. For the scale parameters the conditions are shown. A distinction is made between two different testing situations. These situations are:

- An extreme stiff situation ($k \rightarrow \infty$). In which the dynamic characteristics (m, k and c) and the displacement (Δy) of the model are irrelevant.
- A low stiffness model ($k \neq \infty$). In this case the dynamic characteristics and the displacement are relevant for the results of the tests.

The table also shows the role of the parameter in relation to the above explained situations. The table below shows clearly that the 15 variables from Table 3-1 can be rewritten to 12 dimensionless parameters. The Froude number (Π_6) is not relevant in both cases. Because a situation of a closed culvert has to be simulated.

The scale factors of the model have to be checked. Because there is no specific prototype the Cauchy number (Π_2), the damping factor (Π_5) and the density ratio (Π_8) cannot be checked. These numbers could be used to scale the results to a future design. In § 4.6 this is attempted. For the remaining scale parameters (Reynolds number Π_3 and length factor Π_{10}) it has been assumed, that they do not affect the vibration phenomena. This will be checked in a later stage of the report (§ 4.2).

#	Name	Formula	Type	Conditions	Extremely Stiff Model	Low Stiffness Model
Π_1	Dimensionless Force Amplitude	$\frac{\Delta F}{\rho \cdot U^2 \cdot b^2}$	Output		Present	Present
Π_2	Cauchy Number	$\frac{k}{U^2 \cdot \rho \cdot b}$	Scale	Equal to prototype	To Infinity	Present
Π_3	Reynolds Number	$\frac{U \cdot \rho \cdot b}{\mu}$	Scale	$> 10^5$	Present	Present
Π_4	Strouhal Number	$\frac{f_{exc} \cdot b}{U}$	Output		Present	Present
Π_5	Damping Factor	$\frac{c}{2 \cdot \sqrt{k \cdot m}}$	Scale	Equal to prototype	irrelevant	Present
Π_6	Froude Number	$\frac{\Delta H \cdot g}{U^2}$	Input	Freely to chose	Irrelevant	Irrelevant
Π_7	Frequency Ratio	$\frac{f_{exc}}{f_n}$	Input		irrelevant	Present
Π_8	Density Ratio	$\frac{m}{b^3 \cdot \rho}$	Scale	Equal to prototype	irrelevant	Present
Π_9	Displacement Ratio	$\frac{\Delta y}{b}$	Output		irrelevant	Present
Π_{10}	Length Factor	$\frac{H_1}{\delta}$	Scale	> 2	Present	Present
Π_{11}	Relative Gate Opening	$\frac{\delta}{b}$	Input		Present	Present
Π_{12}	Seal Shape	[-]	Input		Present	Present

Table 3-2: Overview of retrieved Π-terms from the Buckingham-Π theorem and their characteristics

3.1.2 Test Steps

The execution of the tests exists of three main steps. These steps will be explained shortly in this paragraph. A more detailed explanation can be found in Appendix E.

Free-Decay Tests

The first tests executed are free-decay tests. A free-decay test means that the system is given an abrupt external force (in this particular case a small manual tap) after which the model can move freely. From the results the natural frequencies and the damping can be determined. The free-decay tests have been executed under water and above water.

Steady State Measurements

The main test is divided into four individual cases. Every single case has a separate shape as shown in Figure 3-3 and the used names can be found in Table 3-3 (L). The choice for the seal has been based on the objective to test real-life seals. The seals with no. 2 (chamfered-shaped) and no. 3 (point-shaped) are used in practice. The other two seals are based on shapes tested in research from the past. Every seal shape is tested with similar varying parameters. The variable parameters are:

- The spring stiffness (k). By varying the stiffness, the natural frequency of the model can be modified. The different magnitude of spring stiffness are shown in Table 3-3 (R). The calculation of the required spring stiffness can be found in Appendix G. The stiffness has not been related to the real-life stiffness of a hydraulic cylinder but is based on critical areas of vibrations. In Table 3-2 the scaling factor is given that could be used to scale these different degrees of stiffness to a larger and stiffer prototype.
- The flow velocity (U). The flow velocity has been varied between 0.3 m/s (ΔH = 5 mm) and 1.9 m/s (ΔH = 192 mm).
- The gate opening (δ). The opening underneath the valve has been varied between 5 mm and 52 mm.

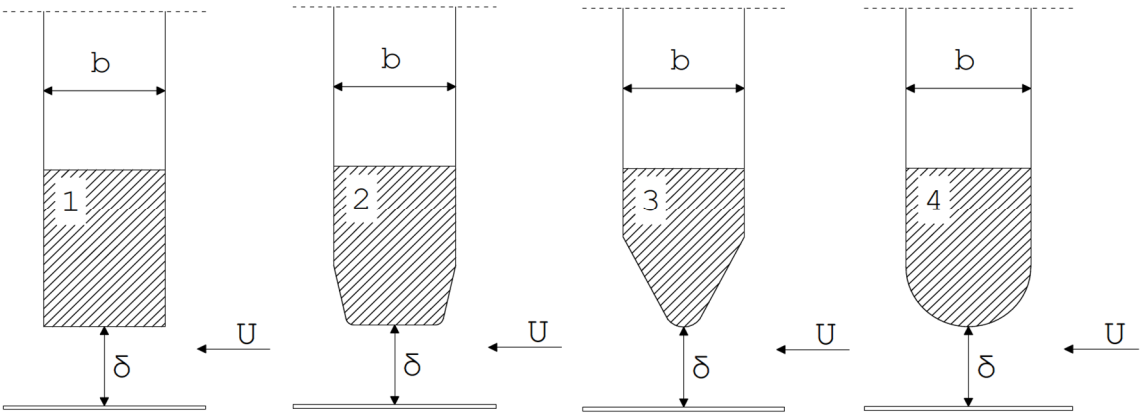

Figure 3-3: The 4 individual test cases during the physical model tests

Seal Shapes	Spring Stiffness [N/mm]
Rectangular-Shaped (1)	1.16
Chamfered-Shaped (2)	5.34
Point-Shaped (3)	5.66
Circular-Shaped (4)	43.2

Table 3-3: (L) Seal shapes used during physical model tests & (R) Spring stiffness used during physical model tests

The tests have been executed under steady state conditions and will therefore be named steady state measurements in the further course of this report. Table 3-4 shows an overview of the expected response of the different shapes to the different types of vibrations. The types of vibrations have been explained in Chapter 2. The full elaboration of these expectations can be found in Appendix E. The expectations are based on theoretical knowledge from the literature study. The numbers between brackets indicate the vulnerability for the different vibration (with 1 is more vulnerable than 2).

#	Seal shape	Turbulence	Instable separation point	Flow reattachment
1	Rectangular-Shaped	Present	Not present	Present (2) only at $\delta < b$
2	Chamfered-Shaped	Present	Not present	Present (1) only at $\delta < b$
3	Point-Shaped	Present	Present (1)	Not present
4	Circular-Shaped	Present	Present (2)	Not present

Table 3-4: Overview of the presence of the different vibration causes related to the seal shape

Contraction Tests

Individual tests have been executed to determine the contraction differences per seal shape. During these tests the flow of the water has been monitored by using dye in the water. From the taken images the contraction coefficient and the related energy losses have been determined.

3.2 Model Set-Up

A more detailed description of the model set-up and the used elements is given in Appendix F. The calculations related to the model set-up can be found in Appendix G. An overview of the set-up is shown in Figure 3-4. The description is divided into 5 main components. These components are:

- The current flume (§ 3.2.1);
- External frame (§ 3.2.2);
- Internal frame (§ 3.2.3);
- Measuring equipment (§ 3.2.4);
- Mass of movable part of the model (§ 3.2.5).

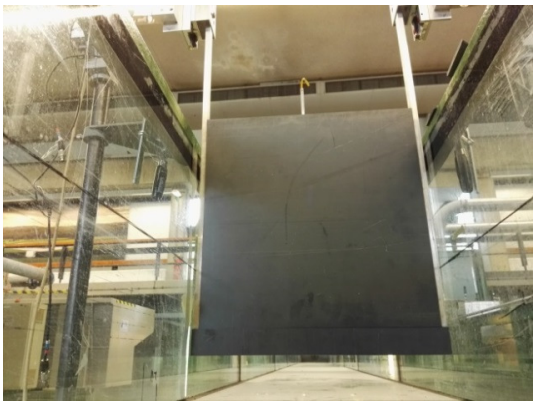

Figure 3-4: (L) Picture of the complete model set-up & (R) Picture of the model from inside the flume

3.2.1 Flume

For the execution of the research a current flume at the University of Technology in Delft, in the Stevin Laboratory, is used. The main characteristics of the used current flume are:

- an effective length of 14.3 metres;
- a width of 0.4 metres;
- a maximum depth of 0.4 metres.

The current flume has a Rehbock weir that measures the return flow of the water. This weir will be used to determine the discharge in a later stage.

3.2.2 External Frame

The external frame connects the movable part of the model set-up with static parts of the model. The current flume can be seen as the main static part of the model set-up. The external frame is shown in Figure 3-4. It is important to make the frame as stiff as possible to minimise noise in the data measurements.

3.2.3 Internal Frame

The internal frame is the movable part of the model set-up. This simulates the valve. The internal frame exists of a number of important elements.

- valve plate;
- lower edges;
- vertical suspension.

The valve plate of the model is made out of PVC (Polyvinylchloride) and has the following dimensions: 400 mm x 400 mm x 30 mm. The plate is shown in Figure 3-4 (L). The figure also shows the different lower edges that can be bolted to the valve plate. The lower edges are also made of PVC.

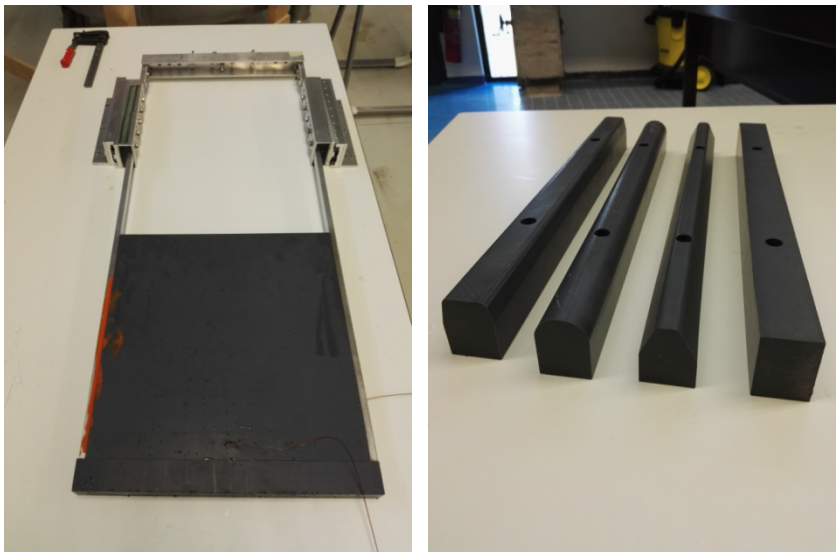

Figure 3-5: (L) Picture of internal frame including sliders, valve plate and lower edge & (R) Picture of used lower edges

The vertical suspension of the system connects the movable part (internal frame) with the static part (external frame). The vertical suspension exists of two elements:

- Springs. The springs are positioned at the top and supply the needed stiffness to the model. They are shown in Figure 3-6. Table 3-5 shows the characteristics of the used springs, from every spring two springs are used simultaneously. The determination of the required spring stiffness can be found in Appendix G.

- Sliders. The sliders will bear the major part of the horizontal force and make sure that the valve is only able to move in the vertical direction. The picture of Figure 3-5 (L) show the sliders that are connected to the internal frame.

Spring Constant [N/mm]	Thickness of wire [mm]	Length of the spring [mm]	Maximum Force [N]
21.65	3.4	104.7	570.0
7.83	4.3	144.8	625.0
2.67	2.5	123.0	237.0
0.58	2.2	122.0	127.0

Table 3-5: The characteristics of used springs

After a first round of tests a horizontal wire had to be attached to the valve plate and a fixed point far away from the model, to minimize the horizontal deflection of the valve plate. The large distance was chosen to minimize the additional vertical force of this wire. More information of the wire can be found in Appendix F.

3.2.4 Measuring Equipment

An important aspect of the model set-up is the choice for the measuring equipment. A detailed elaboration including characteristics can be found in Appendix F. The measured parameters and the related measuring devices are listed below.

- The downstream and upstream water level (H_1 and H_2). The water levels were measured by hand with a standard needle.
- The pressure underneath the valve (p). The pressure is measured with a pressure sensor that is made watertight. The device is integrated in the centre of the lower edge. This point is the lowest point of the valve for all different shapes. This location has been chosen so the exact pressure fluctuations underneath the valve can be measured. A sketch of the integrated pressure sensor is shown in Figure 3-6 (R).
- The vertical displacement (Δy). The vertical displacement is measured by a laser sensor. The laser can be seen in Figure 3-6 (L).
- The vertical force amplitude (ΔF). The force is measured by a load cell that connects the movable part of the model with the external frame. The load cell is shown in Figure 3-6 (L).

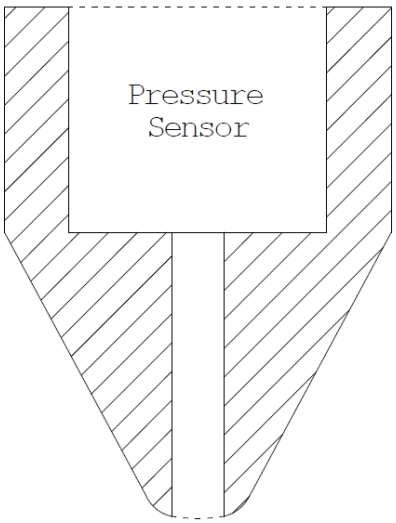

Figure 3-6: (L) Picture of the vertical suspension of the model & (R) Position of integrated pressure sensor

3.2.5 Mass of Model Parts

The first step of the physical model tests was to identify the mass of all the movable parts. The masses are given in Table 3-6. The weight of these elements have a major impact on the natural frequency of the system and therefore also on the response.

Element	Mass of the element [g]
Frame including movable part of sliders	2 450
Connecting piece	171
Plate	5 803
Rectangular lower edge	683
Circular lower edge	613
Point lower edge	553
Chamfered lower edge	657

Table 3-6: Mass of movable parts

It can be concluded that the lower edges have approximately the same mass. Therefore, the natural frequency will not vary much with the different edges. The maximum mass of the movable part is 8936 g. With some additional mass due to the integrated pressure sensor and some screws the total mass of the movable part sums up to 9.0 kg.

Chapter 4 Results and Discussion

This chapter will discuss the results from the physical model test. The results will be elaborated according to the steps of the research. The steps have been elaborated in the previous chapter. The structure of this chapter is shown in Figure 4-1. The following subjects have been treated:

- The natural frequencies of the system (§ 4.1). The natural frequencies of the model have been determined from the results of the free-decay tests. In this paragraph these results will be compared with the theoretical frequencies. A distinction is made between frequencies above water and frequencies under water.
- Model checks (§ 4.2). In the course of the report, some assumptions regarding the model set-up and the conditions of the tests were made. In this paragraph will be checked if these assumptions are valid. The main checks focus on the Reynolds influence, the structural damping of the model and the water level influence.
- Main test (§ 4.3). This paragraph will elaborate on the results of the main part of the physical test. The main part of the test exists of the steady state measurements.
- Energy dissipation (§ 4.4). This section discusses certain aspects of the energy dissipation of the system. Among the discussed subjects are the contraction, the leakage and the dynamic amplification factor.
- Vertical forces (§ 4.5). The paragraph related to the vertical forces arises from the determination of the dynamic amplification factor. The paragraph will focus on any other external forces on the valve in the model.
- Scaling to real prototype (§ 4.6). The final part of this chapter compares the model set-up with real-life designs. The effects of scaling will be described and several scaling factors will be given.

Appendix H gives a detailed elaboration of the spectral analysis that has been used to determine the dominant frequencies and amplitudes from the test data. In Appendix I an overview is given of the executed tests with the test conditions. Appendix J gives some power spectra with a short explanation.

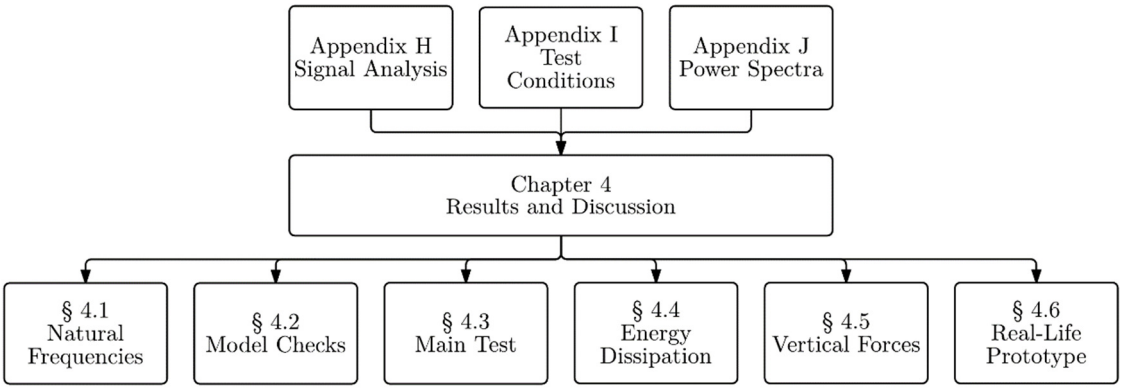

Figure 4-1: The structure of chapter 4

4.1 Natural Frequencies

The first step is the determination of the natural frequencies for the model set-up with different values of stiffness. Two forms of the natural frequency are important for the results in the further course of the report. The forms are:

- The natural frequency in air (§ 4.1.1);
- The natural frequency under water (§ 4.1.2).

4.1.1 Natural Frequency in Air

The natural frequency in air has been determined by a free-decay test under dry conditions. The result from such a test is shown in Figure 4-2. The free-decay tests can also be used to determine the damping of the model. This will be elaborated in the next paragraph. The natural frequency in free air will be addressed as dry natural frequency ($f_{n,dry}$) in the further course of the report.

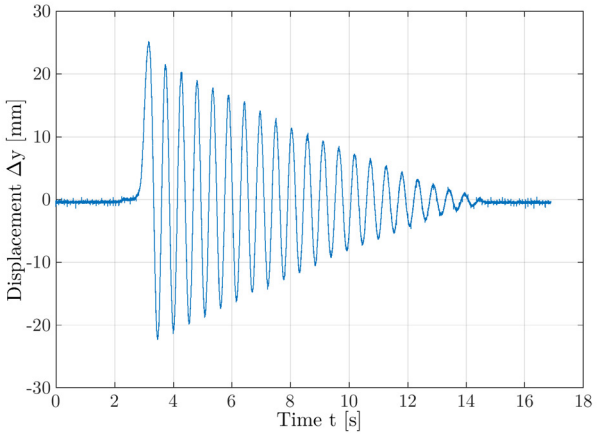

Figure 4-2: Result from a free-decay test above water

Table 4-2 shows an overview of the determined dry natural frequencies for the tests with a rectangular-shaped lower edge. The other shapes have similar frequencies because of a similar mass (the mass difference is a maximum of 90 grams and will therefore be neglected) and similar values of vertical stiffness. The first columns of the table show the theoretical spring stiffness and the theoretical natural frequencies based on the mass (9.0 kg). The final column shows the dry natural frequencies retrieved from the free-decay test data.

Spring stiffness [N/mm]	**Calculated $f_{n,dry}$ [Hz]**	**Measured $f_{n,dry}$ [Hz]**
1.16	1.80	1.77
5.34	3.86	3.79
15.66	6.60	6.54
43.20	10.97	10.88

Table 4-1: Measured and calculated dry natural frequencies of the model set-up with different values of the stiffness

The dry natural frequencies determined from the test data are slightly lower than the frequencies calculated from the relevant characteristics of the dynamic system (m and k). This deviation can be explained by a small error in the calculation of the power spectrum (Appendix H) or a deviation in the spring constant of the ordered springs. The deviations never exceed 2% of the total calculated dry natural frequency.

4.1.2 Natural Frequency under Water

The natural frequency under water differs from the frequency in free air due to the added water effects, as described in § 2.1 and Appendix B. The natural frequency under water is defined as the wet natural frequency ($f_{n,wet}$). The wet natural frequency has also been determined with free-decay tests. In this step the water level (H_1 and H_2, they are equal during the free-decay tests) and de gate opening (δ) are varied to see the effect of these parameters on the wet natural frequency. The tests have been executed with a flow approaching zero, to minimize the effect of the flowing water. A complete lack of flow was impossible in the used current flume. Figure 4-3 (R) shows a result of the free-decay test under water. Again, a rectangular lower edge is used in the model set-up. Table 4-2 shows the results from a test with a vertical spring stiffness of 1.16 N/mm and with a vertical spring stiffness of 5.34 N/mm. The tables show a variation in the frequencies related to the gate opening and to the water level.

$f_{n,dry}$ = **1.77 Hz**			
Water level [mm]	**100**	**200**	**300**
Gate opening [mm]			
45	1.9 Hz	1.8 Hz	2.0 Hz
30	2.0 Hz	1.9 Hz	1.9 Hz
15	2.0 Hz	1.9 Hz	1.9 Hz

$f_{n,dry}$ = **3.79 Hz**			
Water level [mm]	**100**	**200**	**300**
Gate opening [mm]			
45	4.0 Hz	4.1 Hz	4.1 Hz
30	3.9 Hz	4.3 Hz	4.3 Hz
15	3.8 Hz	4.3 Hz	4.5 Hz

Table 4-2: (L) Measured wet natural frequencies for k = 1.16 N/mm & (R) Measured wet natural frequencies for k = 5.34 N/mm

The magnitude of the added mass and added stiffness is calculated to get a better insight into the differences between the wet natural frequency and the dry natural frequency. The added stiffness is estimated using Hooke's law (equation 4.1). Equation 4.2 [20] gives a ratio between the dry natural frequency and the wet natural frequency. This ratio can be used to determine the relevant added water mass, because the added water mass is the only unknown variable in the ratio.

$$F_{upward} = \rho_w \cdot g \cdot V = \rho_w \cdot g \cdot (W \cdot b \cdot u) = k_w \cdot u \rightarrow k_w = \rho_w \cdot W \cdot b \cdot g \tag{4.1}$$

$$\frac{f_{n,wet}}{f_{n,dry}} = \left(1+\frac{k_w}{k}\right)^{1/2} \cdot \left(1+\frac{m_w}{m}\right)^{-1/2} \tag{4.2}$$

Equation 4.1 shows that the added stiffness depends on the intersection surface of the valve with the water. Therefore, the added water stiffness is constant for the model. The added water stiffness is calculated to be 0.12 N/mm. Literature suggests that the added water mass of the valve increases when the water level increases and when the opening underneath the valve decreases [33]. This is not seen in the results from the tables above. The tables show an increasing frequency instead of a decreasing frequency, that is expected with an increase of mass. This could have several explanations:

- a deviation in the calculation of the frequency by means of a spectral analysis.
- the presence of damping. Due to damping the amplitude of the vibrations decreases and the period of the vibrations increases. The increase of the period could affect the determination of the natural frequency. The damping of the system will be elaborated in the next paragraph.
- The lack of completely stationary water. The slightly flowing water provides the system with an additional stiffness (equation 4.3 [33]). This additional stiffness could explain the increase in natural frequency.

$$k_{w\text{-}flow} = \frac{\partial F_y}{\partial y} = \frac{\partial}{\partial y}\left(C_{fy} \cdot \frac{1}{2} \cdot \rho \cdot U^2 \cdot L^2\right) = \frac{1}{2} \cdot \rho \cdot U^2 \cdot L^2 \cdot \frac{\partial C_{fy}}{\partial y} \tag{4.3}$$

4.2 Model Checks

During the design of the model set-up some assumptions were made to come to a satisfying design. These assumptions can be found in Chapter 1 and § 3.1 (following from the dimensional analysis). The main assumptions being checked in this paragraph are listed below.

- The structural damping is assumed to be minimal (§ 4.2.1). In the first section the damping of the model is checked. This is done for tests with varying conditions. In addition to this an explanation will be given of the influence of the present damping in the model on the problem.
- The Strouhal number is independent of the Reynolds number (§ 4.2.2). During the individual tests the value for the Reynolds number varied significantly. It was assumed that this variation did not influence the Strouhal number. This paragraph checks this assumption.
- The water levels on both sides of the valve (H_1 and H_2) do not influence the vibrations (§ 4.2.3). This assumption follows from the starting point that the valve in reality is located in a closed culvert. The assumption that has to be checked is that the flow pattern is independent of the downstream (H_2) and upstream (H_1) water level. This assumption came from the length ratio (Π_{10}) of Chapter 3.

4.2.1 Damping

From the free-decay tests above water and under water the order of magnitude of the damping is estimated. The structural damping of the model has been kept as small as possible to prevent interference of the damping with the results. A complete absence of damping is impossible. The damping of the system varies for a situation under water and a situation above water. Figure 4-3 shows the damping of the system in the form of a decrease of the amplitude in time.

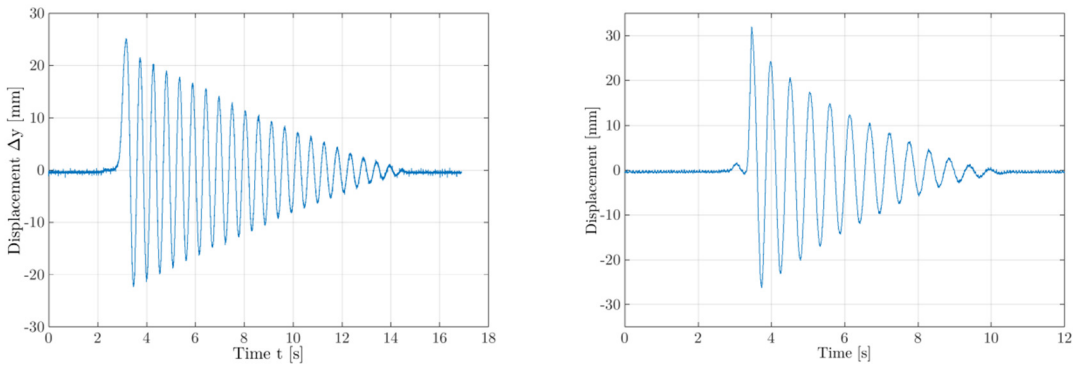

Figure 4-3: (L) Result from a free-decay test above water & (R) Result from a free-decay test under water

The damping factor (ζ) is determined with the logarithmic decrement theory. This theory is based on the assumption that the amplitude in time decreases exponential. Equation 4.4 shows the formula used to determine the damping factor [13].

$$\zeta = \frac{1}{\sqrt{1 + \left(\frac{2 \cdot \pi}{\ln(y_0/y_1)}\right)^2}} \qquad 4.4$$

The calculated damping factors are:

- $\zeta = 0.026$, for a situation under water.
- $\zeta = 0.015$, for a situation above water.

Equation 4.5 shows the envelope of the time varying system that is approached by an exponential function. Figure 4-4 shows the earlier found vibrations with the calculated envelope based on the logarithmic decrement damping factor.

$$Y(t) = Y_0 e^{-\zeta \cdot \omega_n \cdot (t-t_0)} \quad 4.5$$

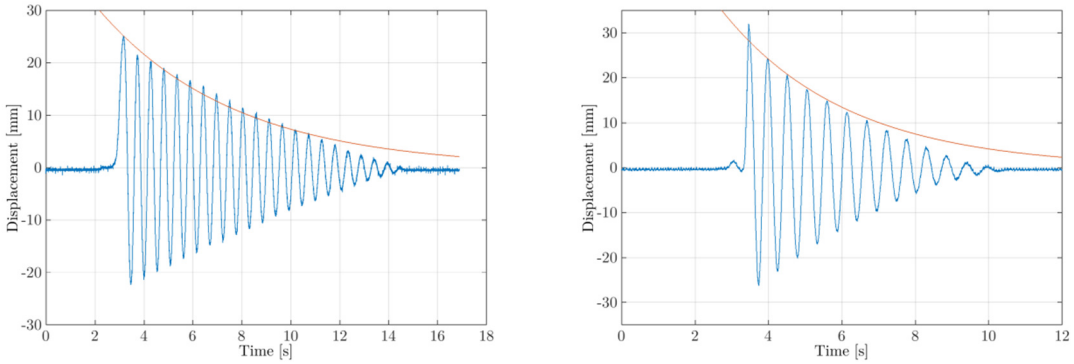

Figure 4-4: (L) Free vibration above water with structural damping approximation & (R) Free vibration under water with structural damping approximation

The determined lines seem to be in line with the assumption that the damping is linear. Only at the start and the end of the vibrations the line no longer follows the decay of the amplitude. The start deviation could be explained by a sudden increase in damping due to the sudden tap to the system. At the end of the vibration the decrease in amplitude shows a more linear behaviour. This behaviour can be explained by the damping due to the friction of the sliders. Both above shown measurements were executed with a relatively low vertical stiffness of 1.16 N/mm. The values of the damping factor have enough margin from the critical damping ($\zeta = 1$) and do not give negative damping ($\zeta < 0$). The damping is minimal but could still influence the resonance frequency. The influence of the damping on the resonance frequency is shown in equation 4.6.

$$f_{resonance} = \frac{1}{2 \cdot \pi} \cdot \sqrt{\frac{k}{m} - \left(\frac{c}{2 \cdot m}\right)^2} = \frac{1}{2 \cdot \pi} \cdot \sqrt{\frac{k}{m} \cdot (1 - \zeta)^2} \quad 4.6$$

The resonance frequencies ($f_{resonance}$) of the model decrease with respectively 2.6% (under water) and 1.5% (above water). The same calculations have been done for a system with a stiffness of 5.34 N/mm. These calculations show similar values for the damping factor as the tests with a vertical stiffness of 1.16 N/mm. The free-decay tests were executed with stationary water which does not show the effect flowing water has on the damping.

After the free-decay tests with stationary water some free-decay tests with flowing water have been executed. Table 4-3 shows the influence of the flowing water and the gate opening underneath the valve on the damping factor as determined. It is shown that the flow velocity (U) and the gate opening (δ) influence the damping factor. In some situations, even a negative damping is observed which leads to an unstable situation. A situation with negative damping is shown in Figure 4-5. In this situation the gate opening was approximately 30 mm and the vibration was stopped manually at approximately 33 seconds.

Velocity U [m/s]	Damping factor ζ [-]	Gate opening δ [mm]
1.36	0.053	14
1.15	0.035	13
0.93	0.016	11
0.74	< 0	32
0.50	< 0	29
1.37	0.015	36
0.76	< 0	56
1.04	< 0	56
1.11	0.012	51

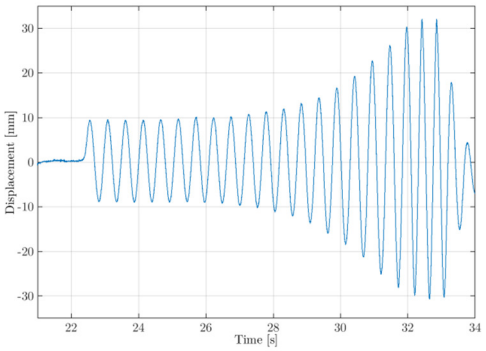

Table 4-3: Damping factor for situation with flowing water

Figure 4-5: Test results that show negative damping ($\zeta < 0$)

Figure 4-6 shows two identical situations except they have a different gate opening (δ). Observed is that the damping in both cases is different. The initial amplitude could have an effect on this damping. The amount of measurements is insufficient to provide a proper conclusion regarding this difference. The damping factors shown are 0.015 (L) and the 0.035 (R).

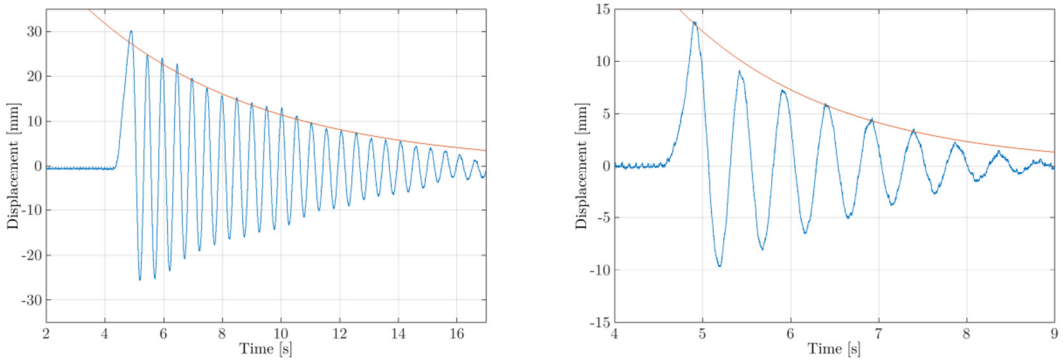

Figure 4-6: (L) Free-decay test result with relatively large gate opening & (R) Free-decay test result with relatively small gate opening

The damping of a vertical lift valve system in practice could not be retrieved and therefore comparison was impossible. From the above elaborated results, the exact physical damping of the system under water can be retrieved with the known stiffness (k) and the known mass (m). This is done using the definition of the dimensionless damping factor. The values retrieved are:

- c = 5.3 Ns/m for the situation under water.
- c = 3.1 Ns/m for a situation above water.

The values above will be used in § 4.6, where the characteristics of the model are compared to real-life designs. The damping could be an interesting design parameter, since its effect on the resonance frequencies and the amplitude of vibration. Future research regarding the damping could focus on the exact damping in the real-life valve system and the effect on damping on the existence of the vibrations.

It can be concluded that the damping in the model is minimal, this is in agreement with the assumption made at the beginning of the report. The damping under water is larger than the damping above water due to the added water damping. The flow velocity (U) and gate opening (δ) appear to have an effect on the amount of damping in the model. Because of a lack of data regarding this damping the exact effects of the flow velocity and the gate opening could not be quantified.

4.2.2 Reynolds Influence

Figure 4-7 shows the relation between the Reynolds number and the Strouhal number. The left figure shows the response frequencies and the right figure shows the excitation frequencies. The two dimensionless numbers have been defined in the previous chapter. At first instance this relation was assumed to be non-existent, meaning that both parameters would not influence each other. However, the figure shows that both parameters do effect each other. The relation shown in Figure 4-7 shows similarities with Figure 4-8 (L), which shows the results of similar tests for flow around a cylinder. These results are similar for flow with water and for flow with wind [14]. Even though the vibration phenomena are not completely similar, the Reynolds dependence has been experienced before. Figure 4-7 (R) shows a similar but less clear relationship.

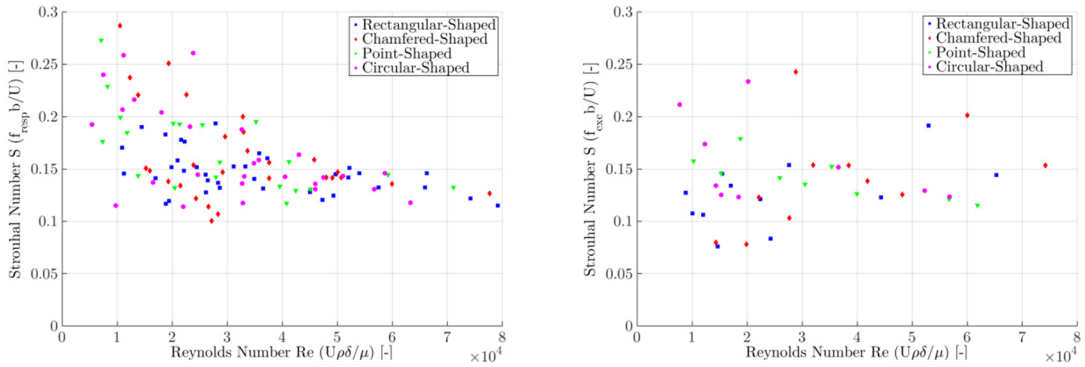

Figure 4-7: Relation between Strouhal number and Reynolds number retrieved from test data

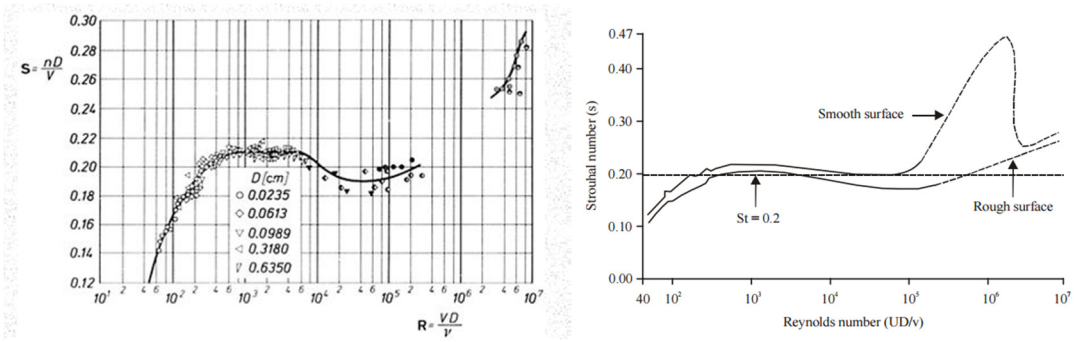

Figure 4-8: (L) Relation between Strouhal number and Reynolds number for flow around a cylinder [63] & (R) Influence of the smoothness of the surface on the Strouhal number and Reynolds number [63]

Another factor that could influence the relation between the Strouhal number and the Reynolds number is the smoothness of the surface. Figure 4-8 (R) shows the results from another research. In this case it also depends on smoothness of the surface. The valve used in the physical model was made out of PVC. A real-life valve is often made out of stainless steel with a rubber seal. This means that the effects could slightly differ. In the further course of the report in some cases the results will be limited to the tests with a Reynolds number larger than $3 \cdot 10^4$. With that limit the Strouhal number tends to be constant and the Reynolds influence can be neglected. Whenever this limit is applied, it will be mentioned.

It can be concluded that there is a clear relationship between the Strouhal number and the Reynolds number. The relation tends to become more constant when the Reynolds number is larger than $3 \cdot 10^4$. From Figure 4-7 (L) can also be concluded that the variation in the Strouhal number related to the Reynolds number is less for the rectangular-shaped lower edge. This means that the rectangular-shaped lower edge has a more predictable response. The Strouhal number of the rectangular-shaped edge varies only between 0.12 and 0.18, where the other shapes reach values of 0.28 and 0.10.

4.2.3 Water Level Influence

The influence of the water level on the vibration phenomena has to be checked. This check focusses on the earlier found ratio Π_{10} (equation 4.7).

$$\Pi_{10} = H_1/\delta \tag{4.7}$$

The check of the water level has been done by keeping the parameters that were varied earlier (k, δ and ΔH) equal while only changing the water levels (H_1 and H_2) on both sides of the valve. Figure 4-9 shows the power spectra of two of these tests. During the test no shooting water has been experienced. Shooting water was avoided to recreate a situation of a closed culvert.

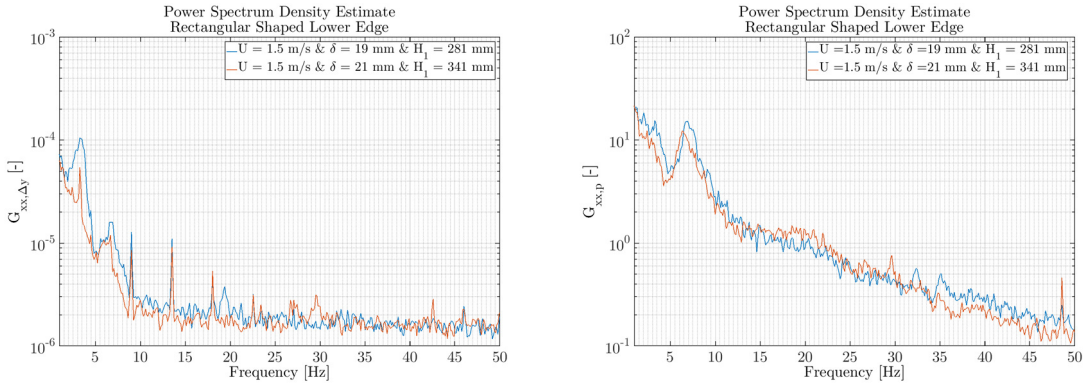

Figure 4-9: (L) Power spectrum of displacement of two tests with same conditions but different water depth & (R) Power spectrum of force of two tests with same conditions but different water depth

The figures above show similar responses regarding the frequencies. However, some small differences can be identified. The experienced energy level is larger for the situations with a larger upstream water level (blue line). The peak frequencies appear to be similar. A proper conclusion cannot be drawn from this result because the results are based on only two tests. The amount of tests is not sufficient enough to show the exact influence of H_1 on the flow-induced vibration phenomena. More tests with a constant ΔH, U and δ and varying H_1 and H_2 should be executed to give a clearer view on the influence of the water level. The limited duration of this research prevented the execution of these tests.

4.3 Main Test

The main test exists of steady state measurements under varying conditions. The exact conditions of the individual tests can be found in Appendix I. The steady state measurements can be divided into two different groups of tests. These groups are tests with an extreme vertical stiffness and tests with a low vertical stiffness. The subjects that are elaborated in this paragraph are listed below.

- Predicted frequencies (§ 4.3.1). Before the test results are processed some predictions regarding the frequencies are being elaborated. This section also explains the possible noise present in the results.
- A situation with an extreme stiff vertical suspension ($k \rightarrow \infty$) (§ 4.3.2). These measurements result in a determination of the excitation frequency related to the flow of the water.
- A situation with varying vertical suspension stiffness ($k \neq \infty$) (§ 4.3.3). These measurements result in a dynamic response of the model on the excitation as determined in § 4.3.2
- Relation between excitation and response of the model (§ 4.3.4).

The frequencies are determined using a spectral analysis based on Welch's Method, the method has been executed with Matlab®. A more detailed explanation of this method is given in Appendix H.

4.3.1 Predicted Frequencies

Before processing the rough test data, the predictions of the frequencies are elaborated. These predictions have been divided into three sections. The sections can be coupled to the structure of the remaining part of the paragraph. The sections are:

- excitation frequency (related to the tests with $k \rightarrow \infty$);
- response frequency (related to the tests with $k \neq \infty$);
- side effects.

Excitation Frequency

The excitation frequencies that can be expected during the tests with an extremely stiff vertical suspension will relate to the Strouhal relationship as shown in equation 4.8. The characteristic length in the relation is open for interpretation and could, therefore, lead to multiple frequencies.

$$T \sim \frac{L}{U} \rightarrow f = \frac{U}{L} \tag{4.8}$$

Different characteristic lengths that could be considered are:

- The gate opening (δ);
- The gate thickness (b);
- The upstream water level (H_1).

The definition of these lengths has been discussed in § 3.1. The different characteristic lengths can be coupled to different types of vibrations. Because the velocity is varied during the tests, the retrieved frequencies will vary per individual test. The critical Strouhal relationship will not be 1.0 but a fraction. In § 4.3.2 an attempt has been made to couple different Strouhal numbers to the shapes of the lower edges. When the number is known, the frequencies per individual situation can be retrieved. The Strouhal relations used in current documentation related to wind actions are 0.12 for a rectangular shape and 0.18 for a circular shape [14]. These Strouhal numbers are related to the vortex shedding phenomena. The vortex shedding phenomena differ from the investigated phenomena in this research.

Response Frequency

The theoretical response of the model has been discussed briefly in § 2.1.3. That paragraph elaborated the natural frequency and response frequency when the force is purely harmonic. Initially, it is expected that the response frequency will be close to the natural frequency of the system. Because the force will not be purely harmonic, energy will be present over a bandwidth of frequencies. Therefore, the system is more likely to be excited by the frequency close to the natural frequency. A first indication has been showed in § 4.2.2 in which this expectation does not seem valid. The response of the model experienced during the tests will be discussed in § 4.3.3.

Side Effects

This part will explain any side effects that can be identified in the results. The side effects exist of effects that are visible in the result (frequencies or amplitudes) but do not result from the problem or test conditions. The side effects elaborated in this section are:

- Horizontal vibrations of the model;
- Surface waves;
- Noise in measuring devices.

Horizontal Vibrations

The horizontal vibrations of the model set-up were clearly seen in the results. The horizontal vibrations do not fall within the scope of the research, because the research focusses on the vertical cross-flow vibrations phenomena only. Two types of horizontal vibrations have been experienced. For the exact calculation of these frequencies a reference is made to Appendix G. The vibrations and frequencies are:

- The horizontal vibration of the model set-up external frame (± 40 Hz). The exact frequency depends on the vertical position of the horizontal top beam. With more stiff springs and a small gate opening the beam is positioned lower and the frequency is experienced to be higher.
- The horizontal vibration of the valve plate (± 120 Hz).

Surface Waves

Another experienced effect were the surface waves. The model has to simulate a valve in a closed culvert, so the surface waves will not be experienced in a real-life situation. The effects related to the surface waves are primarily low frequency vibrations. The waves can exist at the downstream side (H_2) or at the upstream side of the valve (H_1). A first indication of the frequencies of this effect is given by linear wave theory. The flume can be considered as transitional water depth and the dynamic subsurface pressure can be calculated with equation 4.9 [58].

$$p = \rho \cdot g \cdot a \cdot \frac{\cosh\left(k(h+z)\right)}{\cosh(k \cdot h)} \cdot \sin(\theta) \qquad 4.9$$

In which:

p	=	the water pressure [Pa]
z	=	co-ordinate of relative depth to the average water surface [m]
a	=	wave amplitude [m]
θ	=	$\omega t - kx$
k	=	wave number [rad/m]
h	=	water depth [m]

Equation 4.10 [58] can be used to put the equation above in the frequency domain. The wave length experienced was approximately 1.0 metre and the amplitude of the wave is estimated at 0.02 metres. The period of the experienced wave was approximately two seconds.

$$E(f) = \sum_{f=f_i}^{f+\Delta f} \frac{1}{2} \cdot a_i^2 = \sum_{f=f_i}^{f+\Delta f} \frac{1}{2} \cdot p_i^2 \qquad 4.10$$

In which:

E(f)	=	energy related to frequency

The mentioned wave characteristics are put in equation 4.9 with a normal distribution and a small standard deviation. A spectral analysis is applied to these results leads to the graph shown in Figure 4-10. The graph indicate that the surface waves have a high peak at a low frequency (f < 5.0) and produce small noise over the entire spectrum.

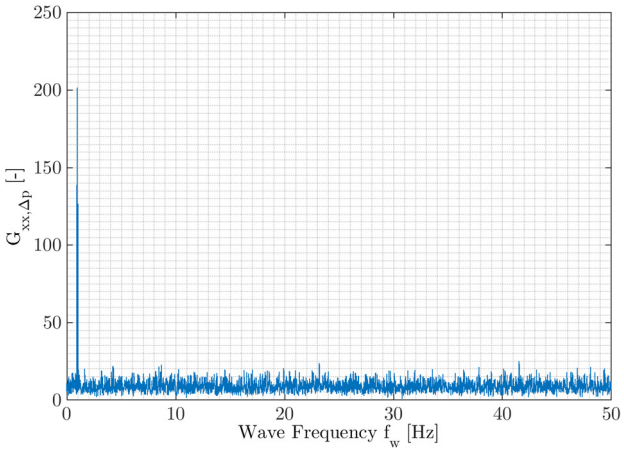

Figure 4-10: Power spectrum of estimated surface waves

The frequency peak is visible at 1.1 Hz. Because the conditions (wave length, amplitude and period) of the experienced surface waves varied, this frequency varies as well. It is assumed that frequencies lower than 3 Hz are due to surface waves.

Noise in Measuring Devices

In addition to the above mentioned side effects, some of the measuring devices showed clear noise peak frequencies. These frequencies cannot be identified as a result of test and are therefore determined in an earlier stage. Appendix F shows the determination of the noise frequencies related to the measuring devices.

Overview

Figure 4-11 shows a power spectrum with identified responses as elaborated above. The low frequency energy as located in the low frequencies (< 3 Hz) due to the surface waves can be seen. The peak at approximately 35 Hz is coupled to the horizontal vibration of the frame. The measuring device of this power spectrum (the pressure sensor) gives a standard peak at approximately 48 Hz. This peak is also shown in the figure below and in Figure 4-12 of the next paragraph.

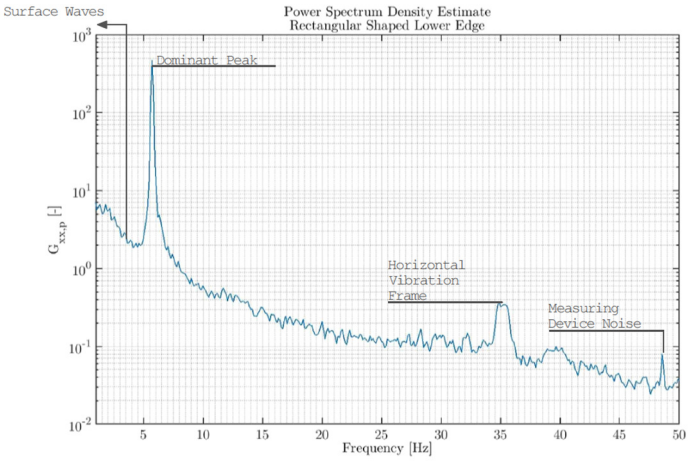

Figure 4-11: Indication of the identified peaks in the power spectrum

4.3.2 Excitation

In this paragraph the excitation frequencies are determined. The excitation frequencies are retrieved from the pressure measurements of the tests with the extreme stiff vertical suspension ($k \rightarrow \infty$). In Appendix F an description and images of the model set-up of these tests are given. Figure 4-12 shows an example of processed data for a rectangular shaped lower edge. The figure shows three measurements with approximately the same gate opening (δ) and a varying flow velocity (U). A clear peak is shown in the power spectra. For all the measurements these peaks have been identified.

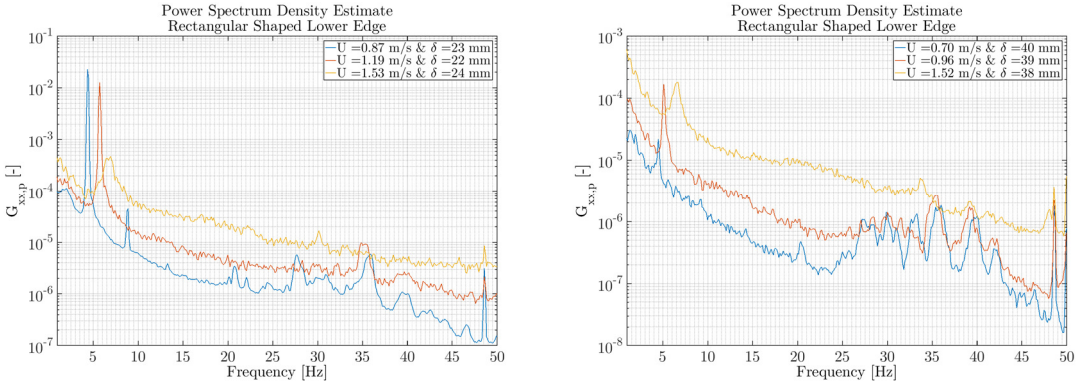

Figure 4-12: Power spectrum estimate diagram of pressure from three measurements with extreme stiff vertical suspension and a rectangular shaped lower edge

The focus is set on the low frequency peaks (between 0 and 15 Hz). These peaks appear to have the largest amount of energy. The figure also shows a peak at the same frequency (± 48 Hz) for all the different velocities, these peaks are the result of deviations in the measuring equipment. These deviations are discussed in Appendix F. Figure 4-13 shows a graph that relates the flow velocity with the identified frequencies. The results show a trend.

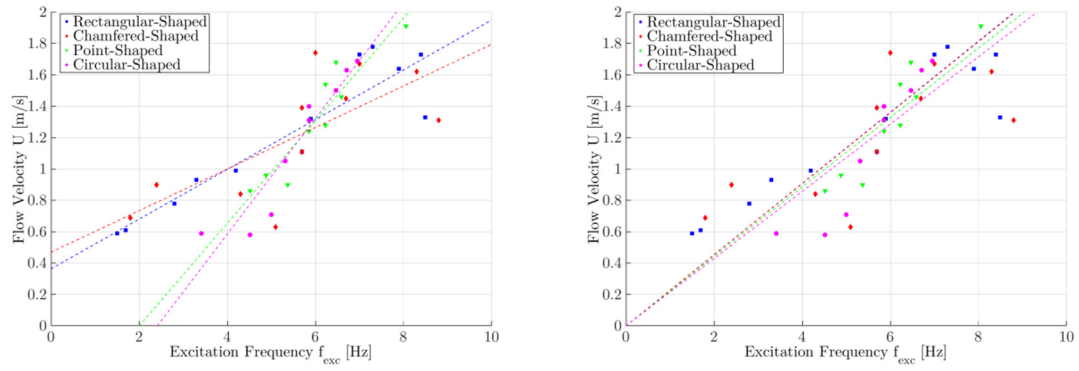

Figure 4-13: Plots of flow velocity versus the frequency with computed trend lines

Table 4-4 shows the characteristics of trend per specific lower edge shape for the left figure of Figure 4-13. From the slope of the trend ($\Delta U/\Delta f$) and the valve thickness (b) a Strouhal number has been retrieved. The trend lines shown do not pass the origin (0,0) of the graph. This is noteworthy, because with no flow velocity no excitation is expected. For that reason, a second graph is shown in Figure 4-13 (R). In this graph the trend lines are plotted through the origin of the graph. The trend line values can be found in Table 4-4.

Shape	R^2	Slope $\Delta U/\Delta f$	Strouhal Number	R^2	Slope $\Delta U/\Delta f$	Strouhal Number
Graph in Figure 4-13		**Left**			**Right**	
Rectangular-Shaped	0.8511	0.157	0.19	0.8565	0.2268	0.132
Chamfered-Shaped	0.5603	0.175	0.17	0.5056	0.2264	0.133
Point-Shaped	0.8743	0.327	0.09	0.7808	0.2212	0.136
Circular-Shaped	0.8921	0.367	0.08	0.7315	0.2143	0.140

Table 4-4: Characteristics of the computed trend lines from Figure 4-13

The values shown in Table 4-4 (related to left figure) do not match with the Strouhal numbers related to vortex shedding. These results give a larger Strouhal number for the rectangular-shaped lower edge compared to the circular-shaped lower edge. The results related to the right figure do show similarities with the vortex shedding Strouhal number (lower for rectangular than circular). The mutually differences are very small.

When the data from Figure 4-13 (R) is adjusted for the Reynolds dependence (§ 4.2.2), the results lead to Figure 4-14. In this particular case only tests with a Reynolds number larger than $3 \cdot 10^4$ are used.

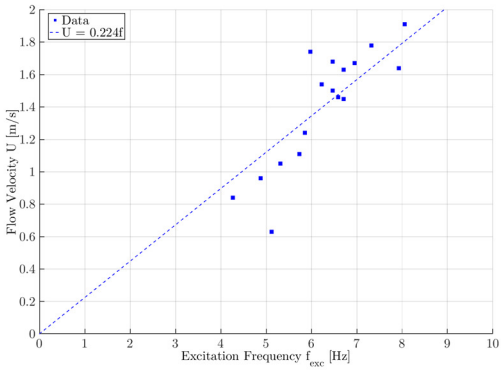

Figure 4-14: Plot of flow velocity versus the frequency for all shapes of the lower edge and Re $> 3 \cdot 104$

The accuracy of the trend is smaller than the previous trend lines ($R^2 = 0.6833$). The retrieved Strouhal number from this figure is 0.13. This number matches with the numbers retrieved from the right graph of Figure 4-13 (varying between 0.13 and 0.14).

It can be concluded that the shape of the valve does not influence the excitation frequency. When the data is filtered for the Reynolds dependency the found Strouhal number of the excitation is 0.13.

4.3.3 Response

This paragraph will focus on the response of the model on the varying conditions as given in Chapter 3. In these steady state tests the model is no longer extreme stiff, but has varying stiffness. During the tests of the response of the model three parameters were measured. The three parameters are:

- the vertical displacement (Δy);
- the vertical force (F);
- the pressure underneath the lower edge of the model (p).

Figure 4-15 shows a situation in which a clear vibration can be identified. The vibrations encountered during the tests have small amplitudes. The results from the steady state measurements are presented in two categories. The two categories are:

- the amplitude of the vibrations;
- the frequency of the vibrations.

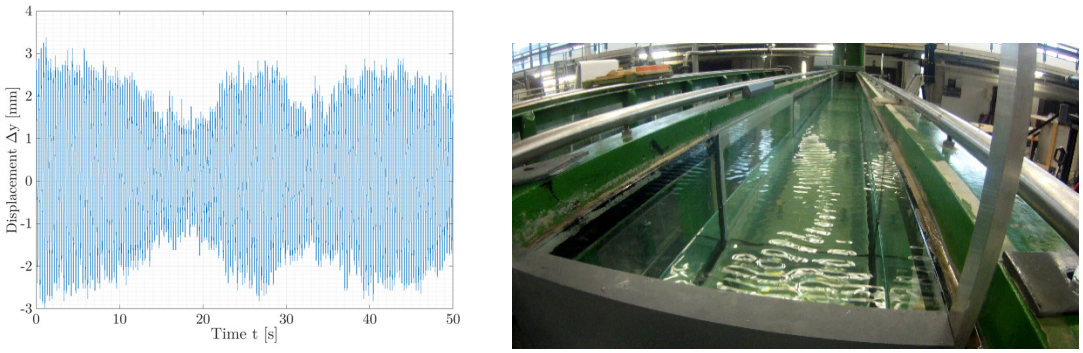

Figure 4-15: (L) Test with clear vibrations visible & (R) Picture of visible small period waves due to vibrations of the valve

The signal shown in Figure 4-15 could be a beat signal in which two sine waves with different periods interfere with each other.

Amplitudes

The elaboration of the amplitude of the vibrations has been divided into a part specifically dedicated to the model set-up and an overall part in which the results are presented in dimensionless quantities as described in Chapter 3.

Model Set-Up

The amplitude of the vertical force indicates the presence and the magnitude of a vibration. Figure 4-16 (L) shows the force amplitude (ΔF) versus the dimensionless Strouhal number (S_n). From the graph can be concluded that the magnitude of the vibrations is significantly larger when the Strouhal number is smaller than 0.3. The amplitudes under the 1.5 N can be neglected, because the amplitude is caused by noise. The Strouhal number in this graph is calculated using the gate thickness (b) as characteristic length and the natural frequency (f_n) as frequency, because these parameters are both design parameters.

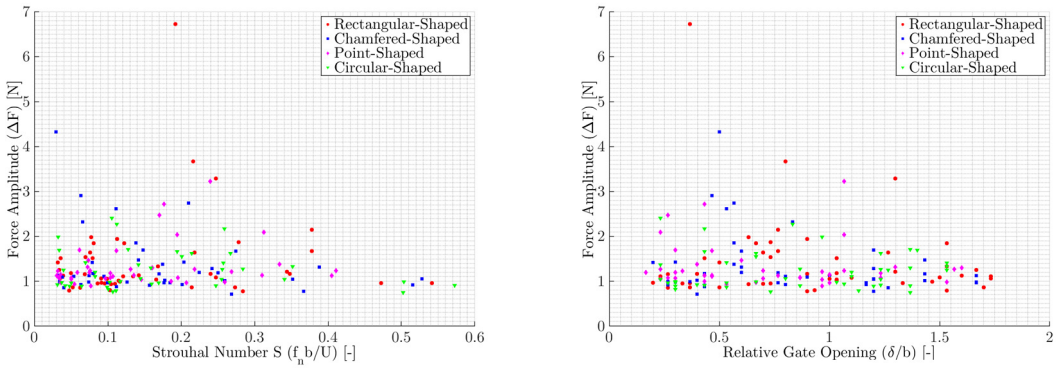

Figure 4-16: (L) Strouhal number versus force amplitude & (R) Force amplitude versus relative gate opening

The rectangular-shaped lower edge shows the highest force amplitude in the vibrations. The chamfered-shaped and point-shaped lower edge show similar magnitudes. However, it seems that the vibrations of the chamfered-shaped edges occur at lower values of the Strouhal number (S_n). The circular-shaped lower edge shows the lowest force amplitudes. Figure 4-16 (R) shows the magnitude of the force amplitude versus the relative gate opening (δ/b) of the individual tests. It can be concluded that magnitude is largest when the relative gate opening (δ) is smaller than 1.0. It should be noted that the major part of the tests has been executed with relative gate openings of $0.5 < \delta/b < 1.5$, which is indicated as critical area in the literature [33].

It can be concluded that the majority of the vibrations occur when the Strouhal number is smaller than 0.3. The vibrations of the rectangular-shaped lower edge have a larger amplitude than the other shapes. In addition to this, the amplitudes of the vibrations are larger when the relative gate opening (δ/b) is smaller than 1.0.

Overall

In this section the graphs presented above are made dimensionless. The graphs are shown in Figure 4-17 and Figure 4-18. Figure 4-17 shows no clear image of the response related to the Strouhal number. A linear relationship appears in the graph. The right graph shows the same graph with the different theoretical natural frequencies. This graph shows that the relation can be coupled to the natural frequency of the system.

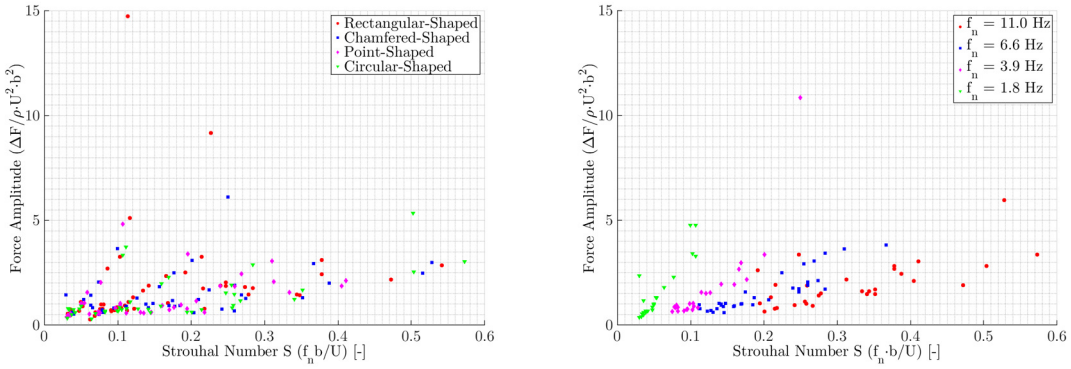

Figure 4-17: (L) Dimensionless force amplitude versus Strouhal number per shape (L) and per natural frequency (R)

Figure 4-17 shows that the amplitudes of the point-shaped lower edge are the smallest and the rectangular-shaped lower edge the largest. This is in agreement with the data presented in Figure 4-16. Figure 4-18 shows the amplitude in relation to the relative gate opening (δ/b). No clear statement can be made based on the graph.

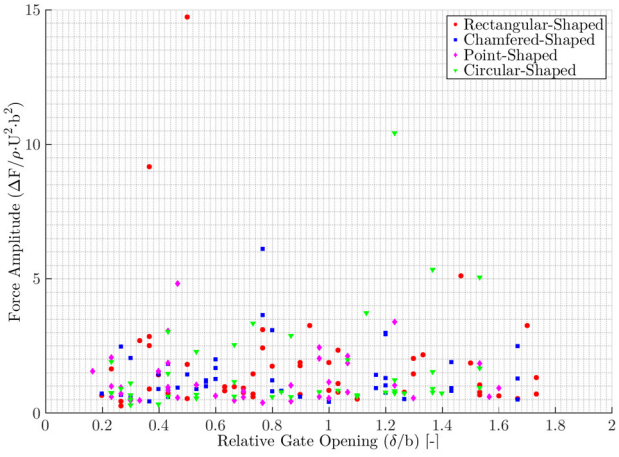

Figure 4-18: Dimensionless force amplitude versus relative gate opening for different seal shapes

From these test results no overall conclusion can be drawn on what the critical Strouhal number is for the initiation of the vibrations. It can be concluded that the amplitudes of the point-shaped lower edge are the smallest, where the rectangular-shaped lower edge shows the largest amplitudes. Based on the data above the relative gate opening does not have an effect on the amplitude of the vibration.

Frequency

The determination of the dominant frequencies of the individual tests has been done using a spectral analysis. The procedure of this analysis is explained in Appendix H. Table 4-5 and Figure 4-19 show the results regarding the identification of a clear dominant response frequency. The results have been divided into three categories. These categories are:

- a clear response frequency in all three measured variables (F, p and Δy);
- a clear response frequency in only two of the three measured variables;
- no clear response frequency at all.

A spectrum with a clear dominant frequency in all three measured variables is shown in Figure 4-22. The range of the conditions during the tests have been kept similar for the different shapes. The percentages of the rectangular-shaped tests do not accumulate to 100% because of a failed test. The final column shows the amount of tests that also showed a high frequency peak (between 20 and 40 Hz). An example of a high frequency response is shown in Figure 4-25. The identification for all the individual tests can be found in Appendix I.

	Total number of tests	**Extreme stiff tests**	**Tests with variable stiffness**	**Clear peak in all three variables**	**Clear peak in two variables**	**No clear peak identified at all**	**High frequency peaks identified**
Rectangular-Shaped	65	13	52	19 (37%)	9 (17%)	23 (44%)	7 (13%)
Chamfered-Shaped	57	15	42	18 (43%)	7 (17%)	17 (40%)	0 (0%)
Point-Shaped	51	11	40	0 (0%)	6 (15%)	34 (85%)	1 (3%)
Circular-Shaped	54	11	43	1 (2%)	11 (26%)	31 (72%)	0 (0%)

Table 4-5: Results of the steady-state measurements regarding the identification of a clear dominant response frequency

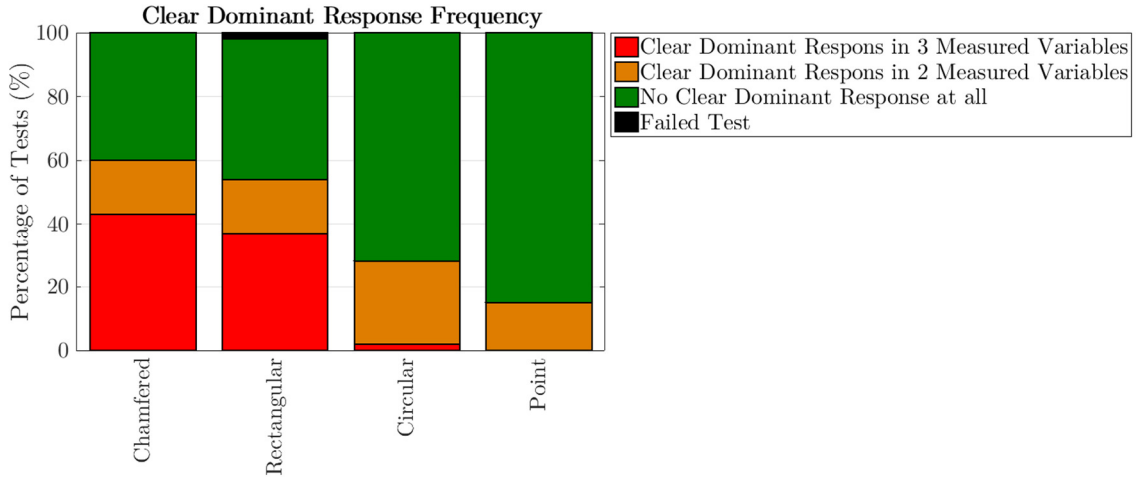

Figure 4-19: Percentages of total number of tests with a clear dominant response frequency

From the table and figure above can be concluded that the rectangular-shaped and the chamfered-shaped lower edge had the most tests with a clear dominant response frequency. The point-shaped lower edge showed the less clear dominant frequencies. The high frequencies responses are only experienced with the rectangular-shaped lower edge. The high frequency responses will be explained in the further course of this paragraph.

Figure 4-20 and Figure 4-21 show the results from above divided into sections related to the relative gate opening (δ/b) and the flow velocity (U). Figure 4-20 shows that the most dominant response frequencies have been found with a relative gate opening between 0.5 and 1.5. Figure 4-21 does not show a clear image. Only the tests with a high velocity (U> 1.5) seem to give less dominant response frequency. It should be noted that this group of tests was very small (only 14 tests in total).

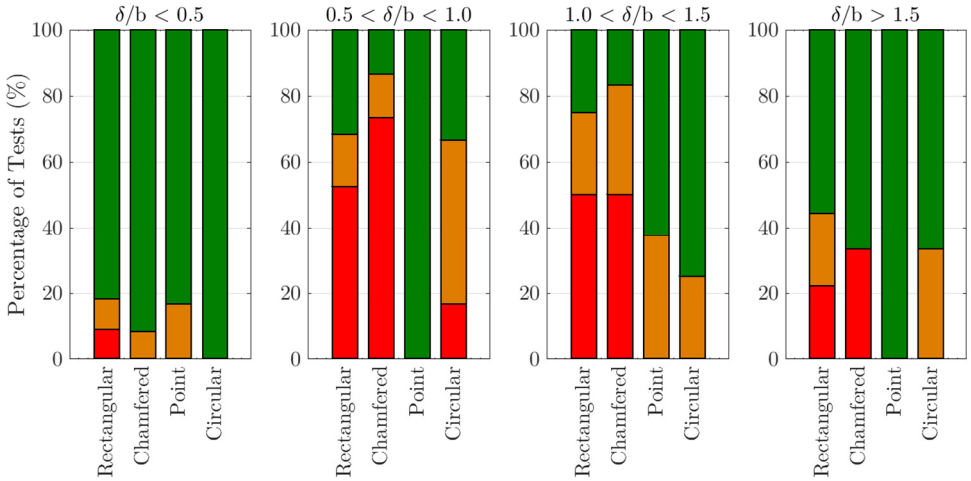

Figure 4-20: The identified response peaks divided into relative gate opening (δ/b) sections

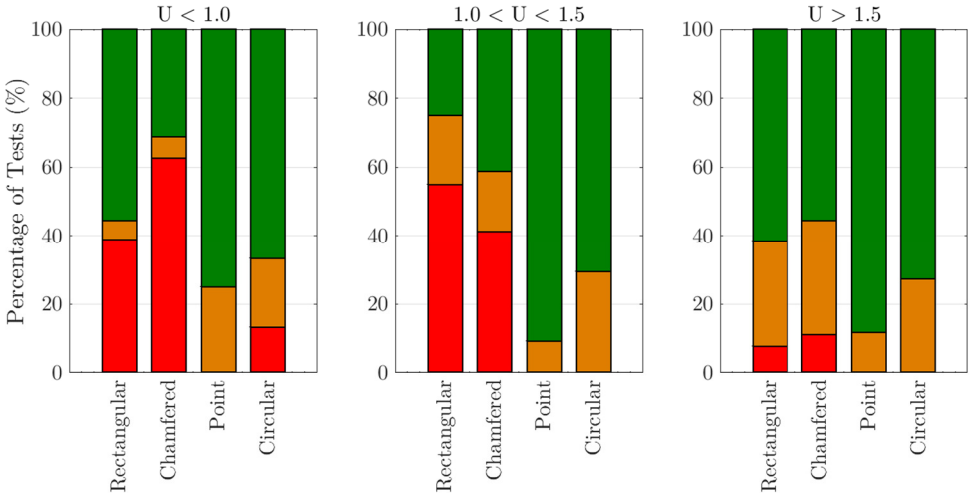

Figure 4-21: The identified response peaks divided into flow velocity (U) sections

Figure 4-22 shows the result of the spectral analysis of one single test with the three measured parameters (ΔF, Δy and p). The vertical lines indicated in the graph are the predicted frequencies as elaborated in § 4.3.1. These frequencies are determined on the characteristic lengths (δ, b or H_1) and the in the previous paragraph determined Strouhal relationship of 0.13. More power spectra, including a brief explanation, can be found in Appendix J.

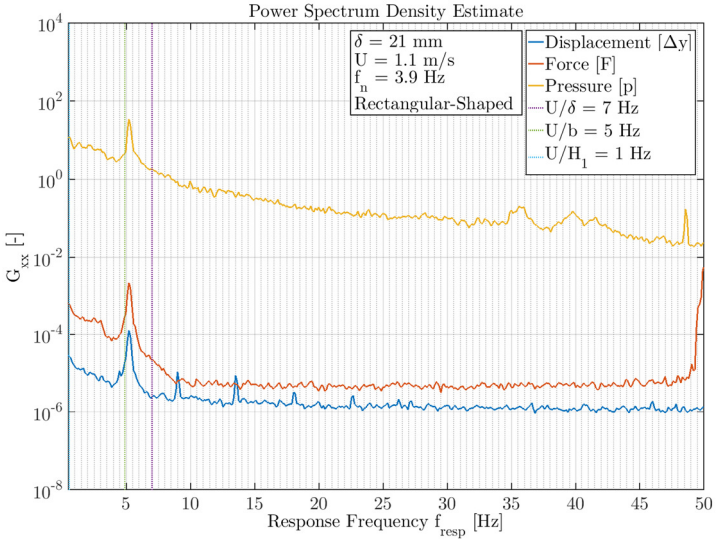

Figure 4-22: Power spectrum of a test with a clear dominant frequency response in all three measured variables

The spectrum above shows a clear peak for all three parameters at approximately 5 Hz. The peak almost coincides with the Strouhal number related to the thickness of the valve (b). These peaks are identified for all individual tests in which a clear peak could be observed and presented in Figure 4-23. The graph shows a similar trend with the graph presented in Figure 4-13 of the previous paragraph. Similar to that case several trend lines can be computed that fit these data points. The characteristics of these trend lines are shown in Table 4-6. Similar to the previous trend lines, these trend lines do not pass the origin of the graph (0,0).

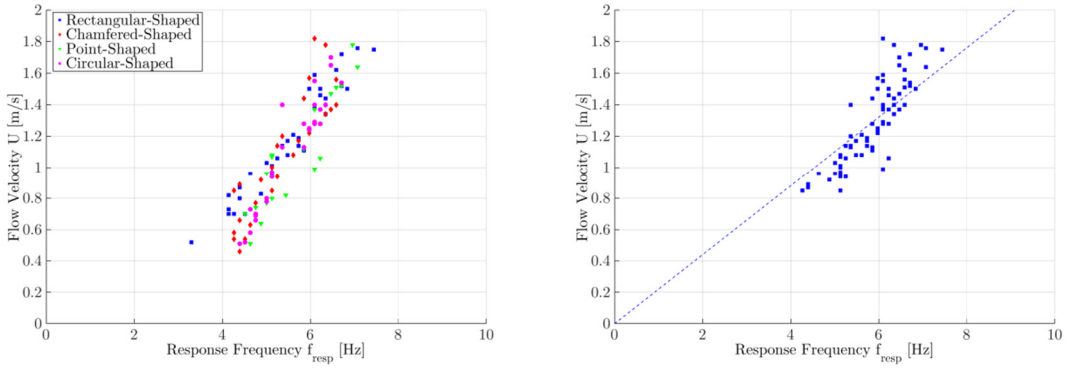

Figure 4-23: Response frequencies versus flow velocity for steady state tests

The right graph of Figure 4-23 shows the data that is filtered for the earlier discussed Reynolds requirement ($Re > 3 \cdot 10^4$). When a trend line is plotted through the origin, it shows that the fit is not completely accurate. The low frequency values can be found under the trend line and the higher frequency values are found above the trend line. The Strouhal number related to the trend line is 0.14, which is a little higher than found with the excitation. From this can be concluded that the valve response is similar to the excitation frequency and not to the natural frequency.

Shape	R^2	Slope $\Delta U/\Delta f$	Strouhal Number
Rectangular-Shaped	0.9234	0.3274	0.09
Chamfered-Shaped	0.8091	0.4214	0.07
Point-Shaped	0.8474	0.4080	0.07
Circular-Shaped	0.8977	0.4810	0.06
Figure 4-23 (R)	0.8161	0.2157	0.14

Table 4-6: Characteristics of the computed trend lines from Figure 4-23

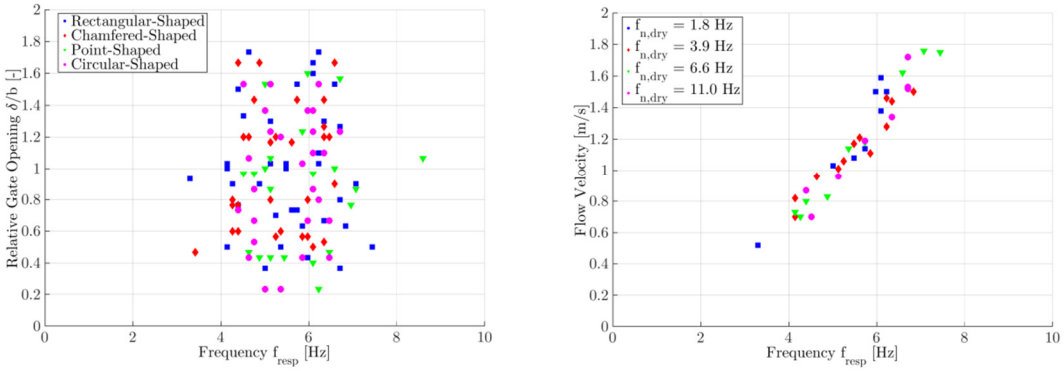

Figure 4-24: (L) Relation between response frequency and gate opening & (R) Relation between frequency and flow velocity with different rigidities for the tests with the rectangular-shaped lower edge

Figure 4-24 (L) shows that the response frequency of the model is not related to the gate opening. This statement only relates to the frequency and not to the magnitude of the vibration. Figure 4-24 (R) shows that also the natural frequency of the system (the rigidity and mass) does not influence the value of this lower frequency. The mass of the valve has not been varied during the tests. The results presented in Figure 4-24 (R) are all retrieved from tests with a rectangular-shaped lower edge.

In addition to the low response frequencies, some tests showed a higher response frequency. Such a response is shown in the power spectrum of Figure 4-25. This spectrum also shows a low frequency peak. This lower frequency peak appears to have less energy than the higher frequency peak. The experienced frequencies did not have a constant value and were found in the region between 25 Hz and 40 Hz.

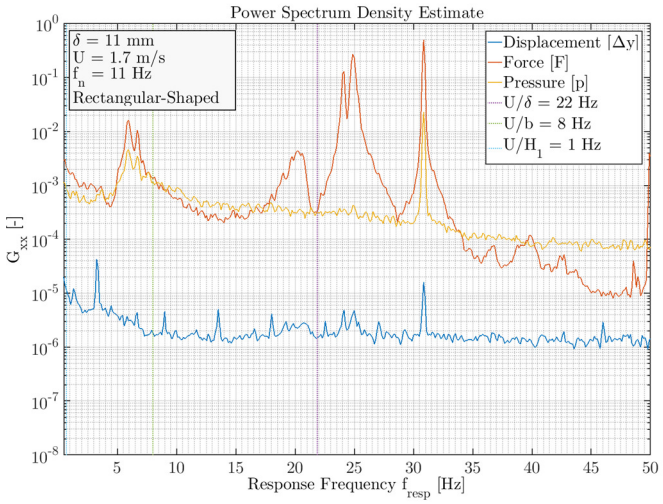

Figure 4-25: Power spectrum of a test with a clear high frequency response

The high frequency vibrations only occurred when the natural frequency was relatively high (in this case the situations with a theoretical natural frequency of 6.6 Hz and 11.0 Hz). The peaks, however, do not correspond with the natural frequencies of the tests. The observed frequency is often two to three times larger than the natural frequency. The amount of tests that show these high frequency peaks are minimal (4% of the total amount of tests).

The peaks can be explained by a difference in two vibration areas described by previous research. ERDBRINK [20] and BILLETER AND STAUBLI [8] both indicated two critical vibration areas. One with a reduced velocity (V_{rd}) between 2 and 3.5 and one area with a reduced velocity larger than 8.5. The reduced velocity is the inverse of the Strouhal number, this is shown in equation 4.11. Appendix D gives a more detailed description of the parameter.

$$V_{rd} = 1/S \tag{4.11}$$

In which: V_{rd} = reduced velocity [-]
S = Strouhal number [-]

It can be concluded that these vibrations are from a different critical area. ERDBRINK couples the high reduced velocity ranges ($V_{RD} > 8.5$) with flow instability (IIE) and the low reduced velocity ranges ($2 < V_{RD} < 3.5$) with vibrations induced by the movement of the valve (MIE) [20]. The low frequency responses are related to the high reduced velocity area and are due to flow instability. Therefore, the high frequency response is coupled to the vibrations induced by the movement of the valve. This type of vibration has been explained before in Chapter 2.

From the data above, it can be concluded that the rectangular-shaped lower edge shows the most dominant responses to the vibrations. The point-shaped lower edge shows the least clear dominant responses. The high frequency responses were only experienced with the rectangular-shaped lower edge. But, too few high frequency responses were experienced to draw a proper conclusion. It can also be concluded that the shape does not have an influence on the response frequency. Neither did the relative gate opening nor the natural frequency of the system. The response of the valve corresponded with the excitation frequency and not with the natural frequency.

4.3.4 Relation Excitation and Response

In this paragraph the same division has been made as in the previous paragraph between a situation specific for the model set-up and a situation regarding and overall part based on dimensionless parameters.

Model Set-up

Figure 4-26 (L) shows the magnitude of the vibrations (the dimensionless force amplitude) as discussed in the previous paragraph versus the ratio between the response frequency and the natural frequency in water (f/f_n). A clear peak is shown at a ratio of approximately 0.6. In a system without damping this peak should be expected at a ratio of 1.0. The theoretical situation is shown in Figure 4-26 (R). The shift in the peak can be explained by the presence of damping.

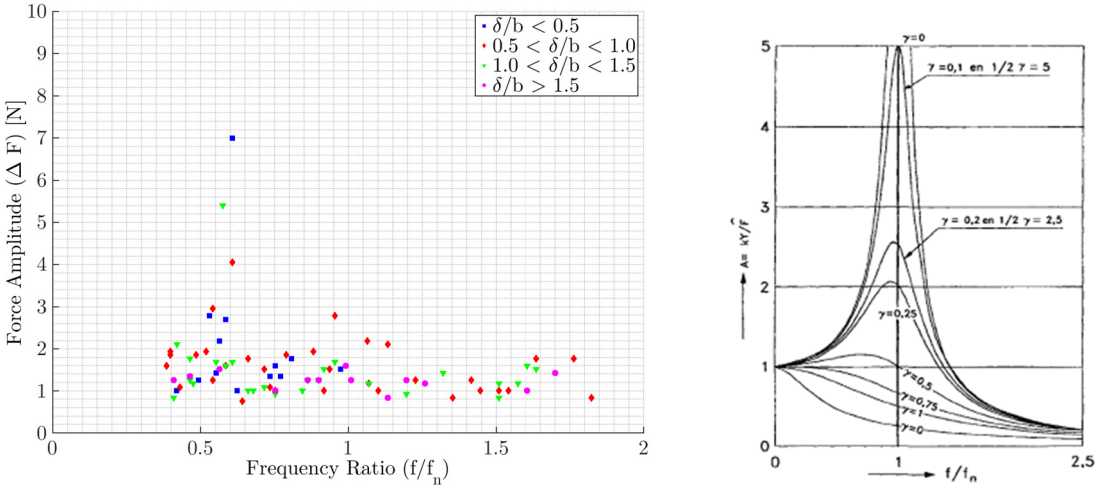

Figure 4-26: (L) Magnitude versus f/fn-ratio & (R) Response diagram of a one degree of freedom mass-spring system [33]

The figure above shows that the presence of damping influences the initiation and amplitude of the vibration, however this effect seems to be large for the minimal amount of damping that is found in the model (§ 4.2.1). Figure 4-26 (R) shows that the shift of the resonance peak is theoretically not as large as the left graph suggests. Figure 4-26 (L) shows that when the relative gate opening (δ/b) is larger than 1.5 no vibrations are experience. A small peak is shown around $f/f_n = 1.0$ only for a relative gate opening between 0.5 and 1.0. Figure 4-27 shows a division of Figure 4-26 for δ/b smaller than 0.5 (L) and δ/b between 0.5 and 1.0.

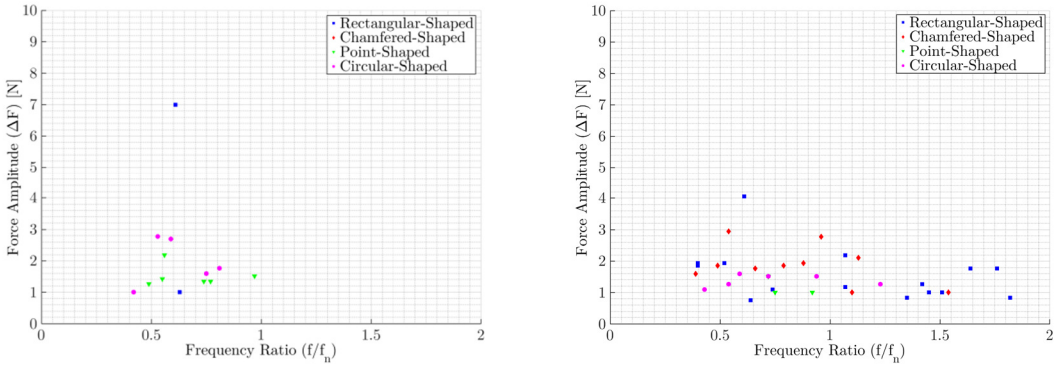

Figure 4-27: (L) Magnitude versus f/f_n-ratio for $\delta/b < 0.5$ & (R) Magnitude versus f/f_n-ratio for $0.5 < \delta/b < 1.0$

The graphs from Figure 4-27 show no clear relation between the amplitude of the force and the frequency ratio.

These damping effects should be investigated in more detail. This could be done by varying the damping during any future tests. For now can be stated that the damping influences the region in which the highest amplitudes are measured. The shift of this region (decrease of f/f_n) interferes with the current design rules ($f_n > 3 \cdot f$) regarding the amplification factor.

Overall

Figure 4-28 displays the dimensionless graph of Figure 4-26. No clear relation is found between the frequency ratio (f/f_n).

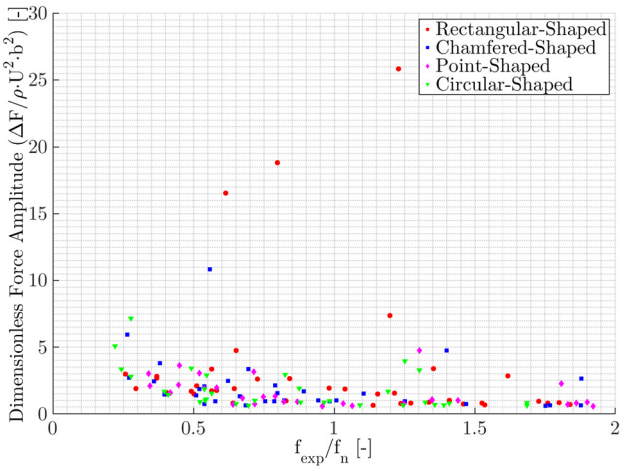

Figure 4-28: Dimensionless force amplitude versus the frequency ratio

The graph above shows that the largest amplitudes are found with the rectangular-shaped lower edge. The point-shaped lower edge shows the lowest force amplitudes. No conclusion can be drawn on which frequency ratio is critical, since no clear image is given in Figure 4-28.

As was concluded in the previous paragraph, the above shown data confirms that the rectangular-shaped lower edge gives the largest amplitudes. The point-shaped lower edge gives the smallest amplitudes. No conclusions can be drawn on which frequency ratio is the most critical.

4.4 Energy Dissipation

During the process of levelling the water in the lock certain types of energy losses can be experienced. This paragraph will give an overview of the energy losses during the test and their consequences on the vibration problems. Some of these results are retrieved from the steady state measurements, others have been retrieved from individual tests as described in Chapter 3. The paragraph exists of the following sections:

- The contraction of the flow underneath the valve (§ 4.4.1). The contraction of the flow is important for the assumption that the flow velocity can be approached with $U = \sqrt{(2 \cdot g \cdot \Delta H)}$.
- The effect of leakage of the model (§ 4.4.2). The leakage will in first instance not lead to direct energy dissipation. However, it does have an effect on the assumption regarding a two dimensional problem.
- The dynamic amplification factor (§ 4.4.3). The final section of this paragraph elaborates the dynamic amplification factor.

4.4.1 Contraction

Because the flow velocity is approximated by the head difference over the valve (ΔH), additional research has been done to the differences in contraction of the different shaped lower edges. The contraction of the flow can be coupled to the energy loss. Figure 4-29 and Figure 4-30 show an example of the images from these measurements. The contraction is taken in the centre underneath the valve because the flow velocity at this point is the most interesting. Full contraction takes place just after the centre of the valve. The measurements are done by a constant discharge (Q). The discharge is measured with a Rehbock weir. Table 4-7 shows the velocities determined with the head difference and with the discharge (equation 4.12). The exact contraction has been determined based on the images of Figure 4-29 and Figure 4-30. Three different cases per shape were observed. The contraction coefficients (μ_c) are given in Table 4-8.

$$U = \frac{Q}{\mu_c \cdot \delta \cdot W} \qquad 4.12$$

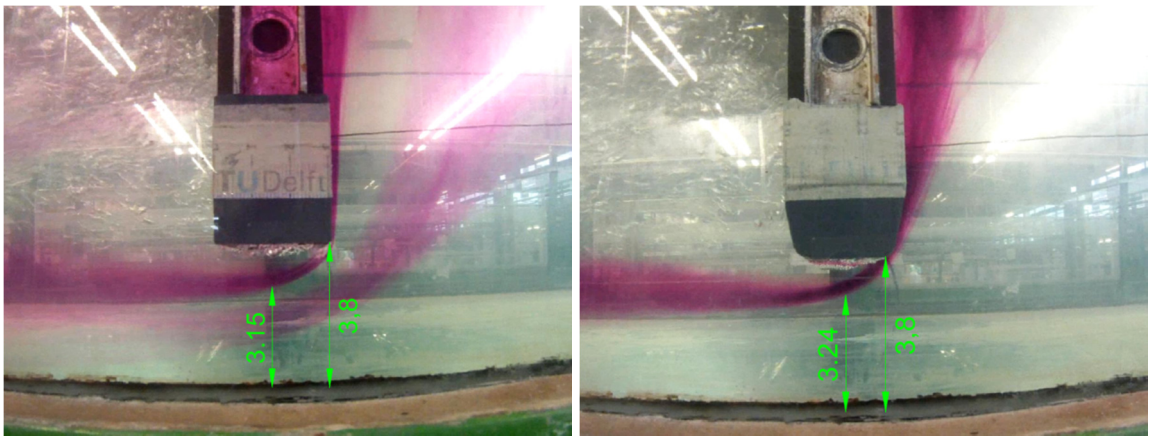

Figure 4-29: Determination of contraction underneath the valve for the rectangular-shaped seal (L) & the chamfered-shaped seal (R)

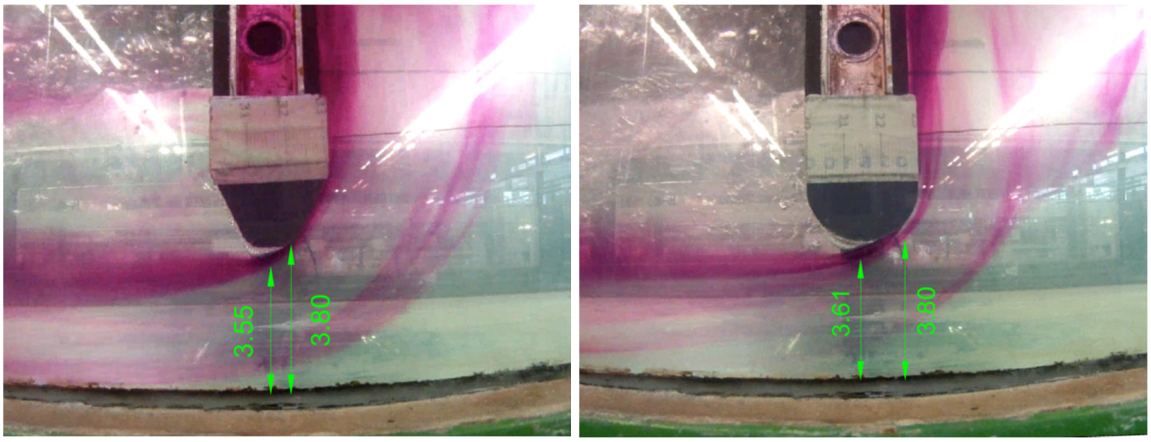

Figure 4-30: Determination of contraction underneath the valve for the point-shaped seal (L) & the circular-shaped seal (R)

	Case 1		Case 2		Case 3	
Velocity [m/s]	0.021 m^3/s Based on ΔH	δ = 38 mm Based on Q	0.011 m^3/s Based on ΔH	δ = 16 mm Based on Q	0.014 m^3/s Based on ΔH	δ = 36 mm Based on Q
Rectangular-Shaped	1.78	1.67	1.70	2.05	1.34	1.42
Chamfered-Shaped	1.65	1.60	1.57	1.87	1.22	1.10
Point-Shaped	1.59	1.46	1.53	1.63	1.11	1.11
Circular-Shaped	1.50	1.44	1.44	1.61	1.06	0.98

Table 4-7: Comparison flow velocity based on head difference (ΔH) and discharge (Q)

Table 4-7 shows that in some cases the flow velocity based on the head difference and based on the discharge varies much. This difference in flow velocity can be explained by some uncertainties in the test data. Because of these deviations is chosen to keep the determination of the flow velocity based on the head difference (ΔH).

Seal Shape	Average contraction coefficient [-]
Rectangular-Shaped	0.75
Chamfered-Shaped	0.85
Point-Shaped	0.92
Circular-Shaped	0.96

Table 4-8: Determined contraction coefficients per seal shape

Table 4-8 shows a difference in contraction coefficients between the different shaped lower edges. It can be concluded that the rectangular-shaped lower edge seal has a lower contraction coefficient which leads to a smaller flow surface by a similar gate opening as any other seal shape.

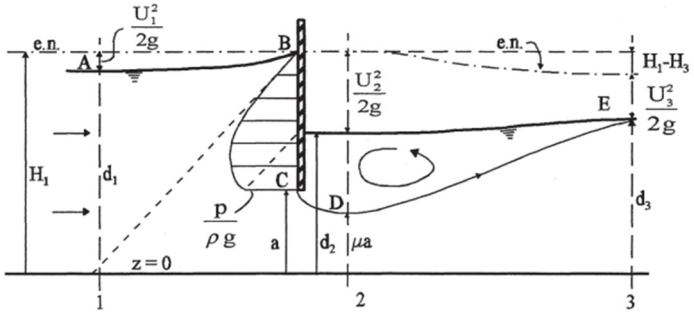

Figure 4-31: Energy situation for a water flow under a valve [3]

Figure 4-31 shows a situation in which water flows underneath a vertical valve. It is shown that the energy level (in the figure indicated as e.n.) drops till the end of the wake. Up to the point where the flow surface is minimal (μa) no energy losses are assumed (losses due to viscous forces are minimal and therefore neglected). Equation 4.13 shows the formula that can be used to determine the amount of head loss due to energy loss. The subscripts used in the equation differ from earlier symbols used for upstream and downstream characteristics. The used subscripts match with Figure 4-31 to prevent confusion.

$$\Delta H_{loss} = H_1 - H_3 = h_1 + \frac{U_1^2}{2g} - \left(h_3 + \frac{U_3^2}{2g}\right) \quad 4.13$$

Because only the upstream and downstream water levels are measured the up- and downstream flow velocities (U_1 and U_3) have to be determined on the results from the Rehbock weir. The tests were executed under steady state conditions, so the discharge was constant.

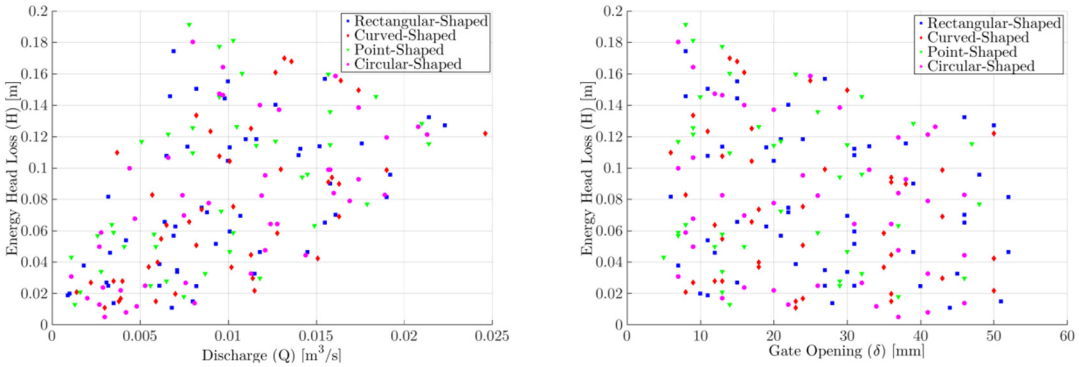

Figure 4-32: (L) Head loss versus discharge (Q) & (R) Head loss versus gate opening (δ)

The figures above do not show a clear relation between the energy losses and the shape of the lower edges. It can be concluded that the shape does not influence the total amount of energy loss.

From the above figures can be concluded that the total loss of energy is not related to the shape of the lower edge or to the gate opening underneath the valve. Also can be concluded that the contraction coefficient from the rectangular-shaped lower edge is the smallest. In ascending order are following the chamfered-shaped, the point-shaped and finally the circular-shaped lower edge seal.

4.4.2 Leakage

The initial physical model showed significant leakage between the valve plate and the side walls of the flume. A device has been used to guide the flow away from the side walls and decrease the amount of side leakage. This device is explained and shown in Appendix F. The result from this device was not significant enough to prevent the leakage. Therefore, the influence of the leakage could not be determined correctly. In addition to the minimal effect of the device on the leakage, it also initiated additional turbulence that could affect the results of the tests.

The amount of leakage will have an effect on the determined flow velocity. The part of the discharge underneath the valve will be lower and therefore also the flow velocities. In addition to the effect on the determination of the velocity the leakage also affects the damping of the system. In a two-dimensional model (as was pursued in this case) the leakage is not included.

It is recommended to test the effect of leakage in future research. Especially, because a real-life design will also experience small amounts of leakage through the sides. The effect of leakage can be tested by designing a model that prevents leakage and compare those results with the results from a test with leakage.

4.4.3 Dynamic Amplification Factor

An important factor during the design of a valve are the forces on the operating machinery. These forces depend partly on the dynamic amplification factor (DAF) that increases the force on the lower edge of the valve through the dynamical system. The dynamic amplification factor is a dimensionless number that describes how often the force caused by a static load should be multiplied when a dynamic load is applied. The current design rules focus on this amplification factor and prescribe a maximal amplification factor of 1.1 [33]. A more detailed explanation of the factor can be found in Appendix B. Figure 4-33 shows a schematization of the model set-up, including damping and spring stiffness.

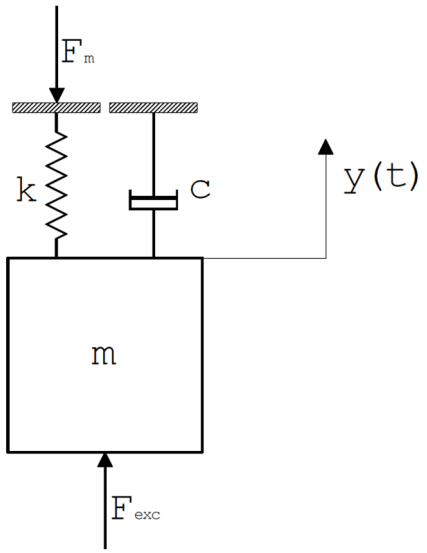

Figure 4-33: Schematization of forces on the valve in the model set-up

The force of an extreme stiff ($k \rightarrow \infty$) situation should be compared with a force retrieved from a similar situation but with a lower stiffness to get a better insight of the amplification factor. The extreme stiff test simulates the static situation. The relative difference (increase or decrease) in force is the amplification factor of the specific situation. This amplification factor should be related to the relative frequency (f/f_n), to see with which values the amplification factor is the largest. The current tests executed with a stiffness to infinity, however, did not record a proper force due to the placement of the load cell parallel to a massive block of wood. Appendix F gives a more detailed explanation of this model set-up.

Because of the above mentioned reason, an exact dynamic amplification factor cannot be determined. For that reason, an approximation is tried. In equation 4.14 the equation of motion of Figure 4-33 is shown. It should be noted that the force measured is equal to the force in the spring, because it is the connection between the valve plate and the stationary world. The damping is not connected to the load cell and is therefore displayed separate from the stiffness. Therefore, the damping can be neglected in this approach.

$$F_{exc} = m \cdot \ddot{y} + c \cdot \dot{y} + k \cdot y \qquad 4.14$$

In which:

	F_m	=	measured force by load cell [N]
	y	=	vertical position [m]
	F_{exc}	=	excitation force [N]
	m	=	mass of valve [kg] = 9.0 kg
	c	=	structural damping [Ns/m]

Because the force in the spring is measured, the expression from equation 4.15 is valid. With the given assumptions equation 4.14 can be rewritten to equation 4.16.

$$F_m = k \cdot y \rightarrow y = F_m/k \rightarrow \ddot{y} = (1/k) \cdot \ddot{F}_m \quad 4.15$$

$$F_{exc} = F_m + m \cdot \ddot{y} = F_m + \frac{m}{k} \cdot \ddot{F}_m = F_m + \omega_0^{-2} \cdot \ddot{F}_m \quad 4.16$$

When assumed is that the force is sinusoidal (equation 4.17), the equations above can be rewritten to equation 4.18. From this equation the amplitude of the excitation force can be derived. This amplitude is the amplitude of the movement, multiplied with the factor: $1 - (\omega/\omega_0)^2$.

$$F_m = a \cdot \sin(\omega \cdot t) \quad 4.17$$

$$F_{ex} = \left(a - a\left(\omega/\omega_0\right)^2\right) \cdot \sin(\omega \cdot t) \quad 4.18$$

The measured force (F_m) is compared with the pressure force (F_p) to get a slight idea of the amplification factor. The pressure force is determined by multiplying the measured pressure with the surface of the lower edge. From the measured force the self-weight of the valve is subtracted ($9 \cdot 9.81 = 88.3$ N). The results are plotted against the frequency ratio (f_{exc}/f_n) and shown in Figure 4-34 (L). Notable are the lines which seem to increase. Figure 4-34 shows that the increase can be explained by the natural frequency of the system.

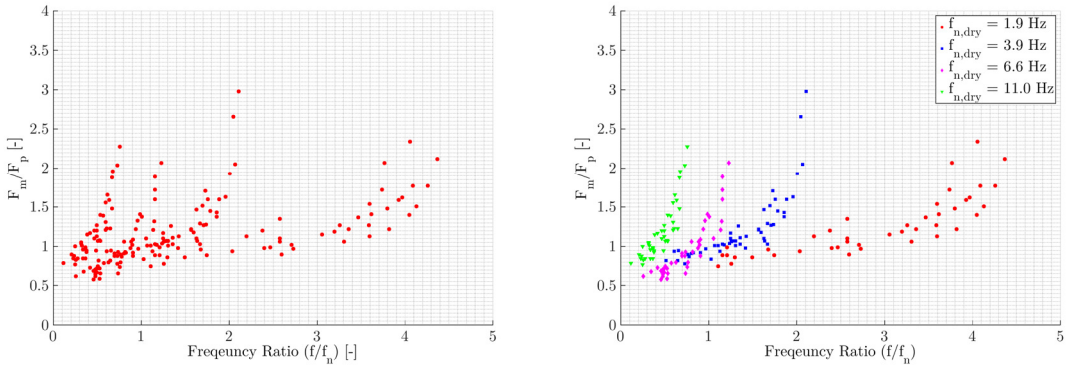

Figure 4-34: Ratio Fm/Fp versus the frequency ratio

A peak at a frequency ratio of 1.0 would be expected, so a form of resonance would be shown. The excitation frequencies used in Figure 4-34 are based on the Strouhal number as determined in the previous paragraph ($S = 0.13$). Therefore, the frequencies have a linear relationship with the flow velocity. Bernoulli's principle says that the pressure decreases when the speed increases. This explains the shape of the graphs. Equation 4.19 gives the steps of this argumentation.

$$U\uparrow \rightarrow f\uparrow \,\&\, p\downarrow \rightarrow f/f_n\uparrow \,\&\, F_m/F_p\uparrow \quad 4.19$$

It can be concluded that this method does not give any information regarding the dynamic amplification factor. A proper result regarding the dynamic amplification factor could be found when the vertical force is measured in the extreme stiff tests. If this force is compared with tests under the same conditions with a low stiffness vertical suspension a clearer and proper view on the amplification factor can be obtained. The next paragraph will go deeper into the vertical force equilibrium.

4.5 Vertical Forces

The final elaboration of the previous paragraph could be a first step in the determination of any vertical forces on the model. The vertical forces discussed in this paragraph have been divided into two sections. These sections are:

- External Force (§ 4.5.1). This paragraph focussed on the vertical force equilibrium between the two measured forces (by the load cell and the pressure sensor) and the self-weight of the model. The result of the elaboration will be any external forces working on the model.
- Hydraulic Down Pull Force (§ 4.5.2). One of the forces resulting from the first paragraph will be the hydraulic down pull force. The hydraulic down pull force will be elaborated in this paragraph.

4.5.1 External Force

When no external forces work on the model the forces measured by the load cell and pressure sensor should make an equilibrium with the mass of the valve. An overview of the forces is shown in Figure 4-35.

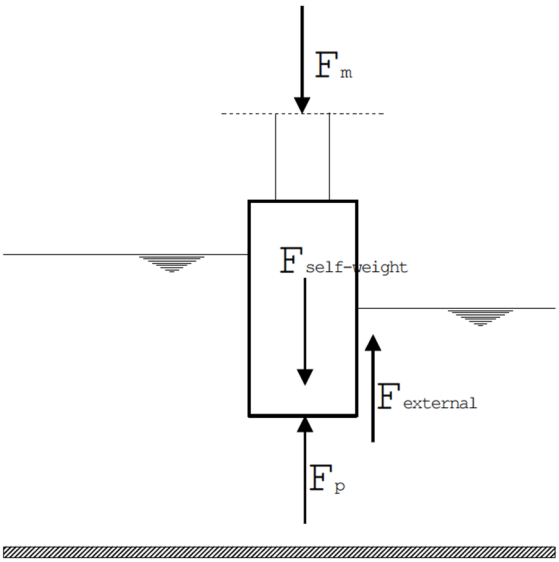

Figure 4-35: Overview of the main vertical forces

The total mass of the valve is known (§ 3.2). The other known forces are the force measured by the load cell (F_m) and the force measured by the pressure sensor under valve (F_p). Here is checked if any other external vertical forces are present in the model. An equilibrium situation of these forces is given in equation 4.20.

$$F_{external} = F_{sw} - F_p - F_m \qquad 4.20$$

In which:

F_m	=	force measured by load cell [N]
$F_{external}$	=	external force [N]
F_{sw}	=	force due to self-weight [N]
F_p	=	force measured by pressure sensor [N]

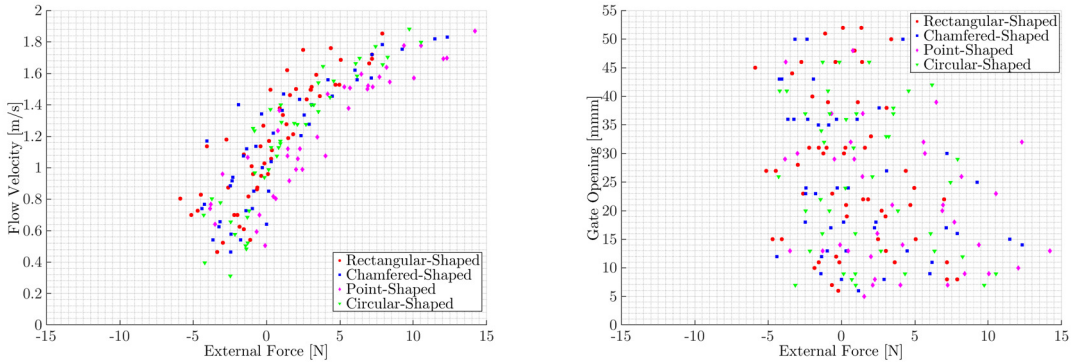

Figure 4-36: The calculated external force versus the flow velocity (L) and the gate opening (R)

Figure 4-36 shows the results of equation 4.20 with the average forces retrieved from the test data. The right figure shows a scatter around an external force of 0 N. This means that the present external force does not depend on the gate opening. The left figure on the other hand shows an increase in the external force as the flow velocity increases. This increase could be explained by a vertical force in the horizontal tensioned wire. The wire has not been tensioned completely horizontal but under a small angle. The increase in flow velocity is coupled to an increase in head difference. An increase in head difference means a larger horizontal force on the valve and because of the small angle a larger vertical force due to the wire. Therefore, it can be concluded that the tensioned wire has an effect on the model. The related vertical force could influence the results of the tests.

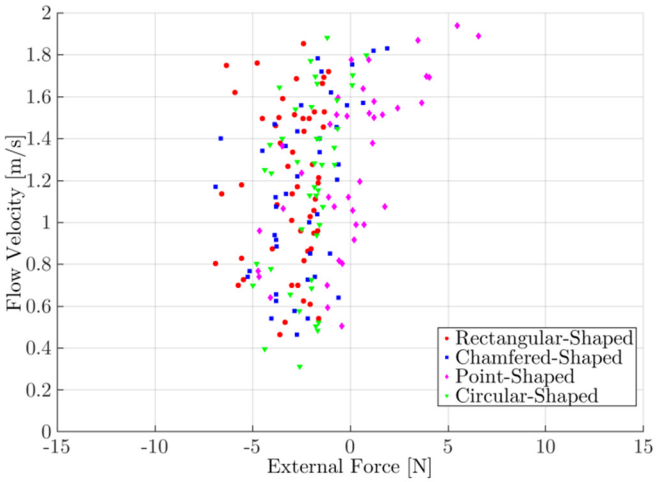

Figure 4-37: Calculated external force as function of the flow velocity adjusted for the vertical wire force.

Figure 4-37 shows the same graph as presented in Figure 4-36 (L). However, this graph has been adjusted for the vertical wire force. An approximation of the force is based on the head difference (ΔH) and the angle of the wire. The figure shows that the external force slightly tends to the negative side. This could imply that a down pull force is present. The down pull force will be elaborated in the next paragraph.

4.5.2 Hydraulic Down Pull Force

In the previous paragraph the presence of the vertical force due to the wire has been proved. Another force seems to be present as well. This force is assumed to be the hydraulic down pull force. In Figure 4-38 the hydraulic down pull force has been added to the vertical force equilibrium. Earlier research proved that the hydraulic down pull force relates to the shape of the valve. A formula for the down pull force is shown in Equation 4.22 [17].

$$F_{down\,pull} = \gamma \cdot K \cdot A \cdot \Delta H \qquad 4.21$$

In which:

$F_{downpull}$	=	down pull force [N]
γ	=	specific weight of water [N/m^3]
K	=	hydraulic down pull coefficient [-]
A	=	cross-sectional area of the valve [m^2] = b · W

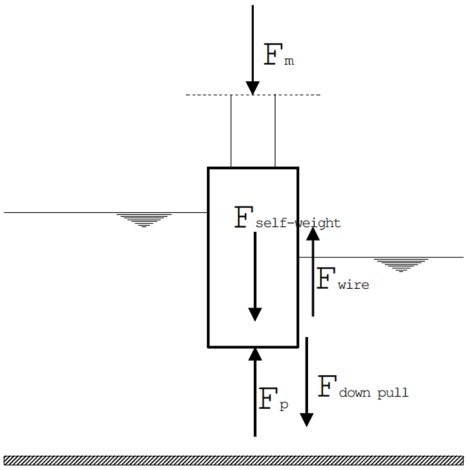

Figure 4-38: Overview of the vertical forces adjusted for the wire force

Based on the equilibrium state of Figure 4-38, an estimation can be made for the hydraulic down pull force ($F_{downpull}$) and the down pull coefficient (K) of the model. The estimation of the down pull coefficient is shown in Figure 4-39. Earlier research indicated that the shape of the lower edge could affect the down pull coefficient [17].

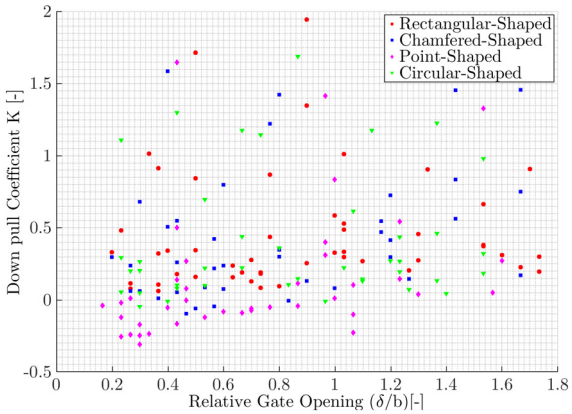

Figure 4-39: Down pull coefficient versus the relative gate opening

The figure above shows that there is no clear relation between the relative gate opening and the down pull coefficient as determined during this research. This means that the test data does not give a clear view on the down pull force. The shape of the lower edge seal does not affect the down pull coefficient.

4.6 Real-Life Prototype

In the final paragraph of this chapter the results from the previous paragraphs will be compared to a real-life design. Two real-life designs are used for this comparison. In the further course of this paragraph, these designs will be named prototype #1 and prototype #2. The comparison between the model and the prototypes has been made with help of the determined dimensionless Π-factors and the test conditions as presented in Chapter 3. The discussed items are:

- Length scale (§ 4.6.1);
- Dynamic characteristics (§ 4.6.2);
- Reynolds scale (§ 4.6.3);
- Excitation frequency (§ 4.6.4);

4.6.1 Length Scale

The first point of focus is the length scale of the model compared to the prototypes. Two important length scales are discussed in this paragraph. The two relevant lengths are:

- The dimensions of the valve (W, b and D). Special attention is paid to the thickness of the valve, because this length has a direct influence on the flow-induced vibrations.
- The head difference over the valve (ΔH). The head difference is a measure for the flow velocity.

Dimensions

The most important dimension of the valve design regarding the vibrations is the thickness of the valve (b). In the model set-up of this research the thickness of the valve was 30 millimetres. The thickness of the real-life designs are 200 millimetres (#1) and 500 millimetres (#2). The thickness used is the thickness of the lowest part of the valve. In some designs the thickness varies over the height of the valve. Table 4-9 displays also other relevant dimensions of the model set-up in comparison with the prototypes.

	Model	Prototype #1	Prototype #2
Width of the valve W [m]	0.4	1.8	2.4
Height of the valve D [m]	0.4	2.25	3.0
Thickness of the valve b [m]	0.03	0.2	0.5
Length scale related to the thickness [-]	-	6.7	16.7

Table 4-9: Dimensions of model versus prototypes

Table 4-9 shows that the length scale of the prototypes (related to the gate thickness) is 6.7 for prototype #1 and 16.7 for prototype #2. This was expected because the tests are executed on a scale model.

Head Difference

The head difference of real-life navigation locks varies much The head difference of the prototypes are shown in Table 4-10. The flow velocity underneath the valve depends on the head difference. The flow velocities are also shown in Table 4-10. The determined velocities will be used in the further course of the chapter to show the scale of the Reynolds number.

	Model	Prototype #1	Prototype #2
Maximal head difference ΔH [m]	0.2	9.9	5.0
Maximum flow velocity U [m/s]	1.9	13.9	9.9

Table 4-10: The head difference and the flow velocity of the model and the prototypes

It should be noted that the head differences in Table 4-10 are without the additions of a dynamic safety factor. In some cases, this safety factor is applied and the head difference in the calculations is larger. Safety factors are neglected to compare with a real-life situation.

4.6.2 Dynamic Characteristics

This paragraph will focus on the comparison of the dynamic characteristics of the model with the dynamic characteristics of the two prototypes. The dynamic characteristics discussed are:

- the mass;
- the stiffness;
- the damping.

Mass

The mass of the valve in the model set-up and of the valves of the prototype is given in Table 4-11. The table also gives the density ratio (Π_s) as a dimensionless scaling factor.

		Model	Prototype #1	Prototype #2
Total mass [kg]		9.0	1 500	2 800
Density ratio [-]	$\frac{m}{V \cdot \rho_w}$	1.9	1.9	0.8

Table 4-11: Mass of model set-up and prototypes

The values from the table show that the model and prototype #1 are similar regarding the density ratio. Prototype #2 has a relative lower density.

Stiffness

Table 4-12 shows the variations of the Cauchy number (presented in Chapter 3) that have been achieved during the research.

Flow velocity [m/s]	**0.3**	**1.9**
Stiffness [N/mm]		
1.16	430	11
5.34	1 978	49
15.66	5 800	145
43.2	16 000	399

Table 4-12: Cauchy numbers reached during the research

	Model	Prototype #1	Prototype #2
Stiffness [N/m]	See Table 4-12	67 400 000	99 000 000
Cauchy number [-]	11 – 16 000	1735	2018

Table 4-13: Stiffness of model and prototypes

Table 4-13 shows the dimensionless Cauchy numbers from the two prototypes. It shows that the prototypes have a Cauchy number that falls within the variation achieved during the physical model tests. The presented Cauchy numbers seem to correspond the best with the 5.35 N/mm vertical stiffness and the low flow velocity (0.3 m/s).

Damping

The damping of a real-life prototype is not known or investigated. The damping is caused to a large extent by the friction between the skin plate of the valve and the seals attached to the culvert. A drawing of such a connection is shown in Appendix A. The friction depends on the head difference and the (static and dynamic) friction coefficient of the two materials (the skin plate and the seal). Because the damping due to friction cannot be modelled as viscous damping (by a dashpot) a new schematization is given in Figure 4-40. The friction in this case is called Coulomb friction [30].

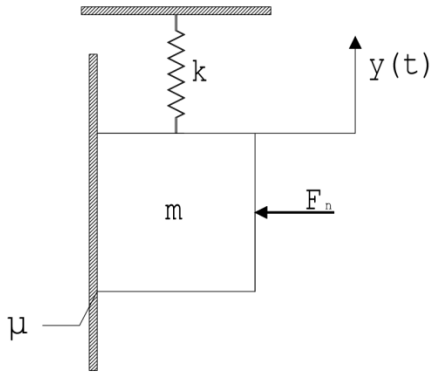

Figure 4-40: Schematization of the dynamic model with friction

The conditions for this type of friction are shown in equation 4.23 [11]. The overall equation of motion (equation 4.22) is non-linear because it changes with every half period of the vibration. The current used friction coefficient (μ) for a valve in a culvert is 0.2 [42]. This is the static coefficient for stainless steel on UHMWPE (Ultra-high-molecular-weight polyethylene) and is over dimensioned because it is used to determine vertical force needed for the hydraulic cylinder. UHMWPE is a plastic material often used in the guidance elements of the valve. In this example this value is used for both prototypes.

$$m\ddot{x} + kx = F_c(\dot{x}) \tag{4.22}$$

$$F_c(\dot{x}) = \begin{cases} -\mu \cdot F_n & \dot{y} > 0 \\ 0 & \dot{y} = 0 \\ \mu \cdot F_n & \dot{y} < 0 \end{cases} \tag{4.23}$$

In which: F_c = friction force [N]
F_n = normal force [N]
μ = friction coefficient [-]

The normal force shown in Figure 4-40 is the hydrostatic force due to the head difference (ΔH). Based on the head differences from Table 4-10 and the earlier described dimensions a first estimation for the friction force can be made. The friction forces are shown in Table 4-14.

	Prototype #1	**Prototype #2**
Maximal head difference ΔH [m]	9.9	5.0
Normal force F_n [N]	393 000	353 000
Friction force F_c [N]	79 000	71 000

Table 4-14: Vertical maximum friction forces of the prototypes

The Coulomb friction can be approximated by an equivalent viscous damping. This can be done by comparing the dissipated energy of the two types of damping. When the energy equals the equivalent viscous damping of the Coulomb friction is found. Equation 4.24 (Coulomb friction) and equation 4.25 (viscous damping) show the dissipated energy per damping type [11]. The dissipated energy is the damping force

multiplied by the covered distance and can therefore be approached by the surface of the graphs in Figure 4-41.

$$E_F = 4 \cdot F_c \cdot \Delta y \quad 4.24$$

$$E_D = \pi \cdot c \cdot \omega \cdot \Delta y^2 \quad 4.25$$

In which:

E_F	=	energy dissipated by coulomb friction [Nm]
E_D	=	energy dissipated by viscous damping [Nm]
F_c	=	friction force [N]
Δy	=	deflection [m]
c	=	damping [Ns/m]
ω	=	radial frequency of the force [rad/s]

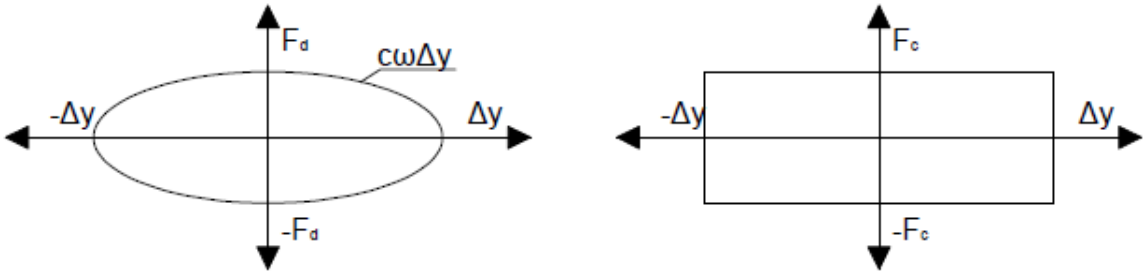

Figure 4-41: (L) Viscous damping force versus amplitude & (R) Friction force versus amplitude

From the dissipated energy equations above the equivalent viscous damping of the coulomb damping can be derived. The equivalent viscous damping is shown in equation 4.26.

$$c_{eq} = \frac{4 \cdot F_c}{\pi \cdot \omega \cdot \Delta y} \quad 4.26$$

For the angular frequency (ω) two values are used. The natural angular frequency and the angular frequency of the force as determined in the next paragraph. Only the deflection (Δy) is unknown. The deflection is more difficult to estimate, because it was difficult to identify the value in the model. It is assumed that the deflection in the model is only 2.0 mm. This deflection is made dimensionless with the length factor π_9 ($\Delta y/b$) from the dimensional analysis. The ratio is 0.033. With the ratio the amplitudes of the prototypes have been estimated. The damping factor of the model under water has already been determined in § 4.2 and was 0.026.

	Model	**Prototype #1**	**Prototype #2**
Estimated deflection Δy [mm]	2.0	13.3	33.3
Natural angular frequency ω_n [rad/s]	-	212.0	188.0
Equivalent viscous damping c_{eq} [Ns/m] (with ω_n)	-	35 400	14 300
Damping factor ζ [-] (with ω_n)	0.026	0.056	0.014
Angular frequency of force ω [rad/s]	-	61.8	17.4
Equivalent viscous damping c_{eq} [Ns/m] (with ω)	-	122 600	154 800
Damping factor ζ [-] (with ω)	0.026	0.193	0.147

Table 4-15: Damping characteristics of the model and the prototype

Table 4-15 shows that a first estimate of the damping factor of the prototypes is comparable to the damping factor of the model. The elaboration above shows that the damping in the system is comparable to the damping in the model. This means that the response of the system is expected to be similar (with similar stiffness and mass). The damping described above is only due to friction, while there are other elements (for example the hydraulic cylinder and the guidance elements) that also add damping to the system. It is assumed that the damping due to these elements is relatively low.

4.6.3 Reynolds Number

The variation of the Reynolds number strongly depends on the earlier discussed length scale and the flow velocity. The Reynolds numbers achieved during the steady state tests have been extensively discussed in § 4.2. Table 4-16 shows the Reynolds numbers related to the prototype. It should be noted that the characteristic length in this determined Reynolds number is varied. Because in other literature other characteristic lengths could be used. For this reason, the Reynolds numbers calculated are related to the height of the culvert (D), the hydraulic diameter (D_H) and the gate thickness (δ). The results are shown in Table 4-16.

		Model	Prototype #1	Prototype #2
Reynolds number [-]	$Re = \frac{U \cdot \rho \cdot b}{\mu}$	$0.9 \cdot 10^4 - 5.7 \cdot 10^4$	$2.9 \cdot 10^6$	$5.0 \cdot 10^6$
Reynolds number [-]	$Re = \frac{U \cdot \rho \cdot D}{\mu}$	$1.2 \cdot 10^5 - 7.6 \cdot 10^5$	$3.1 \cdot 10^7$	$3.0 \cdot 10^7$
Reynolds number [-]	$Re = \frac{U \cdot \rho \cdot D_H}{\mu}$	$0.3 \cdot 10^5 - 1.9 \cdot 10^5$	$7.0 \cdot 10^6$	$6.6 \cdot 10^6$

Table 4-16: Reynolds numbers of model and prototypes

From Table 4-16 can be concluded that the Reynolds numbers in the model are smaller than the Reynolds numbers reached in the prototypes. This Reynolds number influences the Strouhal number and therefore the excitation frequency. It can be concluded that the excitation effect will differ in a larger scale prototype.

4.6.4 The Excitation Frequency

In § 4.3 a Strouhal number was found related to the excitation frequency (S = 0.13). This was done by capturing a relation between the excitation frequency (f_{exc}), the flow velocity (U) and the thickness of the valve (b). In this paragraph this process is reversed and are possible excitation frequencies coupled to the different Strouhal numbers and prototypes. These approximations are based on the maximum values of the flow velocity. Table 4-17 shows the results from these approximations. This frequency has also been used by the determination of the damping (§ 4.6.2).

	Prototype #1	Prototype #2
Excitation frequency (f_{exc}) from Strouhal number $\left(S = \frac{f_{exc} \cdot b}{U} = 0.13\right)$	9.76 Hz	2.77 Hz

Table 4-17: Predicted excitation frequencies (f_{exc}) of the prototypes related to the determined Strouhal number (S)

With this approximation should be kept in mind that this frequency only includes the lower frequency peak. Also has the statement from § 4.6.3 (regarding the Reynolds number) a major effect on the existence of the turbulence and other instability effects of the flow. Therefore, the values from Table 4-17 are expected to be not fully correct. The calculation done here is purely based on the experienced effects of this research (§ 4.3) and is not used in de real-life designs.

	Model	Prototype #1	Prototype #2
Natural Frequency [Hz]	1.81 -11.0	33.74	29.93
Frequency Ratio [f_{exc}/f_n]	-	0.29	0.09

Table 4-18: Natural frequencies of the physical model and the prototypes

Table 4-18 shows the natural frequencies and the frequency ratios of the prototypes It can be concluded, provided that the excitation frequencies are correct, that the prototypes are out of the critical area of resonance. This critical area is when $f_{exc}/f_n = 1.0$.

4.6.5 Conclusion

Table 4-19 gives an overview of the most important scaled characteristics from the model to the two real-life prototypes.

#	Name	Formula	Model	Prototype #1	Prototype #2
Π_2	Cauchy number	$\frac{k}{U^2 \cdot \rho \cdot b}$	10.7 – 16 000	1735	2018
Π_3	Reynolds number	$\frac{U \cdot \rho \cdot b}{\mu}$	$9.0 \cdot 10^3 – 5.7 \cdot 10^4$	$2.9 \cdot 10^6$	$5.0 \cdot 10^6$
Π_5	Damping factor	$\frac{c}{2\sqrt{km}}$	0.026	0.056	0.014
Π_8	Density ratio	$\frac{m}{V \cdot \rho_w}$	1.9	1.9	0.8
	Length scale		-	6.7	16.7

Table 4-19: Comparison of the important characteristics of model and the prototypes

The table above shows that the Reynolds numbers as reached in the model are much lower than are reached in a real-life situation. This difference could influence the excitation frequency, because the Reynolds number has a large impact on the stability of the flow, which is related to the excitation frequency.

The damping in the real-life prototypes is a different type of damping than the damping found in the model. The damping found in the model was assumed to be viscous, where the damping in a design from reality is a damping due to friction, also called Coulomb damping. The real value of damping in the prototypes is not known yet. An equivalent viscous damping can be found for the Coulomb damping. When this equivalent is used the damping factor becomes very low. The damping factor of the model is similar to the damping factors of the real-life designs.

The expected frequencies differ from current design rules, because they are based on the Strouhal number found in an earlier course of this research.

Chapter 5 Conclusions and Recommendations

In this report research is done on the vertical flow-induced vibrations of a valve in a navigation lock. This has been done by performing tests on a physical model in a current flume. More specifically the goal was to assess the impact of the lower edge seal shape on the excitation and response of the valve. This chapter will discuss the conclusions (§ 5.1) and recommendations (§ 5.2) resulting from the research.

5.1 Conclusions

This first paragraph gives the most important conclusions that are drawn from the research. The conclusions have been divided into the answers to the research questions (§ 5.1.1) and additional conclusions that were drawn during the research that has been carried out or were stated in the objectives (§ 5.1.2). The research questions and objectives have been introduced in Chapter 1.

5.1.1 Research Questions

Below an overview of the answers to the research questions is given. A distinction has been made between sub-questions and the main research question, as was done in Chapter 1.

Main Question

What is the effect of the shape of the lower edge seal on the vertical flow-induced vibrations of a valve in a filling and emptying culvert?

The different tested seal shapes did not show any influence on the excitation frequency from the flowing water. For all the different shapes a constant Strouhal number of 0.13 has been determined (§ 4.3.2). This Strouhal number has the gate thickness as characteristic length. The value of this number is influenced by other factors that will be discussed in the further course of this paragraph.

Not in all cases a clear dominant response peaks could be distinguished. The chamfered-shaped lower edge showed to be the most sensitive to vertical excitations. 60% of the total tests executed with this shape showed a clear frequency response. The chamfered-shaped lower edge is followed by the rectangular-shaped (54%), the circular-shaped (20%) and eventually the point-shaped (16%) (§ 4.3).

The shape also has an effect on the amplitude of the vibration. The rectangular-shaped lower edge showed significantly larger amplitudes compared to the other shapes. The point-shaped lower edge showed the smallest amplitude in the vibrations (§ 4.3.3). These amplitudes have an effect on the vertical forces in the hydraulic cylinder.

Sub-Questions

What are the critical conditions for the initiation of the flow-induced vertical vibrations of a valve in a culvert?

The critical conditions for the initiation of the vibrations are related to the dimensionless Strouhal number. The critical range seems to be when the Strouhal number is lower than 0.3. This Strouhal number consists of the natural frequency, gate thickness and the flow velocity.

Another important parameter is the relative gate opening, the gate opening relative to the thickness of the valve. The majority of the vibrations have been experienced when this ratio is between 0.5 and 1.0. The vibrations were not experienced at all with a relative gate opening above 1.5. While the gate opening did influence the presence of the vibration it did not influence the excitation frequency.

What is the relation between the excitation frequency, response frequency of the system and natural frequency of the system?

The different frequencies have a clear theoretical relationship. The natural frequency depends on the dynamic characteristics of the model and the excitation frequency on the flow velocity and a characteristic length (brought together in the Strouhal number). The response of the system was observed not to match with the natural frequency, but to coincide with the excitation frequency.

The response frequency can be divided into two critical areas. One is a low frequency response (0 – 15 Hz) related to a Strouhal number of 0.13 and the other one is a high frequency response (15 – 40 Hz) that was rarely encountered. The high frequency response was only experienced with the rectangular-shaped lower edge. This response requires more attention because of the limited appearances during these tests. Literature relates the two response frequencies to two different types of excitation. The low frequency vibrations are induced by the flow instability (IIE) and the high frequency vibrations are induced by the movement of the valve [20].

What is the difference in excitation frequency for the different lower edge seal shapes? And is this coupled to a constant critical Strouhal number for a specific shape?

The differently shaped lower edges did not show any difference in excitation frequency. For all the shapes the determined Strouhal number was similar (S = 0.13). A relationship between the Strouhal number and the Reynolds number has been experienced. With an increase of the Reynolds number ($> 3.0\ 10^4$), the Strouhal number tends to be more constant. Therefore, the Reynolds number does influence the excitation frequency (§ 4.2.2). The Reynolds variation did differ for the different seal shapes. The rectangular-shaped seal showed to be less impacted by a change in the Reynolds number. The other three shapes (the chamfered-shaped, point-shaped and circular shaped) showed a similar larger variation.

What is the impact of the shape of the lower edge seal on the vertical hydraulic down pull force? And is there a clear way to quantify the value of the hydraulic down pull force?

It is not possible to quantify the hydraulic down pull force on the lower edge of the valve with this test data. In literature the down pull coefficient varied per investigated valve [17]. Without the down pull coefficient, there is no clear way to determine the down pull force analytically. The down pull force depends on the turbulence of the flow, which is unpredictable. The force depends on a lot of other factors as well; flow velocity, gate opening, gate thickness, up- and downstream water level. The point-shaped lower edge seal seemed to have an effect on the hydraulic down pull, because the determined coefficients were the smallest.

5.1.2 Additional Conclusions

In addition to the research questions answered in the previous section, some other conclusions were drawn from the results of the physical model test or the literature study. Some of these conclusions are related to the defined objectives in Chapter 1 or can be coupled to a paragraph of Chapter 4.

Information of the effect of the lower edge seal shape, as used in practice, on the flow-induced vibrations is lacking in current literature (§ 2.2).

One of the objectives was to make an inventory of the existing and the missing information of the vibrations of the valve. Most of the work related to this objective has been done in the literature study. From the earlier research it was concluded that information regarding the effect of the shape of the lower edge was missing in the existing literature. Especially, the information regarding the seal shapes used in practice is lacking. Previous studies were mainly executed using only basic shapes and not shapes as used in practice.

It is possible to test the flow-induced vibrations of a valve with a physical model test (§ 3.2).

Another objective of the research was to design and construct a model set-up that was able to experience the effects of cross-flow induced vibrations. This research proved that it is possible to create an accurate physical model. 40% of all executed steady state measurements showed a clear response frequency. The model has been compared to real-life prototypes. During this comparison it was noted that the real-life Reynolds numbers are much larger than reached in the model. These differences are relatively large and play a significant role in the excitation due to the flowing water. In addition to the real-life Reynolds number, the real-life damping is a different type of damping than found in the model. In real-life the system contains coulomb damping, which is a non-linear type of damping, compared to the viscous damping in the model, which is linear damping.

The structural damping of the model has an effect on the resonance frequencies of the valve (§ 4.2.1 & § 4.6).

The structural damping in the model influenced the amplitude and the conditions in which the vibrations occurred. The damping under water was larger than the damping above water. The flow velocity and the gate opening underneath the valve have an impact on the damping as well. From the literature study followed that the presence of damping decreases the resonance frequency ($f_{exc}/f_n < 1$). This shift brings the current design natural frequency ($f_n = 3 \cdot f_{exc}$) closer to the resonance frequency. It also lowers the amplification factor which is a positive contributor when it comes to a vibration free design of valves.

The Reynolds number influences the Strouhal number (§ 4.2.2).

A clear relation between the Strouhal number and the Reynolds number was found. The Strouhal number tends to become constant with larger Reynolds numbers ($Re > 3 \quad 10^4$). The Strouhal number related to the rectangular-shaped lower edge is less dependent on the variation in the Reynolds number compared to the other shaped lower edges. Therefore, the rectangular-shaped lower edge behaves more predictable.

The response of the valve is in agreement with the excitation frequency and not with the natural frequency (§ 4.3.3).

The response of the system was not in agreement with the natural frequency of the system. It was expected that the system would vibrate in a frequency close to the natural frequency. However, this was not experienced. Instead the majority of the vibrations were experienced close to the excitation frequency. Also no signs of the lock-in effect were experienced, in which the excitation frequency was clearly affected by the natural frequency.

The different shapes of the lower edge seal have varying contraction coefficients, but the shape does not have an effect on the total energy loss over the valve (§ 4.4).

The different shaped lower edges have a different contraction coefficient. The total energy dissipated does not depend on the shape of the lower edge. In ascending order, the shape with the smallest contraction coefficients, hence largest contraction, are the rectangular-shaped, the chamfered-shaped, the point-shaped and the circular-shaped. The shape only affects the flow behaviour under the valve. The overall flow behaviour is similar for all different kind of lower edge shapes.

5.2 Recommendations

In this paragraph an overview is given of the recommendations, following from the research carried out. The recommendations are divided into two subsections to give a more clear overview. These subsections are:

- Possible future research (§ 5.2.1);
- The physical model test (§ 5.2.2).

5.2.1 Possible Future Research

The recommendations in this paragraph involve possible research in the future.

More research has to be done to get a more realistic view on the damping of a real-life design (§ 4.6.2).
During the research the effect of damping on the vibrations was a recurring subject. The damping has an effect on the response frequency of the system (the resonance frequency is affected) and on the amplitude of the vibration (the amplification factor). It appears no information exists of damping in a real-life situation. It is recommended to do more research on the real-life damping of a vertical lift valve in a filling and emptying culvert.

More research has to be done on the effects of the excitation related to the value of the Reynolds number (§ 4.2.2 & § 4.6.3).
The Reynolds numbers reached during the tests have been significantly lower than the Reynolds numbers during a real-life prototype. It was found that the Reynolds number has an effect on the excitation frequency (Strouhal number). Because the real-life Reynolds numbers are much larger (§ 4.6) the excitation frequency may differ from the results from this physical model test. The Reynolds number also has an effect on the instability of the flow. With higher Reynolds number the flow tends to get unstable faster and instability induced vibrations could occur at different conditions. Therefore, it is recommended to do more research in situations with a higher Reynolds number. Preferably, the tests should be executed with Reynolds numbers comparable to real-life situations. This can be achieved by using a larger flume and a larger scale model or use a different substance (for example air).

The influence of the water levels on both sides of the valve on the flow-induced vibrations should be investigated (§ 4.2.3).
The influence of the water level on both sides of the valve on the excitation is an underexposed subject during this research. The water level and water head will be considerably larger in a design from reality. A lack of data made a proper conclusion regarding this influence impossible. Therefore, it is advised to do more research regarding the influence of the up- and downstream water level on the excitation due to the flowing water. During these tests the gate opening and the water head over the valve should be kept constant and only the water levels on both sides of the valves should be varied. The water levels could influence the phenomena in the form of added water effects (mass, stiffness and damping). An important point of notice is that the model was in an open current flume where the real-life valve is positioned in a closed culvert. In a closed culvert the flow conditions can differ significantly from an open flume. The surface effects will also have less influence in a closed culvert.

5.2.2 The Physical Model Test

This paragraph includes recommendations specifically focussed on the model set-up used during this research. It will give advice regarding modifications to fulfil the recommendations made in § 5.2.1 and optimising the current model set-up.

The position of the pressure sensor in the lower edge should be optimised.

During this research the pressure sensor was integrated in the lower edge and in contact with the flowing water through a small tube. This tube is vulnerable for the entrance of air and therefore possibly influencing the results. In some cases, abnormal pressure data was found, which could be related to this aspect. In addition to the one pressure sensor used during this research a model could be manufactured with multiple pressure sensors. In the current research the pressure was only measured at the centre of the lower edge, fluctuations can, however, occur over the whole thickness of the valve. Therefore, important fluctuations could not be present in the research data.

The position of the load cell in a vertically extreme stiff test should be adjusted.

During the test with an extreme stiff situation it was chosen to lock the movable part with an extremely stiff object. The object was situated parallel to the load cell and, therefore, the results retrieved from the load cell during the extreme stiff situation were not usable. It is advised to make the model extremely stiff by connecting the side of the valve with the side of the possible flume. Consequently, it will be possible to measure the force during the extreme stiff situation.

The effects of leakage of water between the valve plate and the side walls should be investigated more thoroughly.

This research was not able to show the effects of the leakage between the valve and the wall. This leakage could influence the vibration phenomena because of added damping and stiffness. The solutions tried to prevent leakage during did not give sufficient results. A model should be created with minimal leakage and minimal added dynamic characteristics to get a proper insight of the effect of leakage.

A more accurate method to measure small vertical displacements should be found.

The displacements experienced were very small and therefore often not measured by the used laser sensor. A future possibility will be to use an accelerometer attached to the valve which is able to measure accurate accelerations. Accelerometers are often more sensitive. The measured accelerations can also be used during an accurate calculation of the amplification factor (§ 4.4.3).

A solution should be found to improve the horizontal support of the valve model without the use of a horizontal tensioned wire.

During first tests a significant horizontal deflection was experienced because of the water head differences and the related hydrostatic force. A horizontal tension wire had to be installed to compensate for this deflection. The wire was not installed completely horizontal due to problems with the attachment. Because of this small angle the wire produced a vertical force on the model that could possibly interfere with the results (§ 4.5). It is advised to design a model without the wire or to make sure the wire is tensioned completely horizontal.

The effects of the surface waves should be minimised in any future research.

A higher upstream and downstream water level could prevent the effect of the surface waves on the results in the model. In a real-life situation the water level on both sides are much higher than in the used current flume. The model was scaled properly, but showed clear low frequency results due to surface waves. The use of a larger flume, to be able to reach larger water levels, is recommended to limit the effects of surface waves.

The effect of the mass of the movable part of the model on the response of the excitations should be investigated.

In future research the mass of the valve plate should be varied to investigate the effect of this mass. The mass influences the natural frequency but is also one of the three major forces (self-weight, buoyancy force and the hydraulic down pull force) that play a role in the vertical force equilibrium. With a same natural frequency, but different mass the force equilibrium is significant different.

References

[1] Amir, M., Nikora, V.I. & Stewart, M.T. (2014). *Pressure forces on sediment particles in turbulent open-channel flow: a laboratory study.* Journal of Fluid Mechanics 757, 458-497.

[2] Anami, K., Ishii, N. & Knisley, C.W. (2012). *Added mass and wave radiation damping for flow-induced rotational vibrations of skin plates of hydraulic gates*. Journal of Fluids and Structures 35, 213-228.

[3] Battjes, J.A. (2002). *Vloeistofmechanica*. Delft, The Netherlands: Delft University of Technology.

[4] Battjes, J.A. & Labeur, R.J. (2014). *Open channel flow*. Delft, The Netherlands: Delft University of Technology.

[5] Bendat, J.S. & Piersol A.G. (1986). *Random Data: Analysis and measurement procedures (second edition)*. New York, US: John Wiley & Sons.

[6] Blevins, R.D. (1977). *Flow-induced vibration*. New York City, US: Van Nostrand Reinhold Co.

[7] Billeter, P. (1998). *Strömungsinduzierte Schwingungen von Schützen mit mehreren Freiheitsgraden*. Zürich, Switzerland: Versuchsanstalt für Wasserbau, Hydrologie und Glaziologie der eidgenössischen technischen Hochschule Zürich.

[8] Billeter, P. & Staubli, T. (1999). *Flow-induced multiple-mode vibrations of gates with submerged discharge*. Journal of Fluids and Structures, 14, 323-338.

[9] Blauwendraad, J. (2016). *Dynamica van systemen*. Delft, The Netherlands: Delft University of Technology.

[10] Brown University. (n.d.). *Introduction to Dynamics and Vibrations*. Retrieved from: http://www.brown.edu/Departments/Engineering/Courses/En4/Notes/vibrations_forced/vibrations_forced.htm

[11] Chopra, A.K. (2000). *Dynamics of structures. Theory and Applications to Earthquake Engineering*. Upper Saddel River, US: Prentice Hall.

[12] De Jong, R.J. & Jongeling, T.H.G. (1995). *In-Flow Vibrations in Hydraulic Structures*. Delft, The Netherlands: Delft Hydraulics.

[13] De Silva, C.W. (Ed.) (2005). *Vibration and Shock Handbook*. Boca Raton, US: Taylor & Francis Group.

[14] EN 1991-1-4 (2005). *Eurocode 1: Actions on Structures Part 1-4: General Actions – Wind Actions*. Brussels, Belgium: CEN, European Committee for Standardization.

[15] EN 1993-1-4 (2005). *Eurocode 3: Design of Steel Structures. Part 1-1: General Rules and Rules for Buildings.* Brussels, Belgium: CEN, European Committee for Standardization.

[16] EN 1993-1-4 (2006). *Eurocode 3: Design of Steel Structures. Part 1-4: General Rules – Supplementary Rules for Stainless Steel.* Brussels, Belgium: CEN, European Committee for Standardization.

[17] Erbisti, P.C.F. (2014). *Design of Hydraulic Structures*. London, United Kingdom: CRC Press/Balkema.

[18] Erdbrink, C.D., Krzhizhanovskaya, V.V. & Sloot, P.M.A. (2014). *Reducing cross-flow vibrations of underflow gates: Experiments and numerical studies*. Journal of Fluids and Structures 50, 25-48.

[19] Erdbrink, C.D. & Jongeling, T.H.G. (2010). Dynamica van beweegbare waterkeringen: Trillingen in onderstroomde schuiven en uitgangspunten voor een schaalmodelopstelling. Delft, The Netherlands: Deltares. Report 1200216-00.

[20] Erdbrink, C.D. (2012). *Physical model tests on vertical flow-induced vibrations of an underflow gate: schaalmodelonderzoek verticaal trillende schuif: deel 3 analyse, resultaten en conclusies*. Delft, The Netherlands: Deltares.

[21] Ettema, R. (2000). *Hydraulic Modelling: Concepts and Practice*. Reston, US: ASCE.

[22] Frostick, L.E., McLelland, S.J. & Mercer, T.G. (Eds.) (2010). *Users guide to physical modelling and experimentation.* Leiden, The Netherlands: CRC Press/Balkema.

[23] Gatti, P.L. & Ferrari, V. (1999). *Applied structural and mechanical vibrations: theory, methods and measuring instrumentation*. London, UK: E & FN Spon.

[24] Glerum, A. & Vrijburcht, A. (Eds.) (2000). *Ontwerpen van schutsluizen: deel 1*. Utrecht, The Netherlands: Rijkswaterstaat.

[25] Glerum, A. & Vrijburcht, A. (Eds.) (2000). *Ontwerpen van schutsluizen: deel 2*. Utrecht, The Netherlands: Rijkswaterstaat.

[26] Hardwick, J.D. (1974). *Flow-induced Vibration of Vertical-lift gate*. Journal of Hydraulics division, proceedings of ASCE vol. 100, 631-644.

[27] Haszpra, O. (1978). *Modelling hydro elastic vibrations*. Budapest, Hungary: Akadémiai Kiadó.

[28] Heller, V. (2010). *Scale Effects in physical hydraulic engineering models*. Journal of Hydraulic Research 49, 293-306.

[29] Holthuijsen, L.H. (2007). *Waves in Oceanic and Coastal Waters.* Cambridge, The United Kingdom: Cambridge University Press.

[30] Inman, D.J. (2008). *Engineering Vibration, third edition.* Upper Saddle River, US: Pearson education, Inc.

[31] Jongeling, T.H.G. (1986). *Onderzoek in een hydraulisch model naar het ontstaan van in-flow trillingen in schuifranden*. Delft, The Netherlands: Delft Hydraulics Laboratory, Report M1906.

[32] Kaneko, S., Nakamura, T., Inada, F. & Kato, M. (eds.) (2008). *Flow-induced vibrations: classifications and lessons from practical experiences*. Oxford, United Kingdom: Elsevier.

[33] Kolkman, P.A. & Jongeling, T.H.G. (1996). *Dynamisch gedrag van waterbouwkundige constructies: deel A constructies in stromingen*. Delft, The Netherlands: Rijkswaterstaat.

[34] Kolkman, P.A. & Jongeling, T.H.G. (1996). *Dynamisch gedrag van waterbouwkundige constructies: deel C methoden van rekenen en experimenteel onderzoek.* Delft, The Netherlands: Rijkswaterstaat.

[35] Lewin, J. (1995). *Hydraulic gates and valves: in free surface flow and submerged outlets*. London, United Kingdom: Thomas Telford Publishing.

[36] Martins, R. (ed.) (1989). *Recent Advances in Hydraulic Physical Modelling*. Dordrecht, The Netherlands: Kluwer Academic Publishers.

[37] Massey, B. (2006). *Mechanics of Fluids, Eighth Edition*. Milton Park, United Kingdom: Taylor & Francis Group.

[38] Mathworks (2002). Signal Processing Toolbox, for use with Matlab®: User's Guide (version 6). Natick, US: The Mathworks Inc.

[39] Micro-Epsilon (n.d.). *Instruction manual optoNCDT1300 [Manual].* Ortenburg, Germany: Micro-Epsilon.

[40] Molenaar, W.F. (2011). *Hydraulic structures: locks*. Delft, The Netherlands: Delft University of Technology.

[41] Naudascher, E. & Rockwell, D. (1994). *Flow-induced vibrations: An engineering guide*. New York City, US: Dover Publications.

[42] NEN 6786 (2001). *Rules for the design of movable bridges*. Delft, The Netherlands: Het Nederlands Normalisatie-Instituut.

[43] Novak, P., Guinot, V., Jeffrey A. & Reeve, D.E. (2010). *Hydraulic Modelling – an Introduction; Principles, methods and applications.* London, UK: Spon Press.

[44] Païdoussis, M.P. (2006*). Real-life experiences with flow-induced vibration*. Journal of Fluids and Structures 22, 741-755.

[45] Solomon Jr., O.M. (1991). *PSD Computations using Welch's Method*. Albuquerque, US: Sandia National Laboratories.

[46] Schiereck, G.J. (2007). *Concise overview of scale rules in coastal engineering*. Hanoi, Vietnam.

[47] Schneeberger (n.d.). *Slides: Dynamic and Precise [Manual]*. Retrieved from: https://www.schneeberger.com/en/products/slides-and-miniature-tables/frictionless-tables/type-nkl/#downloadscatalogue

[48] Sharp, J.J. (1981). *Hydraulic Modelling*. London, UK: Butterworth & Co.

[49] Stockstill, R.L., Hammack, E.A. & Hite Jr., J.E. (2011). *Lock Culverts Valves; Hydraulic design Considerations*. Washington DC, US: U.S. Army Corps of Engineers.

[50] Sun Scale (n.d.). *STS Metric Load Cell [Manual]*. Retrieved from: http://www.adminstrumentengineering.com.au/sense/sts-metric-s-beam-load-cell-sts-metric

[51] Telgársky, R. (2013). *Dominant frequency Extraction*. Albuquerque, US: Central New Mexico Community College.

[52] Thang, N.D. & Naudascher, E. (1986). *Self-excited vibrations of vertical-lift gates*. Journal of Hydraulic Research 24, 391-404.

[53] Thang, N.D. (1990). *Gate Vibrations due to unstable flow separation*. Journal of Hydraulic Engineering 116, 342-361.

[54] Totten, G.E. & De Negri, V.J. (eds.) (2012). *Handbook of hydraulic fluid technology*. Boca Raton, US: CRC Press Taylor & Francis Group.

[55] Trelleborg (n.d.). *Rubber hydraulic seals: technical manual [Manual]*. Retrieved from: http://www.trelleborg.com/en/engineered-products/products--and--solutions/seals/membrane--seals.

[56] Uwland, J. (1979). *Stabiliteitsgedrag van schuiven met diverse onderrandvormen, bij een vertikale bewegingsmogelijkheid*. Delft, The Netherlands: Delft Hydraulics Laboratory, Report M1490.

[57] Vereide, K., Lia, L. & Nielsen, T.K. (2015). *Hydraulic scale modelling and thermodynamics of mass oscillations in closed surge tanks*. Journal of Hydraulic Research 53:4, 519-524.

[58] Vrijling, J.K., Bezuyen, K.G., Kuijper, H.K.T., Van Baars, S., Molenaar, W.F. & Voorendt, M.Z. (2015). *Manual Hydraulic Structures*. Delft, The Netherlands: Delft University of Technology.

[59] Vrijer, A. (1977). *Toegevoegde watermassa en instabiele trillingen van schuiven met een vertikale bewegingsmogelijkheid*. Delft, The Netherlands: Delft Hydraulics Laboratory, Report M1322.

[60] Weaver, D.S., Adubi, F.A. & Kouwen, N. (1978). *Flow Induced Vibrations of a Hydraulic Valve and their elimination*. Journal of Fluids Engineering 100, 239-245.

[61] Welch, P.D. (1967). *The use of Fast Fourier Transform for the estimation of power spectra: A method based on time averaging over short, modified periodograms*. IEEE transactions on audio and Electroacoustic, Vol AU-15, 70-73.

[62] Willems, J. & Busscher, T. (2015). *Het leervermogen versterkt: aanbevelingen voor de Nederlandse sluizensector*. Groningen, The Netherlands: the University of Groningen.

[63] Zahari, M.A. & Dol, S.S. (2015). *Effects of Different Sizes of Cylinder Diameter on Vortex-Induce Vibration for Energy Generation*. Journal of Applied Sciences 15, 783-791.

[Page intentionally left blank]

Nomenclature

Symbol	Description	Unit
A	Amplification factor	-
b	Gate thickness	m
c	Damping	Ns/m
c_{cr}	Critical damping	Ns/m
c_w	Added water damping	Ns/m
Ca	Cauchy number	-
d	Submergence depth of valve	m
D_H	Hydraulic diameter	m
D	Height of the culvert/Height of the valve	m
E	Young's modulus	N/m^2
Eu	Euler number	-
f	Frequency	$Hz = s^{-1}$
f_{exc}	Excitation frequency	$Hz = s^{-1}$
f_n	Natural frequency	$Hz = s^{-1}$
$f_{n,air}$	Natural frequency in air	$Hz = s^{-1}$
$f_{n,wet}$	Natural frequency under water	$Hz = s^{-1}$
$f_{n,damped}$	Damped natural frequency	$Hz = s^{-1}$
f_{resp}	Response frequency	$Hz = s^{-1}$
$f_{resonance}$	Resonance frequency	$Hz = s^{-1}$
F	Force	N
$F_{buoyancy}$	Buoyancy force	N
$F_{downpull}$	Hydraulic down pull force	N
F_{hor}	Horizontal force	N
F_m	Force measured by load cell	N
F_p	Force due to pressure measured with pressure sensor	N
F_{sw}	Self-weight	N
F_{upward}	Upward force	N
F_{ver}	Vertical force	N
Fr	Froude number	-
g	Gravitational acceleration	m/s^2
H	Water level	m
H_1	Upstream water level	m
H_2	Downstream water level	m
ΔH	Head difference	m
k	Spring stiffness	N/m
k_w	Added water stiffness	N/m
K	Down pull coefficient	-
L	Characteristic length	m
m	Mass	kg
m_w	Added water mass	kg
M	Mach number	-
Ma	Mass number	-
n	Scale factor	-
p	Pressure	Pa
Q	Discharge	m^3/s
Re	Reynolds number	-
S	Strouhal number	-
S_n	Strouhal number with natural frequency	-
t	Time	s
U	Flow velocity	m/s
V	Volume	m^3
V_{rd}	Reduced velocity with excitation frequency	-
$V_{rd,0}$	Reduced velocity with natural frequency	-

Symbol	Description	Unit
W	Width of valve/Width of flume	m
We	Weber number	-
y	Vertical position	m
Y_0	Vertical amplitude	m
Δy	Vertical displacement	m
α_T	Down pull coefficient top of valve	-
α_B	Down pull coefficient bottom of valve	-
δ	Gate opening underneath the valve	m
ζ	Dimensionless damping	-
Π	Term dimensional analysis	-
ρ	Density of material	kg/m^3
ρ_w	Density of water	kg/m^3
σ	Surface tension	N/m
μ	Dynamic viscosity	Pa·s
μ_c	Contraction coefficient	-
ν	Kinematic viscosity	m^2/s
ϕ	Phase difference	rad
ω	Angular frequency	rad/s
ω_n	Natural angular frequency	rad/s

Abbreviations	
DAF	Dynamic Amplification Factor
EIE	Extraneously Induced Excitation
FIV	Flow-Induced Vibrations
IIE	Instability-Induced Excitation
MIE	Movement-Induced Excitation

List of Figures

Main Report

Appendix

List of Tables

Main Report

Appendix

Appendix A Lock System

The focus of this research is a valve in a lock system. In this appendix a background is given of the position and function of the valve in a navigation lock. This will be done by elaborating the following subjects:

- General information (§ A.1). A lot of different types of locks exist. The types with the most important elements will be discussed in this paragraph.
- Filling and emptying system (§ A.2). One of the functions of a navigations lock is the levelling of the water in the lock chamber. This levelling is done by the filling and emptying system. An important part of this system is the valve. The filling and emptying system will be the main subject of this paragraph.
- Valve (§ A.3). The final section focusses on the valve with a basic design and the relevant components regarding vibration problems. In this paragraph the different used types of skin plates, operating machinery, guidance elements and seals will be elaborated in detail.

Figure A-1 shows a diagram of the place of the valve in the total system. The structure of this figure will also be the structure of this appendix. Eventually the focus should be narrowed down to the final row, involving the elements of the valve that could influence or initiate the vibrations.

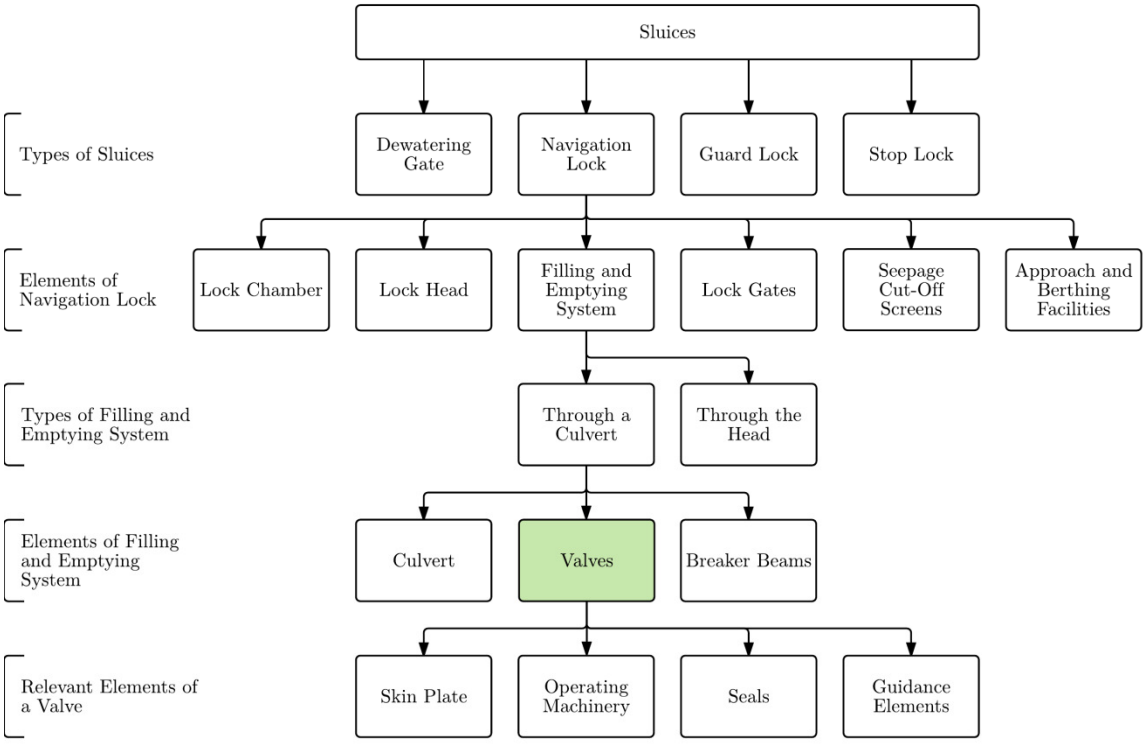

Figure A-1: Diagram of relation of elements of a lock

A.1 General

The lock is part of a larger category of sluices. MOLENAAR [40] uses for the definition of sluices the definition set by Webster's Universal College which is stated as: "*An artificial channel for conducting water often fitted with a gate at the upper end for regulating the flow*". Some of the most common types of sluices are [40]:

- Dewatering gate. The main function of a dewatering gate is to discharge water in favour of controlling the water level behind the gate. In some cases, the gate is also used to protect the area behind the gate against higher water levels from outside or to control the separation between a salt water area and a fresh water area.
- Stop lock. The functions of a stop lock and a dewatering gate are comparable. The major contrast between both sluices is that a stop lock is opened when the reservoir level is significant higher than the external water level. By opening the gate, the sediments, debris and pollutants are flushed out.
- Guard lock. Guard locks have to protect the hinterland against floods and extreme water levels from outer waters (in most cases a sea). An example of a large guard lock is a storm surge barrier.
- Navigation lock. The main function of a navigation lock is the transfer of vessels from one section of the waterway to another one. In most cases a navigation lock is located at the beginning or the end of a channel with a regulated water level. Figure A-2 shows a navigation lock in Lith, The Netherlands.

Figure A-2: Navigation lock in Lith, The Netherlands [24]

A.1.1 Navigation Lock

This research will focus on a navigation lock. Therefore, the main components of the navigation lock will be shortly discussed here. An example of a navigation lock is shown in Figure A-2 and Figure A-3 shows a lay-out of a standard navigation lock. A standard navigation lock exists of six main elements. These elements are [40]:

- Lock chamber (Figure A-3, no. 5). The lock chamber will accommodate the vessels during the filling and emptying process. In addition to the accommodation of the vessels the lock chamber also could have a soil retaining function.
- Lock head (Figure A-3, no. 4). The main function of the lock head is the accommodation of the lock gates. The lock head has a soil and water retaining function and has to transfer most of the loads from the gates to the foundation.
- Lock gates (Figure A-3, no. 3). The lock gates are responsible for withstanding the water level difference over the two sections of the waterways and make sure that vessels will be able to pass. Many types of gates are possible. Examples are vertical-lift gates, mitre gates and roll gates.
- Filling and emptying system (Figure A-3, no. 6). When the gates are closed the water level in lock chamber has to be levelled. For the levelling of the water a filling and emptying system is used.
- Seepage cut-off screens (Figure A-3, no. 7). Because there will be a water head difference over the lock, water wants to flow under and around the structure. This flow of water could lead to stability problems due to piping issues. The seepage cut-off screens are installed to prevent problems due to piping.
- Approach structures and berthing facilities (Figure A-3, no. 1 and no. 2). Approach structures are constructed in the area before the lock (no. 2) to prevent vessels from colliding with the expensive hydraulic structure. When the lock is not available for entering in some cases the vessels have to wait and therefore berthing facilities will be present in the area before the lock (no. 1).

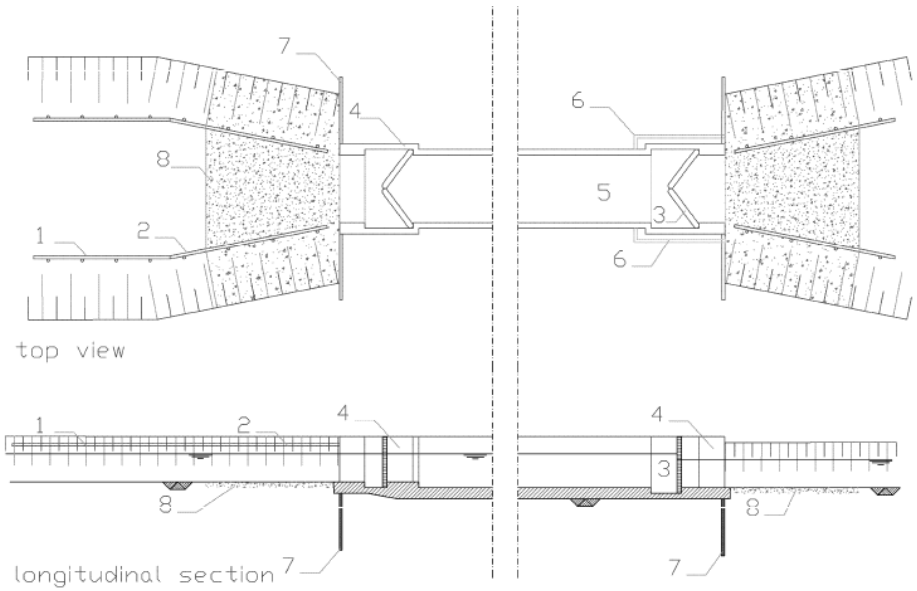

Figure A-3: Lay-out navigation lock [40]

The bottom protection (no. 8) is not mentioned above but is shown in Figure A-3. The bottom protection has to prevent erosion. This erosion could have a negative effect on the stability of the navigation lock.

A.2 Filling and Emptying System

This paragraph will focus on the filling and emptying system as an element of the navigation lock. This will be done be following the next steps:

- General (§ A.2.1). Different types of filling and emptying systems are elaborated in this paragraph.
- Process (§ A.2.2). This part describes the process of levelling the water in the lock chamber and transfer of the vessels.
- Elements (§ A.2.3). The final part will focus on the elements of the filling and emptying system that have an influence on the state of vibrations.

A.2.1 General

The position of the valves depends mainly on the choice of type of filling and emptying system. The filling and emptying system is responsible for the levelling of the water in the lock chamber. The two main systems are [40]:

- a “through the heads system”;
- a “longitudinal culvert system”.

The choice for the filling and emptying system will influence the position of the valves. A “through the head system” involves levelling of the water level through the gates. In Figure A-4 (L) gate valves that are used in this system are shown. In an optimum situation these valves are located as low as possible.

A “longitudinal culvert system” uses culverts constructed outside or inside the lock chamber to provide the in- and outflow of water. An application in which the culverts are located in the lock chamber is shown in Figure A-4 (R). When the culverts are positioned outside the lock chamber they are often integrated in the bottom or wall of the chamber. A culvert system is most of the times applied by locks with a large head difference, to minimize the disturbance of the water in the lock chamber. The use of culverts can control the magnitude and location of these disturbances. Culverts are also used in locks with a salt/fresh water separation system [24].

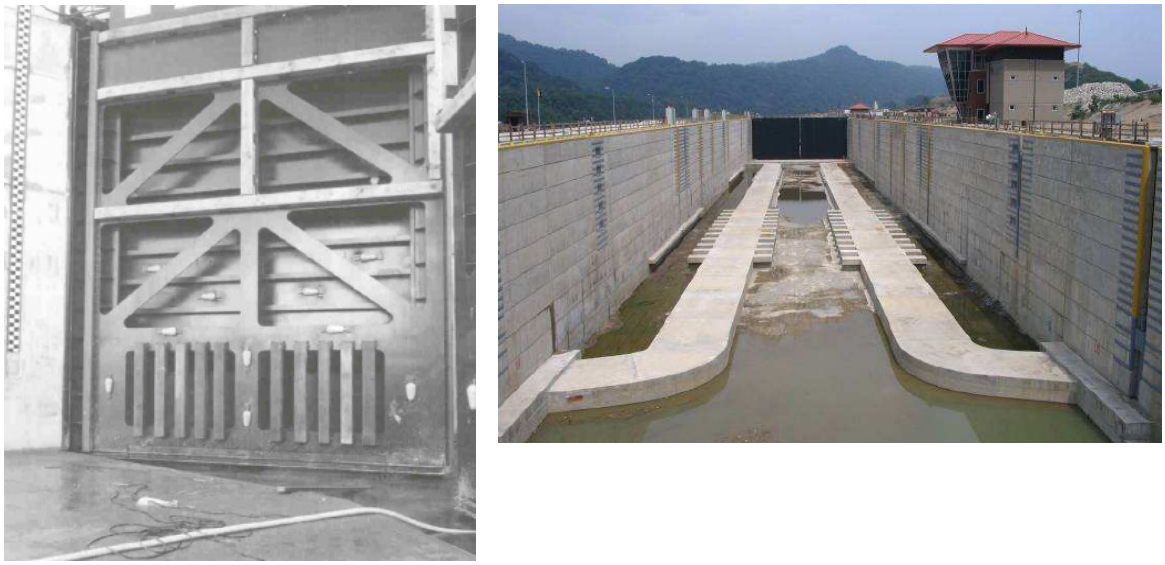

Figure A-4: (L) Valves and breaker plates in a gate [40] & (R) In-chamber longitudinal culvert system, Marmet Lock (US) [40]

A.2.2 Process

The process of levelling the water in a navigation lock can as be described by three stages. These stage are shown in the figures below.

- Stage 1: In first stage the upper gates and filling valve are open (Figure A-5). The vessel is now able to enter the lock chamber of the navigation lock. The water level in the lock chamber has a similar level as the upstream water level.

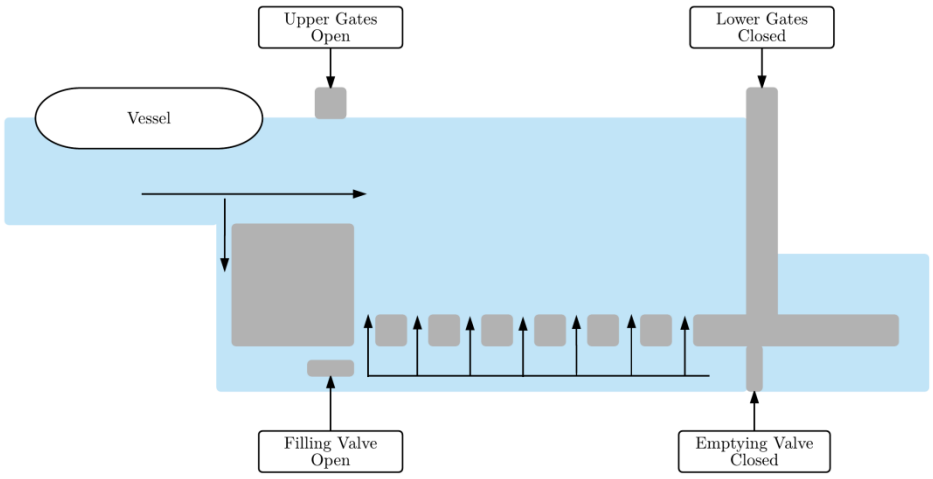

Figure A-5: Stage 1 in levelling process of the navigation lock

- Stage 2. In the second stage both gates are closed and only the emptying valve is open (Figure A-6). During this stage the actual levelling is done. The vessel is located in the lock chamber.

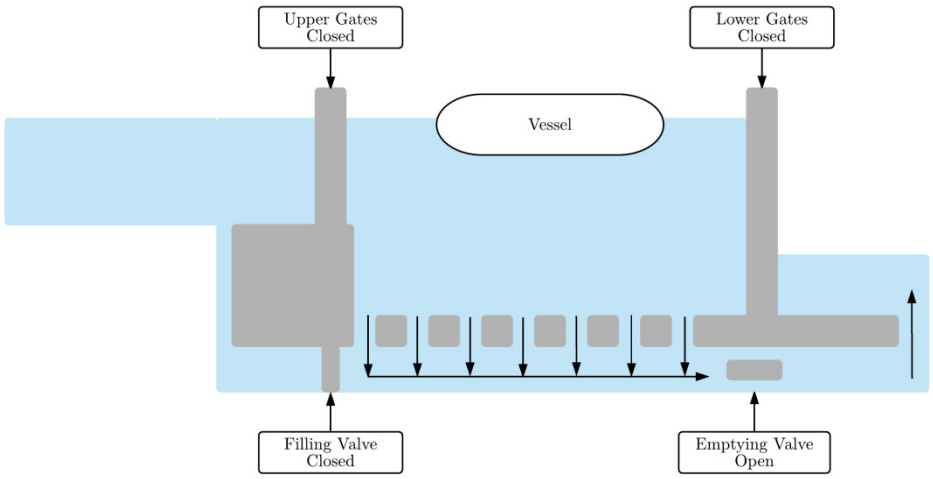

Figure A-6: Stage 2 in levelling process of the navigation lock

- Stage 3. In the final stage the water level is levelled to the downstream water levelled the lower gates can be opened (Figure A-7). The vessel is now able to leave the lock chamber.

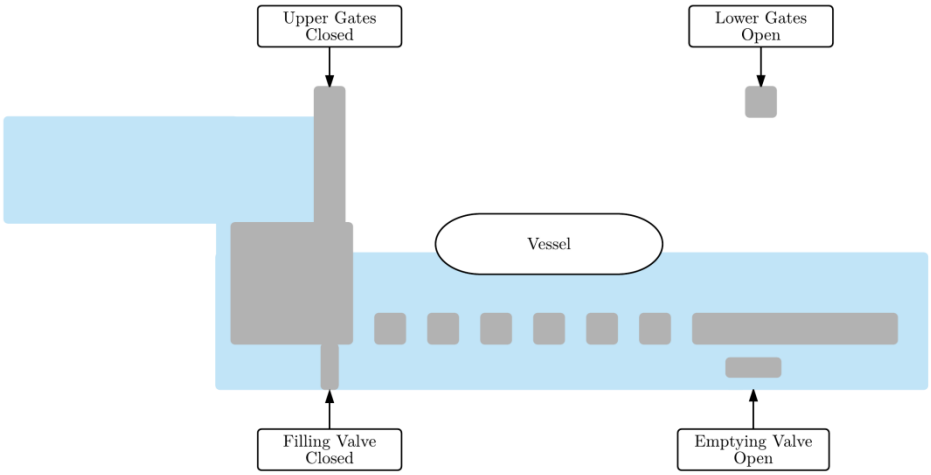

Figure A-7: Stage 3 in levelling process of the navigation lock

The process is reversible when the vessel has to transfer in the other direction.

A.2.3 Elements of the Filling and Emptying System

A basic filling through a longitudinal culvert system exists of several elements that will individually be discussed in this part of the report. Figure A-8 shows an overview of a longitudinal culvert system. The most important elements are:

- a culvert;
- a valve(s);
- breaker beams, in most cases only applied with a through the head system. The breaker beams are not visible in Figure A-8, but can be seen in Figure A-4 (L).

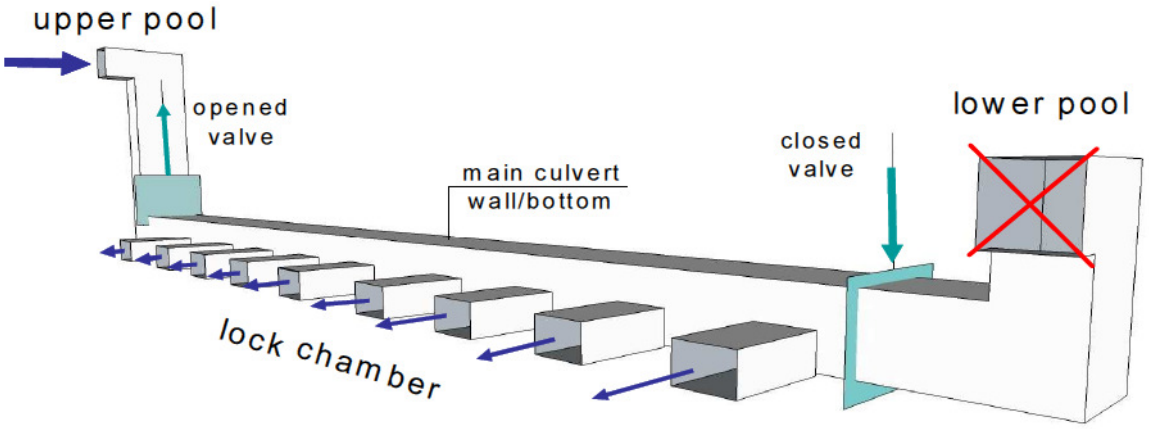

Figure A-8: Overview of a longitudinal culvert system [40]

Culvert

The culvert is a long pipe or tube through which the water is transported. Figure A-8 shows the place of the culvert in the total system. When a choice is made for the filling and emptying system through the head a culvert is not used. However, when the gate has a significant thickness, a tube will be constructed in the gate, which in some cases can be seen as a small culvert. Because the culvert has no further effect on the vibrations of the valve more details regarding the culvert will be omitted.

Valve

The valve is the main controlling element in the system. By closing and opening of the valve(s) the in- and outflow of water into the lock chamber is regulated. The valve will be the crucial element during this research and will therefore be discussed in detail in § A.3.

Breaker Beams

When flow enters and leaves a culvert or valve opening in a gate, in some cases breaker beams could be applied to disperse energy from the flowing water and create a calmer environment for vessels in the lock chamber. The turbulence existing from this breaker beams could lead to a dynamical load on the valve, which could lead to vibrations. This specific vibration is called an excitation due to turbulence [33] and will be further elaborated in Appendix C. A vertical version of these breaker beams is shown Figure A-4 (L).

A.3 Valve

This paragraph will focus on the design of the valve. First a distinction is made based on the retaining function of the valve after which the different relevant elements will be discussed.

A.3.1 General

A distinction between the valves can be made on the retaining function. The two basic types are [24]:

- one-sided retaining;
- two-sided retaining.

The choice for the different types is related to the water levels on both sides of the navigation lock. When a one-sided retaining valve is used the valve is mostly positioned on the high water level side of the gate, with the steel plate directed towards the low water side (see Figure A-9). When a two-sided retaining valve is used than the design will be slightly different.

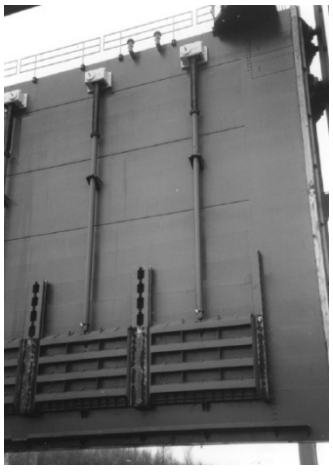

Figure A-9: One-sided retaining valve in a gate [24]

One-sided Retaining

The basic design of a valve exists of a main stiffened thin plate or solid thick plate with on all sides seals to avoid any kind of leakage. The valve moves guided by guidance elements constructed in the door or culvert [24]. If the valve is one-sided retaining the steel plate has a synthetic strip over the whole perimeter which is pressed against steel strips on the perimeter of the opening. This will ensure a watertight connection. In Figure A-10 (L) cross-sections of a one-sided retaining valve are shown. This valve design could be used as a two-sided retaining valve if small amounts of leakage are allowed.

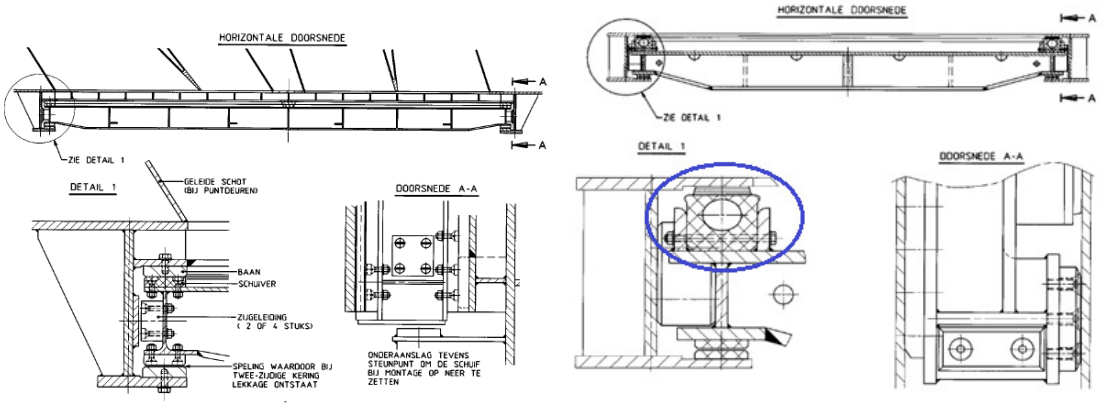

Figure A-10: (L) One-sided retaining valve design [24] & (R) Two-sided retaining valve structure [24]

Two-sided Retaining

Figure A-10 (R) shows the same cross-sections of a typical double-sided retaining valve as Figure A-10 (L) shows for a one-sided retaining valve. In contrast to a one-sided water retaining valve, the two-sided retaining valve has a rubber profile on one side that has to function as stop for the opposite retaining. The rubber profile prestresses the valve in the guidance system and is positioned at the side with the largest pressure. See detail 1 (blue circle) in Figure A-10 (R) for the position of the rubber profile.

When the valve is located in a culvert the design will not have many differences. The major differences can be found regarding the costs and the maintenance [24]. A valve in a culvert will be constructed in the lowest part of the culvert and will therefore be difficult to reach.

A.3.2 Elements of a Valve

A valve system has four critical elements that could have an effect on the vibrations. These elements are:

- skin plate (Figure A-11, no. 1);
- operating machinery;
- guidance elements (Figure A-11, no. 2);
- seals.

Figure A-11 does not show the operating machinery, which is often position far above the valve. Also the seals are not explicitly shown. The individual parts will be explained below.

Skin Plate

The skin plate is the major part of the valve. The design of the skin plate is rather straightforward. The function of the skin plate is to retain the largest part of the water. In Figure A-11 the skin plate is shown in the design as a simple straight plate. The plate is most of the time made out of a metal and can be completely solid or can be stiffened using crossbeams and horizontal beams. These beams are shown in Figure A-11 (L).

Operating Machinery

TWO types of operating machinery are used in present valve systems [24]. The two types are:

- a hydraulic cylinder;
- a mechanical spindle.

In this paragraph they will be discussed in more detail, including the relevant aspects regarding the vibrations of the entire valve system.

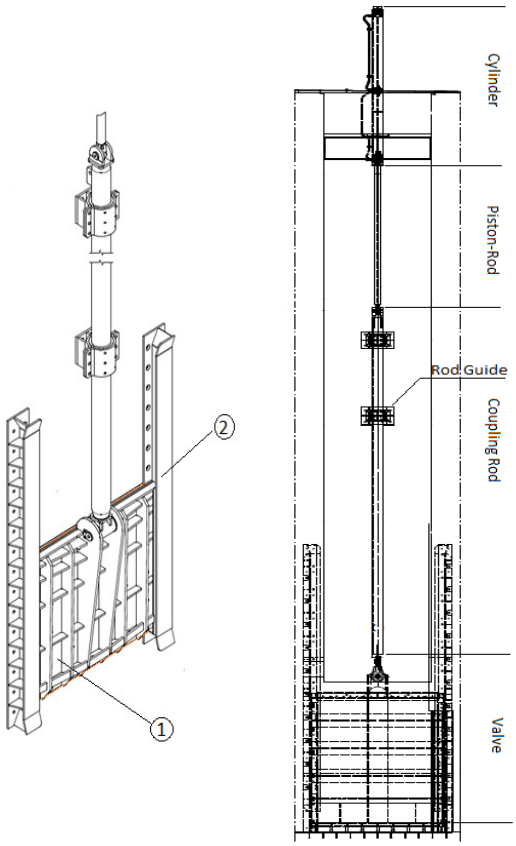

Figure A-11: (L) Valve & (R) Valve with hydraulic cylinder system

Hydraulic Cylinder

When a hydraulic cylinder system is used to open and close the valve several structural elements are present. These structural elements are:

- cylinder;
- piston;
- piston-rod;
- coupling rod;
- rod guides;
- oil tank and pipelines;
- pump.

The required lift force depends on the head difference over the valve and the friction of the valve and the seals with the guidance elements. In some cases, the hydraulic cylinder should be able to push when the upward force of the flowing water is higher than the force due to the mass of the valve. Figure A-12 shows a hydraulic lifting cylinder and Figure A-11 (R) shows the position of the elements related to each other in a vertical hydraulic cylinder. The hydraulic cylinder is currently the most used operating machinery.

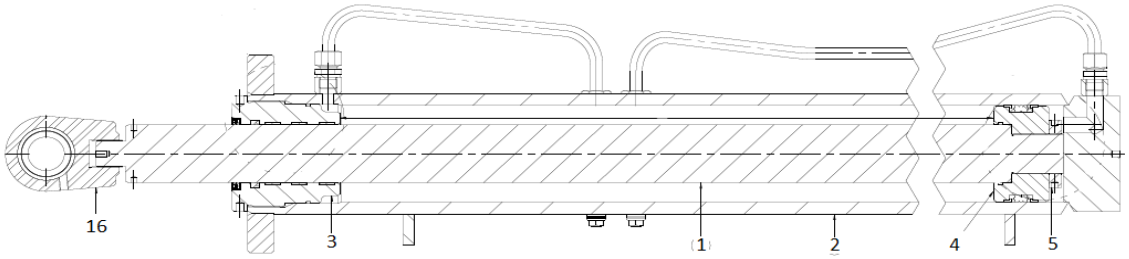

Figure A-12: Hydraulic lifting cylinder

A hydraulic cylinder exists of the following elements [24]:

- Cylinder (Figure A-12, no. 2 and no. 3). The cylinder exists of a cylinder pipe (no. 2) and a cylinder head (no. 3). In the cylinder the oil pressure is varied to push or attract the piston-rod. The cylinder is placed as high as possible to prevent it from water damage and to make it easy accessible for maintenance and repair works.
- Piston (Figure A-12, no. 4). The piston is responsible for the oil pressure in the cylinder and is therefore connected to the oil tank and possible electronic motor. See also the pipelines in the figure.
- Piston-rod (Figure A-12, no. 1). The piston-rod connects the cylinder with the piston-rod eye, indicted with no. 16 in Figure A-12. The piston-rod should be able to move in and out of the cylinder and will therefore be a slender element. The piston-rod eye will connect the cylinder system with a coupling rod.
- Coupling rod (Figure A-11). Because the cylinder will be placed above a certain level most of the times a coupling rod is used to connect the piston-rod with the valve. The length of this coupling rod depends on the distance between the cylinder and valve. The connection with the valve will be described in the next paragraph.
- Rod guides (Figure A-11). Rod guides are used when the whole system, including coupling rods, becomes long. The guides are used to give the slender rods more stability and direction.
- Oil tank. The oil tank is not shown in Figure A-11, but is mostly responsible for the stiffness of the operating machinery. The compressibility of the oil will therefore be important.
- Pump. The pump is responsible for pumping the oil from the tank to the piston. The pump is not shown in Figure A-11.

Mechanical Spindle

A spindle system as operation system is a mechanical system in which the rotating movement from a motor is translated in a vertical movement of a rod by a gear wheel [24]. In present designs the mechanical spindle is a lesser used method than a hydraulic cylinder due to experiences with large amounts of wear in the spindle bolt. See Figure A-13 (L) for an image of a mechanical spindle.

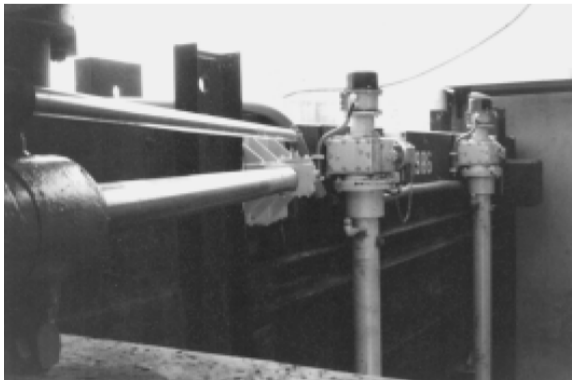

Figure A-13: (L) Mechanical spindle [24]

Guidance Elements

Two guidance systems could be used to guide a valve during the opening and closing process. [24] The two types of guidance systems are:

- wheel supports;
- slide supports.

Both types are described in this section. The guidance elements for a vertical lifting valve are comparable with those of a vertical lifting gate.

Wheel Supports

With the wheel supports the valve is guided by wheels that are connected to the valve. The wheels will roll in niches constructed in the side walls of the gate or culvert. In Figure A-14 a schematization of a wheel support is shown. On both sides of the wheels, rubbers are placed that have to make the connection water tight. An advantage of this kind of support is that the wheels will have a relative low friction coefficient compared to slide supports. A disadvantage is that the wheels require a lot of maintenance, which is difficult due to the location of the valve.

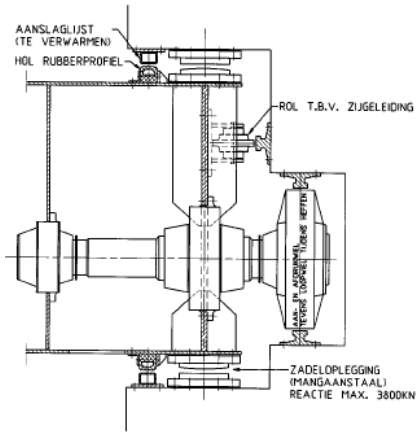

Figure A-14: Wheel supports [24]

Slide Supports

The slide support is the most used support in current valve designs. From a functional point of view, the operation between a slide support and a wheel support does not differ that much. The slide support has more friction compared to a wheel support, but needs on the other hand less maintenance. The friction of such a support could have a beneficial effect on vertical vibrations due to additional damping and energy dissipation. The slide support can also be seen in Figure A-11.

Seals

Leakage can have a negative effect on the valve. For that reason, seals are applied to make the water passage as water tight as possible. In this section the seals will be elaborated. The description is based on:

- the position;
- the material;
- the shape.

Position

When a valve is located in a culvert the skin plate is surrounded entirely by seals. This means that there are three kinds of seals:

- top seal (Figure A-15, blue);
- bottom seal (Figure A-15, red);
- side seals (Figure A-15, green).

In some cases, the top seal is not positioned at the ultimate top but on the backside of the valve (Figure A-15 (R)). This can also influence the vertical vibrations of the valve. The bottom seal, the seal located at the lower edge of the valve is the most interesting seal regarding the initiation of vertical vibrations. This is because of their shape and stiffness. The requirements regarding this seal are contradictory. On one hand the seal has to be stiff so the passing water flow can be as stable as possible and on the other hand the seal should prevent leakage which can be accomplished by making the seal less stiff.

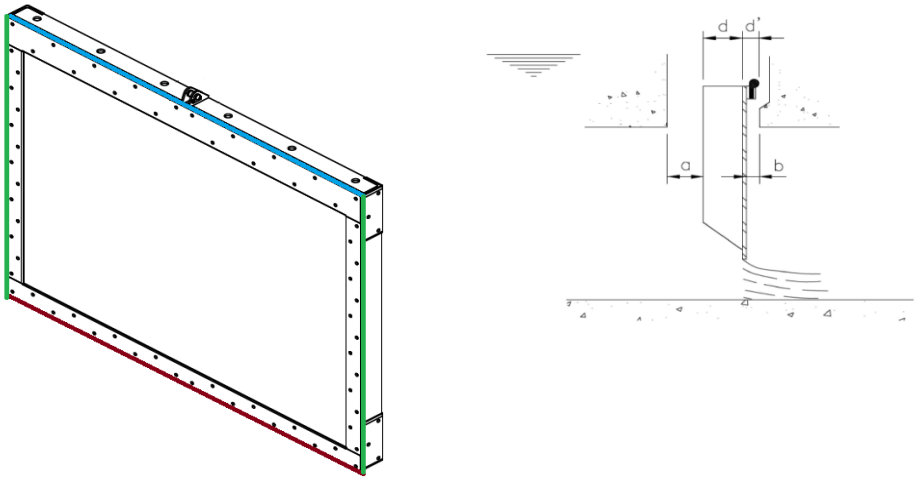

Figure A-15: (L) Position of the seals & (R) Top seal at back of valve [17]

Seal Material

One of the first materials applied as a seal was timber [17]. In current designs this is only used for small head gates or specific applications in rolling gates or mitre gates. When it comes to slide gates metallic seals can be used to provide water tightness and to transfer the force to the sill. The most used material however is rubber. An advantage of using rubber is that the seal can be manufactured in every desirable shape and stiffness. The shapes will be discussed further in the follow part of this paragraph.

Seal Shapes

The shape of the seal depends on its location on the valve (bottom seal, side seal or top seal) and the forces on the seal. It is also depending on if the valve is one-sided or two-sided retaining. The most common used shapes are [17]:

- J-seal (music note);
- hump seal;
- flat seal;
- lip seal.

The different shapes will be discussed below. The seals can achieve sealing by compression or deflection. In addition to the above mentioned types nowadays also Gina-type and similar compression seals are used. In the current days the manufacturers can produce every type and shape that is designed for a specific project.

J-Seal

The music note or J-seal is one of the most used types of seals for a one-sided retaining valve. This kind of seal is most of the time used as a side seal. The J-seal is based on a deflection due to the water pressure on one side. The deflection can be in the bulb, see Figure A-16 (L), or in the stem, see Figure A-16 (R). The bulb deflection occurs when the bulb is under a high compression force. On the other hand, stem deflection is more useful when the compression forces are lower, when the sealing surface is more irregular or when there are large tolerances in the gate dimensions [55].

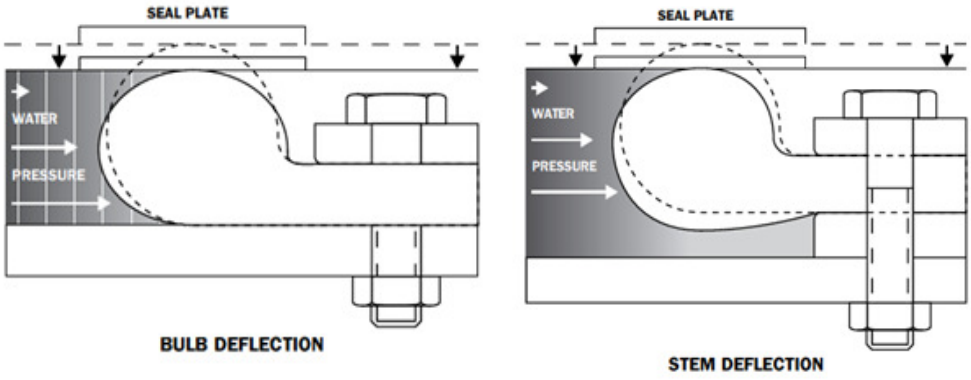

Figure A-16: (L) J-seal with bulb deflection [55] & (R) J-seal with stem deflection [55]

It has to be noted that the J-seal as shown in Figure A-16 is only applicable to a one-sided retaining valve. The seals could be manufactured with either a solid bulb or a hollow bulb, the choice for this type depends on the hydrostatic force on the seal. A solid profile is less vulnerable for compression while the hollow type is more useful in situations with lower hydrostatic pressures.

Hump Seal

The hump seal is applied in two basic forms: The single hump (Figure A-17 (L)) and the double hump seal (Figure A-17 (R)). Both forms are based on sealing by compression as can be seen in the figures. The double humps are mostly used as side seals in a two-sided retaining construction. And the single hump seals are often used as top seals in a submerged vertical-lift gate.

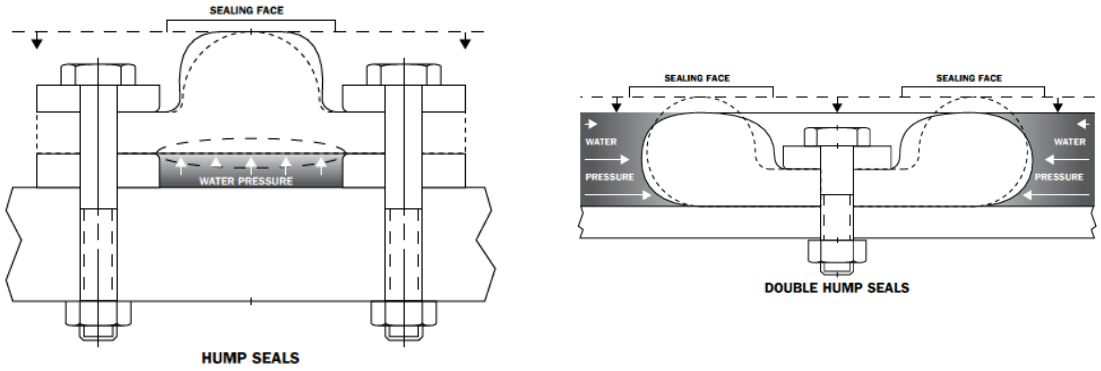

Figure A-17: (L) Single hump seal [55] & (R) Double hump seal [55]

Flat Seal

Flat seals can have a flat, chamfered or radius face and are mostly used as bottom seal. The flat seal works based on the compression principle which is shown in Figure A-18 (L). When a chamfered or radius seal is used the contact area between the seal and the sill is reduced, thereby space is created for the rubber to deflect. Figure A-18 (L) shows a deflected radius flat seal.

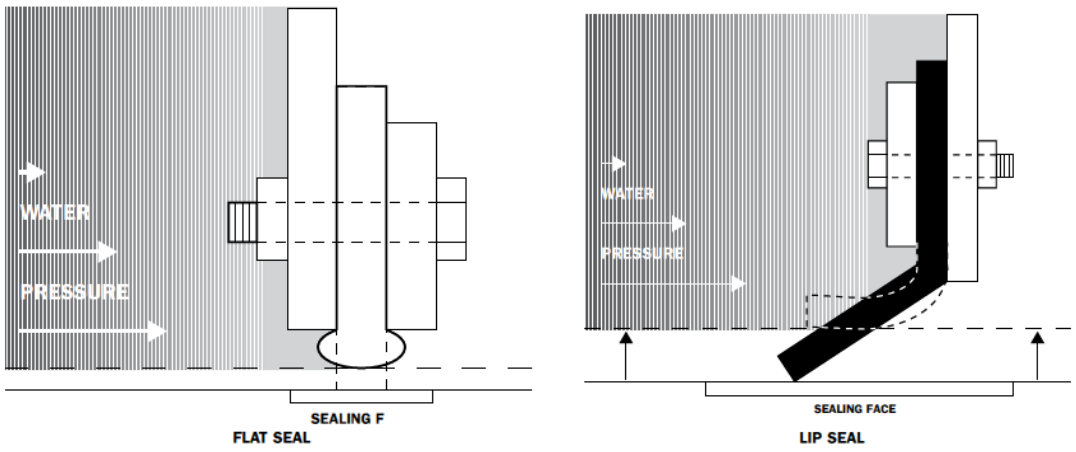

Figure A-18: (L) Flat seal [55] & (R) Lip seal [55]

Lip Seal

Lip seals are available in different lengths and angles. The lip seal functions based on the deflection principle. The application of lip seals is constricted to movement in one single plane. This means that they can only be applied by radial or vertical-lift gates. Sealing is achieved by the water pressure that works on the seal lip, because of that the seal lip deflects and is pushed to the sill. This can be seen in Figure A-18 (R).

Gina-Type Seal

The Gina-type seal was originally developed to be used in the expansion joint between two elements of an immersed tunnel. In current days they are also used to seal a vertical lift gate. In Figure A-19 (L) the Gina-type seal is shown in a compressed state, Figure A-19 (R) shows the Gina-type seal without compression. The shape of the Gina has a small tip so the initial contact surface is small and will become larger during compression. Manufacturers produce the seals often in combination with a compression and force graph. This can be used to fulfil certain criteria regarding the ratio between the horizontal and vertical pressure of the seal.

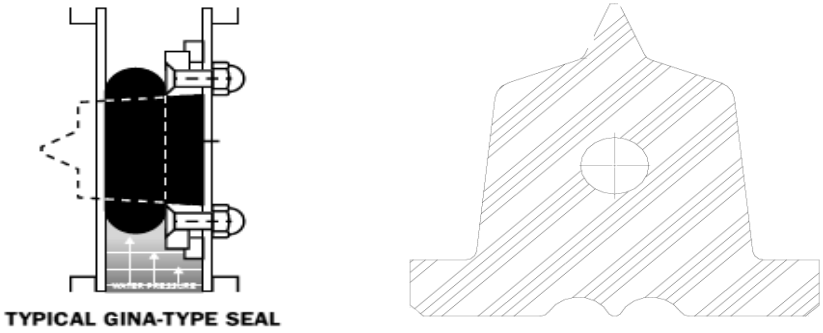

Figure A-19: (L) Compressed Gina-type seal [55] & (R): Gina-type seal [55]

Compression Seal

Some current designs have a seal comparable to the Gina-type seal and the flat seal, but slightly different. Such a seal was applied in a current project at the Wilhelmina channel, see Figure A-20. This seal is an example of a specifically designed seal.

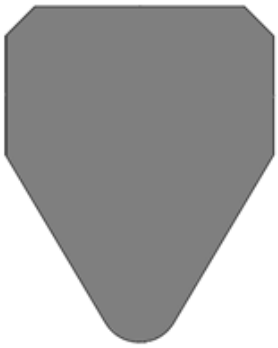

Figure A-20: Shape seal Wilhelmina channel

A.4 Conclusion

This appendix has described the place of the valve in the navigation lock system. A navigation lock is used to the transfer vessels from one section of the waterway to another one. This is mostly done by levelling of the water. The levelling of the water level is executed by a filling and emptying system. With a valve in the filling and emptying system is it possible to control the levelling. The valve exists of multiple elements that could have an effect on the vibrations. The most important elements are:

- skin plate;
- operating machinery;
- guidance elements;
- seals.

These elements can be executed and designed in multiple ways. The focus will be set on a design with a hydraulic cylinder because this is the most applied type of operating machinery. Also will the design have a slide support. The shape of the closing seal will be the focus of the research.

Appendix B Dynamics of the System

This appendix will focus on the dynamic aspects of a valve in a culvert. The aspects are divided into two categories. The categories are:

- Added water effects (§ B.1). This paragraph focusses on the additional effects for a system under water. The relevant effects are the added water mass, the added water stiffness and the added water damping. The added water effects will be elaborated individually.
- Dynamic characteristics (§ B.2). This section exists of an elaboration of some important characteristics regarding the vibration phenomena. Examples of these characteristics are the natural frequency, the damping factor and the amplification factor.

B.1 Added Water Effects

This section will elaborate the difference between a mass-spring-damping system in free air and under water. The additional effects of a system under water are called the added water effects. At first an introduction is given after which the different effects are elaborated.

A mass-spring-damping system under water has some additional terms compared to the same system in free air. These additional terms are all related to the added water mass. The added mass can be defined as a fictitious mass that vibrates together with the structural object in the same frequency [59]. The additional water body will have three effects on the dynamic system. The effects are:

- added water mass (§ B.1.1);
- added water stiffness (§ B.1.2);
- added water damping (§ B.1.3).

The additional factors can also be identified in equation B.1. Equation B.1 shows a basic equation of motion adjusted for system under water.

$$(m + m_w) \cdot \frac{\partial^2 y}{\partial t^2} + (c + c_w) \cdot \frac{\partial y}{\partial t} + (k + k_w) \cdot y = F_w\left(t, y, \frac{dy}{dt}, \text{etc.}\right) \qquad \text{B.1}$$

In which:

	m	=	mass [kg]
	m_w	=	added water mass [kg]
	c	=	damping [Ns/m]
	c_w	=	added water damping [Ns/m]
	k	=	stiffness [N/m]
	k_w	=	added water stiffness [N/m]
	$F(t)$	=	external force [N]
	t	=	time [s]
	y	=	vertical position [m]

B.1.1 Added Water Mass

The simplest effect of the added water is an increase in mass. Figure B-1 (L) shows the simplest kind of added mass.

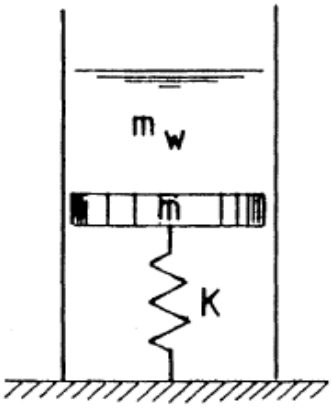

Figure B-1: (L) Most simple form of added mass [35]

ERDBRINK [20] determined the added mass of a valve using an experimental set-up. He measured the free vibrations of his system in open air and under water and concluded from the results the mass and the damping under water. The test was repeated with different water levels. The formula used for determining the added mass is shown in equation B.2. This method is also used in Chapter 4.

$$\frac{f_{n,wet}}{f_{n,air}} = \left(1+\frac{k_w}{k}\right)^{\frac{1}{2}} \cdot \left(1+\frac{m_w}{m}\right)^{-\frac{1}{2}} \qquad \text{B.2}$$

The formula uses in addition to the unknown added mass (m_w) also the unknown added stiffness (k_w). This could be determined by combining the Archimedean force acting on the submerged part of the gate and Hooke's law [20]. See the equations B.3 and B.4.

$$F_{upward} = \rho_w \cdot g \cdot V = \rho_w \cdot g \cdot (W \cdot b \cdot u) = k_w \cdot u \qquad \text{B.3}$$

$$k_w = \rho_w \cdot g \cdot W \cdot b \qquad \text{B.4}$$

In which:

k_w	=	added stiffness [N/m]
ρ_w	=	density of water [kg/m^3]
V	=	volume of submerged part of valve [m^3] = $W \cdot b \cdot u$
W	=	width of the gate in cross-flow direction [m]
b	=	gate thickness in in-flow direction [m]
u	=	submergence depth [m]
g	=	gravitational acceleration [m/s^2]

See Figure B-2 for an indication of the dimensions mentioned in the equation above.

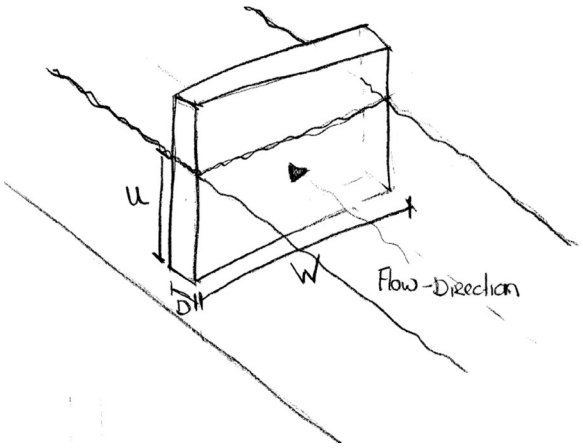

Figure B-2: Indication of the dimension parameters

ERDBRINK [20] concluded from tests that the amount of added mass depends on the opening underneath the gate and the submergence of the gate. This matches with the experiences of equation B.4.

B.1.2 Added Water Stiffness

In the previous paragraph a way is shown how ERDBRINK [20] computed the added stiffness. This will be elaborated in more detail in this paragraph. Three forms of added stiffness have been described earlier. The forms are:

- the additional rigidity because of floating;
- stiffness by quasi-stationary flow;
- stiffness that arises from an abrupt change of position of the object.

According to the given description especially the final one is a special case which will only have an effect on a valve in a culvert, because of the inertia of the discharge. The stiffness of a floating body can be calculated with equation B.4 [33]. In Figure B-2 the used dimensions in equation B.4 are shown. The stiffness due to the quasi-stationary flow can be calculated with equation B.5.

$$k_{w\text{-}flow} = \frac{\partial F_y}{\partial y} = \frac{\partial}{\partial y}\left(C_{fy} \cdot \frac{1}{2} \cdot \rho \cdot U^2 \cdot L^2\right) = \frac{1}{2} \cdot \rho \cdot U^2 \cdot L^2 \cdot \frac{\partial C_{fy}}{\partial y} \qquad \text{B.5}$$

In which:

$k_{w\text{-}flow}$	=	added stiffness due to flow [N/m]
F_y	=	vertical component of the flow force [kN] = $C_{fy} \cdot 1/2 \cdot \rho \cdot V^2 \cdot L^2$
C_{fy}	=	force coefficient [-]
ρ	=	density of fluid [kg/m^3]
U	=	flow velocity [m/s]
L^2	=	flow surface [m^2]

As earlier mentioned the type due to the abrupt change of position plays an important role on a valve construction in a culvert. When the valve suddenly changes its position the flow will not change immediately due to inertia of the flow. Because of this effect the flow underneath the valve will change. The force on the valve which is related to the velocity squared will therefore change according to equation B.6 [33].

$$F_{new} = F_{permanent}\left(\frac{\delta^2}{(\delta+\Delta\delta)^2}\right) \qquad \text{B.6}$$

In which:

δ	=	opening underneath the valve [m]
$\Delta\delta$	=	change in opening underneath the valve [m]

The abrupt added stiffness can be determined by dividing the change in force by –y [33]. See equation B.7.

$$k_{w\text{-}abrupt} = \frac{F_{new} - F_{perm}}{-y} = -F_{perm}\left(\frac{\delta^2}{(\delta + \triangle\delta)^2} - 1\right) \cdot \frac{1}{y} \cong 2 \cdot \frac{F_{perm}}{\delta} \qquad \text{B.7}$$

Concluded from equation B.7 can be that the added stiffness in this case is the largest when the gap underneath the valve is small. What is not shown in the equation is that the stiffness is related to the frequency and will only appear when the vibration has a high frequency, because in this case the discharge tends to be constant, which is needed to get this additional stiffness.

B.1.3 Added Water Damping

In addition to the added mass and added stiffness the valve under water can also experience effects of added water damping. The added damping can have an effect on both the vibrations in in-flow direction and in cross-flow direction. In this particular case only the vibrations in cross-flow direction are considered. For an arbitrary shape of the object the additional damping in cross-flow direction is as shown in equation B.8 [33].

$$c_w = \frac{1}{2} \cdot \rho \cdot U \cdot A \cdot \left(\frac{\partial C_L}{\partial \alpha} + C_W\right) \qquad \text{B.8}$$

In which:

c_w	=	added damping [kg/s]
ρ	=	fluid density [kg/m^3]
U	=	flow velocity [m/s]
A	=	flow surface [m^2]
C_L	=	lift force coefficient [-]
α	=	angle of the flow [°]
C_W	=	flow resistance coefficient [-]

B.2 Dynamic Characteristics

This paragraph elaborates some important characteristics regarding the dynamic system and the vibration phenomena. The characteristics can be derived from the equations of motion and are important to determine the state of the vibrations. The characteristics are:

- the natural frequency (§ B.2.1);
- the damping factor (§ B.2.2);
- the amplification factor (§ B.2.3).

B.2.1 Natural Frequency

The natural frequency is defined as the frequency of a free vibrating system without external force, which lacks any form of damping. The equation of motion in this case will become:

$$m \cdot \frac{d^2y}{dt^2} + k \cdot y = 0 \qquad \text{B.9}$$

The result of this equation will be a harmonic vibration in the form of:

$$y = Y_0 \cdot \sin(\omega t) \qquad \text{B.10}$$

This leads to a natural frequency of:

$$f_n = \frac{\omega_n}{2\pi} = \frac{1}{2\pi}\sqrt{\frac{k}{m}} \qquad \text{B.11}$$

When the same approach is applied to an equation of motion for an underwater system, as mentioned in § B.1, the natural frequency changes to equation B.12.

$$f_n = \frac{1}{2 \cdot \pi}\sqrt{\frac{k+k_w}{m+m_w}} \qquad \text{B.12}$$

B.2.2 Damping Factor

The damping factor is a ratio between the critical damping and the actual damping. The critical damping follows from the solution of the equation of motion of a free vibration with damping. The definition of the critical damping is shown in equation B.13.

$$c_{cr} = 2 \cdot \sqrt{k \cdot m} \tag{B.13}$$

When a similar method is followed for an equation of motion under water the critical damping changes to equation B.15. The damping factor for a situation under water is given in equation B.15.

$$c_c = 2 \cdot (m + m_w) \cdot \sqrt{\frac{k + k_w}{m + m_w}} = 2 \cdot \sqrt{(k + k_w) \cdot (m + m_w)} \tag{B.14}$$

$$\gamma = \frac{c}{c_c} = \frac{c}{2 \cdot \sqrt{k \cdot m}} = \frac{c}{2 \cdot \sqrt{(k + k_w) \cdot (m + m_w)}} \tag{B.15}$$

In the ratio above is assumed that the water will not give an additional water damping. The damping factor is an important number in defining if the dynamical system is stable ($\gamma > 0$) or instable ($\gamma < 0$).

B.2.3 Dynamic Amplification Factor

Figure B-3 shows an example of a response diagram and a phase diagram. Noticeable is that when the excitation frequency and the natural frequency are similar the amplitudes could increase enormously. But when they are almost similar also an increase in amplitude is shown. This can be expressed using the amplification factor. The dynamic amplification factor is shown in equation B.16 [33].

$$A = \frac{k \cdot y}{\hat{F}} = \frac{1}{2 \cdot \gamma} \tag{B.16}$$

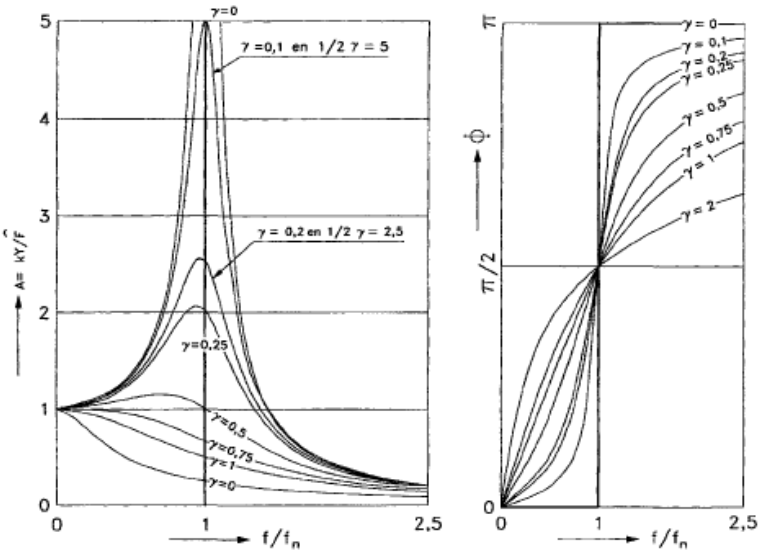

Figure B-3: Response and phase diagram of a one degree of freedom mass-spring system [33]

[Page intentionally left blank]

Appendix C Flow-Induced Vibrations

This appendix will focus on the already existing information regarding flow-induced vibrations on hydraulic structures. During the course of the appendix the following subjects will be described:

- Types (§ C.1). The first paragraph will give the general knowledge regarding flow-induced vibrations. This involves the definitions and types as used in literature.
- Flow characteristics (§ C.2). Because one of the classification systems is defined on basis of the flow characteristics this paragraph is dedicated to the different types of flow.
- Previous research (§ C.3). An important point for this research is the similar research done in the past. This final paragraph will give an overview of five already executed researches.
- The current design rules (§ C.4). The final section will give some information regarding the already available guide lines regarding the vibrations of a valve. Only the relevant vibrations will be elaborated.

C.1 Types

Kaneko, Nakamura, Inada and Kato [32] define the vibration and noise phenomena due to the flow of water or gas as Flow-induced Vibrations (FIV). One of the first written books mentioning the term was written by Blevins [6] in which he classifies the FIV phenomena based on two types of flow: namely steady flow and unsteady flow. The flow conditions will be explained in the next paragraph. FIV phenomena find their origin in many different fields of study. The basic elements of the flow-induced vibrations are [41]:

- Body oscillators. A body oscillator consists of two types. One type is a rigid structure or rigid element that is able to perform angular or linear movements. The other type is a structure or structural part that has elastic properties and can perform flexural movement.
- Fluid oscillators. In comparison to a body oscillator a fluid oscillator exists of mass that can oscillate due to gravity or fluid compressibility. When an excitation frequency coincides with the natural frequency of a body oscillator it can amplify the vibration of the body oscillator.
- Sources of excitation. The sources for excitation in de fluid or body oscillator can be a great many. The sources can be divided into three main categories [41]:
    - Extraneously induced excitation (EIE). This type of excitation arises from fluctuations in flow velocity or fluctuations in pressure that are independent of the structure. Sources for this kind of excitations can be waves, external created turbulence and earthquakes.
    - Instability-induced excitation (IIE). In the case of IIE the source of the excitation is the flow instability. Defined is that the flow instability is related to the flow created by the shape of the structure. Examples from this kind of excitation are vortex shedding behind the structure and impinging of a free shear layer.
    - Movement-induced excitation (MIE). This type of excitation relates to fluctuating forces that arise from the movement of the vibrating oscillator. In other words, these kinds of excitations are self-excited.

The process of the excitations is most of the time not a straight forward process. In most cases combinations of the sources EIE, IIE and MIE are present simultaneously. The same applies to the presence of a body oscillator and a fluid oscillator.

Kolkman and Jongeling [33] defined in a later stage of research five specific types of initiated excitations, related to the design of hydraulic structures. In Figure C-1 an overview is shown from the different vibrations related to a rod or beam (top row) and a valve (bottom row). These excitations are:

- excitation due to turbulence (Figure C-1, no. 1);
- excitation due to flow instability (Figure C-1, no. 2);
- self-excitation (Figure C-1, no. 3);
- increase of excitation by liquid resonance (Figure C-1, no. 4);
- excitation due to liquid oscillations in a basin (Figure C-1, no. 5).

The further course of this paragraph will elaborate those five types and place them into the classification of Naudascher and Rockwell [41].

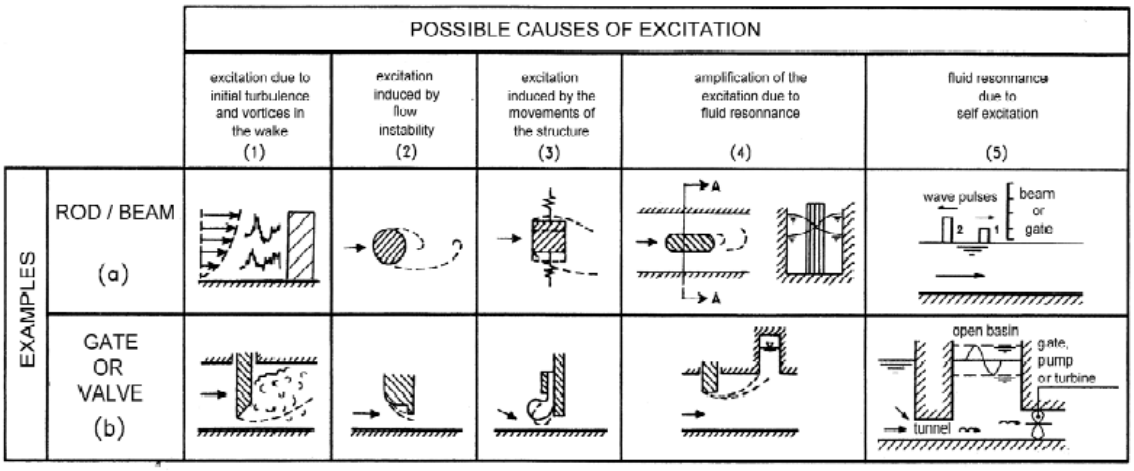

Figure C-1: Different types of vibrations on hydraulic structures [33]

C.1.1 Excitation due to Turbulence

Where Kolkman and Jongeling [33] describe this vibration as one, the classification of Naudascher and Rockwell [41] indicates that it can be considered as an EIE and an IIE. As shown in Figure C-1 (image 1a) an initial turbulence in the flow is the source for the vibration which would indicate that the vibration would be classified as an EIE. On the other hand (Figure C-1, image 1b) the vibration is caused because of wake behind the valve, which is initiated by the structure itself; this is the main condition for an IIE.

C.1.2 Excitation due to Flow Instability

As the name of the excitation already indicates the vibration can be classified as an IIE. This definition includes all excitations caused by flow instability induced by the shape of the object. Important aspects are the separation point of the shear layer and a possible reattachment points of the shear layer. When these points do not have stable position vertical pressure fluctuations can arise which will initiate a vibration in the valve. Figure C-2 shows the possible forms of reattachment.

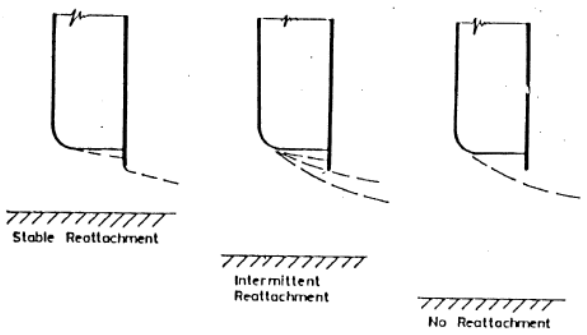

Figure C-2: Forms of shear layer reattachment [35]

C.1.3 Self-Excitation

Self-excitation is a typical vibration of an MIE in the classification system of Naudascher and Rockwell [41]. When the excitation force of the vibration and the vibration self are harmonic than self-excitation is possible. When self-excitation occurs the amplitude of the vibration will increase exponential until a physical border is reached, when such a border is not present the structure will fail. A lot of mechanisms exist from which a self-excitation can arise; one example is the bath plug phenomenon, in which a bath plug starts self-excitation due to the fluctuations in the discharge and velocity under the plug. All mechanisms of self-excitation have in common that the entire systems damping is negative.

C.1.4 Increase of Excitation by Liquid Resonance

This kind of vibration can be classified in EIE category of Naudascher and Rockwell [41]. The vibration occurs when the fluid oscillator (in this case the added water) is going to resonance with the initial vibration of the valve. When both excitation frequencies are close to the natural frequency of the valve resonance could occur. Resonance could lead to high amplitudes and possible failure.

C.1.5 Excitation due to Liquid Oscillations in a Basin

The final form described by Kolkman and Jongeling [33] is an excitation that is initiated by an excitation in a liquid. For this excitation the same category counts as the earlier mentioned increase of excitation by a liquid resonance, namely EIE. The final both vibrations will not play a role in this research.

C.1.6 Other Causes

This paragraph describes phenomena that are not mentioned in relation with flow-induced vibrations, but could initiate similar vibrations. These other causes are:

- cavitation;
- leakage;
- reflected wave.

Cavitation

Cavitation is a cause of vibration which is not described by Kolkman and Jongeling [33]. Lewin [35] describes this type as: "*Cavitation is caused by local pressure on the downstream side of a valve by the accelerated flow of the water as it contracts to pass through the valve opening and by the generation of turbulence*". This process involves forming of eddies in the shear layer downstream of the valves. The pressure in these eddies is much lower than in the accelerated flow. When the pressure reaches the vapour pressure, cavitation bubbles could arise. Due to viscous forces and ambient pressure increase these bubbles will become unstable and collapse. The collapsing of the bubbles creates locally significant noise and vibration which could lead to multiple forms of damage and malfunctioning.

Leakage

Another cause of vibrations is related to leakage underneath or sideways of the valves. Regarding the leakage underneath the valve the lower edge closing seals play a major role. PAÏDOUSSIS [44] describes this form of vibration to be notorious for its destructiveness. Kept in mind should be that researches mentioned by PAÏDOUSSIS [44] are related to other fields of study. A beneficial aspect of excitation due to leakage is that the amplitude cannot increase more than a present physical boundary layer (the sill on the bottom of the culvert), therefore resonance is almost impossible. Leakage past side seals rarely results in vibration of the gate as a whole [35]. It could have an effect on local structural elements and have a very noisy effect.

Reflected Wave

A vibration phenomenon only found by valves in a conduit is caused by a reflected wave. LEWIN [35] states that the variation in discharge underneath the valve gives a pressure wave, which could be reflected on an upstream object. When returned to the valve this wave could have a frequency that could lead to an instable valve system.

C.2 Flow Characteristics

As earlier mentioned one of the first distinctions made in the types of flow-induced vibrations was the one related to the type of flow [6]. KANEKO *et al.* [32] describes three forms of flow:

- steady flow;
- unsteady flow;
- two-phase flow.

Another aspect of flow conditions is the location of the valve. According to MOLENAAR [40], the flow situation from a hydraulic point of view varies for both earlier mentioned filling and emptying systems (see Appendix A). By using head filling the flow is characterized as 'open channel flow' and by using a culvert system the flow is known as a 'closed conduit flow'. Both types of flow have their individual characteristics. Main difference is that 'closed conduit flow' has an energy loss due to friction with the walls and therefore will have a lower velocity.

C.2.1 Steady and Unsteady Flow

BLEVINS [6] made a first distinction between flow-induced vibrations based on type of flow. He distinguished vibrations due to steady flow and vibrations due to unsteady flow. Steady flow is a flow in which the properties of the flow do not depend upon time. Examples of these properties are velocity and pressure. Unsteady flow represents all other kinds of flow in which the properties do depend upon time. When focussed on a flow underneath a valve both types of flow can occur. Flow underneath a valve will mainly be unsteady flow due to the continuously change in the boundary conditions [4]. The most important boundary conditions are the water head difference, which will reduce during the process, and the gate opening, that will increase during the process. Both boundary conditions have an effect on the flow velocity and therefore the flow velocity will be continuously changing in time.

C.2.2 Two-Phase Flow

Two-phase flow is generally a flow of a liquid and gas combined. An example of this two-phase flow is the earlier described cavitation. When used in research two-phase flows could be described by the dimensionless Weber number which relates the fluids inertia to its surface tension. According to LEWIN [35] it is hard to study the effects of two-phase flows in a model study due to scaling problems. For that reason, the two-phase flow will be out of the scope of this research.

C.3 Previous Research

In the past some research has been done regarding flow-induced vibrations. The researches described in this paragraph have either a similar aim or a similar approach. The researches elaborated in this paragraph will be:

- A research focused on the added mass and instable vertical vibrations executed by Vrijer [59].
- A research focused on different lower edge shapes of a valve and their effect on the vertical vibrations performed by Uwland [56].
- A research focused on vertical flow-induced vibrations of an underflow gate executed by Erdbrink [20].
- A research on the horizontal in-flow vibrations done by Jongeling [31].
- A research on flow-induced multiple mode vibrations of gates with submerged discharged executed by Billeter and Staubli [8].

In the recent researches this reduced velocity is also used in combination with the response frequency, which is in case the inverse of the normal Strouhal number (see equation 2.10). This reduced velocity is noted as V_{rd}. A crucial point in comparing researches that use the Strouhal number or the reduced velocity is the definition of the characteristic length (L), therefore Table C-1 also shows what the different researches defined as characteristic length. Important for this specific research is the range in which the previous researches found their vibration phenomena, which will in a later phase be used to determine the test conditions. Also has the use of natural frequency and the response frequency not been constant during these researches.

Research	Critical Range for Vibrations		Definition Characteristic Length (L)
Vrijer [59]	$S > 0.012$	$S < 0.20$	Gate Opening (δ)
Uwland [56]	$S > 0.012$	$S < 0.20$	Gate Opening (δ)
Kolkman and Jongeling [33]	$S > 0.2$	$S < 0.3$	Gate Opening (δ)
Erdbrink [20]	$V_{rd} > 2$	$V_{rd} < 3.5$	Gate Thickness (b)
	$V_{rd} > 8.5$		Gate Thickness (b)
Billeter and Staubli [8]	$V_{rd} > 2$	$V_{rd} < 4$	Gate Thickness (b)
	$V_{rd} > 10$		Gate Thickness (b)

Table C-1: Results retrieved of previous researches

Table C-1 shows the results retrieved from researches done in the past. The oldest studies, from Vrijer [59] and Uwland [56], found the same results based on the same definition for the Strouhal number. However, Uwland based a large part of his research on the earlier done research of Vrijer. The numbers found during these researches correlate with the high reduced velocity ranges of the more recent researches. These more recent researches, those of Erdbrink [20] and Billeter and Staubli [8], show also a major similarity regarding the critical ranges. They both describe two ranges, one with a low reduced velocity and one with a high reduced velocity. However, both give contradictory explanations for the cause of these two ranges. Erdbrink relates the high reduced velocity ranges ($V_{rd} > 8.5$) with flow instability (IIE) and the low reduced velocity areas ($2 < V_{rd} < 3.5$) with vibrations induced by the movement of the valve (MIE) [20]. Billeter and Staubli on the other hand state the exact opposite, in which the low reduced velocity ranges are caused by flow instability and the high reduced velocity ranges are caused by movement induced causes. The statement made by Kolkman and Jongeling [33] contradicts with all the other researches (Table C-1).

C.4 Current Design Guidelines

Kolkman and Jongeling [33] state that there is no method to assure a vibrations free design regarding a structure in flowing water. However, with the present knowledge major design mistakes can be avoided. This paragraph will elaborate the current rules and guidelines regarding the design. The design rules regarding the vibrations will be elaborated as classified by Kolkman and Jongeling [33] (§ C.1). The relevant types of vibrations have been elaborated in more detail in an earlier stage of this report and are:

- the excitation due to turbulence (§ C.4.1).
- the excitation due to flow instability (§ C.4.2).

C.4.1 Excitation due to Turbulence

The first type of excitation mentioned was the excitation due to turbulence. According to Kolkman and Jongeling [33] the initial turbulence due to external effects (for example breaker plates as described in Appendix A) will not have an effect on the valve, because the initial velocity is significantly low with respect to the crucial velocity underneath the valve. Therefore, only turbulence initiated by the valve itself has to be taken into account during the design. This turbulence can initiate a vibration parallel to the flow as well as cross-flow vibration. Kolkman and Jongeling [33] and Lewin [35] use for both types of vibrations the same earlier done researches from Abelev [as cited in [33]] and Naudascher [as cited in [35]] In both cases the situations were linked to the dimensionless Strouhal number. The definition of the Strouhal number is shown in equation C.1. The Strouhal number will return in the dimensional analysis of Appendix D.

$$S = \frac{f_{exc} \cdot L}{U} \qquad \text{C.1}$$

In which:

S	=	Strouhal number [-]
f_{exc}	=	excitation frequency [Hz]
L	=	a representative length of the flow geometry [m]
U	=	flow velocity [m/s]

Horizontal Excitation

For the conditions regarding the horizontal excitation of the valve Kolkman and Jongeling [33] give Figure C-3, that shows the critical areas in which the vibrations occur. The figure and values were retrieved from an old research done by Abelev [as cited in [33]]. Coupled to this figure is the next condition regarding the earlier described Strouhal number shown in equation C.2.

$$0.5 < S < 3 \qquad \text{C.2}$$

Based on this condition and the figure, the dominant excitation frequency from the flow can be determined. Kolkman and Jongeling [33] recommend to fulfil the next condition regarding the Strouhal number:

$$\frac{f_n \cdot L}{U} > (2 \text{ a } 3) \cdot S \qquad \text{C.3}$$

This condition states that the natural frequency of the valve system should be at least two or three times larger than the dominant excitation frequency retrieved from the first condition (equation C.3). In practice the factor 3 is mostly used.

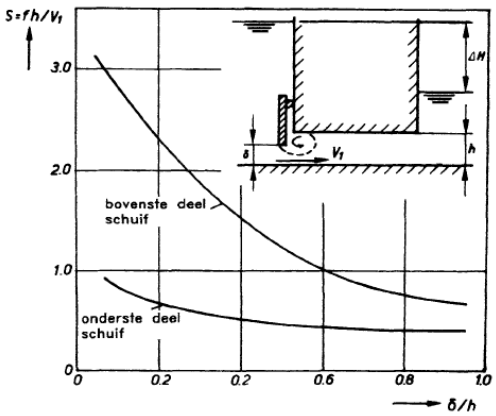

Figure C-3: Strouhal numbers for horizontal excitation for design of valves [33]

Vertical Excitation

The design regarding the vertical excitation due to turbulence follows a similar approach as the earlier described approach regarding horizontal vibrations. For this particular case KOLKMAN AND JONGELING [33] and LEWIN [35] describe the same approach, based on a research of NAUDASCHER [as cited in [35]]. Figure C-4 shows the results. Related to this figure the next condition is set:

$$0.2 < S < 0.3 \qquad \text{C.4}$$

From this condition the dominant excitation frequency in vertical direction can be determined and again the next condition has to be met as shown in equation C.5.

$$\frac{f_n \cdot L}{U} > (2 \text{ a } 3) \cdot S \qquad \text{C.5}$$

This leads again to a natural frequency of the system that should be at least 3 times larger than the dominant excitation frequency in vertical direction of the flow. Important point to notice is that the natural frequency is related to the system and in vertical direction will have additional elements regarding the mass, damping and stiffness, some of these elements are the operational machinery, seals and guidance systems (Appendix A).

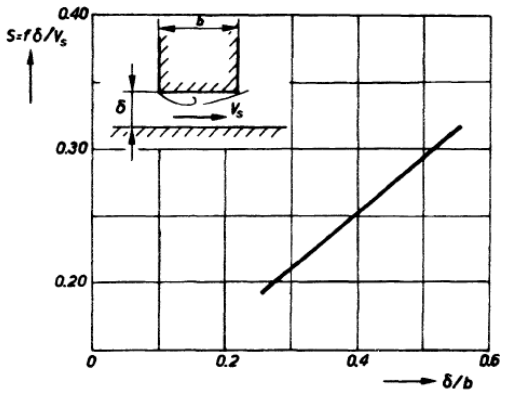

Figure C-4: Strouhal numbers for vertical excitation [33]

C.4.2 Excitation due to Flow Instability

Regarding the excitations due to flow instability no clear design calculations are available. The criteria that are given by some literature are mostly rules based on the shape of the valve. KOLKMAN AND JONGELING [33] describe situations that should be avoided during the design of the valve. These situations are:

- A situation in which there is not a constant separation point. This means that separation point of the shear layer varies, what will result in fluctuations in the vertical hydraulic pull force. This can occur when a circular-shape is used as lower edge.
- A condition in which flow after releasing attaches again at a wall of plate of the valve lower edge from which the reattachment point is not constant in place (Figure C-5 (L,2a)).
- When the flow reattaches and the reattachment point is stable free shear layer with waves can arise. The enclosed wake can experience pressure fluctuations what could initiate a vibration in the valve (Figure C-5 (R)).

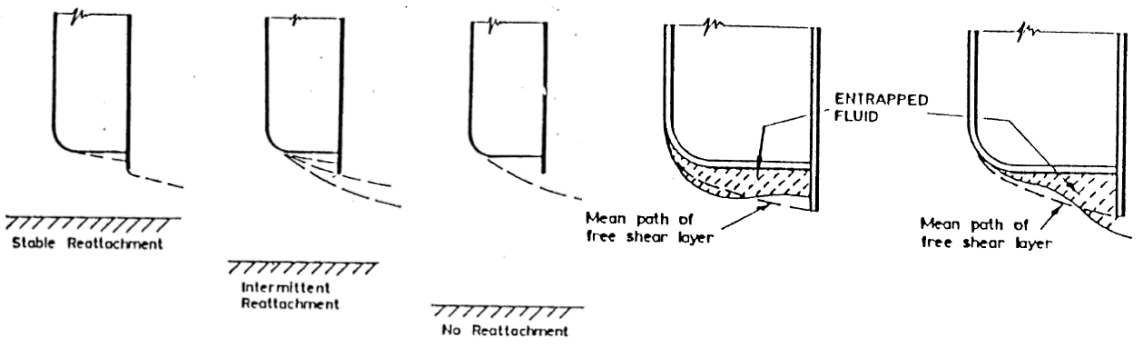

Figure C-5: (A) separated flow (B) possible shear layer deflection of entrapped fluid [35]

Comparable to the situations that should be avoided described by KOLKMAN AND JONGELING [33], LEWIN [35] some standard design guide lines regarding the shape of the valve. These rules are:

- No structural member downstream or upstream of the control point should protrude into a line at 45° from the point of flow control (Figure C-6). Upstream is advised to keep this angle at 60°, this is in contrast with see Figure C-6.
- It is better to arrange for vortex trail to be shed from the extreme downstream edge of the gate in order to achieve flow conditions that are as steady as possible.
- A sharp cut-off point should be provided at the lower edge. In other to keep the positon of the separation point stable.

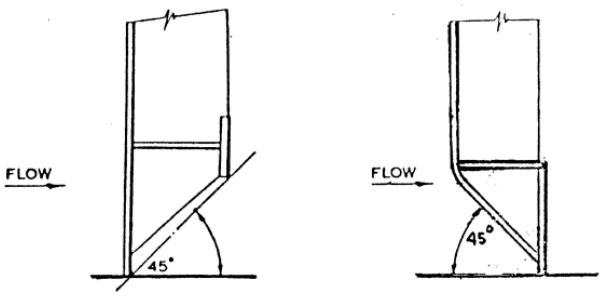

Figure C-6: Arrangement of structural members at the bottom of a valve [35]

C.5 Conclusion

The definitions given in various literature to flow-induced vibrations differ significantly. NAUDASCHER AND ROCKWELL [41] give a distinction between the causes. The three described vibrations are:

- extraneously induced excitation (EIE);
- instability-induced excitation (IIE);
- movement-induced excitations (MIE).

This research will only focus on the vibrations caused by flow instability (IIE) and the effect on a rigid body oscillator, this means that flexural movement should be kept as low as possible. This will lead to model in which the valve is infinitely stiff. There are two types of vibrations described by KOLKMAN AND JONGELING [33] that could be classified as IIE. These vibrations are:

- excitation due to turbulence (caused by the shape of the valve);
- the excitation due to flow instability.

The main vibration treated in this research will be the vibration caused by flow instability, however it will be impossible to separate the both types of vibrations. Therefore, the vibration due to turbulence will also return occasionally in the further course of this report. Also the other causes of vertical vibrations (cavitation, leakage and reflected wave) will be neglected in this research. It should however be kept in mind that possible design rules regarding these vibrations should be applied, because this would also be the case in a real-life design.

One of the most used rules regarding the vibrations is the relation between the dominant excitation frequency of the flow and the natural frequency of the structure. Current literature indicates that the structure will not fail due to vibrations as long as the natural frequency is at least 3 times the excitation frequency which is derived from equation C.6. This basic rule applies to the excitation due to turbulence, as well in horizontal direction as vertical direction.

$$\frac{f_n \cdot L}{U} > (2 \text{ a } 3) \cdot S \qquad \text{C.6}$$

For the excitation due to flow instability no exact design rules regarding frequency or forces are mentioned. When it comes to such a vibration the shape of the valve is normative. Important points of notice are:

- the separation point;
- possible reattachment point.

An instability in one of these two points could lead to vertical vibrations due to flow instability.

[Page intentionally left blank]

Appendix D Dimensional Analysis

This appendix explains the dimensional analysis that has been executed to determine the methodology and the model set-up. This analysis exists of the following subjects:

- Buckingham Π-theorem (§ D.1). This part explains the applied Buckingham Π-theorem that has been executed to create a dimensionless space. In this dimensionless space all relevant variables are present.
- Variables (§ D.2). This section is in continuation to the previous paragraph and presents all variables retrieved from the Buckingham Π-theorem. A distinction is made between input parameters, output parameters and scale parameters.

D.1 Buckingham Π-Theorem

The first step of the dimensional analysis is the execution of the Buckingham Π-theorem. This paragraph will elaborate the execution of this method. The main goal of this method is to create a dimensionless field in which the results can be interpreted. An additional benefit is that the number of variables reduces, this will be explained in a later stage of this paragraph. The first step of the theorem is to indicate all variables that are involved or could have an effect on the problem [57]. These variables are shown in Figure D-1 and described in Table D-1.

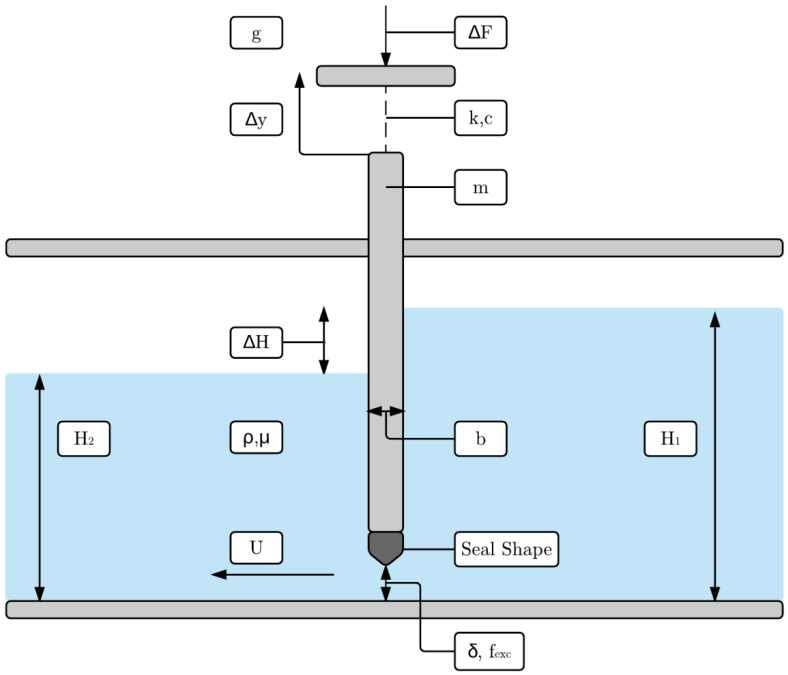

Figure D-1: Overview of involved variables

The units of the variables in Table D-1 are all rewritten in International System of Units (SI) base units. The final column shows that all variables depend on only 3 different SI base units (r = 3). These units are metres (length), seconds (time) and kilograms (mass). At this point the seal shape is defined as an additional external variable with no unit. This sums the total amount of variables up to 14 (n = 14). The result of the Buckingham Π-theorem will therefore only give (n - r = 14 - 3) 11 dimensionless parameters. This shows that the initial problem described by 14 individual parameters, will now be described by 11 individual parameters.

Variables	Symbol	Unit	SI-Unit
Stiffness	k	$N/m = (kg \cdot m/s^2)/m = kg/s^2$	$[M/T^2]$
Mass	m	kg	[M]
Damping	c	$(N \cdot s)/m = kg/s$	[M/T]
Vertical displacement of the valve	Δy	m	[L]
Upstream water level	H_1	m	[L]
Head difference	ΔH	m	[L]
Gate thickness	b	m	[L]
Gate opening	δ	m	[L]
Water density	ρ	kg/m^3	$[M/L^3]$
Excitation frequency	f_{exc}	$Hz = 1/s$	[1/T]
Flow velocity	U	m/s	[L/T]
Dynamic viscosity	μ	$Pa \cdot s = (N/m^2) \cdot s = kg/(m \cdot s^2) \cdot s = kg/(m \cdot s)$	$[M/(L \cdot T)]$
Gravitational acceleration	g	m/s^2	$[L/T^2]$
Vertical force amplitude	ΔF	$N = kg \cdot m/s^2$	$[M \cdot (L/T^2)]$
Seal shape	-	-	[-]

Table D-1: Parameters of the problem

All these variables are in some way connected to amplitude of the vertical force. The vertical force amplitude is chosen to be the outcome of the problem. Therefore, the equations D.1 and D.2 can be written.

$$\Delta F = f(k, m, c, \Delta y, \Delta H, b, \delta, \rho, \mu, U, H_1, f_{exc}, g) \quad \text{D.1}$$

$$\Delta F = k^a \cdot m^b \cdot c^c \cdot \Delta y^d \cdot \Delta H^e \cdot b^f \cdot \delta^g \cdot \rho^h \cdot \mu^i \cdot U^j \cdot H_1^k \cdot f_{exc}^l \cdot g^m \quad \text{D.2}$$

Because all variables depend on only 3 SI-unit's equation D.2 can be rewritten to equation D.3. This equation shows the basic problem in terms of only the SI basic units.

$$\left[\frac{M \cdot L}{T^2}\right] = \left[\frac{M}{T^2}\right]^a \cdot [M]^b \cdot \left[\frac{M}{T}\right]^c \cdot [L]^d \cdot [L]^e \cdot [L]^f \cdot [L]^g \cdot \left[\frac{M}{L^3}\right]^h \cdot \left[\frac{M}{L \cdot T}\right]^i \cdot \left[\frac{L}{T}\right]^j \cdot [L]^k \cdot \left[\frac{1}{T}\right]^l \cdot \left[\frac{L}{T^2}\right]^m \quad \text{D.3}$$

Comparing the SI-units in equation D.3 gives the conditions stated in equations D.4. The first step to a dimensionless space is found when equation D.2 is combined with the conditions from equation D.4. The results of this step are shown in equation D.5 and equation D.6.

$$\begin{aligned} \text{M: } 1 &= a + b + c + h + i \quad &\rightarrow h &= a - b + j + l + 2m - 1 \\ \text{L: } 1 &= d + e + f + g - 3h - i + j + k + m \quad &\rightarrow f &= a - 3b - c - d - e - g - k + j + 2l + 3m \\ \text{T: } -2 &= -2a - c - i - j - l - 2m \quad &\rightarrow i &= 2 - 2a - c - j - l - 2m \end{aligned} \quad \text{D.4}$$

$$\Delta F = k^a \cdot m^b \cdot c^c \cdot \Delta y^d \cdot \Delta H^e \cdot b^{a-3b-c-d-e-g-k+j+2l+3m} \cdot \delta^g \cdot \rho^{a-b+j+l+2m-1} \cdot \mu^{2-2a-c-j-l-2m} \cdot U^j \cdot H_1^k \cdot f_{exc}^l \cdot g^m \quad \text{D.5}$$

$$\Delta F = \left(\frac{\mu^2}{\rho}\right) \cdot \left(\frac{k \cdot b \cdot \rho}{\mu^2}\right)^a \cdot \left(\frac{m}{b^3 \cdot \rho}\right)^b \cdot \left(\frac{c}{b \cdot \mu}\right)^c \cdot \left(\frac{\Delta y}{b}\right)^d \cdot \left(\frac{\Delta H}{b}\right)^e \cdot \left(\frac{\delta}{b}\right)^g \cdot \left(\frac{U \cdot \rho \cdot b}{\mu}\right)^j \cdot \left(\frac{H_1}{b}\right)^k \cdot \left(\frac{f_{exc} \cdot b^2 \cdot \rho}{\mu}\right)^l \cdot \left(\frac{b^3 \cdot \rho^2 \cdot g}{\mu^2}\right)^m \quad \text{D.6}$$

The created dimensionless space is shown in equation D.7. The initial results are shown in Table D-2. Equation D.7 and equation D.1 show the exact same problem but with less parameters.

$$\frac{\Delta F \cdot \rho}{\mu^2} = f\left(\left(\frac{k \cdot b \cdot \rho}{\mu^2}\right), \left(\frac{m}{b^3 \cdot \rho}\right), \left(\frac{c}{b \cdot \mu}\right), \left(\frac{\Delta y}{b}\right), \left(\frac{\Delta H}{b}\right), \left(\frac{\delta}{b}\right), \left(\frac{U \cdot \rho \cdot b}{\mu}\right), \left(\frac{H_1}{b}\right), \left(\frac{f_{exc} \cdot b^2 \cdot \rho}{\mu}\right), \left(\frac{b^3 \cdot \rho^2 \cdot g}{\mu^2}\right)\right) \quad \text{D.7}$$

Number	Π_1	Π_2	Π_3	Π_4	Π_5	Π_6	Π_7	Π_8	Π_9	Π_{10}	Π_{11}
Formula	$\frac{\Delta F \cdot \rho}{\mu^2}$	$\frac{k \cdot b \cdot \rho}{\mu^2}$	$\frac{m}{b^3 \cdot \rho}$	$\frac{c}{b \cdot \mu}$	$\frac{\Delta y}{b}$	$\frac{\Delta H}{b}$	$\frac{\delta}{b}$	$\frac{U \cdot \rho \cdot b}{\mu}$	$\frac{H_1}{b}$	$\frac{f_{exc} \cdot b^2 \cdot \rho}{\mu}$	$\frac{b^3 \cdot \rho^2 \cdot g}{\mu^2}$

Table D-2: The initial dimensionless factors resulting from the Buckingham Π-theorem

The results from Table D-2 are combined to come to predefined and useful dimensionless numbers that have been used in research before. Multiplying and dividing with dimensionless numbers keeps resulting in dimensionless numbers. In the final results all parameters shown in Table D-2 have to return. The combinations made are shown in equations D.8 up to D.15.

$$\Pi_{?1} = \frac{\Pi_{10}}{\Pi_8} = \frac{\left(\frac{f_{exc} \cdot b^2 \cdot \rho}{\mu}\right)}{\left(\frac{U \cdot \rho \cdot b}{\mu}\right)} = \frac{f_{exc} \cdot b}{U} \tag{D.8}$$

$$\Pi_{?2} = \frac{\Pi_2}{\Pi_8^2} = \frac{\left(\frac{k \cdot b \cdot \rho}{\mu^2}\right)}{\left(\frac{U \cdot \rho \cdot b}{\mu}\right)^2} = \frac{k}{\rho \cdot U^2 \cdot b} \tag{D.9}$$

$$\Pi_{?3} = \sqrt{\frac{\Pi_4^2}{\Pi_2 \cdot \Pi_3}} = \sqrt{\frac{\left(\frac{c}{b \cdot \mu}\right)^2}{\left(\frac{k \cdot b \cdot \rho}{\mu^2}\right) \cdot \left(\frac{m}{b^3 \cdot \rho}\right)}} = \frac{c}{\sqrt{k \cdot m}} \tag{D.10}$$

$$\Pi_{?4} = \frac{\Pi_{10}}{\sqrt{\Pi_2 / \Pi_3}} = \frac{\left(\frac{f_{exc} \cdot b^2 \cdot \rho}{\mu}\right)}{\sqrt{\left(\frac{k \cdot b \cdot \rho}{\mu^2}\right) / \left(\frac{m}{b^3 \cdot \rho}\right)}} = \frac{\left(\frac{f_{exc} \cdot b^2 \cdot \rho}{\mu}\right)}{\sqrt{\left(\frac{k \cdot b^4 \cdot \rho^2}{\mu^2 \cdot m}\right)}} = \frac{\left(\frac{f_{exc} \cdot b^2 \cdot \rho}{\mu}\right)}{\sqrt{\frac{k}{m}} \cdot \frac{b^2 \cdot \rho}{\mu}} = \frac{f_{exc}}{\sqrt{\frac{k}{m}}} \tag{D.11}$$

$$\Pi_{?5} = \frac{\Pi_{?4}}{\Pi_{?1}} = \frac{\left(f_{exc} / \sqrt{\frac{k}{m}}\right)}{\frac{f_{exc} \cdot b}{U}} = \frac{U}{b \cdot \sqrt{\frac{k}{m}}} \tag{D.12}$$

$$\Pi_{?6} = \frac{\Pi_{11}}{\Pi_8^2} \cdot \Pi_6 = \frac{\left(\frac{b^3 \cdot \rho^2 \cdot g}{\mu^2}\right)}{\left(\frac{U \cdot \rho \cdot b}{\mu}\right)^2} \cdot \frac{\Delta H}{b} = \frac{\Delta H \cdot g}{U^2} \tag{D.13}$$

$$\Pi_{?7} = \frac{m}{b^3 \cdot \rho} = \frac{m}{V \cdot \rho} \tag{D.14}$$

$$\Pi_{?8} = \frac{\Pi_1}{\Pi_8^2} = \frac{\frac{\Delta F \cdot \rho}{\mu^2}}{\left(\frac{\mu}{U \cdot \rho \cdot b}\right)^2} = \frac{\Delta F}{U^2 \cdot \rho \cdot b^2} \tag{D.15}$$

The final dimensionless parameters from the dimensionless space are shown in Table D-3. The numbers are given a name.

Number	Name	Formula	Number	Name	Formula
Π_1	Dimensionless force amplitude	$\frac{\Delta F}{U^2 \cdot \rho \cdot b^2}$	Π_7	Frequency ratio	$\frac{f_{exc}}{\sqrt{k/m}}$
Π_2	Cauchy number	$\frac{k}{U^2 \cdot \rho \cdot b}$	Π_8	Density Ratio	$\frac{m}{V \cdot \rho}$
Π_3	Reynolds number	$\frac{U \cdot \rho \cdot b}{\mu}$	Π_9	Displacement ratio	$\frac{\Delta x}{b}$
Π_4	Strouhal number	$\frac{f_{exc} \cdot b}{U}$	Π_{10}	Length factor	$\frac{H_1}{\delta}$
Π_5	Damping number	$\frac{c}{\sqrt{k \cdot m}}$	Π_{11}	Relative Gate Opening	$\frac{\delta}{b}$
Π_6	Froude number	$\frac{\Delta H \cdot g}{U^2}$	Π_{12}	Seal shape	[-]

Table D-3: Derived Π-terms from the Buckingham Π-theorem

The term Π_7 (frequency ratio) will be rewritten to the ratio between the excitation frequency and the natural frequency (as described in the next paragraph). This definition is shown in equation D.16. A similar step has been taken to take the dimensionless damping to a definition used often in literature. The damping number is rewritten to the damping factor as shown in equation D.17.

$$\Pi_7 = \frac{f_{exc}}{f_n} = \frac{f_{exc}}{\frac{1}{2\pi} \cdot \sqrt{\frac{k}{m}}} \qquad \text{D.16}$$

$$\Pi_5 = \frac{c}{2 \cdot \sqrt{k \cdot m}} \qquad \text{D.17}$$

D.2 Variables

After the dimensionless numbers have been defined in the previous, this section will be the next step in the dimensional analysis. In this paragraph the results from the previous paragraph will be classified within three categories. The categories will be discussed individually and are listed below.

- input variables (§ D.2.1);
- output variables (§ D.2.2);
- scale factors (§ D.2.3).

D.2.1 Input Variables

Not all of the variables shown in Figure D-1 and used in the last paragraph for the Buckingham Π-theorem can be regulated during the tests. The below listed four variables will be input variables. Behind the variable the related Π-term is indicated:

- the flow velocity underneath the valve (Π_6);
- the shape of the lower edge seal (Π_{12});
- the natural frequency of the valve system (Π_7);
- the gate opening underneath the valve (Π_{11}).

The above mentioned variables could depend on other sub variables. This will be discussed in the further course of this paragraph in which the variables will be elaborated separately.

Flow Velocity (Π_6)

The velocity underneath the valve depends on the head difference over the valve and the discharge underneath the valve. This can be related to the Π_6-term from Table D-3, which also represents the Froude number. The velocity cannot be calculated based on the discharge and the opening under the valve, because of the unknown contraction of the flow. Because of the contraction the flow will not use the entire area underneath the valve. For this reason, the formula shown in equation D.18 should be used to determine the flow velocity based on the head difference over the valve.

$$U = \sqrt{2 \cdot g \cdot \Delta H} \qquad \text{D.18}$$

In which:

	U	=	average profile velocity [m/s]
	g	=	gravitational acceleration [m/s^2]
	ΔH	=	head difference over the valve [m]

Equation D.18 shows the resemblance with Π_6. The Froude number will not have any effect in this model because there is no free surface flow in the real-life situation. The flow velocity can be varied by changing the discharge and as a result the head difference over the valve. The flow velocity is also a part of the Strouhal number (Π_4), which is an important factor during the determination of the excitation frequency (f_{exc}). Kept in mind should be that the lower edge of the valve should be submerged at all-time.

For rigid structures with an elastic suspension the velocity scale may be freely chosen, if only the Reynolds number does not drop below a critical value [36]. This is the case in this model, because the viscous force does not play a significant role in the vibration phenomena, as described above. Because the velocity scale is free to choose a choice can be made to pick a scale corresponding to the Froude law. In this case a closed conduit flow could be scaled according to the Froude law [27]. The flow velocity during tests has been varied between 0.3 m/s (ΔH = 5 mm) and 1.9 m/s (ΔH = 192 mm).

Seal Shapes (Π_{12})

The shape of the seal is one of the main focus points of this research and is represented by Π_{12} in the dimensional analysis. The factor has been included as an external Π-term. The choice for the shapes is based on the vulnerability for the different kinds of vibrations. A more detailed elaboration of these vulnerabilities is given in Appendix C. The shapes used during the research are:

- rectangular-shaped profile (Figure D-2, no. 1);
- rectangular profile with chamfered edges (Figure D-2, no. 2). In the further course of the report this shape is referred to as chamfered-shaped;
- point-shaped profile with rounded edges (Figure D-2, no. 3). In the further course of the report referred to as point-shaped;
- circular-shaped profile (Figure D-2, no. 4).

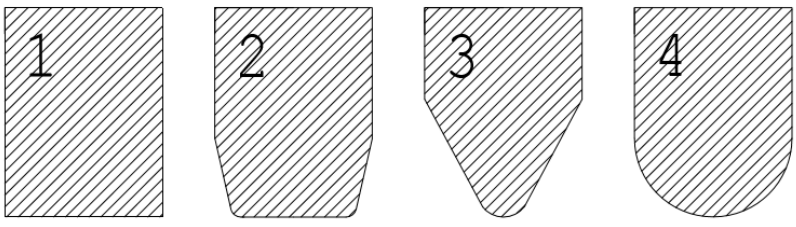

Figure D-2: Different lower edge seal shapes used during the research

Natural Frequency of the System (Π_7)

The natural frequency of the system returns in the Π_7-term and is made dimensionless with help of the excitation frequency (f_{exc}). The natural frequency of the valve system is given by equation D.19. The natural frequency is affected by two single parameters of the model. These parameters are:

- the stiffness;
- the mass.

$$f_n = \frac{1}{2 \cdot \pi} \cdot \sqrt{\frac{k}{m}} \qquad \text{D.19}$$

With the determined mass of 9.0 kg (Chapter 3) and the used rigidities. The calculation of the spring rigidities can be found in Appendix G. The calculated theoretical natural frequencies are shown in Table D-4.

Spring Stiffness [N/mm]	Natural Frequency [Hz]
1.16	1.8
5.34	3.9
15.66	6.69
43.2	11.0

Table D-4: Used different types of stiffness and natural frequencies

Gate Opening (Π_{11})

The final parameter that can be varied during the process is the opening underneath the gate. The gate opening is made dimensionless with the gate thickness. This relation is shown in equation D.20.

$$\delta / b \qquad \text{D.20}$$

In which: δ = opening under the valve [m]
b = width of the valve [m]

The gate opening is relevant for the instability of the flow. Literature indicates that effects due to reattachment of the flow only occurs at relative opening of $\delta/b < 1$. This is only experienced for a valve with a shape vulnerable for this type of vibrations (rectangular) [34]. Recent research found the major vibrations phenomena also in this range [20].

Based on literature three different relative gate openings are used during the test. The different openings are:

- $\delta/b = 0.5$. With this opening reattachment phenomena should occur for the vulnerable shapes.
- $\delta/b = 1$. This opening is a borderline case. Extreme vulnerable shapes will show vibrations due to reattachment, less vulnerable shapes most probably not.
- $\delta/b = 1.5$. In none of the cases any vibrations due to reattachment should occur with this opening.

Because it was not possible to fix the gate opening exact at the above mentioned values. The opening was varied between 5 mm and 52 mm.

D.2.2 Output Variables

As earlier discussed the output is given in dimensionless parameters so the results can be applied on real-life design in the future. Therefore, it has been tried to present the results based on parameters that could be influenced and changed in the design phase. The following output variables are discussed in this paragraph:

- vertical force amplitude (Π_1);
- excitation frequency (Π_4);
- vertical displacement (Π_9).

Vertical Force Amplitude (Π_1)

One of the outputs should be the amplitude of the vertical force of the initiated vibrations, which will be presented in the Π_1-term. Equation D.21 presents a formula from literature combining the vertical down pull force with the characters of the flow and structural parts. This formula could be used to determine if the shape of the valve has influence on the down pull coefficient as mentioned in the formula. Because the valve and model are solely being under flown the relevant coefficient is the bottom coefficient (α_B), the top coefficient (α_T) can be neglected.

$$F = (\alpha_T - \alpha_B) \cdot b \cdot d \cdot \rho \cdot (U^2/2) \qquad \text{D.21}$$

In which:

F	=	down pull force [N]
α_T	=	down pull coefficient at the top of the valve [-]
α_B	=	down pull coefficient at the bottom of the valve [-]
b	=	width of the gate [m]
d	=	depth of the gate [m]
ρ	=	density of water [kg/m^3]
U	=	velocity under the valve [m/s]

Excitation Frequency (Π_4)

One of the measured values will be the excitation frequency (f_{exc}) that returns in Π_4. In case of extreme stiff situation, the excitation frequency can be measured with a pressure sensor. For more information of a pressure sensor see Appendix F. When movement is possible, not the excitation frequency (f_{exc}) but the response frequency (f_{resp}) is measured. This frequency is not only related to the excitation frequency but also to the natural frequency (f_n) of the system. Crucial in this part is the definition of the Strouhal number. The multiple definitions of the Strouhal number are:

- Strouhal number based on the excitation frequency (S), see equation D.22.

$$S = \frac{f_{exc} \cdot b}{U} \qquad \text{D.22}$$

In which:

S	=	Strouhal number based on excitation frequency [-]
U	=	flow velocity [m/s]
f_{exc}	=	excitation frequency [Hz]
b	=	thickness of the valve [m]

- Strouhal number based on the natural frequency (S_n), see equation D.23.

$$S_n = \frac{f_n \cdot b}{U} \qquad \text{D.23}$$

In which:

S_n	=	Strouhal number based on natural frequency [-]
f_n	=	natural frequency [Hz]

- A critical Strouhal number has been defined in this report. This number is a constant factor at which the vibrations occur (S_c), see equation D.24 and Figure D-3.

$$S_c = \frac{f_{exc,\,dom} \cdot b}{U} \qquad \text{D.24}$$

In which: S_c = critical Strouhal number [-]

$f_{exc,dom}$ = dominant excitation frequency [Hz]

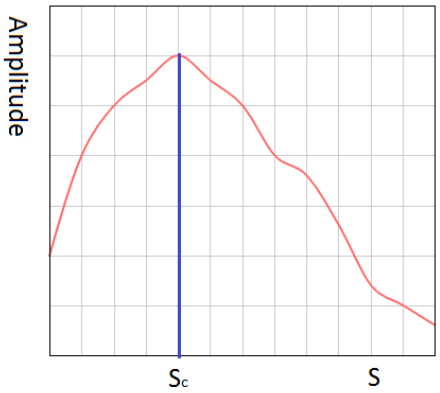

Figure D-3: Definition of the critical Strouhal number

An often used way to present results regarding the effects of flow-induced vibrations is the reduced velocity. The definitions of the reduced velocity parameters are coupled to the definitions of the above mentioned Strouhal number, see equations D.25 and D.26.

$$V_{rd} = 1/S \qquad \text{D.25}$$

In which: V_{rd} = reduced velocity [-]

S = Strouhal number based on excitation frequency [-]

$$V_{rd,n} = 1/S_n \qquad \text{D.26}$$

In which: $V_{rd,n}$ = reduced velocity based on natural frequency [-]

S_n = Strouhal number based on natural frequency [-]

$$V_{rd,r} = \frac{U}{f_{resp} \cdot b} \qquad \text{D.27}$$

In which: $V_{rd,r}$ = reduced velocity based on response frequency [-]

f_{resp} = response frequency system [Hz]

Equation D.27 shows a special form of the reduced velocity which is used during the most recent researches to display a critical range in which the vibrations occur, this definition is used here to determine the range of expected vibrations. The previous researches made a distinction between high reduced velocity ranges ($10 < V_{rd,r} < 80$), which indicates vibrations due to flow instability (IIE), and low reduced velocity ranges ($2 < V_{rd,r} < 3.5$), which indicate vibrations induced by the movement of the valve (MIE) [20]. Researches from the same period indicate the same reduced velocity areas, but contradict the causes [8].

It should be noted that the use of reduced velocity (and the Strouhal number) has not been a clear process. In some past researches the characteristic length (L) was defined as the gate opening (δ) [56] [59]. In the most recent researches the width of the gate (b) is used as characteristic length [20] [8]. When you present your results using the dimensionless reduced velocity this could give a skewed view on the problem. Table D-5 shows the critical vibrations ranges found in the most recently done research.

Research	Critical Range for Vibrations	
ERDBRINK [20]	$V_{rd,r} > 2$	$V_{rd,r} < 3.5$
	$V_{rd,r} > 8.5$	
BILLETER AND STAUBLI [8]	$V_{rd,r} > 2$	$V_{rd,r} < 4$
	$V_{rd,r} > 10$	

Table D-5: Critical vibration ranges in previously done research

With a valve width (b) of 0.03 m and $\Delta H_{max} = 0.1$ m and $\Delta H_{min} = 0.02$ m. The expected response frequencies based on previous done researches can be calculated. The frequencies are based on valve with a rectangular shape, for the other shapes the response frequencies are assumed to be in the same range. The difference in range will be a result of the shape. See for the calculated expected frequencies Table D-6. These expected frequencies are the basis for the determination of the stiffness of the system.

Critical Range		f_{resp} [Hz]	f_{resp} [Hz]
Flow Velocity		$U_{max} = 1.4$ m/s for $\Delta H_{max} = 0.1$ m	$U_{min} = 0.6$ m/s for $\Delta H_{min} = 0.02$ m
Low Range	$V_{rd,r} = 2.0$	23.35 Hz	10.44 Hz
	$V_{rd,r} = 3.5$	13.34 Hz	5.97 Hz
High Range	$V_{rd,r} = 8.5$	5.49 Hz	2.46 Hz
	$V_{rd,r} = 80$	0.58 Hz	0.26 Hz

Table D-6: Expected response frequency

Vertical Displacement (Π_9)

The vertical displacement will be the output of the model and can be made dimensionless using the Π_9-term. The vertical displacement could also be used to calculate the vertical force when the stiffness (k) is known.

D.2.3 Scale Parameters

The model used is not based on a real-life prototype. Most of the numbers from the dimensional analysis have been presented as an input or an output number. The remaining numbers will have an effect on the scaling. This means that they have to go to a limit or stay constant to maintain a proper scale. There are three types of scaling:

- geometric scaling;
- kinematic scaling;
- dynamic scaling;

In this research the dynamic scaling is the most important. Dynamic similarity requires constant ratios of all forces [28]. See equation D.28 [22] that gives the ratios between the 6 most important forces in fluid dynamics. These forces are:

- inertia force;
- gravity force;
- viscous force;
- elastic compression force;
- pressure force;
- surface tension force.

$$\frac{(F_i)_n}{(F_i)_m} = \frac{(F_g)_n}{(F_g)_m} = \frac{(F_\mu)_n}{(F_\mu)_m} = \frac{(F_e)_n}{(F_e)_m} = \frac{(F_p)_n}{(F_p)_m} = \frac{(F_s)_n}{(F_s)_m} \qquad \text{D.28}$$

In which:

F_i	=	inertia force [N]
F_g	=	gravity force [N]
F_μ	=	viscous force [N]
F_e	=	elastic compression force [N]
F_p	=	pressure force [N]
F_s	=	surface tension force [N]

Because inertia is usually the most relevant force in fluid dynamics [28], these ratios are given by 5 dimensionless numbers, see equations D.29 up to D.33 for the definitions of these numbers.

Froude:
$$Fr = \left(\frac{\text{Inertial Force}}{\text{Gravity Force}}\right)^{1/2} = \frac{U}{(g \cdot L)^{1/2}} \qquad \text{D.29}$$

Reynolds:
$$Re = \frac{\text{Inertial Force}}{\text{Viscous Force}} = \frac{L \cdot U}{\nu} \qquad \text{D.30}$$

Weber:
$$We = \frac{\text{Inertial Force}}{\text{Surface Tension Force}} = \frac{\rho \cdot U^2 \cdot L}{\sigma} \qquad \text{D.31}$$

Euler:
$$Eu = \frac{\text{Pressure Force}}{\text{Inertial Force}} = \frac{p}{\rho \cdot U^2} \qquad \text{D.32}$$

Cauchy:
$$Ca = \frac{\text{Inertial Force}}{\text{Elastic Force}} = \frac{\rho \cdot U^2}{E} \qquad \text{D.33}$$

In which:

U	=	characteristic velocity [m/s]
g	=	gravitational acceleration [m/s^2]
L	=	characteristic length [m]
ν	=	kinematic viscosity [m^2/s]
ρ	=	fluid density [kg/m^3]
σ	=	surface tension [N/m]
p	=	pressure [Pa]
E	=	Young's modulus [N/m^2]

This information is combined with the Π-terms. That shows that the Weber number is not relevant in this problem, because the surface tension has been left out of the dimensional analysis. This can be checked in Weber is smaller than 11 [43]. This also counts for the Mach number, because the fluid was assumed to be incompressible from the start of the research. The Mach number should kept small ($M < 0.3$) [43] to ensure there are no compressibility effects.

In an earlier phase has been stated that a closed conduit has to be simulated and that makes the Froude number irrelevant. These statements lead to the remaining of 5 Π-terms as scaling parameter.

- Reynolds number (Π_3);
- Cauchy number (Π_2);
- damping factor (Π_5);
- mass number (Π_8);
- length ratio (Π_{10});

Reynolds Number (Π_3)

The Reynolds number is given by Π_3 and has to reach a limit value to ensure a turbulent situation and a possible excitation frequency. When the Reynolds number is high enough, viscous forces can be neglected. The limit for the Reynolds number is given in equation D.34 [43]. This limit has to be met to ensure that the friction of the walls does not play a role in the velocity determination.

$$\mathrm{Re} > 10^5 \qquad \text{D.34}$$

The official equation of the Reynolds number is given in equation D.35.

$$\mathrm{Re} = \frac{U \cdot L \cdot \rho}{\mu} = \frac{U \cdot L}{\nu} \qquad \text{D.35}$$

In which:

Re	=	Reynolds number [-]
U	=	characteristic velocity [m/s]
L	=	characteristic length [m]
ρ	=	density liquid [kg/m^3]
μ	=	dynamic viscosity liquid [Pa·s]
ν	=	kinematic viscosity liquid [m^2/s] = $1.2 \cdot 10^{-6}$ m^2/s for water of 14° C

The possible ranges that can be achieved in the tests depend on the thickness of the valve and the possible flow velocities as determined in an earlier stage of this appendix. The Reynolds value is strongly dependable on definition of the characteristic length. The values do not exceed the limit stated in equation D.34. In this state is assumed that the value is large enough. This should be checked during the test phase.

Cauchy Number (Π_2), Damping Factor (Π_5) and Density Ratio (Π_8)

The Cauchy number (stiffness), the damping factor (damping) and density ratio (mass) do all influence the dynamical characteristics of the system as elaborated in Appendix B. In a situation in which the system is kept extreme stiffness, all these scale factors no longer play a significant role. When a prototype model was scaled these factors should be kept constant. In this case no prototype is available.

Length Ratio (Π_{10})

The only Π-term left is a length ratio presented by Π_{10}. Assumed is that this parameter has an influence on the flow pattern. This is shown in Figure D-4. Assumed is that the ratio H_1/δ should be at least 2 but as high as possible. This is assumed to recreate a drowned situation as is also the case in a closed conduit culvert.

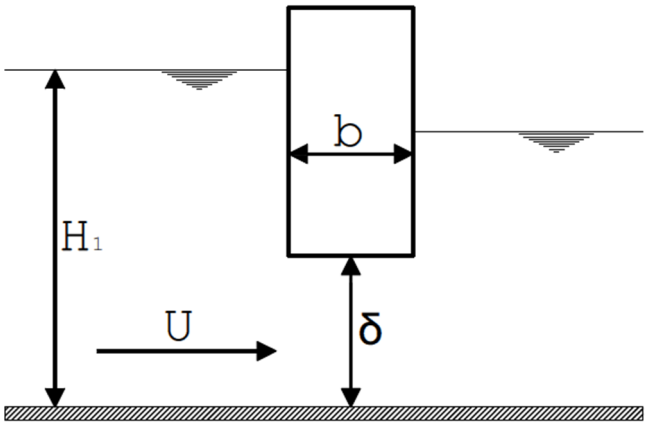

Figure D-4: Schematization of the relation between H_1 and b

D.3 Conclusion

Table D-7 shows the relevant dimensionless parameters retrieved from the Buckingham Π-theorem and their role in the model (input/output or scale parameter). For the scale parameters the conditions are shown and their relevance to the two situations as described earlier. The two situations are:

- an extreme stiff situation. In which the dynamic characteristics (m, k and c) and the displacement ($\triangle y$) of the model are irrelevant.
- low stiffness model. In this case the dynamic characteristics and the displacement are relevant for the results of the tests.

The table below shows clearly that the 15 variables from Figure D-1 and Table D-1 are rewritten to 12 dimensionless parameters. The Froude number (Π_6) is not relevant in both cases because a situation of a closed culvert is simulated.

#	Name	Formula	Type	Conditions	Extreme stiff model	Low stiffness model
Π_1	Dimensionless force amplitude	$\frac{\triangle F \cdot \rho}{\mu^2}$	Output		Present	Present
Π_2	Cauchy number	$\frac{k}{U^2 \cdot \rho \cdot b}$	Scale	Constant with prototype	Irrelevant	Present
Π_3	Reynolds number	$\frac{U \cdot \rho \cdot b}{\mu}$	Scale	$> 10^5$	Present	Present
Π_4	Strouhal number	$\frac{f_{exc} \cdot b}{U}$	Output		Present	Present
Π_5	Damping factor	$\frac{c}{2 \cdot \sqrt{k \cdot m}}$	Scale	Constant with prototype	Irrelevant	Present
Π_6	Froude number	$\frac{\triangle H \cdot g}{U^2}$	Input	Freely to chose	Irrelevant	Irrelevant
Π_7	Frequency ratio	$\frac{f_{exc}}{f_n}$	Input		Irrelevant	Present
Π_8	Density Ratio	$\frac{m}{V \cdot \rho}$	Scale	Constant with prototype	Irrelevant	Present
Π_9	Displacement ratio	$\frac{\triangle x}{b}$	Output		Irrelevant	Present
Π_{10}	Length factor	$\frac{H_1}{\delta}$	Scale	> 2	Present	Present
Π_{11}	Length factor	$\frac{\delta}{b}$	Input		Present	Present
Π_{12}	Seal shape	[-]	Input		Present	Present

Table D-7: Overview of Π-terms and characteristics

Appendix E Methodology

This appendix gives an explanation of the methodology used during the research. The appendix has been divided into two main parts. The two parts are:

- Process steps (§ E.1). The first part of the appendix describes the steps taken during the execution of the tests.
- The different test cases (§ E.2). This paragraph will give a more detailed description of the different test cases. It will also describe the expectations of the response of the different cases to the different vibration phenomena.

E.1 Process Steps

The process of testing has been divided into different steps. These steps are elaborated in this paragraph. The different steps are:

- the determination of the mass of the model (§ E.1.1);
- the determination of natural frequency in free air and in stationary water (§ E.1.2);
- the steady state measurements under varying conditions (§ E.1.3);
- check of assumptions made during the dimensional analysis and the design of the model set-up (§ E.1.4).

E.1.1 Determine Mass

The first step of the tests is to determine the mass of the movable part of the model. Kept in mind should be that any penetrated water should be taken into account. This can be done by repeating this step at the very end of the testing period. In a further stage of this paragraph the changing of the seal is mentioned. This change can affect the mass of the entire movable part and should therefore be measured again. The mass should be identified individually for all shapes of lower edge seals. This can be done by weighing the individual parts.

E.1.2 Determine Natural Frequency

The natural frequency is related to the mass and stiffness of the model, which differs in free air from a situation in water. This is due to added water effects as described in Appendix B. One of the effects is the added mass that relies on the submergence of the gate and therefore depends on the height of the water level. The natural frequency can be determined by a free decay test. During this test the system is given a simple tap and the movement is monitored. For both cases (in free air and under water) this can be done in a similar way. Because the added water mass depends on the immergence of the gate under water this process should be repeated with the different gate openings and water levels. The water test should be executed in a stationary situation ($Q_{pump} = 0$). During this step also the structural damping can be measured. The damping is determined by executing the logarithmic decrement method. The is shown on Chapter 4.

E.1.3 Steady State Measurements

During the main stage of the research the measurements are executed in a steady state situation. During these steps the important values to measure are the flow velocity (U) (related to ΔH), the response frequency (f_{resp}) and the vertical displacement (Δy). The varying variables during these steady state measurements are:

- 4 different shapes of lower edges;
- varying flow velocities (U), related to the head difference over the valve (ΔH);
- varying gate openings (δ);
- the natural frequency (f_n), which is varied by the stiffness of the system (k).

Different seal shapes, a total of 4, are going to be tested with similar conditions (same δ, U and f_n). The seals have been explained in Appendix D. The individual cases are elaborated in more detail in the next paragraph.

E.1.4 Additional Tests

Because the model is made on scale and some effects are neglected, during the tests some of these assumptions should be tested. The tests are summarized under the name of additional tests. In Chapter 1 and Appendix D the assumptions are explained. The tests will focus on:

- the sensitivity of the water depth on the phenomenon.
- the effects in relation to the Reynolds number.
- the contraction effects underneath the valve.

Sensitivity Water Depth

The sensitivity of the water depth is checked by executing tests with similar conditions but varying water depths. The conditions (U, δ and k) should be kept constant and only the water depth on both sides of the valve (H_1 and H_2) should be varied. The results of these variations should be compared.

Reynolds Number

The influence of the Reynolds number should be checked during the tests. This can be done by varying the Reynolds number as presented in Chapter 3. The varying parameter in this definition will be the flow velocity (U).

Contraction Effects

The different seal shapes show different effects regarding contraction and energy losses. These effects have an effect on the assumption that the flow velocity (U) can be approached by only using the head difference (ΔH). The effects have been checked by making a video of the flow and using a dye to visualize the flow. The video is eventually used to retrieve images with clear contraction. On the lower edges a part of a tape-measure has been attached, so afterwards it is possible to scale the obtained images.

E.2 Cases

This paragraph describes the 4 different cases (each with a different seal shape) and the expectations regarding the response of these different shapes to the different types of vibrations. The expectations are divided into three possible causes as described in Appendix C. These causes are:

- turbulence;
- instability separation point;
- flow reattachment.

E.2.1 Case 1

In the first situation a rectangular lower edge shape is applied (as used by ERDBRINK [20]) and has been tried to create conditions in which the valve intends to vibrate (Figure E-1). When the gate opening is differed the type of vibrations should be recognisable. In this situation is the width of the valve defined as b (Figure E-1). During the change of the valve shape this definition will stay the same. In the first state the flow velocity is kept constant. Literature prescribes that reattachment of the flow on a rectangular shaped valve only occurs when the gate opening (δ) is smaller than the width of the gate (b) [33]. When varying the gate opening (δ) multiple scenarios will occur. The step described in the previous paragraph (determine the added mass) should be repeated for every seal shape to determine the natural frequency under water. Figure E-1 shows the case with the most important characteristics.

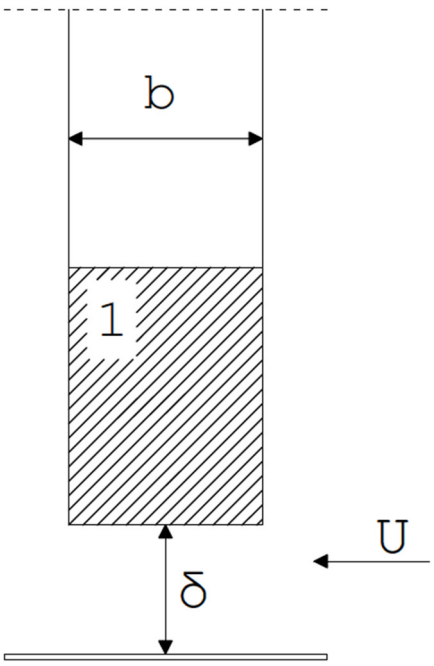

- Rectangular-shaped seal.
- Intend to let the valve vibrate, based on previous researches.
- Width of valve (b) kept constant
- Flow velocity (U) varied.
- Variation in natural frequency (f_n) to obtain relation between natural frequency (f_n), response frequency (f_{resp}) and excitation frequency (f_{exc}).
- 3 predefined gate openings (δ) to distinguish different vibration causes.

Figure E-1: Case 1 with a rectangular shaped seal

Turbulence: Vibrations due to turbulence will be present under all conditions.

Instability separation point: Because the valve has no round shapes no instable separation point should occur.

Flow reattachment: Because of the rectangular shape reattachment is possible, it will only occur when the gate opening (δ) is smaller than the width of the gate (b). Reattachment does not always lead to vibrations. When the situation is stable (stable reattachment point, no fluctuations in entrapped fluid) the valve will not vibrate.

E.2.2 Case 2

In case 2 a real-life used lower edge seal is used. The shape of the seal has been referred to as chamfered-shaped. The basic conditions regarding velocity (U) and gate width (b) are kept similar. The lower edge seal used is a shape that is used in real-life however it is not the most used type. The mass of the different lower edge seals is almost similar. Therefore, the natural frequency (f_n) will not vary per case.

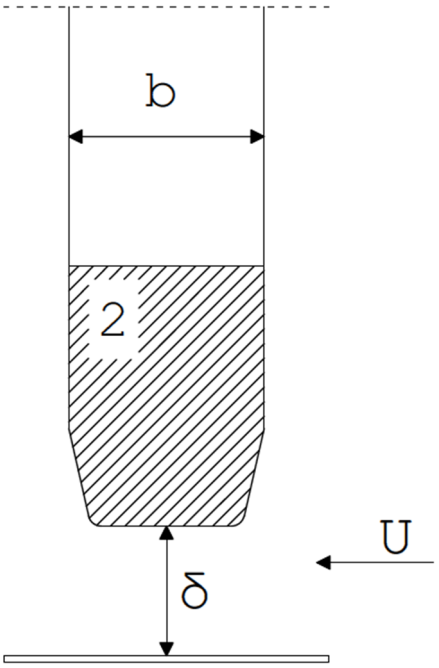

- Rectangular shape seal with chamfered corners.
- Determine wet natural frequency. System expected to have higher mass and lower added stiffness.
- Same flow velocities (U) as in previous case.
- Same gate opening (δ) as in previous case.
- Same structural stiffness (k) as in previous case.

Figure E-2: Case 2 with a chamfered- shaped seal

Turbulence: Vibrations due to turbulence will be present under all conditions.

Instability separation point: Similar to situation 1 there will be no instable separation point, because the valve has no round shapes.

Flow reattachment: For this case the same as for situation 1 applies. However, expected is that the flow reattachment occurs with only small relative gate openings (δ/b). This can be explained by the cut-off corners that makes horizontal surface on the lowest point smaller. The flow has less range to reattach.

E.2.3 Case 3

Case 3 uses one of the most applied seals nowadays. The seal is designed under an angle of 60°, as stated in the design guide lines [33], and has a sharp tip as possible, this should prevent any vibrations due to flow reattachment. The shape has been referred to as point-shaped.

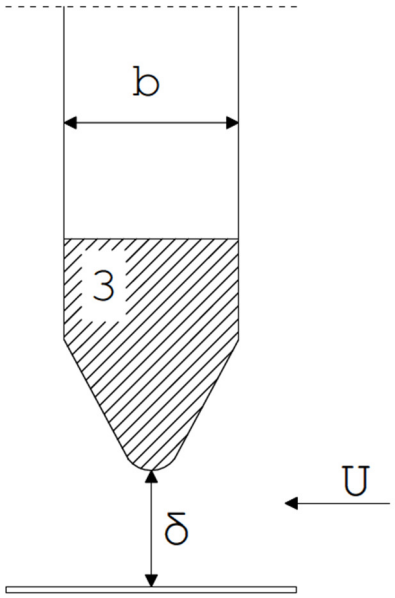

- Point-shaped seal.
- Same flow velocities (U) as in previous case.
- Same gate opening (δ) as in previous case.
- Same structural stiffness (k) as in previous case.

Figure E-3: Case 3 with a point-shaped seal

Turbulence: Vibrations due to turbulence will be present under all conditions.
Instability separation point: Because the tip still has a small radius some vibrations due to instability of the separation point can be expected. During the design of the seal has been tried to keep the tip as sharp as possible to prevent this phenomenon.
Flow reattachment: Because of the applied angles as described before, no flow reattachment is possible. So no vibrations due to this phenomenon should occur with this shape.

E.2.4 Case 4

The fourth and final case will be with a round shape. This basic form is still used a lot during the design of vertical lift valves.

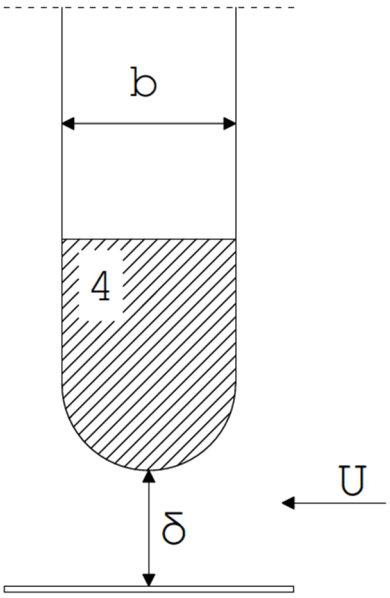

- Circular-shaped seal.
- Same flow velocities (U) as in previous case.
- Same gate opening (δ) as in previous case.
- Same structural stiffness (k) as in previous case.

Figure E-4: Case 4 with a circular-shaped seal

Turbulence: As long as there is a flow velocity the vibrations due to turbulence will be present. Lower flow velocities most probably show less excitation.

Instability separation point: This seal should be, compared with the shapes from the other situations, the most vulnerable for vibrations due to an instable separation point.

Flow reattachment: Due to the shape of the seal no flow reattachment should occur, so no vibrations due to this cause will take place.

E.3 Conclusion

This appendix elaborated the relevant input variables and the process steps. The varying parameters are:

- the seal shapes. The names of the different seal shapes are shown in Table E-1 .
- the spring stiffness (k). By varying the stiffness, the natural frequency of the model can be modified. The used springs are shown in Table E-1.
- the flow velocity (U). The flow velocity has been varied between 0.3 m/s ($\Delta H = 5$ mm) and 1.9 m/s ($\Delta H = 192$ mm).
- the gate opening (δ). The opening underneath the valve has been varied between 5 mm and 52 mm.

Seal Shapes	Spring Stiffness [N/mm]
Rectangular-Shaped	1.16
Chamfered-Shaped	5.34
Point-Shaped	15.66
Circular-Shaped	43.2

Table E-1: Test parameters

The process steps taken during one single case are:

- measure mass;
- free-decay tests in free air;
- free-decay tests in stationary water;
- steady state measurements;
- additional tests.

Table E-2 gives an overview of the expected response of the individual seal shapes to the different types of vibrations.

Situation	Turbulence	Instable Separation Point	Flow Reattachment
Rectangular-Shaped	Present	Not Present	Present (2) only at $\delta < b$
Chamfered-Shaped	Present	Not Present	Present (1) only at $\delta < b$
Point-Shaped	Present	Present (1)	Not Present
Circular-Shaped	Present	Present (2)	Not Present

Table E-2: Overview presence different vibration causes

Appendix F Model Set-Up

This appendix will elaborate the set-up of the model. The chapter is divided into different subjects, these subjects are the main elements of the model set-up. This appendix only focusses on the set-up of the model for any calculations is forwarded to Appendix G. The discussed subjects are:

- The flume (§ F.1). This paragraph gives some details about the flume that is used during the research. In this flume the model is placed
- The external frame (§ F.2). This part describes the external frame that will connect the moving part with the flume and other static elements.
- The internal frame (§ F.3). The internal frame is the name of the movable part of the model.
- Measuring equipment (§ F.4). The final section will exist of the elaboration of the measuring equipment used.
- Additional Elements (§ F.5). In the final paragraph some additional elements are discussed. These elements are a special design leakage device and a horizontal tensioned wire.

F.1 The Flume

For the execution of the research only a current has to be simulated, waves can be neglected in the simulation. A basic current flume is therefore sufficient for the experiment. Figure F-1 gives an indication of the dimensions of the chosen flume. The used flume is shown in Figure F-2 (L). The characteristics of the chosen flume are:

- an effective length of 14.3 metres;
- a width of 0.4 metres;
- a maximum depth of 0.4 metres

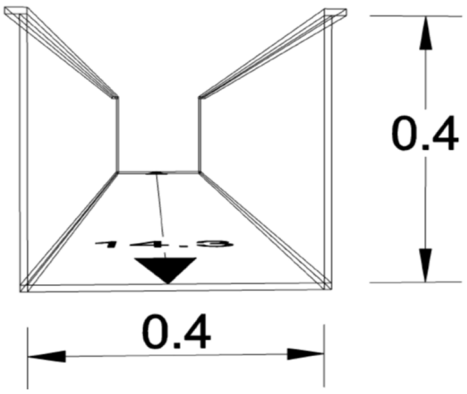

Figure F-1: Dimensions of the used current flume

The flume also has a plate on the end of the flume that can regulate the water level at the downstream side of the valve. A picture of this regulation plate is shown in Figure F-2 (R). The flow also has a Rehbock weir, which is used to determine the discharge through the flume.

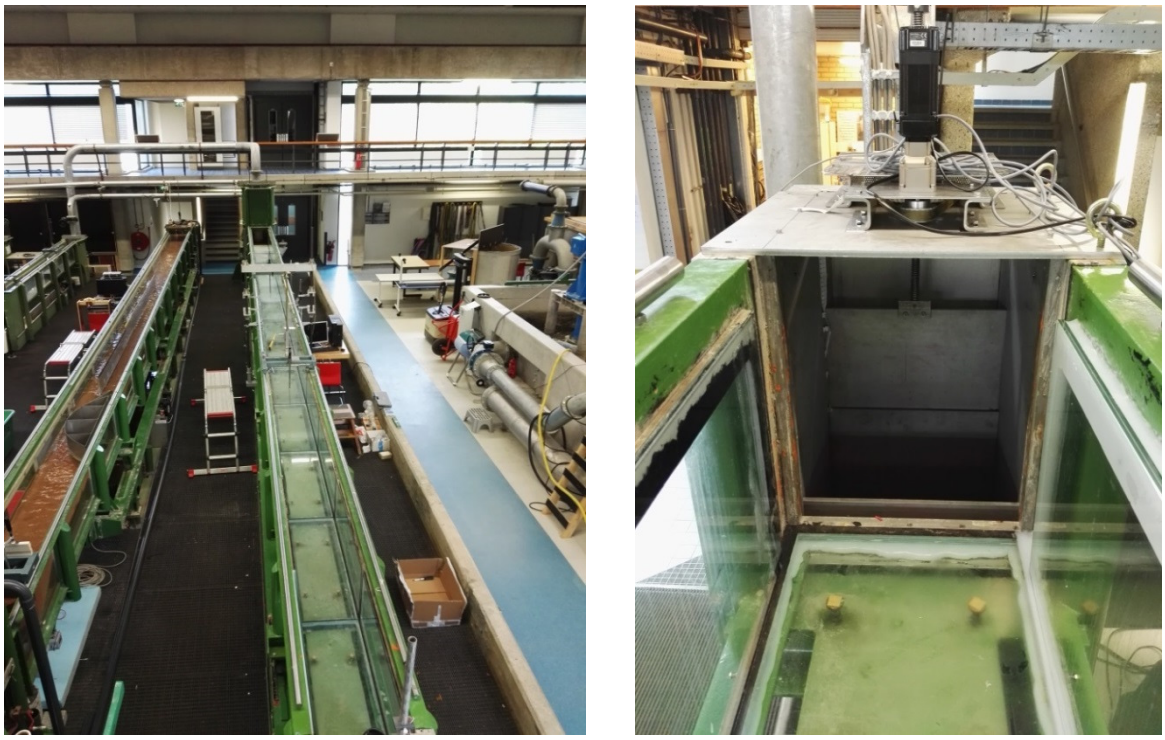

Figure F-2: (L) Picture of the used flume & (R) Picture of regulation flume at the end of the flume

F.2 The External Frame

The external frame has to make sure that the valve is connected to a fixed point and the only force affecting the valve will be the force of the water flow and the gravity of the valve system. The frame is shown in the picture of Figure F-3.

Figure F-3: Picture of the external frame

The frame exists of multiple parts, which are all visible in the picture of Figure F-3. These parts are:

- A lower horizontal beam that is connected to the flume with clamps and bolts (Figure F-4 (L)).
- Two vertical poles, that connect the horizontal beams (Figure F-5). In the picture is an additional connection to the flume shown. This connection is made to create additional horizontal stiffness for the entire set-up.
- An upper horizontal beam that connects the external frame with the movable part of the internal frame, including the valve, with help of vertical suspension springs. The upper horizontal beam is shown in Figure F-5 (L). The connection between the vertical pole and this beam is shown in Figure F-4 (R). Important aspect is that this connection should be easily relocated, because it will influence the opening underneath the valve (δ), which is a varying parameter in the research.

Figure F-4: (L) Picture of lower horizontal beam with clamp & (R) Picture of connection between vertical pole and horizontal top beam

Figure F-5: (L) Picture of upper horizontal beam with the vertical suspension connections & (R) Picture of vertical pole with a n additional connection to the flume.

F.3 The Internal Frame

The internal frame exists of multiple important elements. These elements are:

- the vertical suspension (§ F.3.1). The vertical suspension connects the internal frame with the external frame and will exists of two sliders and multiple springs.
- the valve plate (§ F.3.3). The valve plate simulates the skin plate of the vertical lift valve.
- the lower edges (§ F.3.4). The lower edges are available is 4 different shapes (Appendix D). The shapes are easily replaceable.

Figure F-6 shows the steel frame of the internal frame, with the steel hooks on top to connect the springs. In the picture also the vertical sliders are shown. The valve plate is missing the picture below.

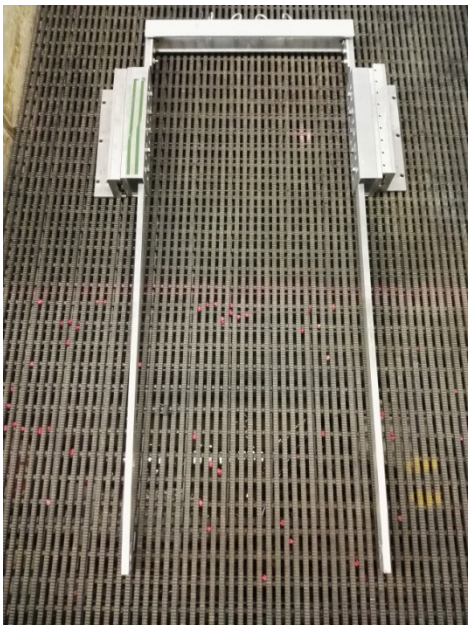

Figure F-6: Picture of the internal frame including the sliders

F.3.1 Vertical Suspension

The main vertical suspension will exist of two parts. This paragraph will elaborate these parts. The parts are:

- the sliders;
- the springs.

In addition to these two elements, several tests have been executed with an extreme stiff situation. The model set-up has been slightly adjusted to achieve this extreme stiffness. These adjustments will also be discussed in this paragraph.

Sliders

Two vertical sliders are used in the model set-up to avoid damping and friction in the vertical direction. The sliders can be seen in Figure F-7 (R). The forces on the sliders and the resistance of the sliders is further elaborated in Appendix G. The sliders are connected to the external frame with load cells, which are able to measure the horizontal force. However, the horizontal force is not relevant for this research and therefore they will not be used. The connection with the load cells is shown in Figure F-7. Figure F-6 shows the sliders and the entire internal frame connected to the external frame.

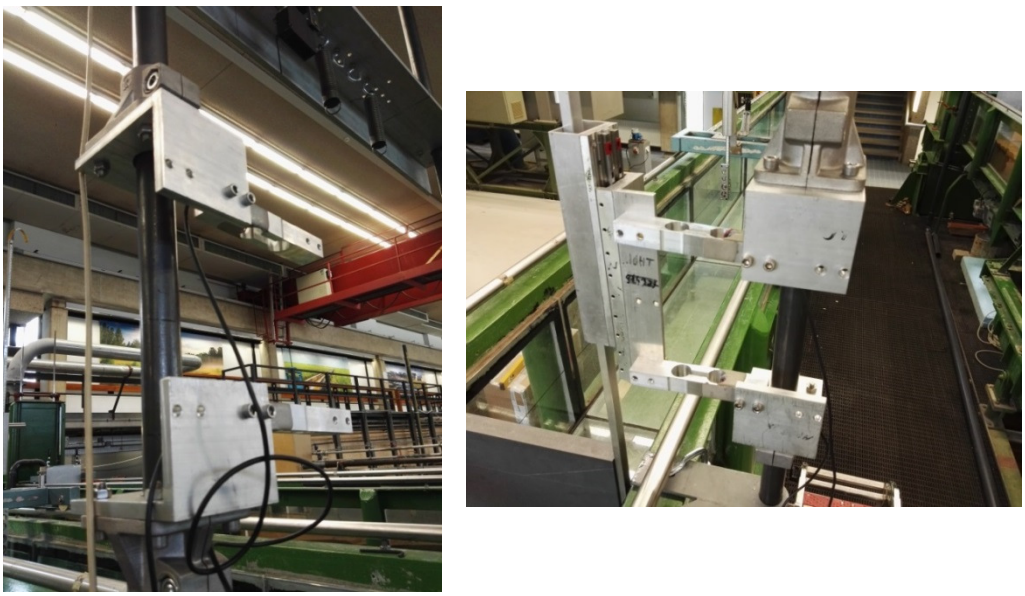

Figure F-7: (L) Picture of load cells and connections to the external frame & (R) Picture of sliders and internal frame connected to the external frame

Springs

Another part of the vertical suspension are the springs. The springs are used to vary the stiffness of the entire system and are placed between the internal and external frame as shown in Figure F-8 The springs used are shown in Table F-1. The calculation of the needed stiffness is shown in Appendix G.

Figure F-8: Picture of spring connection between internal frame and external frame

Spring Constant [N/mm]	Thickness of wire [mm]	Length of the spring [mm]	Maximum Force [N]
21.65	3.40	104.70	570.00
7.83	4.25	144.80	625.00
2.67	2.50	123.00	237.00
0.58	2.20	122.00	127.00

Table F-1: Characteristics of used springs

F.3.2 Extreme Stiff Suspension

Figure F-9 shows the adjustment made to create an extreme stiff vertical suspension. During the tests with the extreme stiff vertical suspension only the pressure measurements are interesting. Therefore, the springs are removed and the top part is locked with help of a piece of timber.

Figure F-9: Extreme stiff vertical suspension

F.3.3 Valve

One of the most important parts of the model set-up will be the plate that simulates the valve. Some requirements were set to come to a choice. These requirements are:

- The valve plate should be infinitely stiff. By making the valve extremely stiff no flexural movement is allowed. If the valve is bending this influences the amount of added water mass, what will have an effect on the response of the valve
- No penetration of water into the valve. This requirement is similar to the previous requirement, because penetration of water into the valve will change the mass of the valve during test what influences the response.
- The valve should have a low mass. By keeping the mass as low as possible the vibrations will be initiated easier.
- Easy connection with the different shapes of lower edge. The lower edge is one of the variables in the research and it should be easy to replace the seal in between the tests.
- The leakage flow between the valve and the side walls should be minimized. This leakage flow can have a beneficial effect on the prevention of any vibration. Some leakage through the sides of the valve is allowed.

Because in an earlier stage of the research an assumption has been made that the valve plate is infinitely stiff a choice has been made to use PVC as material for the plate, this material is often used to model steel [43]. The width of the valve will be 0.03 metres and the height will be 0.4 metres, including the attached lower edge the valve will have a larger height than the flume. The valve will have a width equal to the flume of 0.40 metres. See for the dimensions of the valve in the model Figure F-10, the dimensions are given in millimetres.

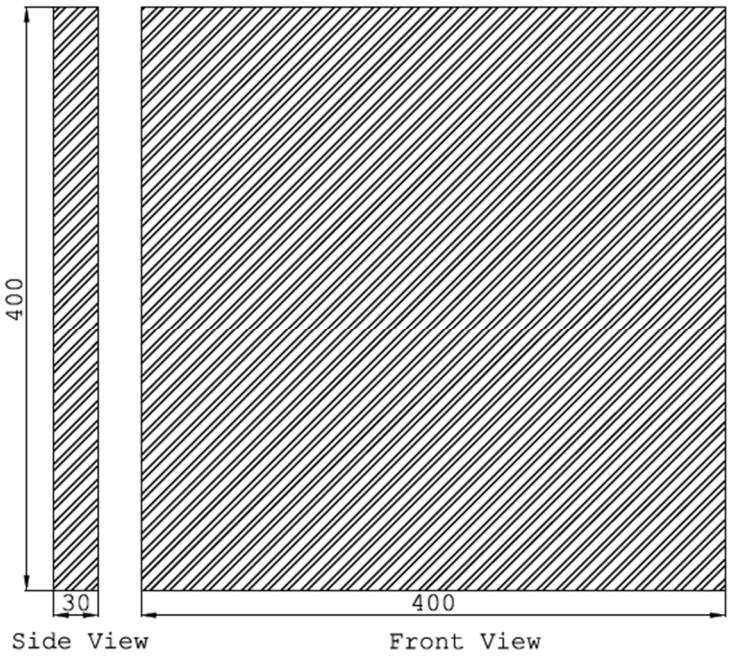

Figure F-10: Dimensions of the valve plate of the model

The deformation of the valve under extreme conditions has been checked and is minimal. The check is given in Appendix G. Figure F-11 shows how the plate is bolted to the internal frame and the entire internal frame including the steel frame, lower edges and sliders.

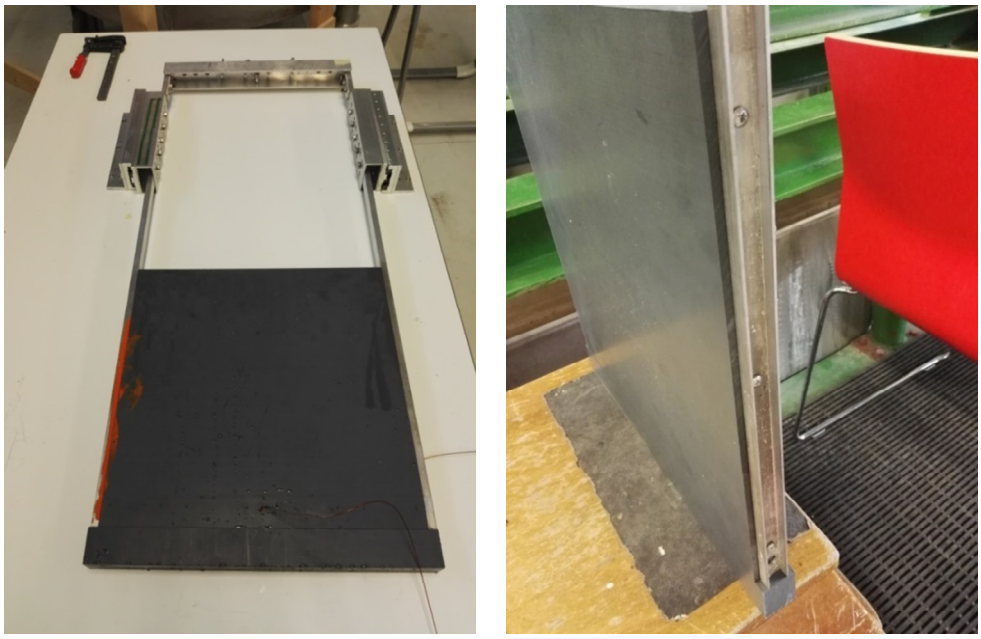

Figure F-11: (L) Picture of the internal frame with plate, lower edge and sliders & (R) Picture of the connection between the internal frame and the PVC plate

F.3.4 Lower Edge

During the tests 4 seals shapes are used. The shapes are shown in Figure F-12 with the reel dimensions. The seals are scaled down to fit with the valve plate. The seals have retained their specific shape. Figure F-12 (R) shows boring holes what makes the lower edges easy to connect to the plate by using two bolts.

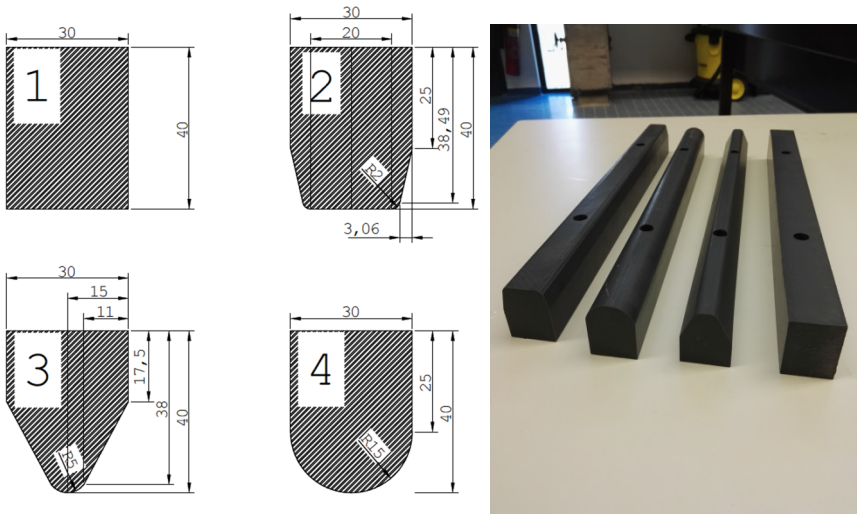

Figure F-12: (L) Dimensions lower edges & (R) Picture of the 4 different used lower edges

F.4 Measuring Equipment

An important aspect of the model set-up is the choice for the measuring equipment. This paragraph will shortly elaborate the used devices and the errors involved with this type. The parameters that have to be measured are:

- The upstream and downstream water level. The water levels are measured with standard needles. This will not be elaborated in more detail, because it is a straightforward process.
- The pressure underneath the valve (§ F.4.1). The pressure underneath the valve in measured with a pressure sensor in the lower edge that is made watertight.
- The vertical displacement (§ F.4.2). The vertical displacement is measured by a laser sensor.
- The vertical force (§ F.4.3). For the vertical force a load cell has been used.

Besides the elaboration of these devices a test has been executed in which these devices are not loaded to check for any flaws in the devices. The results of this test are presented in § F.4.4. All the tests have been executed with a sample frequency of 1000 Hz.

F.4.1 Pressure Sensor

The pressure sensor used was a Honeywell piezo-resistive senor that was made fully water tight for measurements under water. Figure F-13 shows the position of the pressure sensor in the lower edge and the watertight sell of the pressure sensor. The pressure sensor has a natural frequency of 400 Hz [1]. This frequency is far away from the frequencies that are aimed for. Therefore, no interference will be expected.

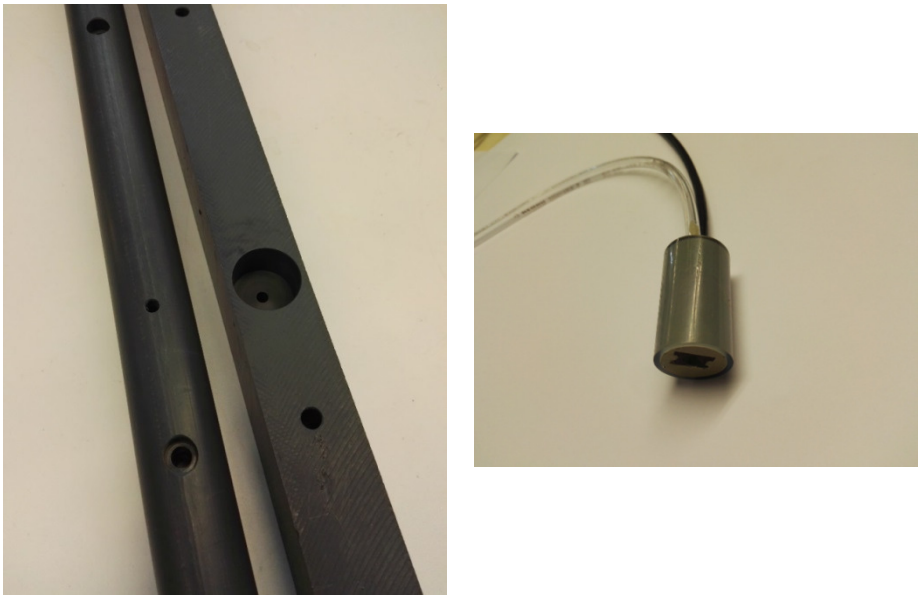

Figure F-13: (L) Picture of position of pressure sensor in the lower edge & (R) Picture of the water tight shell of the pressure sensor

Figure F-14 shows the calibration of the pressure sensor. The result of the calibration is the equation shown in equation F.1 with a R^2- value of 0.9551.

$$p = -193.4 \cdot V + 920.2 \qquad \text{F.1}$$

In which: p = pressure measured [N/m^2]
V = voltage measured [V]

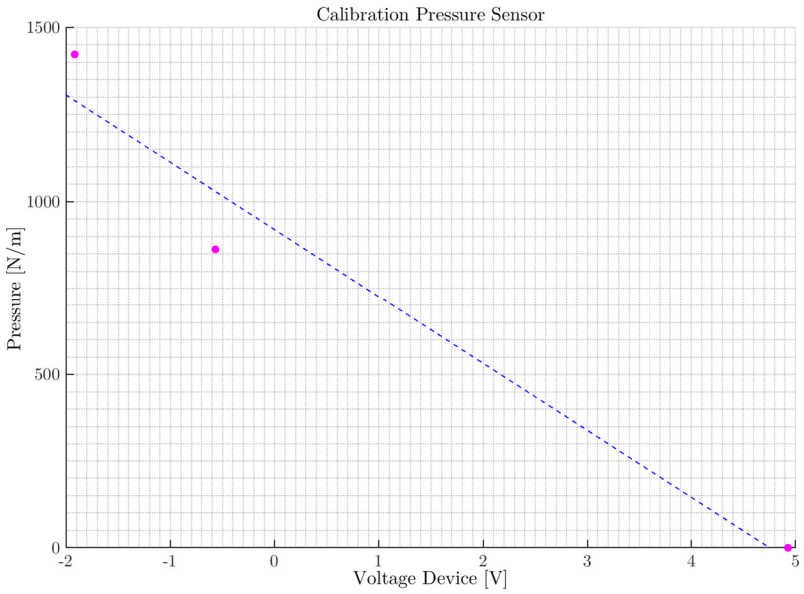

Figure F-14: Calibration pressure sensor

F.4.2 Laser

The used laser is a micro-epsilon optoNCDT1300 as shown in Figure F-15. The position of the laser in the model set-up can be found in Figure F-16 (R).

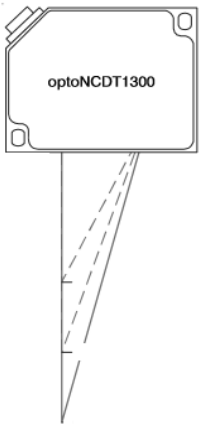

Figure F-15: Schematization of the used laser device [39]

The sampling rate of the device is 500 Hz and it has a range from 60 mm to 260 mm. These values are coupled to respectively 2.0 V and 10.0 V, which leads to the calibration formula shown in equation F.2. The resolution of the device is 0.02 %. [39]

$$\Delta y = 25 \cdot V + 10 \qquad \text{F.2}$$

In which: Δy = measured displacement [mm]

V = voltage measured [V]

F.4.3 Load Cell

The load cell used is a AE sensors STS Metric load cell with accuracy class C2. Figure F-16 shows a schematization of the load cell and the position of the load cell in the model set-up. Figure F-17 shows a diagram of the calibrated values of the used load cell. The calibration equation is given in equation F.3.

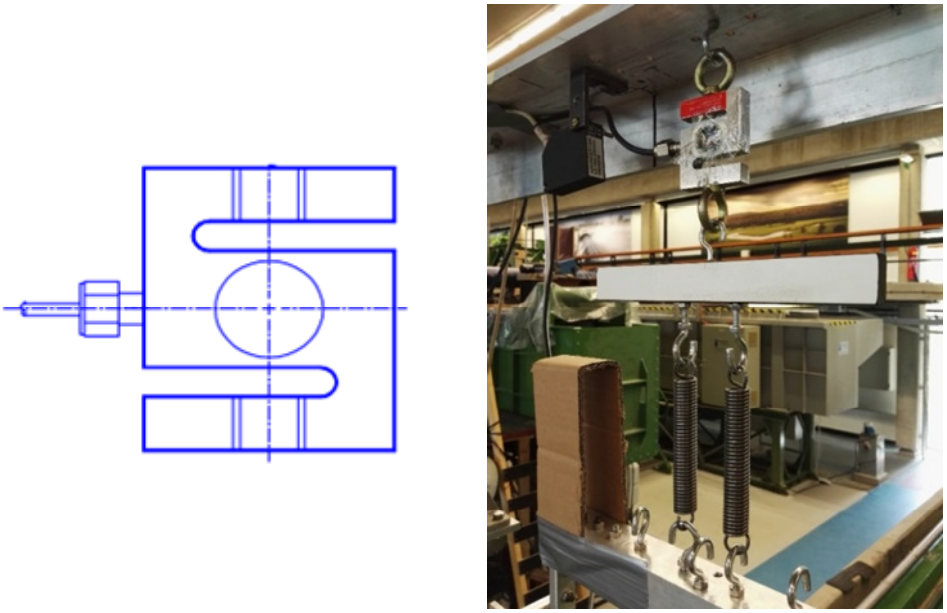

Figure F-16: (L) Schematization load cell [50] & (R) Picture of load cell in model set-up

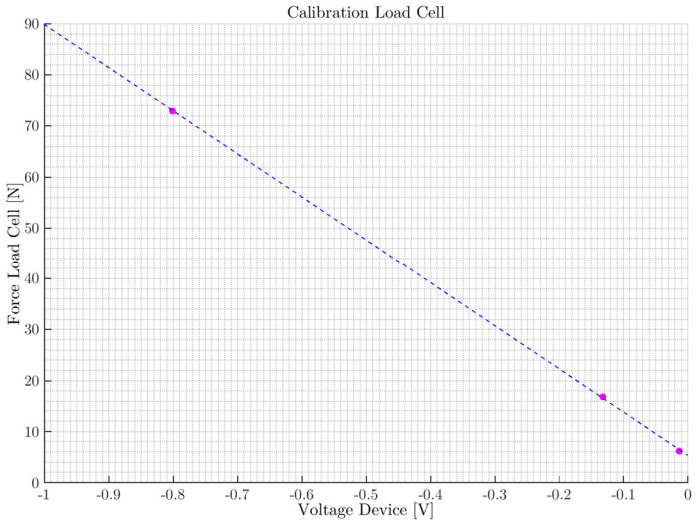

Figure F-17: Calibration of the load cell

$$F = -89.11 \cdot V + 5.13 \qquad \text{F.3}$$

In which: F = force measured [N]
V = voltage measured [V]

The combined error is 0.025 % of rated output. The rated output of the used model is 3.0 mV/V. [50]

F.4.4 Check

A power spectrum is made from a signal of the not used measuring devices to check the equipment for possible deviating results. This means that they were disconnected form the model and put on a stable surface. The pressure sensor was left in a container with stationary water. The results from this test are shown in Figure F-18.

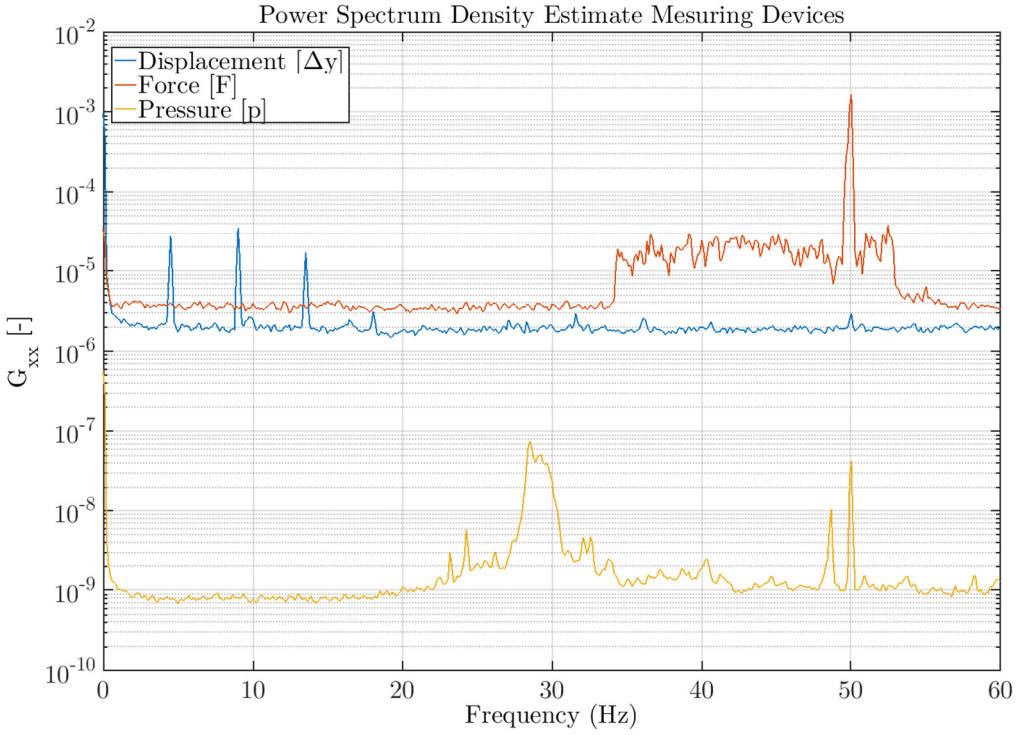

Figure F-18: Power spectrum density of the measuring equipment

The figure above clearly shows some returning frequencies that are caused by the devices or any surroundings. These frequencies are not part of the investigated problem and can therefore be ignored during the processing of the data. Table F-2 shows the retrieved frequencies from this test.

Device	**Frequencies [Hz]**				
Load Cell					50.05
Pressure Sensor	25.58	48.71			50.05
Laser	4.52	9.03	13.55	17.95	50.05

Table F-2: Retrieved frequencies

The 50 Hz frequency can be explained by the power net. The other frequencies however seem to come from the sensors or surroundings. Most of these frequencies have also been detected in the steady state measurements. Assumed can be that these frequencies are not part of the problem investigated.

F.5 Additional Elements

This paragraph describes a few elements that were used or added to the basic model set-up as described in the previous paragraphs. The additional elements used and described are:

- leakage device (§ F.5.1).
- tension wire (§ F.5.2).

F.5.1 Leakage Device

Figure F-19 shows a device that was used to prevent the leakage between the flume side and the valve plate. The device redirects the flow and minimizes the leakage. The dimensions are equal to the dimensions of the flume, so the water flow is forced to pass the device through one side of the device.

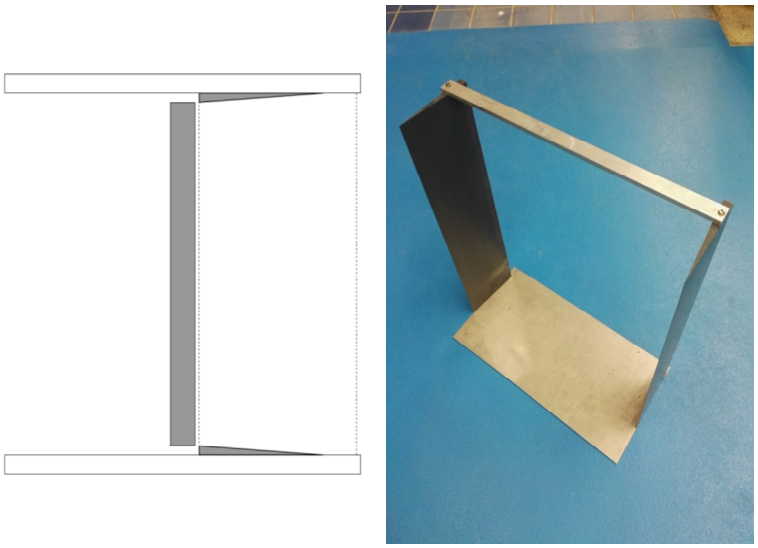

Figure F-19: (L) Sketch of device to prevent leakage & (R) Picture of device to prevent leakage

F.5.2 Tension Wire

After a first stage of tests it was experienced that the valve plate of the model showed a lot of horizontal deflection, which had a major impact on the results. Therefore, a horizontal wire was tensioned to prevent the plate from bending. The wire was not attached completely horizontal because it was impossible to attach in the current flume. Figure F-20 shows a sketch of the tension wire. Noted should be that the sketch is not in scale. In the next appendix the calculation of the wire is shown.

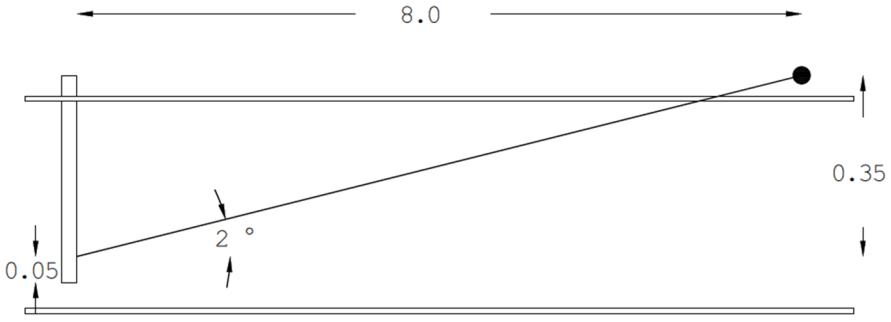

Figure F-20: Sketch of horizontal tension wire

[Page intentionally left blank]

Appendix G Model Set-Up Calculations

This appendix will exist of some detailed calculations that have been executed for the design of the model set-up. In this appendix the next specific calculations will be discussed:

- Forces (§ G.1). This paragraph elaborates the forces that will have an effect on the model set-up.
- Valve Plate Deformation (§ G.2). This paragraph gives a small calculation that proves that the deformation of the valve plate as used in the model is minimal under extreme conditions.
- Horizontal Excitation (§ G.3). This paragraph focusses on the initiation of horizontal vibrations and the response of the model to these vibrations.
- Vertical Suspension (§G.4). the vertical suspension exists of springs from which the stiffness is determined in this paragraph
- Horizontal Suspension (§ G.5). During the tests the model should be able to withstand horizontal forces. These forces will be taken by sliders and a horizontal wire. In this paragraph a capacity check has been done. Also will the effects of the horizontal wire be discussed.

G.1 Forces

This paragraph will give the calculations made to determine the forces on the model. The forces are divided into vertical (§ G.1.1) and horizontal forces (§ G.1.2).

G.1.1 Vertical Forces

The major vertical forces that work on the model are shown in Figure G-1 and are:

- Self-weight (F_{sw});
- Buoyancy ($F_{buoyancy}$);
- Hydraulic down pull force ($F_{downpull}$).

Except the self-weight of the valve all these forces are varying in the time.

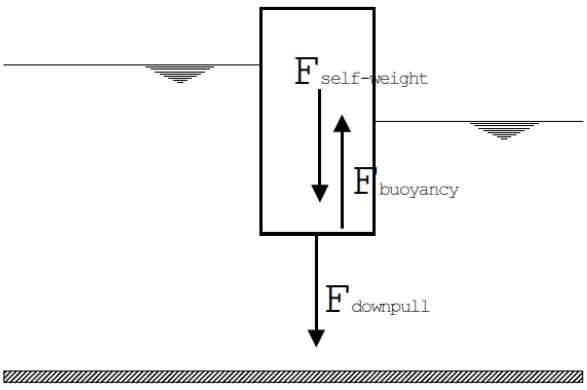

Figure G-1: Overview of major vertical force on the model

Self-Weight

The self-weight of the model is crucial for the vibration phenomena because of its involvement in the natural frequency of the system. Besides the mass of the system also the added water mass is important. In this section only the self-weight is discussed. The determination of the added mass has been described in § E.1.2. Equation G.1 gives a simple definition of the formula for the self-weight.

$$F_{sw} = V \cdot \rho \cdot g \qquad \text{G.1}$$

In which:

F_{sw}	=	self-weight of model [N]
V	=	volume valve model [m^3]
ρ	=	density material [kg/m^3]
g	=	gravitational acceleration [m/s^2]

The exact weight including the weight of the added mass of the water has be determined in one of the first steps of the testing process and is set on 9.0 kg. In the initial design step a mass of 8.9 kg was assumed which is approaches this value accurately.

Buoyancy Force

The buoyancy of the model construction depends on volume of immergence of the valve, which is clearly shown in Figure G-2. This graph is based on a valve thickness of 0.03 metres. The buoyancy force can be simply calculated based on the principle of Archimedes.

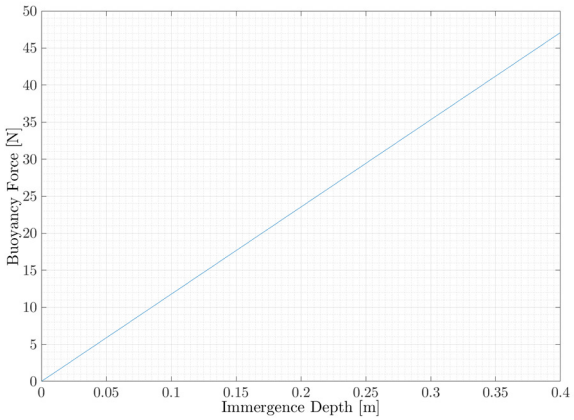

Figure G-2: $F_{buoyancy}$ related to immergence depth

In most cases the valve will be fully under water. In this stage an immergence depth of 0.3 metres is assumed. This leads to a buoyancy force as calculated in equation G.2.

$$F_{buoyancy} = (0.03 \cdot 0.4 \cdot 0.3) \cdot 1000 \cdot 9.81 = 35.3 \text{ N} \qquad \text{G.2}$$

The exact buoyancy force will vary during the course of the test, because the valve will be tested under different immergence conditions.

Hydraulic Down Pull Force

The hydraulic down pull force will be caused by the flow under the valve and will be the initiating force of the vibrations. Any fluctuations in this force are responsible for the vibrations, crucial in this step is the frequency of the fluctuations. This frequency is called the excitation frequency (f_{exc}). Equation G.3 [35] shows a formula from literature to determine the down pull force, the uncertainty in this force are the coefficients.

$$F_{downpull} = (\alpha_T - \alpha_B) \cdot b \cdot W \cdot \rho_w \cdot (U^2/2) \quad \text{G.3}$$

In which:

F	=	down pull force [N]
α_T	=	down pull coefficient at the top of the valve [-]
α_B	=	down pull coefficient at the bottom of the valve [-]
b	=	thickness of the gate [m]
W	=	width of the gate [m]
ρ_w	=	density of water [kg/m^3]
U	=	velocity under the valve [m/s]

With a coefficient of 1, in practice this will always be less, the maximum hydraulic down pull force will be:

$$F_{downpull} = 1 \cdot 0.03 \cdot 0.4 \cdot 1000 \cdot (1.6^2/2) = 15.4 \text{ N} \quad \text{G.4}$$

This down pull force will have an amplitude that eventually will coupled to the amplitude of the vibration. However, this calculation is solely based on a flow and does not take into account instability phenomenon.

G.1.2 Horizontal Force

The horizontal force on the model depends completely on the head difference over the valve. The maximum head difference over the valve is assumed to be 0.2 metres, because the valve should be in a drowned condition to simulate the culvert. Most probably this maximum head difference will be larger, however to come to a safe design the 0.2 metres is assumed in this case. The maximum upstream water level is set on 0.4 metres (the height of the flume) and the maximum downstream water level is set on 0.2 metres. The total horizontal force can be calculated using equation G.5. The resulting situation is shown in Figure G-3. The resulting horizontal force due to hydrostatic force is 235 N.

$$F_{hor} = \frac{1}{2} \cdot \rho \cdot g \cdot W \cdot (H_1^2 - H_2^2) \quad \text{G.5}$$

In which:

F_{hor}	=	horizontal force [N]
ρ	=	density [kg/m^3] = 1000 kg/m^3
g	=	gravitational constant [m/s^2] = 9.81 m/s^2
H_1	=	upstream water level [m] = 0.4 m
H_2	=	downstream water level [m] = 0.2 m
W	=	width of valve [m] = 0.4 m

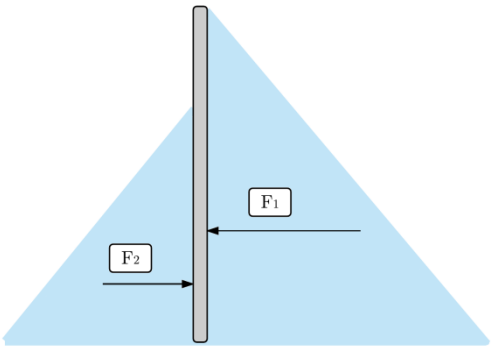

Figure G-3: Hydrostatic horizontal forces

G.2 Valve Plate Deformation

A small calculation is made to make sure the deformation of the PVC valve when loaded with the maximum horizontal force will not be too large. This deformation depends on the Young's modules of steel. The lower limit of this modulus is set on:

$$E_{pvc} = 2.4 \text{ GPa} = 2.4 \cdot 10^9 \text{ N/m}^2 \qquad \text{G.6}$$

A first indication is made on a simplified idea of beam with the use of a standard formula. This formula is given in equation G.9 [58].

$$w = \frac{5}{384} \cdot \frac{q \cdot l^4}{EI} \qquad \text{G.7}$$

In which:

w	=	horizontal deflection [m]
q	=	distributed load [N/m]
l	=	length [m]
E	=	Young's modulus [N/m^2]
I	=	moment of inertia [m^4]

When the valve is cut up in a beam with a width of 0.10 metre the deflection (w) in an extreme situation ($\Delta H = 0.2$ m) will become 0.12 mm.

G.3 Horizontal Excitation

The model can be excited in the horizontal direction due to two structural elements. These elements will be discussed separately here. The elements are:

- The valve (§ G.3.1);
- The external frame (§ G.3.2).

The frequencies determined in this paragraph could return during the processing of the results. These frequencies can be neglected because they are not related to the important phenomena of this research.

G.3.1 Valve

Any form horizontal excitation has to be minimized. The horizontal excitation frequencies of the valve can be calculated using the graph shown in Figure G-4. This graph is based on research done in the past. Some detailed explanation about this excitation can be found in 103

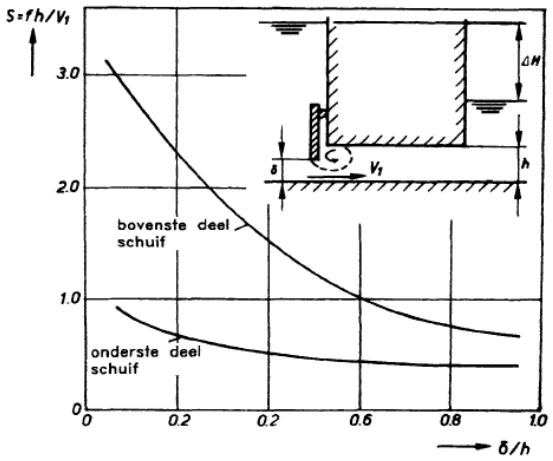

Figure G-4: Critical horizontal Strouhal numbers [33]

For only excitation of the bottom the Strouhal number will have a maximum value of:

$$S_0 = 1.0 \qquad \text{G.8}$$

Using equation G.9 that has derived from Figure G-4, the maximum horizontal excitation frequency (related to the maximum flow velocity of 1.40 m/s) of the model is 3.50 Hz.

$$f_{exc} = \max(S_0) \cdot {}^{U}/_{h} \qquad \text{G.9}$$

In which:

f_{exc}	=	excitation frequency [Hz]
S_0	=	critical Strouhal number for the bottom edge, from Figure G-4 [-] = 1.0
U	=	flow velocity [m/s] = 1.4 m/s
h	=	height of culvert [m] = 0.4 m

With a higher δ/h - ratio this excitation frequency will become even smaller due to the decrease of the critical Strouhal number. See Figure G-4. The natural frequency of the valve in horizontal direction can be calculated using equation G.10 [16].

$$f_n = \frac{(n \cdot \pi)^2}{2 \cdot \pi \cdot L^2} \cdot \sqrt{\frac{EI}{m}} \qquad \text{G.10}$$

In which:

f_n	=	natural frequency [Hz]
n	=	resonance mode [-]
L	=	width of valve [m]
E	=	Young's modulus [N/m^2]
I	=	moment of inertia [m^4]
m	=	mass [kg]

The horizontal mass exists besides the mass of the valve of additional mass due to the water. This is similar to the earlier described added mass however this time it is in the horizontal direction. This mass can be calculated using equation G.11 [33]. The second term can be eliminated based on the assumption that the water level in the model will be as high as the height of the valve. See also Figure G-5 for the exact definition of the dimensions.

$$m_w = \frac{\pi}{4} \cdot \rho \cdot d^2 + \frac{2}{\pi} \cdot \rho \cdot d \cdot \ln\left(\frac{h}{d}\right) = \frac{\pi}{4} \cdot \rho \cdot d^2 \qquad \text{G.11}$$

In which:

m_w	=	added water mass per width [kg/m]
ρ	=	density of water [kg/m^3]
d	=	height of valve [m]

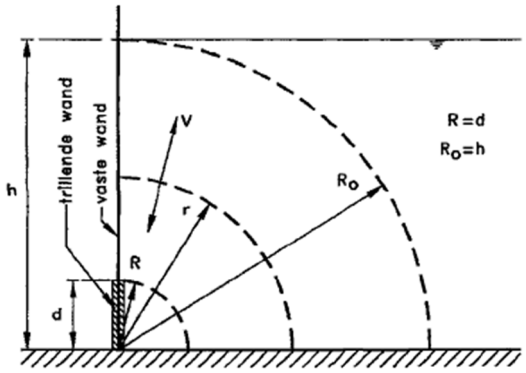

Figure G-5: Added horizontal water mass [33]

The additional water mass becomes 125.7 kg/m, which brings the total mass that affects the horizontal vibration to 59.3 kg. Adding this value to equation G.10 the natural frequency in horizontal direction becomes 187.4 Hz. This frequency is significant larger than the maximum expected excitation frequency (3.5 Hz). Therefore, the response of the model due to horizontal excitations should be very low.

G.3.2 External Frame

The frame is considered to be a cantilever with in addition to its own mass also has a top mass. This assumption is made to calculate the horizontal natural frequency of the external frame. Figure G-6 gives a schematization of this assumption.

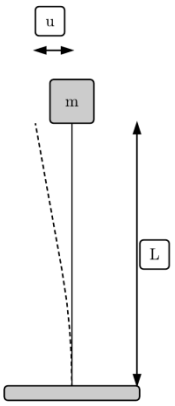

Figure G-6: Schematization of the external frame with top mass

For a cantilever the formula for the deflection of the tip known. This formula is presented in equation G.12.

$$u = \frac{F \cdot L^3}{3 \cdot EI} \tag{G.12}$$

From this statement the stiffness of the entire system can be determined as shown in equation G.13.

$$k = \frac{\text{load}}{\text{deflection}} = \frac{F}{u} = \frac{3 \cdot EI}{L^3} \tag{G.13}$$

With the known stiffness the natural frequency can be determined using the basic equation.

$$f_n = \frac{1}{2 \cdot \pi} \sqrt{\frac{3 \cdot EI}{m \cdot L^3}} \tag{G.14}$$

Because the frame has two steel poles, with a uniformly distributed mass, and a top mass, the horizontal beam, the mass has to be compensated. The distributed mass has to be compensated according to equation G.15.

$$m_e = m \cdot \frac{L}{4} \tag{G.15}$$

The system is considered of two identical steel poles with a top load, horizontal top beam, when the steps presented are being followed the retrieved natural frequency is approximately 40 Hz.

G.4 Vertical Suspension

The vertical suspension has been determined when the weight of the model was not yet known. Figure G-7 shows the natural frequency of the system in relation to the stiffness and the mass. Resonance is not necessary for the research however a clear amplitude should be visible. When the amplification factor becomes too low (with a high $f_{resp}\backslash f_n$-ratio) the vibrations will be less visible and the obtaining of the results will be more difficult.

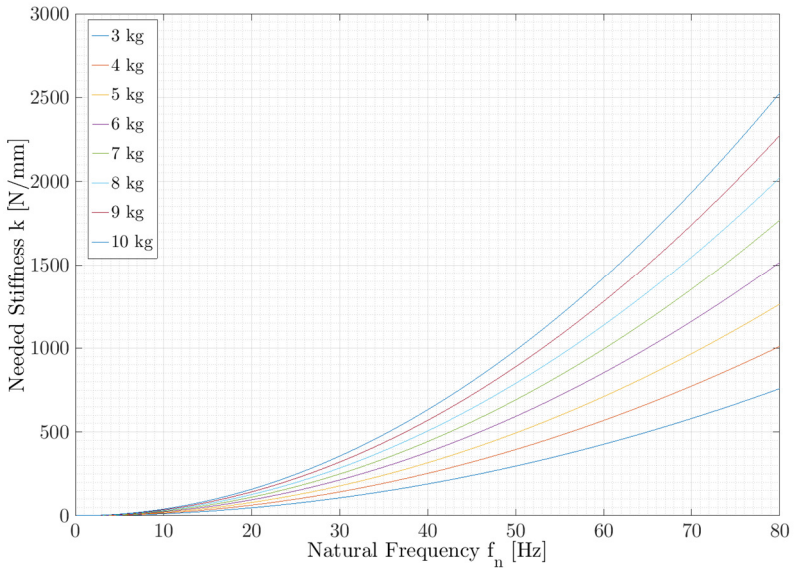

Figure G-7: Needed stiffness versus natural frequency of the system

The needed stiffness can be supplied by multiple springs if necessary, with a maximum of 4 springs, this limitation is given by the frame. With a first assumption of 9 kilograms and the determined response frequencies of Appendix D. The characteristics of the springs that will be used during the research are given in Table G-1.

Spring Constant [N/mm]	Thickness of wire [mm]	Length of the spring [mm]	Maximum Force [N]
21.65	3.40	104.70	570.00
7.83	4.25	144.80	625.00
2.67	2.50	123.00	237.00
0.58	2.20	122.00	127.00

Table G-1: Characteristics of used springs

Stiffness [N/mm]		1.16	5.34	15.66	43.2
Natural Frequency [Hz]		1.8	3.9	6.6	11.0
Reduced velocity [-] with varying	0.3	5.6	2.6	1.5	0.9
flow velocities [m/s]	1.9	35.2	16.2	9.6	5.8

Table G-2: Expected reduced velocities

Table G-2 shows the reduced velocities with regard to the natural frequencies that can be achieved using this stiffness's and the earlier determined values for the minimum and maximum velocity. Clearly shown in the major range of reduced velocities possible with these spring combinations. The different springs could be combine into a lot more different combinations. Table G-3 shows the relation between the expected response frequencies (f_{resp}) and the calculated natural frequencies (f_n). This relation gives an indication of the response of the system. A ratio close to 1 indicates possible resonance, what leads to large amplitudes.

Flow Velocity [m/s]	V_{rd} [-]	f_{resp} [Hz]	f_n [Hz]			
			1.16	5.34	15.66	43.20
1.9	2	31.7	27.3	5.9	2.0	0.7
	3.5	18.1	15.6	3.4	1.2	0.4
	8.5	7.5	6.4	1.4	0.5	0.2
	80	0.8	0.7	0.1	0.1	0.0
0.3	2	5.0	4.3	0.9	0.3	0.1
	3.5	2.9	2.5	0.5	0.2	0.1
	8.5	1.2	1.0	0.2	0.1	0.0
	80	0.1	0.1	0.0	0.0	0.0

Table G-3: $f_{resp}\backslash f_n$-ratio of the used springs

G.5 Horizontal Suspension

This paragraph will focus on the horizontal suspension. The will be achieved by elaborating the following subjects:

- The Slider Capacity (§ G.5.1). This part will calculate if the used sliders are able to resist the extreme loads. It will also include the forces that have to be taken by any other horizontal supports
- Tensioned Wire (§ G.5.2). Related to the previous paragraph a tensioned wire has been used to prevent the valve from flexural movement.

G.5.1 Slider Capacity

Applying the sliders as presented in Appendix F the moment capacity of these sliders is limited. The limitations regarding the slides are given in Table G-4 and Figure G-8. Without any additional horizontal support and a maximum horizontal loading over the valve model of $\Delta H = 0.2$ m, the sliders will most probably not be able to handle the moment forces. Therefore, a horizontal tension wire has been attached to the valve. This wire is elaborated in the next paragraph.

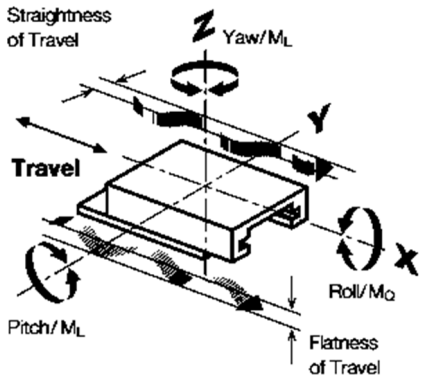

Characteristics		Value
C	Vertical Allowable Force	3770 N
M_L	Allowable Moment	36.40 Nm
M_Q	Allowable Moment	52.78 Nm
	Weight	1.2 kg

Figure G-8: Direction of moments on slider [47]

Table G-4: Characteristics of the available sliders [47]

In these calculation is assumed that the valve is fully closed and the upstream water level reaches the maximum value of 0.4 metres. The position of the horizontal wire is crucial for the distribution of the loads. Figure G-8 shows the support forces for the valve with the forces presented in Figure G-9. The distance from the slider to the end of the valve is assumed to be 0.5 metres, because the slider has to be positioned above the flume.

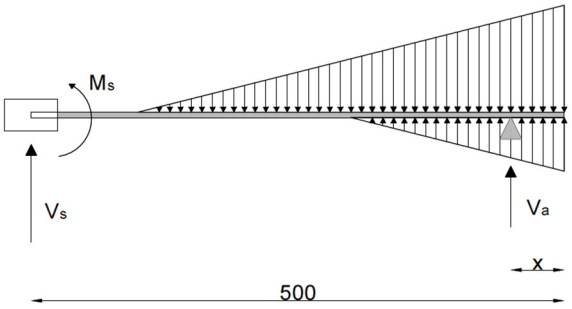

x [m]	M_s [Nm]	V_s [N]	V_a [N]
No Support	40.5	117.7	-
0.0	7.2	51.0	66.6
0.05	5.0	38.6	79.1
0.1	2.5	22.7	95.0
0.15	0.1	1.7	116.0

Figure G-9: Schematization valve with loads and supports

Table G-5: Support forces

The maximum support moment in the slider will exceed the capacity when no support is present. The horizontal wire is tensioned and attached to the valve to prevent the exceedance of the capacity. The wire should be as small as possible to minimize the amount of additional damping. In a maximum situation with $\Delta H = 0.2$ m, the tension force will become 100 N.

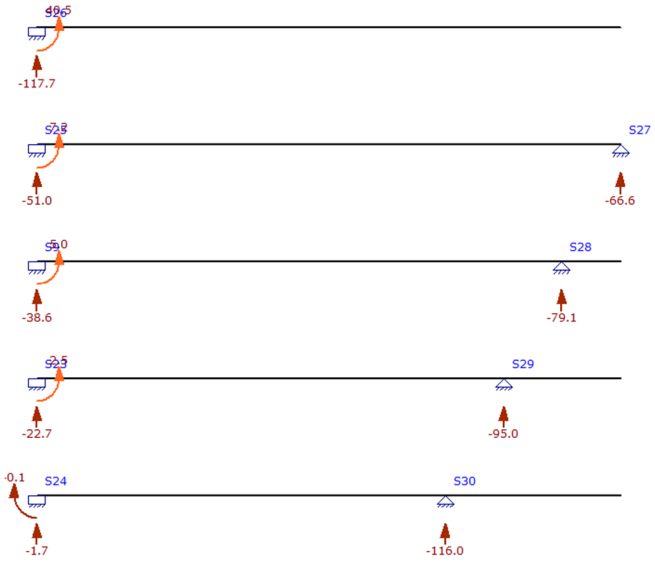

Figure G-10: Support forces in a valve with different positions of back support

G.5.2 Tension Wire

As discussed in the previous paragraph a tension wire is necessary to prevent the valve from bending and to limit the flexural forces in the sliders. Because the wire could not be attached fully horizontal a small vertical force will be introduced in the system. This force could influence the vibration phenomena. The total length of the wire was 8 metres and it was attached 35 centimetres higher than it was attached to the valve. The maximum horizontal hydrostatic force is (over $\Delta H = 0.2$ m) is 235 N. the angle of the wire is 2.5°. The additional vertical force is 1.1 N. This is approximately 1.5 % of the self-weight force, what is relatively small.

[Page intentionally left blank]

Appendix H Signal Analysis

This appendix will describe the steps taken during the processing of the data. A power spectrum density (PSD) estimation has been made to determine the dominant frequencies of the phenomenon. This way it is possible to distinct the dominant frequencies from the noise vibrations. The dominant frequencies will carry the most energy which will be described in a later part. The elaboration of the signal analysis is divided into two single parts. These parts are:

- A theoretical background of a spectral analysis (§ H.1).
- The determination of specific variables of the analysis for this research and a sample calculation (§ H.2).

H.1 Theoretical Background

The analysis starts with the transformation of the signals in the time domain to signals in the frequency domain. In most cases this is done by executing a Fast Fourier Transform (FFT) [20]. A special form of a Fourier analysis is Welch's method [5]. This method is used in this particular research. This choice will be elaborated in § H.2. The first step of the method is dividing the whole sample in segments which are overlapping. A schematization is given in Figure H-1.

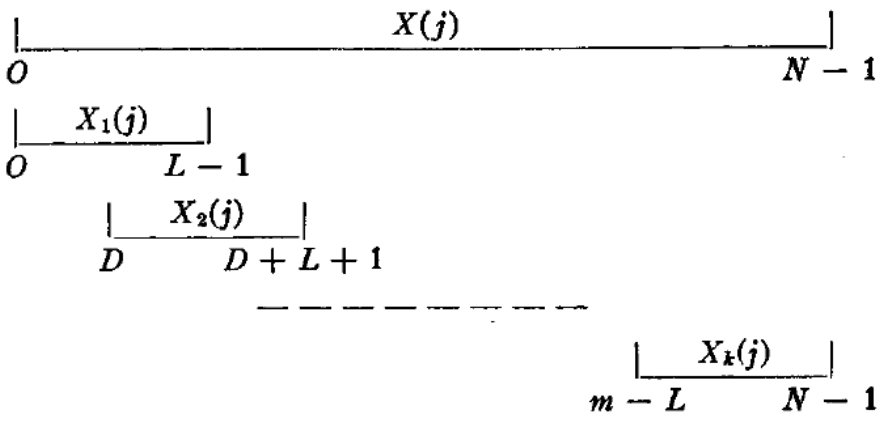

Figure H-1: Record segmentation with overlap [61]

The dividing of the sample in K segments can be expressed as shown in equation H.1.

$$\begin{aligned} &\text{Segment } 1: x(0), x(1), \ldots, x(M\text{-}1) \\ &\text{Segment } 2: x(S), x(S\text{+}1), \ldots, x(M\text{+}S\text{-}1) \\ &\vdots \\ &\text{Segment K}: x(N\text{-}M), x(N\text{-}M\text{+}1), \ldots, x(N\text{-}1) \end{aligned} \qquad \text{H.1}$$

In which:
- M = number of points in each segment
- S = number of points to shift the beginning of the segment
- K = number of segments

When the segments are determined a Discrete Fourier Transform (DFT) is taken from every single segment according to equation H.2. Before this is done the segments are multiplied with a window function.

$$X_k(v) = \sum_m x(m) \cdot w(m) \cdot e^{-j \cdot 2\pi \cdot v \cdot m} \qquad \text{H.2}$$

In which:
- m = $(k\text{-}1)\cdot S, \ldots, M+(k\text{-}1)\cdot S\text{-}1$
- w(m) = window function

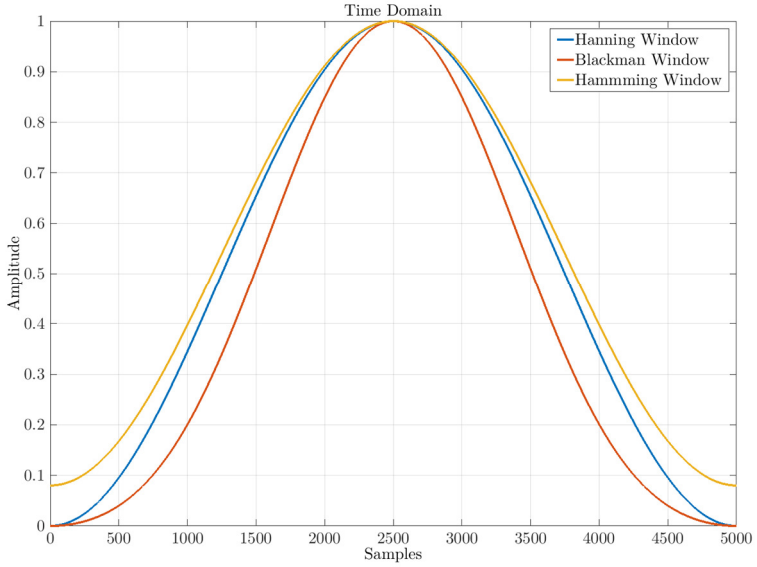

Figure H-2: Hamming, Blackman and Hanning window functions with 5000 samples

The window function multiplies the considered segments with a value and the not used segments with 0. It also increases the middle part of the vibration envelope and tapers the beginning and the end of the segment. The most used windows are a Hann window, a Hamming window and a Blackman window. All windows are shown in Figure H-2 with a window length of 5000 samples. The windows have in common that they are all based on a cosine function. Chosen is for a Hanning window, because it is the most used window when working with random vibration data. Equation H.3 gives the analytical expression of this window.

$$w(m) = \frac{1}{2}\left(1\text{-}\cos\left(\frac{2\pi \cdot m}{N\text{-}1}\right)\right) \qquad \text{H.3}$$

The next step will be to form the modified periodogram values of the DFT results. This is done according to the equation shown below.

$$P_k(v) = \frac{1}{W} \cdot |X_k(v)|^2 \qquad \text{H.4}$$

In which the window function returns according to equation H.5.

$$W = \sum_{k=1}^{K} w^2(m) \qquad \text{H.5}$$

The final step involves the averaging of the periodograms calculated in the previous steps to obtain Welch's estimate of the PSD. This averaging is shown in equation H.6.

$$S_x(v) = \frac{1}{K} \sum_{k=1}^{K} P_k(v) \qquad \text{H.6}$$

The major advantage of using such a PSD diagram is that is relatively easy to determine the energy related to a certain frequency. This can be done by taken the integral of the function. This is shown in equation H.7.

$$m_0 = \int S \cdot df \qquad \text{H.7}$$

A difference in this method related to other similar method's is the overlap in segments.

$$G_{xx}(f_k) = \frac{2}{n_d \cdot N \cdot \Delta t} \sum_{i=1}^{n_d} |X_i(f_k)|^2 \qquad \text{H.8}$$

The indices (p, F and Δy) indicate the type of measurement that is used to come to a PSD. The used variables are the pressure, the force and the displacement.

H.2 Sample

To show the accuracy of the Welch's method and the FFT a simple example is elaborated here. The used function is shown in equation H.9 and Figure H-3.

$$y(t) = 10 \cdot \sin(4 \cdot \pi \cdot t) \qquad \text{H.9}$$

From this equation the frequency can be determined easily as $4\pi/2\pi = 2$ Hz and the amplitude is set on 10. The sampling rate is set on 1000 Hz to resemble the sampling rate of the measurements. Crucial in this step are the transform length (the number of output points) and the window length (the length of the input signal) [5]. The transform length is advised to keep as a power of 2 to improve the accuracy of the results [38]. The full window length is in the case of a 300 seconds measurement 300 s $\cdot$ 1 000 Hz = 300 000 samples. Because the Welch's method is used this window length can be cut up in smaller pieces as described in the previous paragraph.

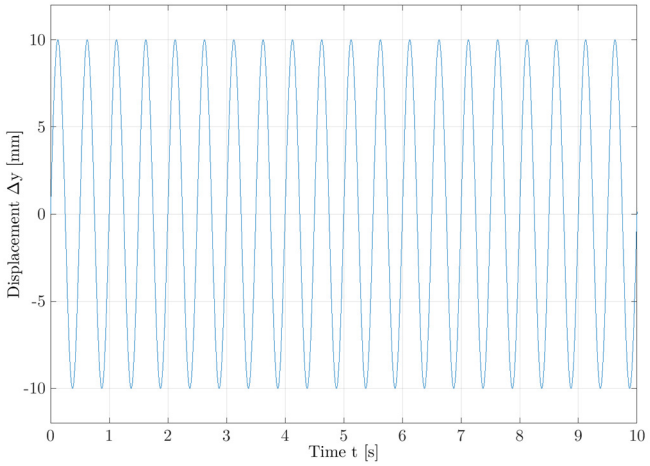

Figure H-3: Time-Place diagram of example function

The basic Matlab function PWELCH (see equation H.10) uses as standard value an overlap of 50% and a transform length (nfft) as the next power of 2 of the window length. Figure H-4 shows the determined dominant frequency of the signal with varying window length. It shows that the result becomes more accurate as soon as the window length is larger than $2^{15} = 32\,768$. This means that the window length should kept larger than this length and the transform length will become $2^{16} = 65\,536$ samples.

pwelch (x,window,noverlap,nfft,fs) H.10

In which:

	x	=	input variable
	window	=	window type and length = hanning (2^{16})
	noverlap	=	overlap between segments
	nfft	=	transform length = next power of 2 of window length
	fs	=	sampling frequency = 1000 Hz

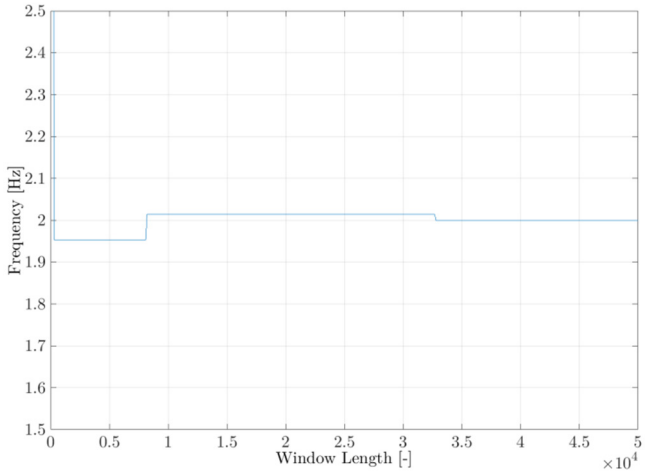

Figure H-4: Determined frequency with varying window length

Window Length	**sin (4πt)**		**sin (6πt)**		**sin (8πt)**	
	f [Hz]	Deviation	f [Hz]	Deviation	f [Hz]	Deviation
2^{12} = 4096	1.95	2.4 %	2.93	2.3 %	3.91	2.4 %
2^{13} = 8192	1.95	2.4 %	3.05	1.7 %	4.03	0.7 %
2^{14} = 16384	2.01	0.7 %	2.99	0.3 %	4.03	0.7 %
2^{15} = 32768	2.01	0.7 %	3.01	0.2 %	4.00	0.1 %
2^{16} = 65536	2.00	0.1 %	3.00	0.1 %	4.00	0.1 %

Table H-1: Deviation of the real amplitude of the vibration

In contrast with the earlier mentioned 2^{16} as window length the window length is set to 2^{14}. Table H-1 shows the deviations of the determined frequencies with the real frequencies. Shown is that the "error" is small with a window length of $2^{14} = 16384$. A major advantage of a smaller window length is the smoothing of the graph and therefore avoiding small peaks.

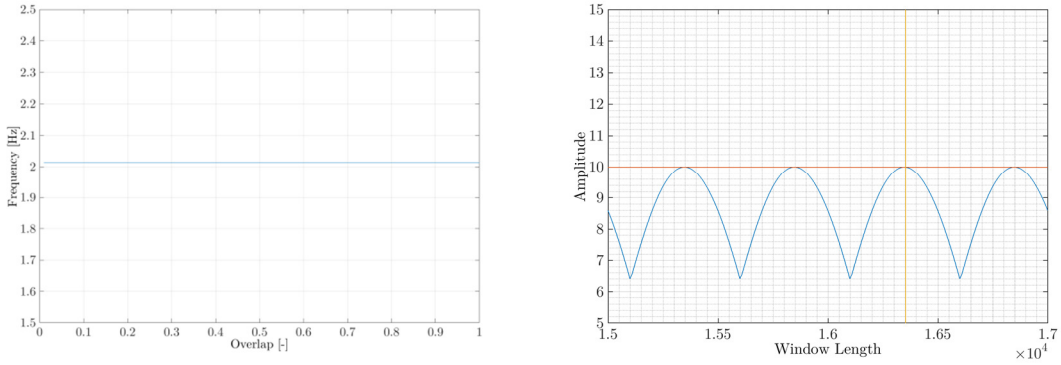

Figure H-5: (L) Influence of overlap on dominant frequency & (R) Determined amplitude versus window length

With the determined window length and transform length the overlap has been varied. As shown in Figure H-5 the overlap does not have a major influence on the final result. Therefore, the setting is set on the standard 50%. The determination of the amplitude of the variable related to the specific frequencies has to be done by using a basic FFT. This FFT is shown in equation H.11. Both parameters can have two relations:

- If n > x, then the x signal will be padded with trailing zeros.
- If n < x, then the x signal will be truncated.

$$\text{fft}(x,n) \tag{H.11}$$

In which: x = input variable
n = window length

Figure H-5 shows that the determined amplitude with a window length of 2^{14} samples will be 9.90. In comparison with the real amplitude of 10 this can be seen as accurate.

[Page intentionally left blank]

Appendix I Overview Test Conditions

This appendix gives an overview of the conditions during the different executed tests. The overview of the tests conditions has been divided into several subsections. The subsections are according to the process steps mentioned in Appendix E.

I.1 Free-Decay Tests

The first step in the process were the free-decay tests to determine the natural frequencies. The conditions regarding these tests are given in the paragraph. Table I-1 shows the conditions for the tests above water and Table I-2 the conditions for the tests under water.

Name of Data File	Seal Shape	Stiffness k [N/mm]
TestF-002-001-a	Rectangular-Shaped	1.16
TestF-002-001-b	Rectangular-Shaped	1.16
TestF-002-001-c	Rectangular-Shaped	1.16
TestF-002-002-a	Rectangular-Shaped	5.34
TestF-002-002-b	Rectangular-Shaped	5.34
TestF-002-002-c	Rectangular-Shaped	5.34
TestF-002-003-a	Rectangular-Shaped	15.66
TestF-002-003-b	Rectangular-Shaped	15.66
TestF-002-003-c	Rectangular-Shaped	15.66
TestF-002-004-a	Rectangular-Shaped	43.2
TestF-002-004-b	Rectangular-Shaped	43.2
TestF-002-004-c	Rectangular-Shaped	43.2

Table I-1: Free-decay test conditions above water

Name of Data File	Seal Shape	Stiffness k [N/mm]	Gate Opening δ [mm]	Downstream Water Level H_2 [mm]	Upstream Water Level H_1 [mm]
TestA-002-001-a	Rectangular-Shaped	1.16	45	10	10
TestA-002-001-b	Rectangular-Shaped	1.16	45	10	10
TestA-002-001-c	Rectangular-Shaped	1.16	45	10	10
TestA-002-001-d	Rectangular-Shaped	1.16	30	10	10
TestA-002-001-e	Rectangular-Shaped	1.16	30	10	10
TestA-002-001-f	Rectangular-Shaped	1.16	30	10	10
TestA-002-001-g	Rectangular-Shaped	1.16	15	10	10
TestA-002-001-h	Rectangular-Shaped	1.16	15	10	10
TestA-002-001-i	Rectangular-Shaped	1.16	15	10	10
TestA-002-002-a	Rectangular-Shaped	5.34	45	10	10
TestA-002-002-b	Rectangular-Shaped	5.34	45	10	10
TestA-002-002-c	Rectangular-Shaped	5.34	45	10	10
TestA-002-002-d	Rectangular-Shaped	5.34	30	10	10
TestA-002-002-e	Rectangular-Shaped	5.34	30	10	10
TestA-002-002-f	Rectangular-Shaped	5.34	30	10	10
TestA-002-002-g	Rectangular-Shaped	5.34	15	10	10
TestA-002-002-h	Rectangular-Shaped	5.34	15	10	10
TestA-002-002-i	Rectangular-Shaped	5.34	15	10	10
TestA-002-003-g	Rectangular-Shaped	21.3	15	10	10
TestA-002-003-h	Rectangular-Shaped	21.3	15	10	10

Name of Data File	Seal Shape	Stiffness k [N/mm]	Gate Opening δ [mm]	Downstream Water Level H_2 [mm]	Upstream Water Level H_1 [mm]
TestA-002-003-i	Rectangular-Shaped	21.3	15	10	10
TestA-002-004-a	Rectangular-Shaped	1.16	45	20	20
TestA-002-004-b	Rectangular-Shaped	1.16	45	20	20
TestA-002-004-c	Rectangular-Shaped	1.16	45	20	20
TestA-002-004-d	Rectangular-Shaped	1.16	30	20	20
TestA-002-004-e	Rectangular-Shaped	1.16	30	20	20
TestA-002-004-f	Rectangular-Shaped	1.16	30	20	20
TestA-002-004-g	Rectangular-Shaped	1.16	15	20	20
TestA-002-004-h	Rectangular-Shaped	1.16	15	20	20
TestA-002-004-i	Rectangular-Shaped	1.16	15	20	20
TestA-002-005-a	Rectangular-Shaped	5.34	45	20	20
TestA-002-005-b	Rectangular-Shaped	5.34	45	20	20
TestA-002-005-c	Rectangular-Shaped	5.34	45	20	20
TestA-002-005-d	Rectangular-Shaped	5.34	30	20	20
TestA-002-005-e	Rectangular-Shaped	5.34	30	20	20
TestA-002-005-f	Rectangular-Shaped	5.34	30	20	20
TestA-002-005-g	Rectangular-Shaped	5.34	15	20	20
TestA-002-005-h	Rectangular-Shaped	5.34	15	20	20
TestA-002-005-i	Rectangular-Shaped	5.34	15	20	20
TestA-002-007-a	Rectangular-Shaped	1.16	45	30	30
TestA-002-007-b	Rectangular-Shaped	1.16	45	30	30
TestA-002-007-c	Rectangular-Shaped	1.16	45	30	30
TestA-002-007-d	Rectangular-Shaped	1.16	30	30	30
TestA-002-007-e	Rectangular-Shaped	1.16	30	30	30
TestA-002-007-f	Rectangular-Shaped	1.16	30	30	30
TestA-002-007-g	Rectangular-Shaped	1.16	15	30	30
TestA-002-007-h	Rectangular-Shaped	1.16	15	30	30
TestA-002-007-i	Rectangular-Shaped	1.16	15	30	30
TestA-002-008-a	Rectangular-Shaped	5.34	45	30	30
TestA-002-008-b	Rectangular-Shaped	5.34	45	30	30
TestA-002-008-c	Rectangular-Shaped	5.34	45	30	30
TestA-002-008-d	Rectangular-Shaped	5.34	30	30	30
TestA-002-008-e	Rectangular-Shaped	5.34	30	30	30
TestA-002-008-f	Rectangular-Shaped	5.34	30	30	30
TestA-002-008-g	Rectangular-Shaped	5.34	15	30	30
TestA-002-008-h	Rectangular-Shaped	5.34	15	30	30
TestA-002-008-i	Rectangular-Shaped	5.34	15	30	30

Table I-2: Free-decay test conditions under water

I.2 Steady State Measurements

The conditions of the steady-state tests have been divided related to the different shapes. The different conditions are shown in:

- Table I-3: the tests with the rectangular-shaped lower edge (§ I.2.1).
- Table I-4: the tests with the chamfered-shaped lower edge (§ I.2.2).
- Table I-5: the tests with the point-shaped lower edge (§ I.2.3).
- Table I-6: the tests with the circular-shaped lower edge (§ I.2.4).

In addition to the test conditions the table shows if a clear vibration has been identified. This is done in the final column by a gradation. The gradation used is:

- The number 1 for a clear peak in all three measured variables (Δy, p and F)
- The number 2 for a clear peak in just one or two measured variables. The variables that have the peak are indicated with the characters F (force), P (pressure) and Y (displacement).
- The number 3 for no clear peak at all.

The character H (high frequency) indicates if the peak was found in the high frequency area (15 – 40 Hz). When no H is noted the peaks were found in the low frequency area (0 – 15 Hz).

I.2.1 Rectangular-Shaped Lower Edge Tests

Table I-3 shows the test conditions of the tests executed with the chamfered-shaped lower edge. Without the test with an extreme vertical stiffness (A total of 13), 52 steady state measurements were done with the chamfered-shaped lower edge of which 19 (37%) showed a clear peak in all three measured variables and 9 (17%) showed only a peak in two measured variables. One of the tests failed (2%). The remaining, 23 tests (44%), did not show a clear peak at all. 7 tests (13%) also showed a high frequency peak.

Name of Data File	Seal Shape	Stiffness k [N/mm]	Gate Opening δ [mm]	Downstream Water Level H_2 [mm]	Upstream Water Level H_1 [mm]	Peak
TestE-001-001-a	Rectangular-Shaped	5.34	31	161	275	Failed
TestE-001-001-b	Rectangular-Shaped	5.34	31	212	321	1
TestE-001-001-c	Rectangular-Shaped	5.34	30	201	271	1
TestE-001-001-d	Rectangular-Shaped	5.34	30	188	222	1
TestE-001-001-e	Rectangular-Shaped	5.34	21	187	244	1
TestE-001-001-f	Rectangular-Shaped	5.34	19	155	218	1
TestE-001-001-g	Rectangular-Shaped	5.34	19	167	281	2 (F,P)
TestE-001-001-h	Rectangular-Shaped	5.34	20	199	304	1
TestE-001-001-i	Rectangular-Shaped	5.34	22	214	289	1
TestE-001-001-j	Rectangular-Shaped	5.34	21	222	341	1
TestE-001-001-k	Rectangular-Shaped	5.34	22	229	370	3
TestE-001-001-l	Rectangular-Shaped	5.34	8	204	350	3
TestE-001-001-m	Rectangular-Shaped	5.34	8	176	351	3
TestE-001-001-n	Rectangular-Shaped	5.34	6	136	218	3
TestE-001-001-o	Rectangular-Shaped	5.34	7	203	241	3
TestE-001-001-p	Rectangular-Shaped	5.34	51	233	248	3
TestE-001-001-q	Rectangular-Shaped	5.34	52	224	271	1
TestE-001-001-r	Rectangular-Shaped	5.34	52	199	282	1
TestE-001-001-s	Rectangular-Shaped	5.34	31	203	255	1
TestE-001-001-t	Rectangular-Shaped	5.34	31	192	217	1
TestE-001-002-a	Rectangular-Shaped	43.2	23	192	231	1
TestE-001-002-b	Rectangular-Shaped	43.2	23	192	231	1

Name of Data File	Seal Shape	Stiffness k [N/mm]	Gate Opening δ [mm]	Downstream Water Level H_2 [mm]	Upstream Water Level H_1 [mm]	Peaks
TestE-001-002-c	Rectangular-Shaped	43.2	22	203	275	1
TestE-001-002-d	Rectangular-Shaped	43.2	24	214	333	2(F,P)
TestE-001-002-e	Rectangular-Shaped	43.2	11	181	332	2(F,P), H1
TestE-001-002-f	Rectangular-Shaped	43.2	11	173	281	3, H1
TestE-001-002-g	Rectangular-Shaped	43.2	12	158	204	3
TestE-001-002-h	Rectangular-Shaped	43.2	11	148	167	3
TestE-001-002-i	Rectangular-Shaped	43.2	40	178	203	3
TestE-001-002-j	Rectangular-Shaped	43.2	39	194	241	2(F,P)
TestE-001-002-k	Rectangular-Shaped	43.2	39	209	300	2(F,P), H2(F,P)
TestE-001-002-l	Rectangular-Shaped	43.2	38	216	333	2(F,P)
TestE-001-003-a	Rectangular-Shaped	1.16	13	178	292	1, H1
TestE-001-003-b	Rectangular-Shaped	1.16	15	185	330	3
TestE-001-003-c	Rectangular-Shaped	1.16	11	163	217	3, H1
TestE-001-003-d	Rectangular-Shaped	1.16	10	151	171	3
TestE-001-003-e	Rectangular-Shaped	1.16	28	158	172	3
TestE-001-003-f	Rectangular-Shaped	1.16	31	186	246	1
TestE-001-003-g	Rectangular-Shaped	1.16	33	206	321	3
TestE-001-003-h	Rectangular-Shaped	1.16	46	208	274	3
TestE-001-003-i	Rectangular-Shaped	1.16	48	221	318	3
TestE-001-003-j	Rectangular-Shaped	1.16	50	231	360	3
TestE-001-003-k	Rectangular-Shaped	1.16	44	165	176	3
TestE-001-004-a	Rectangular-Shaped	15.66	45	193	226	3
TestE-001-004-b	Rectangular-Shaped	15.66	46	208	279	2(F,P)
TestE-001-004-c	Rectangular-Shaped	15.66	46	231	365	2(F,P)
TestE-001-004-d	Rectangular-Shaped	15.66	15	189	345	3, H1
TestE-001-004-e	Rectangular-Shaped	15.66	15	172	238	2(F,P), H1
TestE-001-004-f	Rectangular-Shaped	15.66	15	157	184	1
TestE-001-004-g	Rectangular-Shaped	15.66	27	146	171	3
TestE-001-004-h	Rectangular-Shaped	15.66	27	176	211	1
TestE-001-004-i	Rectangular-Shaped	15.66	27	207	365	3
TestE-001-005-a	Rectangular-Shaped	∞	40	177	196	-
TestE-001-005-b	Rectangular-Shaped	∞	40	196	255	-
TestE-001-005-c	Rectangular-Shaped	∞	40	219	356	-
TestE-001-005-d	Rectangular-Shaped	∞	40	208	298	-
TestE-001-005-e	Rectangular-Shaped	∞	25	204	365	-
TestE-001-005-f	Rectangular-Shaped	∞	25	184	247	-
TestE-001-005-g	Rectangular-Shaped	∞	25	161	179	-
TestE-001-005-h	Rectangular-Shaped	∞	13	161	205	-
TestE-001-005-i	Rectangular-Shaped	∞	13	173	262	-
TestE-001-005-j	Rectangular-Shaped	∞	13	184	337	-
TestE-001-005-k	Rectangular-Shaped	∞	13	155	186	-
TestE-001-005-l	Rectangular-Shaped	∞	9	159	209	-
TestE-001-005-m	Rectangular-Shaped	∞	9	179	332	-

Table I-3: Test conditions for steady state tests with the rectangular-shaped lower edge

I.2.2 Chamfered-Shaped Lower Edge Tests

Table I-4 shows the test conditions of the tests executed with the chamfered-shaped lower edge. Without the test with an extreme vertical stiffness (A total of 15), 42 steady state measurements were done with the chamfered-shaped lower edge of which 18 (43%) showed a clear peak in all three measured variables and 7 (17%) showed only a peak in two measured variables. The remaining, 17 tests (40%), did not show a clear peak at all.

Name of Data File	Seal Shape	Stiffness k [N/mm]	Gate Opening δ [mm]	Downstream Water Level H_2 [mm]	Upstream Water Level H_1 [mm]	Peaks
TestF-001-001-a	Chamfered-Shaped	5.34	13	172	227	3
TestF-001-001-b	Chamfered-Shaped	5.34	13	185	293	3
TestF-001-001-c	Chamfered-Shaped	5.34	14	199	370	2(F,Y)
TestF-001-001-d	Chamfered-Shaped	5.34	13	163	191	3
TestF-001-001-e	Chamfered-Shaped	5.34	6	163	273	3
TestF-001-001-f	Chamfered-Shaped	5.34	24	163	180	1
TestF-001-001-g	Chamfered-Shaped	5.34	24	190	266	1
TestF-001-001-h	Chamfered-Shaped	5.34	25	208	365	3
TestF-001-001-i	Chamfered-Shaped	5.34	23	157	168	1
TestF-001-001-j	Chamfered-Shaped	5.34	50	193	215	1
TestF-001-001-k	Chamfered-Shaped	5.34	50	205	248	3
TestF-001-001-l	Chamfered-Shaped	5.34	50	241	365	3
TestF-001-002-a	Chamfered-Shaped	43.2	18	182	256	1
TestF-001-002-b	Chamfered-Shaped	43.2	17	192	318	2(F,P)
TestF-001-002-c	Chamfered-Shaped	43.2	18	169	206	1
TestF-001-002-d	Chamfered-Shaped	43.2	8	172	255	3
TestF-001-002-e	Chamfered-Shaped	43.2	9	181	315	3
TestF-001-002-f	Chamfered-Shaped	43.2	8	153	174	3
TestF-001-002-g	Chamfered-Shaped	43.2	36	192	237	2(F,P)
TestF-001-002-h	Chamfered-Shaped	43.2	36	211	306	2(F,P)
TestF-001-002-i	Chamfered-Shaped	43.2	36	177	197	1
TestF-001-003-a	Chamfered-Shaped	1.16	35	188	225	1
TestF-001-003-b	Chamfered-Shaped	1.16	38	212	303	3
TestF-001-003-c	Chamfered-Shaped	1.16	11	185	309	3
TestF-001-003-d	Chamfered-Shaped	1.16	15	201	370	1
TestF-001-003-e	Chamfered-Shaped	1.16	9	152	179	3
TestF-001-003-f	Chamfered-Shaped	1.16	23	162	177	1
TestF-001-003-g	Chamfered-Shaped	1.16	24	179	230	1
TestF-001-003-h	Chamfered-Shaped	1.16	27	199	299	3
TestF-001-003-i	Chamfered-Shaped	1.16	30	214	365	3
TestF-001-004-a	Chamfered-Shaped	15.66	18	169	209	1
TestF-001-004-b	Chamfered-Shaped	15.66	17	178	244	1
TestF-001-004-c	Chamfered-Shaped	15.66	17	188	293	1
TestF-001-004-d	Chamfered-Shaped	15.66	16	198	360	2(F,P)
TestF-001-004-e	Chamfered-Shaped	15.66	36	170	185	1
TestF-001-004-f	Chamfered-Shaped	15.66	35	197	256	2(F,P)
TestF-001-004-g	Chamfered-Shaped	15.66	36	208	300	2(F,P)
TestF-001-004-h	Chamfered-Shaped	15.66	12	174	238	3
TestF-001-004-i	Chamfered-Shaped	15.66	12	159	187	3
TestF-001-004-j	Chamfered-Shaped	15.66	43	192	222	1
TestF-001-004-k	Chamfered-Shaped	15.66	43	209	279	1
TestF-001-004-l	Chamfered-Shaped	15.66	43	219	319	1
TestF-001-005-a	Chamfered-Shaped	∞	46	171	191	
TestF-001-005-b	Chamfered-Shaped	∞	46	195	231	
TestF-001-005-c	Chamfered-Shaped	∞	46	219	307	
TestF-001-005-d	Chamfered-Shaped	∞	46	232	365	

Name of Data File	Seal Shape	Stiffness k [N/mm]	Gate Opening δ [mm]	Downstream Water Level H_2 [mm]	Upstream Water Level H_1 [mm]	Peaks
TestF-001-005-e	Chamfered-Shaped	∞	29	171	195	
TestF-001-005-f	Chamfered-Shaped	∞	29	192	255	
TestF-001-005-g	Chamfered-Shaped	∞	29	204	311	
TestF-001-005-h	Chamfered-Shaped	∞	29	214	356	
TestF-001-005-i	Chamfered-Shaped	∞	16	168	209	
TestF-001-005-j	Chamfered-Shaped	∞	16	184	283	
TestF-001-005-k	Chamfered-Shaped	∞	16	194	348	
TestF-001-005-l	Chamfered-Shaped	∞	8	156	204	
TestF-001-005-m	Chamfered-Shaped	∞	8	175	307	
TestF-001-005-n	Chamfered-Shaped	∞	8	179	348	
TestF-001-005-o	Chamfered-Shaped	∞	8	162	231	

Table I-4: Test conditions for steady state tests with the chamfered-shaped lower edge

I.2.3 Point-Shaped Lower Edge Tests

Table I-5 shows the test conditions of the tests executed with the point-shaped lower edge. A total of 51 tests were done with this lower edge. 11 tests with an extreme stiff vertical suspension and 40 with variable stiffness. Of these 40 tests 0 (0%) showed a clear peak in all three measured variables and only 6 (15%) showed a peak in two measured variables. The remaining, 34 tests (85%), did not show a clear peak at all. Only one test (3%) showed a high frequency peak.

Name of Data File	Seal Shape	Stiffness k [N/mm]	Gate Opening δ [mm]	Downstream Water Level H_2 [mm]	Upstream Water Level H_1 [mm]	Peaks
TestG-001-001-a	Point-Shaped	5.34	21	186	259	3
TestG-001-001-b	Point-Shaped	5.34	21	197	315	3
TestG-001-001-c	Point-Shaped	5.34	37	176	194	3
TestG-001-001-d	Point-Shaped	5.34	37	206	270	3
TestG-001-001-e	Point-Shaped	5.34	39	228	358	3
TestG-001-001-f	Point-Shaped	5.34	8	159	223	3
TestG-001-001-g	Point-Shaped	5.34	9	173	295	3
TestG-001-001-h	Point-Shaped	5.34	9	188	370	3
TestG-001-001-i	Point-Shaped	5.34	18	189	316	3
TestG-001-002-a	Point-Shaped	43.2	12	162	212	2(F,P)
TestG-001-002-b	Point-Shaped	43.2	13	187	365	3
TestG-001-002-c	Point-Shaped	43.2	13	158	192	2(F,P)
TestG-001-002-d	Point-Shaped	43.2	7	156	213	3
TestG-001-002-e	Point-Shaped	43.2	7	169	286	3
TestG-001-002-f	Point-Shaped	43.2	8	178	370	3
TestG-001-002-g	Point-Shaped	43.2	32	182	215	3
TestG-001-002-h	Point-Shaped	43.2	32	204	301	2(F,P), H1
TestG-001-002-i	Point-Shaped	43.2	32	218	365	2(F,P)
TestG-001-003-a	Point-Shaped	1.16	29	169	194	3
TestG-001-003-b	Point-Shaped	1.16	26	188	247	3
TestG-001-003-c	Point-Shaped	1.16	30	208	324	2(F,P)
TestG-001-003-d	Point-Shaped	1.16	26	209	346	3
TestG-001-003-e	Point-Shaped	1.16	23	209	370	3
TestG-001-003-f	Point-Shaped	1.16	20	192	307	3
TestG-001-003-g	Point-Shaped	1.16	16	171	221	3
TestG-001-003-h	Point-Shaped	1.16	14	150	163	2(F,Y)
TestG-001-003-i	Point-Shaped	1.16	5	149	192	3
TestG-001-003-j	Point-Shaped	1.16	7	170	229	3
TestG-001-003-k	Point-Shaped	1.16	9	179	305	3

Name of Data File	Seal Shape	Stiffness k [N/mm]	Gate Opening δ [mm]	Downstream Water Level H_2 [mm]	Upstream Water Level H_1 [mm]	Peaks
TestG-001-003-l	Point-Shaped	1.16	10	184	330	3
TestG-001-004-a	Point-Shaped	15.66	30	187	234	3
TestG-001-004-b	Point-Shaped	15.66	29	202	297	3
TestG-001-004-c	Point-Shaped	15.66	29	174	202	3
TestG-001-004-d	Point-Shaped	15.66	13	170	228	3
TestG-001-004-e	Point-Shaped	15.66	14	191	352	3
TestG-001-004-f	Point-Shaped	15.66	14	180	290	3
TestG-001-004-g	Point-Shaped	15.66	13	153	174	3
TestG-001-004-h	Point-Shaped	15.66	46	194	224	3
TestG-001-004-i	Point-Shaped	15.66	48	216	294	3
TestG-001-004-j	Point-Shaped	15.66	47	229	346	3
TestG-001-005-a	Point-Shaped	∞	37	165	175	-
TestG-001-005-b	Point-Shaped	∞	37	194	241	-
TestG-001-005-c	Point-Shaped	∞	37	218	339	-
TestG-001-005-d	Point-Shaped	∞	37	226	370	-
TestG-001-005-e	Point-Shaped	∞	21	185	264	-
TestG-001-005-f	Point-Shaped	∞	21	194	302	-
TestG-001-005-g	Point-Shaped	∞	21	209	395	-
TestG-001-005-h	Point-Shaped	∞	21	174	215	-
TestG-001-005-i	Point-Shaped	∞	12	174	258	-
TestG-001-005-j	Point-Shaped	∞	12	189	355	-
TestG-001-005-k	Point-Shaped	∞	12	159	197	-

Table I-5: Test conditions for steady state tests with the point-shaped lower edge

I.2.4 Circular-Shaped Lower Edge Tests

Table I-6 shows the test conditions of the tests executed with the point-shaped lower edge. A total of 54 tests were done with this lower edge. 11 tests with an extreme stiff vertical suspension and 43 with variable stiffness. Of these 40 tests 1 (2%) showed a clear peak in all three measured variables and only 11 (26%) showed a peak in two measured variables. The remaining, 31 tests (72%), did not show a clear peak at all.

Name of Data File	Seal Shape	Stiffness k [N/mm]	Gate Opening δ [mm]	Downstream Water Level H_2 [mm]	Upstream Water Level H_1 [mm]	Peaks
TestH-001-001-a	Circular-Shaped	5.34	32	177	204	3
TestH-001-001-b	Circular-Shaped	5.34	31	196	261	3
TestH-001-001-c	Circular-Shaped	5.34	33	212	312	3
TestH-001-001-d	Circular-Shaped	5.34	33	212	312	2(F,P)
TestH-001-001-e	Circular-Shaped	5.34	9	163	231	3
TestH-001-001-f	Circular-Shaped	5.34	9	187	352	3
TestH-001-001-g	Circular-Shaped	5.34	9	159	209	3
TestH-001-001-h	Circular-Shaped	5.34	16	158	182	2(F,P)
TestH-001-001-i	Circular-Shaped	5.34	16	178	248	3
TestH-001-001-j	Circular-Shaped	5.34	16	196	337	3
TestH-001-002-a	Circular-Shaped	43.2	37	194	242	2(F,P)
TestH-001-002-b	Circular-Shaped	43.2	37	208	293	2(F,P)
TestH-001-002-c	Circular-Shaped	43.2	37	222	343	2(F,P)
TestH-001-002-d	Circular-Shaped	43.2	37	157	162	3
TestH-001-002-e	Circular-Shaped	43.2	13	154	171	3
TestH-001-002-f	Circular-Shaped	43.2	13	175	258	3
TestH-001-002-g	Circular-Shaped	43.2	13	189	336	3
TestH-001-002-h	Circular-Shaped	43.2	46	179	193	3

Name of Data File	Seal Shape	Stiffness k [N/mm]	Gate Opening δ [mm]	Downstream Water Level H_2 [mm]	Upstream Water Level H_1 [mm]	Peaks
TestH-001-002-i	Circular-Shaped	43.2	46	204	249	3
TestH-001-002-j	Circular-Shaped	43.2	46	221	305	2(F,P)
TestH-001-002-k	Circular-Shaped	43.2	20	184	262	2(F,P)
TestH-001-002-l	Circular-Shaped	43.2	20	199	337	3
TestH-001-002-m	Circular-Shaped	43.2	20	162	184	1
TestH-001-003-a	Circular-Shaped	1.16	34	164	176	3
TestH-001-003-b	Circular-Shaped	1.16	36	187	252	3
TestH-001-003-c	Circular-Shaped	1.16	38	214	308	3
TestH-001-003-d	Circular-Shaped	1.16	42	226	354	3
TestH-001-003-e	Circular-Shaped	1.16	12	184	332	3
TestH-001-003-f	Circular-Shaped	1.16	9	174	281	3
TestH-001-003-g	Circular-Shaped	1.16	8	158	217	3
TestH-001-003-h	Circular-Shaped	1.16	22	156	169	2(F,P)
TestH-001-003-i	Circular-Shaped	1.16	26	194	277	3
TestH-001-003-j	Circular-Shaped	1.16	29	214	354	2(F,P)
TestH-001-004-a	Circular-Shaped	15.66	26	168	193	1
TestH-001-004-b	Circular-Shaped	15.66	24	194	290	2(F,P)
TestH-001-004-c	Circular-Shaped	15.66	25	210	370	2(F,P)
TestH-001-004-d	Circular-Shaped	15.66	7	149	180	3
TestH-001-004-e	Circular-Shaped	15.66	7	178	359	3
TestH-001-004-f	Circular-Shaped	15.66	7	166	266	3
TestH-001-004-g	Circular-Shaped	15.66	41	162	170	3
TestH-001-004-h	Circular-Shaped	15.66	41	193	226	3
TestH-001-004-i	Circular-Shaped	15.66	41	212	292	3
TestH-001-004-j	Circular-Shaped	15.66	41	229	352	3
TestH-001-005-a	Circular-Shaped	∞	21	163	181	-
TestH-001-005-b	Circular-Shaped	∞	21	191	285	-
TestH-001-005-c	Circular-Shaped	∞	21	198	338	-
TestH-001-005-d	Circular-Shaped	∞	35	173	190	-
TestH-001-005-e	Circular-Shaped	∞	35	198	254	-
TestH-001-005-f	Circular-Shaped	∞	35	214	328	-
TestH-001-005-g	Circular-Shaped	∞	35	222	358	-
TestH-001-005-h	Circular-Shaped	∞	11	153	179	-
TestH-001-005-i	Circular-Shaped	∞	11	172	259	-
TestH-001-005-j	Circular-Shaped	∞	11	185	330	-
TestH-001-005-k	Circular-Shaped	∞	11	176	276	-

Table I-6: Test conditions for steady state tests with the point-shaped lower edge

I.2.5 Overview Results

Table I-7 shows an overview of all the steady-state tests with the retrieved peaks.

	Total number of Tests	Tests with Extreme Stiff	Tests with Variable Stiffness	Failed Tests	Peak in all three Variables	peak in two Variables	No clear peak at all	High Peaks Identified
Rectangular-Shaped	65	13	52	1 (2%)	19 (37%)	9 (17%)	23 (44%)	7 (13%)
Chamfered-Shaped	57	15	42	0 (0%)	18 (43%)	7 (17%)	17 (40%)	0 (0%)
Point-Shaped	51	11	40	0 (0%)	0 (0%)	6 (15%)	34 (85%)	1 (3%)
Circular Shaped	54	11	43	0 (0%)	1 (2%)	11 (26%)	31 (72%)	0 (0%)

Table I-7: An overview of the results from the stead-state tests

I.3 Contraction Measurements

The final test conditions given in this appendix are the conditions during the contraction tests. The conditions are given in Table I-8.

Name of Data file	Seal Shape	Stiffness k [N/mm]	Gate Opening δ [mm]	Downstream Water Level H_1 [mm]	Upstream Water Level H_2 [mm]
ContractieA-002	Rectangular-Shaped	∞	38	227	389
ContractieA-003	Rectangular-Shaped	∞	18	193	335
ContractieA-004	Rectangular-Shaped	∞	36	206	298
ContractieB-002	Chamfered-Shaped	∞	38	227	365
ContractieB-003	Chamfered-Shaped	∞	18	193	319
ContractieB-004	Chamfered-Shaped	∞	36	206	282
ContractieC-002	Point-Shaped	∞	38	227	355
ContractieC-003	Point-Shaped	∞	18	193	312
ContractieC-004	Point-Shaped	∞	36	206	269
ContractieD-002	Circular-Shaped	∞	38	227	341
ContractieD-003	Circular-Shaped	∞	18	193	299
ContractieD-004	Circular-Shaped	∞	36	206	263

Table I-8: Test conditions of the contraction tests

[Page intentionally left blank]

Appendix J Power Spectra

This appendix will show some power spectra from individual tests. Per spectra will the notable aspects be described and elaborated as much as possible. The exact test conditions are indicated in the figure or can be found in Appendix I. The tests can be identified by the first character and the second number. The first character indicates:

- Test E: Tests with the rectangular-shaped lower edge.
- Test F: Tests with the curved-shaped lower edge.
- Test G: Tests with the point-shaped lower edge.
- Test E: Tests with the circular-shaped lower edge.

The final number in the test indicates the stiffness of the model set-up. The numbers used are:

- TestX-001-001: These tests are executed with a vertical stiffness of 5.34 N/mm and a natural frequency of 3.88 Hz.
- TestX-001-002: These tests are executed with a vertical stiffness of 43.2 N/mm and a natural frequency of 11.0 Hz.
- TestX-001-003: These tests are executed with a vertical stiffness of 1.16 N/mm and a natural frequency of 1.81 Hz.
- TestX-001-004: These tests are executed with a vertical stiffness of 15.66 N/mm and a natural frequency of 6.64 Hz

§ J.1 shows a power spectra for the determination of the natural frequency, while § J.2 shows several power spectra from the steady state measurements.

J.1 Natural Frequency

Figure J-1 shows a spectrum for a free-decay test with a clear peak of the natural frequency in which the system vibrates.

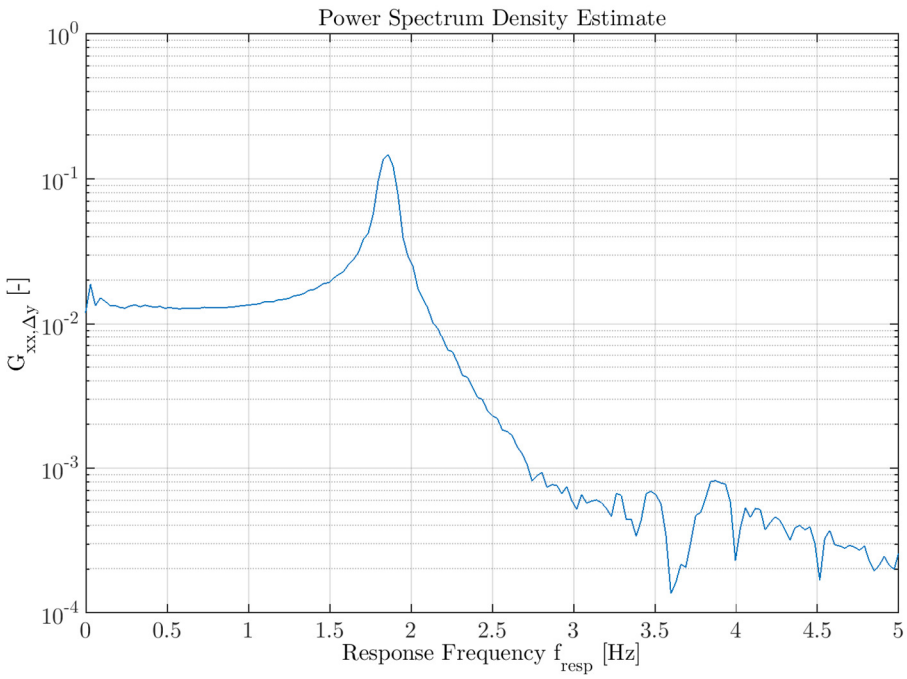

Figure J-1: Power spectrum of a free-decay test

J.2 Steady State Measurements

The power spectrum shown in Figure J-2 shows a clear low frequency peak at approximately 5 Hz. The peak coincides with the green vertical line that represents the Strouhal relationship of 0.13, as retrieved in Chapter 4, and the thickness of the valve (b). The spectrum is also shown in Chapter 4.

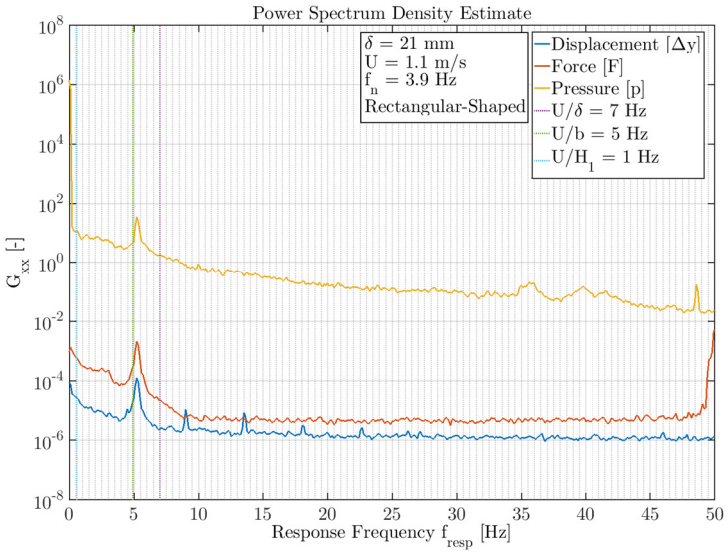

Figure J-2: Power spectrum of TestE-001-001-e

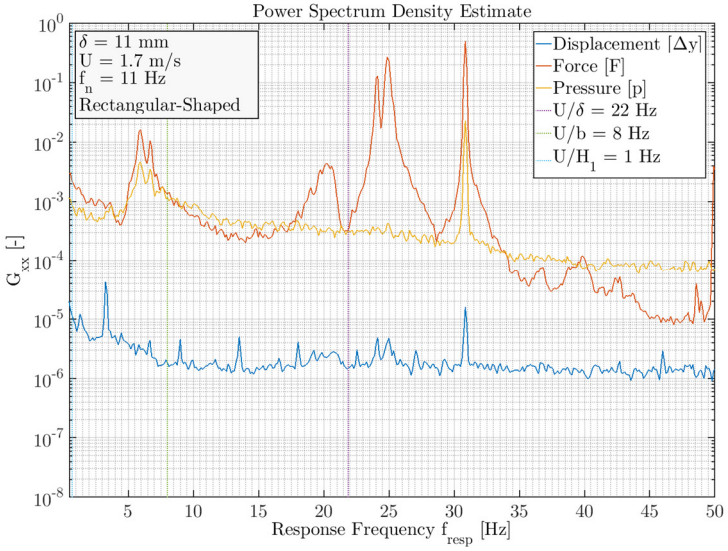

Figure J-3: Power spectrum of TestE-001-002-e

Figure J-3 shows a test result that clearly has a high frequency peak. Besides the high frequency peak, there is also a peak at a lower frequency. This peak coincides with the green vertical line, which is similar to mentioned above with Figure J-2. Figure J-4 shows a similar response with a high and a low frequency response.

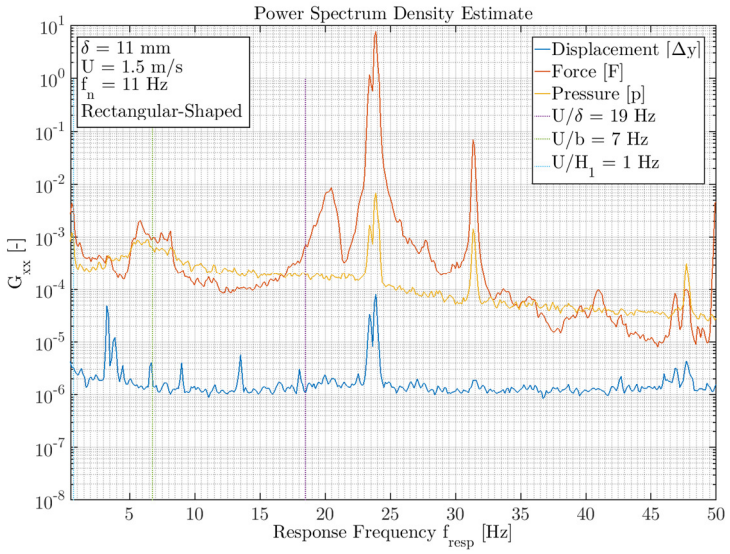

Figure J-4: Power spectrum of TestE-001-002-f

Figure J-5 is an example of a power spectrum that does not show a clear response at all. While Figure J-6 shows a clear response in a test with a chamfered-shaped lower edge. The peak does not coincide with the Strouhal number related to the gate thickness nor to the one with the gate opening. This could mean that the determined Strouhal number (0.13) is not fully correct.

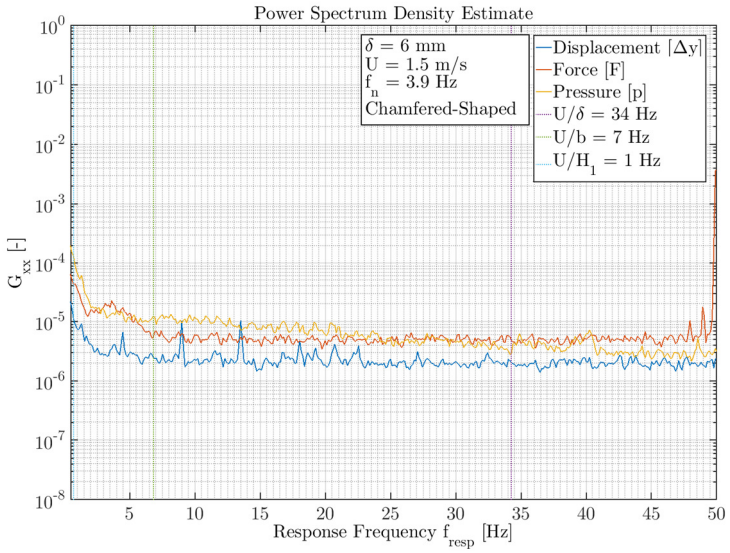

Figure J-5: Power spectrum of TestF-001-001-e

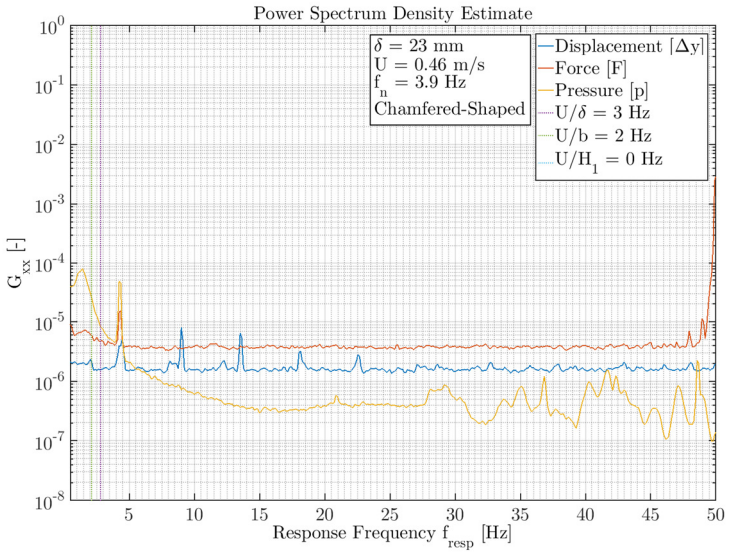

Figure J-6: Power spectrum of TestF-001-001-i

Figure J-7 shows the power spectrum of the only test with a high frequency that was not tested with the rectangular-shaped lower edge. This test was executed with a point-shaped lower edge.

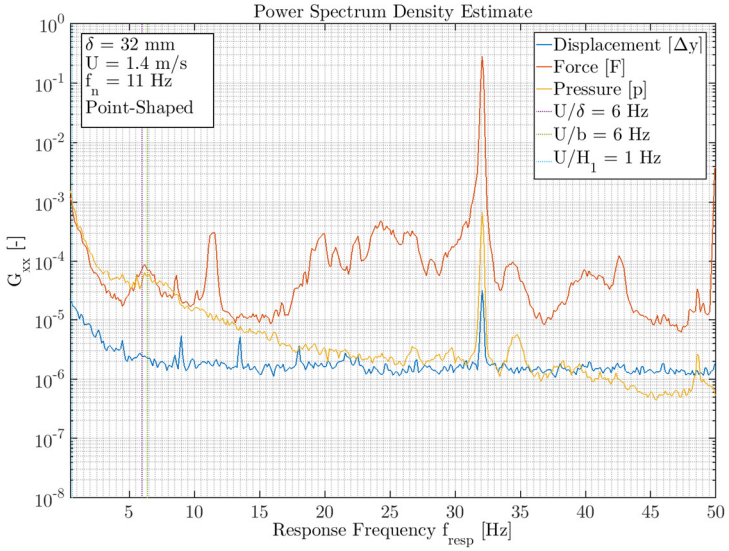

Figure J-7: Power spectrum of TestG-001-002-h

Figure J-8 shows a clear dominant response peak for a test with a circular-shaped lower edge. Shown is that the peak coincides with the Strouhal number related to the gate opening. This is in contrast with the rectangular-shaped where the most peak coincides with the Strouhal number of the gate thickness. A similar effect can be seen in Figure J-9.

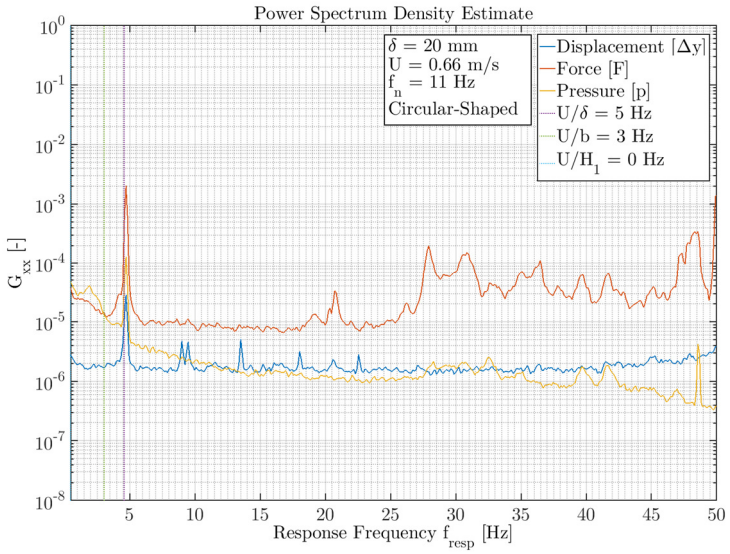

Figure J-8: Power spectrum of TestH-001-002-m

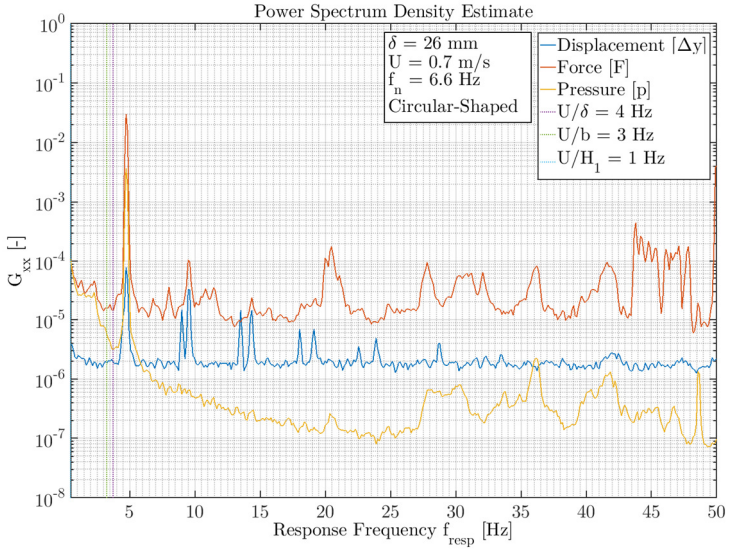

Figure J-9: Power Spectrum of TestH-001-004-a

The power spectra shown are just a few examples of the spectra constructed. In total 227 spectra were created, for every test one. The total amount of tests can be found in Appendix I.